UNIVERSITY OF SOUTHAMPTON

School of Biological Sciences

Predicting the yield and water-use of poplar short rotation coppice under a future climate

by

Rebecca Joy Oliver

Thesis for the degree of Doctor of Philosophy

September 2010

UNIVERSITY OF SOUTHAMPTON

ABSTRACT

SCHOOL OF BIOLOGICAL SCIENCES

Doctor of Philosophy

PREDICTING THE WATER-USE AND YIELD OF POPLAR SHORT ROTATION COPPICE

by Rebecca Joy Oliver

Under the current climate there is significant spatial variation in the yield and water-use of bioenergy crops such as poplar short rotation coppice (SRC). Marked changes in patterns of precipitation and temperature are predicted globally as a result of anthropogenic climate change. This is likely to significantly impact on the yield and transpiration of poplar SRC. The response of poplar SRC to future climate change is unknown and represents a significant knowledge gap in the path to a sustainable future.

This thesis used a land-surface scheme, JULES, to investigate the response of poplar SRC yield and transpiration to the interaction between changes in atmospheric CO_2 concentration and changes in climate. Empirical work generated poplar SRC specific parameter values for use JULES. It was found that V_{max}, a key model photosynthetic parameter, was significantly lower when estimated under the assumption of infinite leaf internal conductance to CO_2. This invalidated the assumption that internal CO_2 transfer has a negligible impact on the drawdown of CO_2 from c_i to c_c. The photosynthesis model in JULES is based on this assumption; however, inclusion of this additional CO_2 transfer pathway in the model did not impact on the accuracy of the simulated carbon assimilation, because the value of V_{max} used in the model compensated for the presence/absence of this pathway. It was concluded that, given the model's high sensitivity to V_{max}, it is essential to calibrate the model with a parameter value estimated under assumptions appropriate for the model. Further modification, calibration and validation enabled JULES to simulate the dynamic growth and water-use of poplar under a managed SRC cycle, which is a novel application for the model. Changes in climate were simulated using an ensemble of GCM anomalies and atmospheric CO_2 concentration was simulated using the SRES A1B emissions scenario. Results of this work highlighted the influence of climate in modifying the yield and transpiration responses to elevated concentrations of atmospheric CO_2. Additionally, for a future climate scenario, these simulations indicated higher yields but also higher water-use of poplar SRC, although the magnitude and direction of response was highly spatially variable.

Contents

List of Figures

Chapter 1

Chapter 2

Chapter 3

Chapter 4

Chapter 5

Chapter 6

Chapter 8

List of Tables

Chapter 2

Chapter 4

Chapter 5

Chapter 6

Chapter 8

I Rebecca Joy Oliver declare that the thesis entitled 'Predicting the yield and water-use of poplar short rotation coppice under a future climate' and the work presented in the thesis are both my own, and have been generated by me as the result of my own original research. I confirm that:

- This work was done wholly or mainly while in candidature for a research degree at this university.
- Where any part of this thesis has previously been submitted for a degree or any other qualification at this University or any other institution, this has clearly been stated.
- Where I have consulted the published work of others, this is always clearly attributed.
- Where I have quoted from the work of others, the source is always given. With the exception of such quotations, this thesis is entirely my own work.
- I have acknowledged all main sources of help.
- Where this thesis is based on work done by myself jointly with others, I have made clear exactly what was done by others and what I have contributed myself.
- Parts of this work have been published as:

Oliver, R. J., Finch, J. W., & Taylor, G. (2009) Second generation bioenergy crops and climate change: a review of the effects of elevated atmospheric CO_2 and drought on water use and the implications for yield. *Global Change Biology Bioenergy*. doi 10.1111/j.1757-1707.2009.01011.x

Signed:
Date: 18.09.2010

Acknowledgements

I would like to thank my supervisors, Jon Finch and Gail Taylor for giving me the opportunity of taking on this exciting PhD, especially Jon whose door was always open. A huge thank you goes to all the people I worked with at the Centre for Ecology and Hydrology, especially Eleanor Blyth, Phil Harris, Lina Mercado, Rich Ellis and Doug Clark. Their help and support over the years was invaluable. I would like to thank my family and friends for their support and encouragement over the years. Finally, special thanks go to Tom for always being there for me and keeping me sane!

Abbreviations

ATP	Adenosine triphosphate
C	Carbon
C_3	Plant using the C_3 photosynthetic pathway
C_4	Plant using the C_4 photosynthetic pathway
CET	Central England Temperature
CO_2	Carbon dioxide
DECC	Department of Energy and Climate Change
DEFRA	Department for Environment, Food and Rural Affairs
DTI	Department of Trade and Industry
FACE	Free-air CO_2 enrichment
GCM	Global Circulation Model
GtC	Giga-tons of Carbon
IEA	International Energy Agency
IPCC	Intergovernmental Panel on Climate Change
IRGA	Infrared gas exchange analyser
JULES	Joint UK Land Environment Simulator
LRT	Likelihood ratio test
MLE	Maximum likelihood estimator
MtC	Mega-tons of Carbon
N	Nitrogen
NAD-ME	NAD-malic enzyme
NADP-ME	NADP-malic enzyme
NADPH	Nicotinamide adenine dinucleotide
OTC	Open-top chamber
PAR	Photosynthetically active radiation
PCK	Phosphoenolpyruvate carboxykinase
PEP	Phosphoenolpyruvate
PFT	Plant functional type
ppm	Parts per million
PSII	Photosystem II
RCEP	Royal Commission on Environmental Pollution
RMSD	Root mean square difference
Rubisco	Ribulose-1,5-bisphosphate carboxylase/oxygenase
RuBP	Ribulose-1,5-bisphosphate
SRC	Short rotation coppice
SRF	Short rotation forestry
SRES	Special Report on Emissions Scenarios
UKCIP	UK Climate Impacts Programme
WUE	Water-use efficiency

Chapter 1

Introduction

1.1 The changing climate

Greenhouse gases in the Earth's atmosphere are responsible for warming the atmosphere, making the planet suitable for life. Atmospheric greenhouse gases absorb outgoing infra-red radiation from the Earth's surface causing some heat to be retained. Without this effect the Earth's surface would be 20 to 30^{o}C colder. Human activity, largely from the burning of fossil fuels and land-use change, has caused the concentration of many greenhouse gases to increase (IPCC, 2007). The major anthropogenic greenhouse gases include carbon dioxide (CO_2), methane and nitrous oxide. Elevated levels of greenhouse gases give rise to an enhanced warming effect as a result of a change in the Earth's radiative budget. In other words, the balance between incoming energy from the Sun and outgoing energy from the Earth is upset as more heat is absorbed by greenhouse gasses and retained. This leads to global warming and changes in the Earth's climate. The most abundant greenhouse gas is CO_2, and in their latest report, the Intergovernmental Panel on Climate Change (IPCC) conceded that the concentration of atmospheric CO_2 as recorded in 2005 far exceeded the natural range over the last 650,000 years (180 to 300 ppm) as determined from ice cores (IPCC, 2007) (Fig. 1). Indeed, since the start of the industrial revolution, the concentration of atmospheric CO_2 has increased markedly as a result of human activities from about 280 parts per million (ppm) to 389 ppm in 2010 (www.co2now.org, last accessed 01.05.10).

The burning of fossil fuels and land-use change are two key causes of the rising concentrations of greenhouse gasses in the atmosphere. Global annual fossil CO_2 emissions increased from an average of 6.4GtC (giga-tons of carbon) per year in the 1990s, to 7.2 GtC per year in 2000-2005. CO_2 emissions associated with land-use change were estimated to be 1.6 GtC per year over the 1990s, but these estimates have a large uncertainty (IPCC, 2007). In Europe (EU15) in 2000, anthropogenic emissions totalled about 0.94 GtC per year, of this the UK emitted roughly 147 MtC (mega-tons of carbon) per year (Cannell, 2003). Projections of future global carbon emissions from 2000 to 2100 were developed by

the IPCC SRES (Special Report on Emissions Scenarios) (Nakicenovic & Swart, 2000). These follow roughly 40 different scenarios in total within four main scenario families. The scenarios were developed to generate trajectories for emissions of greenhouse gases and aerosol precursor emissions into the future, depending on different interactions between global energy demand, economy, demography and land-use change. From 2000 to 2050, across the four scenario families, predictions of future global carbon emissions range from about 9 to 27 GtC (Nakicenovic & Swart, 2000). By 2100, the range of emissions across the 40 SRES scenarios is between 3 and 37 GtC, which reflects either a decrease to half the 1990 levels or, more worryingly, a huge increase by as much as a factor of six (Nakicenovic & Swart, 2000).

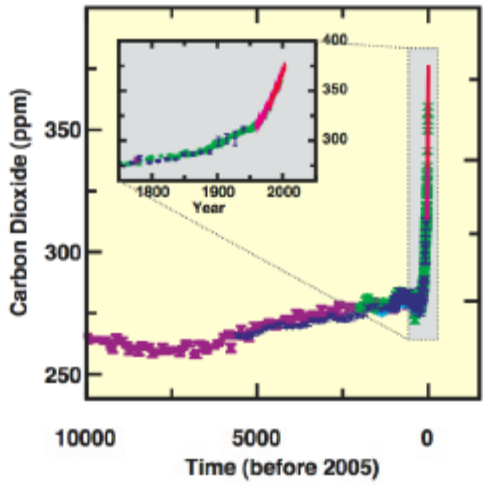

Fig 1. Atmospheric concentrations of CO_2 over the last 10, 000 years (large panel) and since 1750 (inset panel). Measurements are from ice cores (symbols with different colours for different studies) and atmospheric samples (red lines). Reproduced from IPCC (2007).

Direct observations of global climate change are such that the IPCC (2007) report stated that "warming of the climate is unequivocal, as is now evidenced from observations of increases in global average air and ocean temperatures, widespread melting of snow ice, and rising global average sea levels". The global surface temperature record indicates that the Earth has warmed by about 0.74 $^{\circ}$C since the beginning of the last century. Eleven of the last twelve years (1995-2006) are among the twelve warmest years on record (IPCC, 2007). Global average sea level rose at an average of 1.8 mm per year over 1961 to 2003. Declining glaciers and mountain snow is thought to contribute to rising sea levels, as are expanding oceans as they absorb more heat; observations since 1961 show that the average temperature of the global ocean has increased to depths of at least 3000 m and that the

ocean has been absorbing more than 80 % of the heat added to the climate system (IPCC, 2007).

In the UK, Central England Temperature (CET) has increased by roughly 1.0 ^{o}C since the 1970s, and it is very likely that increased anthropogenic greenhouse gas emissions are responsible for this (Jenkins *et al.*, 2009). Temperatures in Wales, Scotland and Northern Ireland have risen by about 0.7 to 0.8 ^{o}C since 1980, and sea surface temperatures around the UK coast have risen by roughly 0.7 ^{o}C over the past three decades (Jenkins *et al.*, 2009). The UK Climate Impacts Programme (UKCIP) looks at climate change scenarios specifically for the UK under medium (A1B), high (A1F1) and low (B1) SRES emissions scenarios (Nakicenovic & Swart, 2000) to provide probabilistic projections of future climate change. By the 2080s, under a medium emissions scenario, mean daily maximum temperature is predicted to increase across the UK. Reported at the 50 % probability level (i.e. central estimate of change), increases in the summer average temperature are up to 5.4 ^{o}C in parts of southern England and 2.8 ^{o}C in parts of northern Britain (Jenkins *et al.*, 2009). Increases in winter daily maximum temperature ranges from 1.5 ^{o}C to 2.5 ^{o}C depending on location (Jenkins *et al.*, 2009). These projections are for the medium emissions scenario, and therefore could change significantly under the high or low scenario.

Unlike annual temperature, there are no historical long-term trends apparent regarding the amount of annual precipitation in the UK. Seasonal-mean precipitation is highly variable, but appears to have decreased in summer and increased in winter (Jenkins *et al.*, 2009). Changes in the intensity of rainfall are also apparent; in winter, all regions of the UK have experienced an increase over the past 45 years of heavy precipitation events. In summer, all regions except North-East England and North Scotland have experienced a decrease in heavy precipitation events (Jenkins *et al.*, 2009). Projected changes in rainfall for the UK under a medium emissions scenario suggest that by 2080, significant changes in winter and summer precipitation are likely, although the magnitude of the change varies depending on region. The western side of the UK sees the biggest changes in winter precipitation, with a central estimate of an increase of up to +33 % (Jenkins *et al.*, 2009). Summer precipitation is projected to decrease significantly (-40 %) in parts of southern England, however minimal change is forecast for parts of northern Scotland.

1.2 Climate change mitigation

Globally, the effects of climate change are clearly evident, and CO_2 emissions are predicted to continue rising steadily and significantly (IPCC, 2007). It is widely agreed in the scientific community that the increase in global temperature should remain below 2 ^{o}C above pre-industrial levels to avoid dangerous anthropogenic interference with the climate system. This was agreed in the Copenhagen Accord at the UN Climate Change Conference in 2009. Therefore, the exploitation of renewable energy sources is likely to make an increasing contribution to climate change mitigation. The UK 'Climate Change Act 2008', a legally binding long-term framework to cut carbon emissions, commits the Government to emissions cuts of 80 % by 2050 from 1990 baseline levels. In light of this, the 'UK Low Carbon Transition Plan' outlines plans to cut emissions by 18 % on 2008 levels by 2020 (over one third reduction on 1990 levels) (DECC, 2009a). As one of a series of measures, the Government has set a target to generate 30% of UK electricity, and 15 % of all energy (electricity, heat and transport), from renewable sources by 2020 (DECC, 2009a). This is a large increase from the 4.2% of total electricity in the UK produced from renewable sources in 2005 (DTI, 2006), and a seven-fold increase in total energy supply from renewables from 2008 levels (DECC, 2009b). The Renewable Energy Strategy (2009b), outlined a significant contribution of bioenergy from biomass to the generation of electricity, heat and transport fuels as part of the low carbon energy mix.

1.2.1 Bioenergy from biomass

Bioenergy from biomass is a broad category of renewable energy that refers to any solid or nonsolid biological energy source including plant material or animal wastes. Bioenergy has been identified as having significant potential to mitigate greenhouse gas emissions and provide a secure and sustainable energy supply. Sources of biomass include crop residues, forest and industrial wood waste, straw, sewage sludge, animal waste and dedicated crops grown for energy production, termed bioenergy crops. In addition to being a source of biomass for the generation of heat and power, these dedicated bioenergy crops are also being hailed as the sustainable alternative to food crops for the generation of liquid transport fuels, termed second-generation bioenergy crops. Across temperate regions these currently include tree species grown under short rotation coppice (SRC) or intensive single stem forest management (SRF), such as species of poplar (*Populus* spp.) and willow (*Salix*

spp.), and C_4 grasses such as miscanthus (*Miscanthus giganteus*) and switchgrass (*Panicum virgatum* L.). In tropical and sub-tropical areas, the oil crop Jatropha (*Jatropha curcas*) has been suggested as a dedicated second generation bioenergy crop (Openshaw, 2000).

Poplar or willow managed as SRC are grown in densely planted plantations of high-yielding varieties. Typically, cuttings of 18-20cm long are planted from which a single stem develops, after one year's growth the trees are cut back to encourage re-growth of multiple stems. SRC plantations are usually harvested on rotations of three to five years, and the plantation may be viable for up to 30 years before re-planting is necessary (DEFRA, 2001b). Inputs of additional nutrients, such as nitrogen fertilisers are usually minimal. SRF involves the cultivation of fast-growing trees in plantation. The trees are single-stemmed and harvested between eight to 20 years after planting. The bioenergy grasses, such as miscanthus and switchgrass are perennial, rhizomatous grasses typically originating from Asia (DEFRA, 2001a). For the genus *Miscanthus x giganteus*, rhizomes are planted in densely stocked plantations, once established the crop can be harvested annually. Plantations usually remain viable for up to 20 years (Karp & Shield, 2008).

Burning bioenergy crops releases CO_2 into the atmosphere, however, plants absorb CO_2 when they photosynthesise; consequently an equivalent amount of CO_2 is taken from the atmosphere as the crops re-grow. Therefore, the carbon balance of bioenergy crops is much more favourable to conventional fossil fuels, the net effect is that bioenergy crops have significantly lower emissions of carbon. A net release of CO_2 can occur if the growing, processing or transporting of the energy crop involves the use of fossil fuels, such as in the production and use of fertilisers, and use of machinery to harvest and transport the crops. However, this is often minimal as energy crops do not require intensive management and can be further reduced if the biomass crop is grown close to where it will be used (RCEP, 2004).

Currently, co-firing of power stations to generate electricity is the dominant end-use for biomass from dedicated perennial bioenergy crops, and has commonly been in operation since 2002. Generating heat by burning biomass is another significant contribution bioenergy could make to reducing reliance on fossil fuels, however is it currently under exploited (DTI, 2006). Production of second-generation biofuels from the high proportion

of lignin and cellulose in these bioenergy crops has some way to go as technologies develop to make the process more efficient, but is another significant end-use for dedicated bioenergy crops. With the increasing demand for energy from bioenergy, the amount of land used to grow dedicated bioenergy crops in the UK is steadily increasing. In 2003, dedicated energy crops such as willow SRC and miscanthus grass occupied less than 2000 ha, as of 2008 this had increased to roughly 15 000 ha in England. The UK government's Biomass Strategy (DEFRA, 2007) suggested that bioenergy crops grown for generating heat and power could occupy up to 1.1 million ha by 2020. However, up to 3.1 million ha has been identified as suitable for planting willow SRC or miscanthus in England (Haughton *et al.*, 2009).

Concerns have been raised over the sustainability of some bioenergy crops, socially and environmentally, and over the greenhouse gas savings they can achieve. The term bioenergy crop, however, encompasses a wide genre, and many of these issues are primarily related to the production of first-generation biofuels (IEA, 2010). These are largely produced from food crops such as grains, sugar cane and vegetable oils, that could potentially compete with land for food-crops. Consequently, a key emphasis of the UK Low Carbon Transition Plan was ensuring the sustainability of bioenergy, including environmental and social impacts, and stability of supply chains.

1.2.2 Greenhouse gas savings and energy efficiency

Dedicated bioenergy crops have been shown to have significantly lower emissions of greenhouse gases compared to conventional fossil fuels. Assessment of life-cycle emissions associated with production, processing and delivery of a wide range of bioenergy feedstocks demonstrated under 'good practice' conditions, greenhouse gas savings can range from 65 % to 95 % compared to natural gas (DECC, 2009b). For SRC crops, greenhouse gas savings were in the region of 96 % to 93 % for chips and 74 % to 56 % for pellets compared to coal and gas respectively (Bates *et al.*, 2009). The higher emissions from SRC pellets resulted from energy used for drying and grinding the chips into pellets. These estimates also assume 'good practice', which means schemes are well operated with efficient processing of the feedstock, and energy crops are planted on good soils achieving reasonable yields (Bates *et al.*, 2009). The emissions abated by bioenergy are significantly affected by transportation distances, management practices i.e. use of

nitrogen fertilisers and heavy machinery. Additionally, land-use change can impact on emissions savings. Using formerly fallow land to grow bioenergy crops can reduce emissions savings by up to 10 %, and planting on permanent grassland is even worse with savings even reversed in some cases (Bates *et al.*, 2009).

Dedicated bioenergy crops have very favourable energy conversion efficiencies. For electricity generation, energy crops and coal are approximate energy equivalents (Cannell, 2003). However, combined heat and power (CHP) energy generation has a conversion efficiency of around 70-80% for bioenergy crops, which is a vast improvement on conventional power stations with conversion efficiencies of just 40-50% (Cannell, 2003) (Fig. 2). Although energy crops, like coal and gas, have some net release of carbon (C) due to production and transportation, whereas the fossil fuels emit 500kg of carbon to the atmosphere, the energy crops recycle it (Fig. 2).

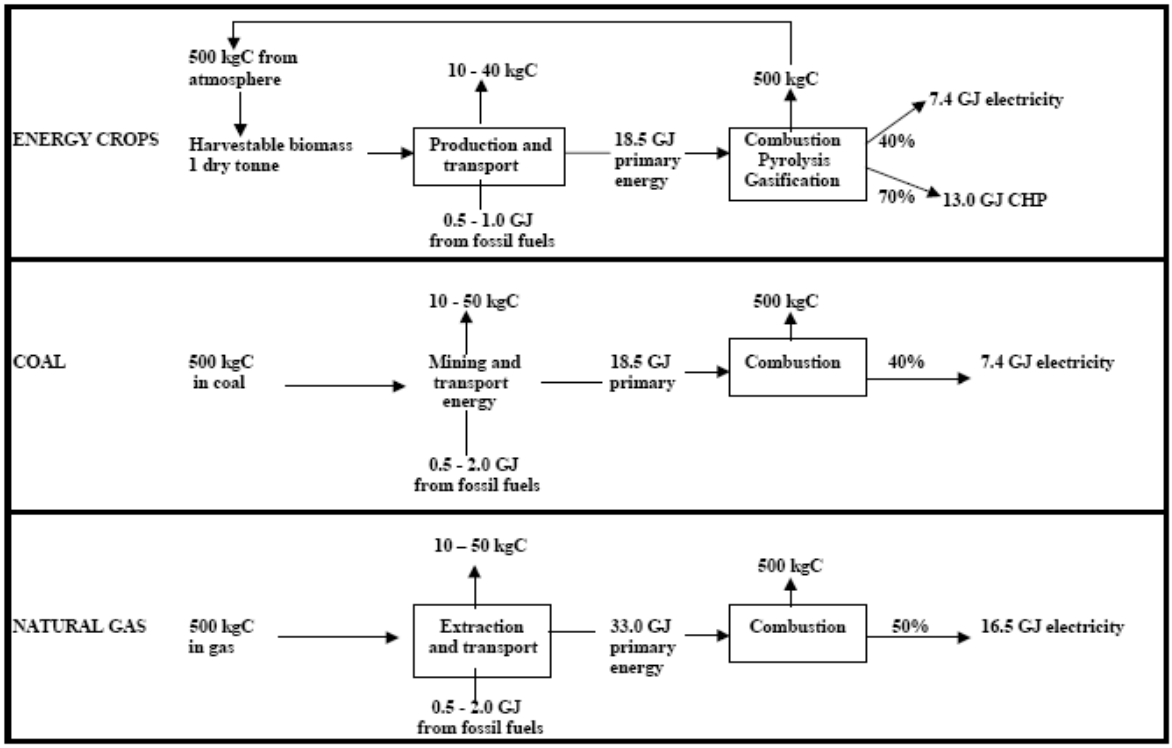

Fig. 2. Simplified schemes of the flows of energy and carbon when generating electricity from energy crops, coal or natural gas. From Cannell (2003).

1.3 Yield of second-generation bioenergy crops in the current climate

SRC crops are fast growing and high yielding which are desirable physiological traits contributing to their economic viability. Average yields of up to 15 dry tons ha^{-1} yr^{-1}, which is equivalent to 6.6 tons of oil for each hectare of coppice have been reported (Anderson *et al.*, 2005). For poplar species, theoretical work suggests values of over 40 t ha^{-1} yr^{-1} should be possible (Nonhebel, 2002), Scarascia-Mugnozza *et al*. (1997) documented yields of up to 35 dry t ha^{-1} yr^{-1} for a genotype of poplar (*P. trichocarpa* x *P. deltoids*). Bunn *et al*. (2004) recorded more conservative values for poplar yields from two sites in the UK ranging from 5.8 to 11.8 dry t ha^{-1} yr^{-1}. Similarly Tubby & Armstrong (2002) observed yields of between 4.90 to 15.87 dry t ha^{-1} yr^{-1} for three genotypes of poplar at two sites in the UK. Interestingly the lowest performer at one site (Trichobel, yield 4.90 dry t ha^{-1} yr^{-1}), had a significantly increased yield when measured at the second site (11.91 dry t ha^{-1} yr^{-1}). A fundamental problem with bioenergy SRC crops is attaining consistently high yields that are economically viable in large-scale plantings across a wide variety of climatic and site conditions. The results of yield trials such as those by Tubby and Armstrong (2002) highlight the importance of selecting suitable sites and matching species and genotypes to site conditions to maximise yields and economic viability.

1.4 Rates of water use of second-generation bioenergy crops in the current climate

Although plant water use depends on genotypic variation, climate and soil conditions, many studies have demonstrated particularly high water use for dedicated SRC bioenergy crops which supports their fast growth rates. An early study of the water use of irrigated poplar coppice carried out in Wisconsin, USA by Hansen (1988) found maximum stand transpiration rates of 4.4 to 4.8 mm day^{-1} during the second to fifth growing seasons. Hinckley *et al*. (1994) found similar maximum stand transpiration rates of 4.8 mm day^{-1} for a four-year-old un-coppiced stand of *P. trichocarpa x deltoides*. Field measurements of transpiration rates from two poplar genotypes (Beaupré and Dorschkamp) at sites in the UK revealed very high transpiration rates, typically up to 8 mm day^{-1} during the growing season (Hall & Allen, 1997) (Fig. 3a). Similarly high transpiration rates were estimated for willow at the same site (Hall *et al.*, 1998). Studies on irrigated willow SRC in Sweden (Lindroth & Cienciala, 1996; Lindroth *et al.*, 1994) and varieties of poplar SRC in the UK (Hall *et al.*, 1996) have shown that they use significantly more water than agricultural

crops and most broadleaved tree species, but not conifers. Less information is available about the water use of miscanthus or switchgrass, but a report by Finch *et al*. (2004), which used a combination of measurements and modelling to quantify evaporation, concluded that although the transpiration rates from miscanthus were high during the growing season, on an annual basis they were comparable to permanent grassland (Fig. 3b). Nevertheless, such seasonal heavy water use demonstrated by miscanthus in synchrony with summer drought could lead to higher impacts on ecosystem water availability compared to permanent grassland.

a

b

Fig. 3a. Measuring transpiration rate in a *Populus* stem, and **b.** A flux station used to quantify evaporation from miscanthus. Source, a. Gail Taylor, Southampton University; b. Jon Finch, Centre for Ecology and Hydrology.

1.5 Additional benefits of bioenergy crops

Further benefits of second-generation, dedicated bioenergy crops include increased energy security, increased biodiversity and increased stability of soils vulnerable to erosion. Global energy demand is forecast to increase by around 45 % between 2006 and 2030, with almost 80 % of this increase coming from fossil fuels (DECC, 2009a). In 2008, the UK imported 25 % of the gas it used, and this is projected to increase (DECC, 2009a). Heavier reliance on imported fossil fuels increasingly exposes the UK to global energy price fluctuations and competition for resources. With an increase in energy generated from bioenergy crops grown within the UK, this would reduce the heavy reliance on an external energy supply.

Indicators of biodiversity, such as butterfly abundance, suggest that perennial bioenergy crops can have positive impacts on biodiversity. The total abundance of butterflies, and abundance of different families of butterflies, were generally found to be greater in the field margins of SRC willow and miscanthus plantations compared to arable fields (Haughton *et al.*, 2009). Therefore, plantations of second-generation dedicated bioenergy crops could help improve biodiversity within dominantly agricultural landscapes. Finally, perennial plantations of bioenergy crops have been shown to reduce the impact of erosion through wind and water on vulnerable soils (IEA, 2010).

1.6 Conclusions

Bioenergy from second-generation, dedicated energy crops, such as SRC poplar and willow and the C_4 grasses, is identified as a renewable and sustainable energy source. Unlike first-generation bioenergy crops, second-generation bioenergy crops are viable on less productive agricultural land, therefore the competition with food crops for land is reduced. These dedicated bioenergy crops have a high energy efficiency, particularly when used in CHP generation. Additionally, they offer significant reductions in greenhouse gas emissions compared to conventional fossil fuels. Therefore, a significant contribution of these dedicated bioenergy crops to a low carbon energy mix in all sectors is proposed by the UK Government in its strategy to achieve emissions reductions targets by 2020 and beyond, with a key focus on sustainability.

Crops identified as suitable for bioenergy production have been primarily selected on the basis of their fast growth rates and high yields. However, particularly for the woody SRC crops, these are associated with high rates of water use. Adequate water availability is necessary to maintain high yields to ensure economic thresholds are achieved and a stable supply chain; however this must not compromise ecosystem water resources for other uses such as agriculture, domestic supply and river and aquifer re-charge. In the UK, predicted future climate scenarios as a result of rising atmospheric CO_2 levels suggest, in general, higher temperatures, wetter winters and drier summers (Jenkins *et al.*, 2009). The UK is dominantly a rain-fed agricultural system, consequently reduced summer precipitation and higher temperatures raises significant concerns over future yields and water-use of bioenergy crops. Under the current climate it is understood that there is significant spatial variation in the yield of bioenergy crops (Aylott *et al.*, 2008; Tubby & Armstrong, 2002).

This variation of supply is likely to significantly shift as the climate changes. Additionally, although plant responses to changes in atmospheric CO_2 concentration have been widely researched, observed responses are still variable. Moreover, how plants respond to changes in CO_2 in concert with additional changes in their environment, such as drought and temperature, have been little researched in dedicated bioenergy crops of this type. This is surprising given their increasing economic value not just in the UK, but globally. The Renewable Energy Strategy (DECC, 2009b) forecast that biomass will increasingly become a globally traded commodity. Consequently, there is a pressing need to increase our understanding of the yield and water-use responses of bioenergy crops to predicted changes in the climate, and how these will impact on the future supply of bioenergy in the UK.

1.7 Research aims

The response of yield and water-use of dedicated bioenergy crops to future climate change, and the impact of this on the variability of supply was identified as a significant research gap. This research has therefore used a combination of fieldwork and modelling to disaggregate and quantify the response of yield and water-use of poplar SRC to changes in climate and atmospheric CO_2.

Because of the increased susceptibility of poplar varieties to rust diseases, willow is currently the favoured SRC crop in the UK. Nevertheless, poplar was used in this study because it was grown as SRC (*Populus x euramericana* and *P. nigra*) in a free-air CO_2 enrichment (FACE) experiment in Italy. This provided a source of data on the growth and transpiration of these two genotypes of poplar managed as SRC under ambient and elevated concentrations of atmospheric CO_2. In addition, poplar is recognised as a model tree (Taylor, 2002) and sequencing of the whole poplar genome (Tuskan *et al.*, 2006) suggests it may return to favour as scientific advances breed more disease resistant varieties.

This research has used the land-surface scheme JULES, (the Joint UK Land Environment Simulator), a third generation land-surface model derived from MOSES 2.1 of the UK Met Office Unified Model. This model includes a physiologically-based model of leaf-level photosynthesis, and leaf-level stomatal conductance is computed as a function of net CO_2

assimilation. The rate of leaf photosynthesis depends on a suit of environmental conditions in addition to internal CO_2 concentration. These leaf-level fluxes are scaled-up to the canopy-level and the simulated available NPP (net primary productivity) is used to simulate vegetation dynamics. Therefore, the JULES model was used in this work as it contains the relevant fluxes of carbon, water and energy to dynamically simulate the yield and water-use of poplar SRC. In addition, it has the potential to be used for global applications, and is a community model. Therefore, work using the JULES model can provide information to a wider JULES modelling community. JULES does not currently include poplar SRC, or any managed perennial bioenergy crop, as a vegetation type. Therefore this work will also contribute to improving simulation of the land-surface in JULES by explicitly representing this significantly increasing land-cover.

With the motivation to determine yield and water-use responses of poplar SRC in the UK to future climate change, and with the need to refine a land-surface model in order to do so, this study addressed the following objectives:

1. What are the genotype-dependent differences between the two varieties of poplar SRC investigated in this study in terms of photosynthetic parameters, stomatal conductance and carbon allocation strategies, and how do these change with water stress?

2. What is the impact of internal conductance to CO_2 on the key photosynthetic kinetic parameters used in the physiologically-based photosynthesis - stomatal conductance model in the land-surface scheme JULES?

3. Using calibrated parameter values, is the accuracy of simulated leaf-level photosynthesis and stomatal conductance improved by including internal CO_2 conductance in the physiologically-based photosynthesis - stomatal conductance model used in JULES?

4. Scaling up from the leaf-level to the canopy-level, can JULES accurately simulate the managed growth cycle, productivity and water-use of poplar SRC?

5. How do changes in climate and atmospheric CO_2 concentration interact to impact on yield and transpiration of poplar SRC in the UK?

6. How does poplar SRC yield and transpiration vary within the UK under current climatic conditions, and how does this change under a future climate scenario?

1.8 Thesis outline

Chapter 2 presents a review of the current knowledge of plant responses to elevated atmospheric CO_2 and its interaction with drought, with a specific focus on perennial bioenergy crops. Details of the direct and indirect leaf-level responses to elevated atmospheric CO_2 and drought are given and how these scale to the whole-plant. In chapter 3, fieldwork was conducted to determine values for the key photosynthetic parameters used in the leaf-level photosynthesis-stomatal conductance model in JULES for both genotypes of poplar SRC. This chapter also investigated the impact of internal CO_2 conductance on estimates of the photosynthetic parameters. In addition, photosynthesis and stomatal conductance that had been measured over the course of the growing season with two periods of imposed drought were used to determine the response of photosynthesis, stomatal conductance and carbon allocation to this environmental stress in both poplar varieties. In chapter 4, data collected in chapter 3 were used to calibrate and validate the leaf-level photosynthesis-stomatal conductance model used in JULES for the two genotypes of poplar. The impact of including the additional internal transfer of CO_2 in the leaf-level photosynthesis-stomatal conductance model on the accuracy of simulated photosynthesis and stomatal conductance was also assessed. In chapter 5, the JULES model was modified and parameterised to simulate the managed growth cycle of poplar SRC and the carbon allocation and water-use. Model performance was validated against observations from a poplar FACE experiment. Chapter 6 used this configuration of the JULES model, calibrated for the two genotypes of poplar SRC, to simulate the transpiration and yield of poplar SRC under the current climate and for a future climate predicted under the SRES A1B emissions scenario using an ensemble of climate predictions. The response to a future climate was fully disaggregated (i.e. climate and CO_2 concentration) to gain a better understanding of the interaction between climate and CO_2.The variation in yield and transpiration of poplar SRC in the UK was assessed under the current and future climate scenario at four locations in the UK, and for three different 'typical' soil types.

Chapter 2

Second generation bioenergy crops and climate change: the effects of elevated atmospheric CO_2 and drought on water-use and yield

2.1 Introduction

Species currently used as second-generation bioenergy crops are suitable as a source of biomass energy because they are fast-growing and high-yielding. However, this is accompanied by high rates of water-use (Hall *et al.*, 1998; Lindroth & Cienciala, 1996; Lindroth *et al.*, 1994). Consequently, the implications of climate change for bioenergy crop production are substantial, particularly with regard to rising atmospheric CO_2 concentrations and forecast increased frequency of summer drought, as these two climate factors are key environmental determinants of productivity and water-use in plants. For the biomass industry to compete successfully with conventional fossil fuel alternatives and flourish, energy yield per hectare must be high and needs to remain so in the face of a changing climate. Additionally, environmental concerns surround bioenergy crop production in relation to their water-use. The C_3 *Salicaceae* trees in particulary have high rates of water-use (Hall *et al.*, 1998; Lindroth & Cienciala, 1996; Lindroth *et al.*, 1994) which, should droughts become more frequent as is forecast, pose a serious threat to ecosystem water resources. Therefore a conflict of interests is reached with the necessity to increase yields on the one hand, and minimise excessive water-use on the other. However, this is complicated by the unknown responses of these second-generation bioenergy crops to the concurrent changes in climate and atmospheric CO_2 concentration. More than ever there is a need to quantify and predict the effects of increasing atmospheric CO_2 and drought on crop growth and water-use, specifically for these species, to ensure both economic and environmental sustainability.

Increased carbon uptake by plants in response to rising concentrations of atmospheric CO_2, termed the "CO_2 fertilisation effect", is predicted to generate higher plant biomass as

a result of increased rates of plant photosynthesis (Norby *et al.*, 2005). However, this response is variable, depending on species and plant age (Körner, 2006; Körner *et al.*, 2005). Plant water-use is also predicted to decline in a future climate as a result of reduced stomatal conductance (*gs*). Enhanced rates of photosynthesis and reduced *gs* lead to increased plant water-use efficiency (WUE) i.e. the amount of biomass produced per unit water used (Ceulemans & Mousseau, 1994; Curtis & Wang, 1998; Drake *et al.*, 1997; Gunderson & Wullschleger, 1994; Norby *et al.*, 1999; Saxe *et al.*, 1998). It is suggested that these responses to an enriched CO_2 atmosphere will improve the drought tolerance of plants by delaying the onset of drought due to enhanced soil water availability.

Currently, low water availability is the main factor limiting plant growth and yield worldwide (Chaves *et al.*, 2003) and, as suggested by GCM (global circulation model) predictions, global change will make water scarcity ever more prominent in many parts of the world. Drought is therefore likely to be the change in climate that has the greatest impact on plant growth, productivity and ecosystem function in most parts of the temperate latitudes. Given the significant environmental limitation on growth due to water availability, this may dominate the effect of elevated atmospheric CO_2 on plant growth and water-use. Therefore, we propose that whilst growth in an elevated CO_2 atmosphere may have beneficial effects on bioenergy crop productivity and water-use, this will strongly depend on the climate, primarily in response to the severity, timing and frequency of drought during the growing season. Increases in temperature are also shown to increase yield and total biomass in many plant species, primarily as a result of increased rates of carbon assimilation and faster development through the growing season, although this response is not universal and there is evidence that suggests photosynthetic responses of plants acclimate to higher temperatures (Morison & Lawlor, 1999; Wheeler *et al.*, 1996; Wheeler *et al.*, 1994). Investigation of the effects of elevated atmospheric CO_2 in concert with stresses such as nutrient availability and atmospheric ozone concentration have already been shown to modify the CO_2 response of some plant species (Karnosky *et al.*, 2003; Oren *et al.*, 2001). Therefore, it is important to understand plant responses to 'multiple' climate changes, not just elevated atmospheric CO_2. This review investigates the physiological responses of second-generation lignocellulosic bioenergy crops to the concurrent climate effects of elevated atmospheric CO_2 and reduced summer precipitation. Although the effects of elevated atmospheric CO_2 on plant functioning have been addressed in many studies and reviewed several times (Ainsworth & Long, 2005;

Ainsworth & Rogers, 2007; Ceulemans & Mousseau, 1994; Drake *et al.*, 1997; Long *et al.*, 2004; Medlyn *et al.*, 1999; Saxe *et al.*, 1998), this review uniquely focuses on the combined effects of CO_2 and drought, and the implications this has for bioenergy crop production.

Information specific to perennial bioenergy crops that are the focus of this review is limited; therefore we draw on examples from other C_3 tree species and C_4 grass species where necessary. The development in recent years of large-scale free-air CO_2 enrichment (FACE) experiments, allowing the exposure of plants to elevated atmospheric CO_2 under natural, field conditions, has contributed significantly to our understanding of plant responses to rising atmospheric CO_2. A recent synthesis of outputs from these experiments suggests that yield enhancement in elevated atmospheric CO_2 is likely to be less than that predicted from work in small- and open-top chamber (OTC) studies (Long *et al.*, 2006). Additionally, well known limitations exist to the use of controlled environment and OTC systems when studying plant physiological responses to elevated atmospheric CO_2 (Arp, 1991; Long *et al.*, 2004; Nowak *et al.*, 2004), consequently our synthesis is based mainly on FACE experiments. Globally, there are many FACE experiments of which two, AspenFACE (Rhinerlander, Wisconsin, USA), and popFACE (Viterbo, Central Italy), use varieties of poplar. *Populus tremuloides* is grown at AspenFACE as a mature, unmanaged stand of trees. Three genotypes of poplar, *P. alba, P. x euramericana* and *P. nigra* are grown at popFACE under SRC management. Data for willow are extremely limited; therefore we draw upon examples from other C_3 woody temperate species where necessary. Data for C_4 bioenergy crops, such as miscanthus and switchgrass, are virtually non-existent, highlighting a gap in research. Examples are drawn from other C_4 grasses and agricultural crops including sorghum (*Sorghum bicolour*) and maize (*Zea mays*) amongst others.

2.2 Plant responses to elevated atmospheric CO_2 concentration

In an attempt to simplify the plant physiological responses to elevated atmospheric CO_2 for C_3 and C_4 lignocellulosic bioenergy crops, two pathways were identified, 'direct' and 'indirect', through which elevated atmospheric CO_2 affects photosynthesis (Fig. 1). The 'direct' CO_2 effect describes the pathway through which elevated atmospheric CO_2 directly influences net photosynthesis (A_{net}) by altering photosynthetic metabolic processes. The

'indirect' CO_2 pathway describes how elevated atmospheric CO_2 can influence A_{net} indirectly via stomatal regulation. An increase in net carbon assimilation rate as a result of either pathway leads to increased capacity to generate energy for growth, ultimately resulting in higher biomass production, which is desirable for a bioenergy crop species (Ainsworth & Long, 2005; Calfapietra *et al.*, 2003b; Ceulemans & Mousseau, 1994; Curtis & Wang, 1998; Gielen & Ceulemans, 2001; Liberloo *et al.*, 2006; Norby *et al.*, 1999; Poorter & Navas, 2003), although this plant response is variable (Körner *et al.*, 2005). Both the direct and indirect pathway are an important component of plant WUE, the direct pathway through stimulating photosynthetic metabolism and the indirect pathway through improving plant-water relations and conserving soil moisture, and both will be discussed.

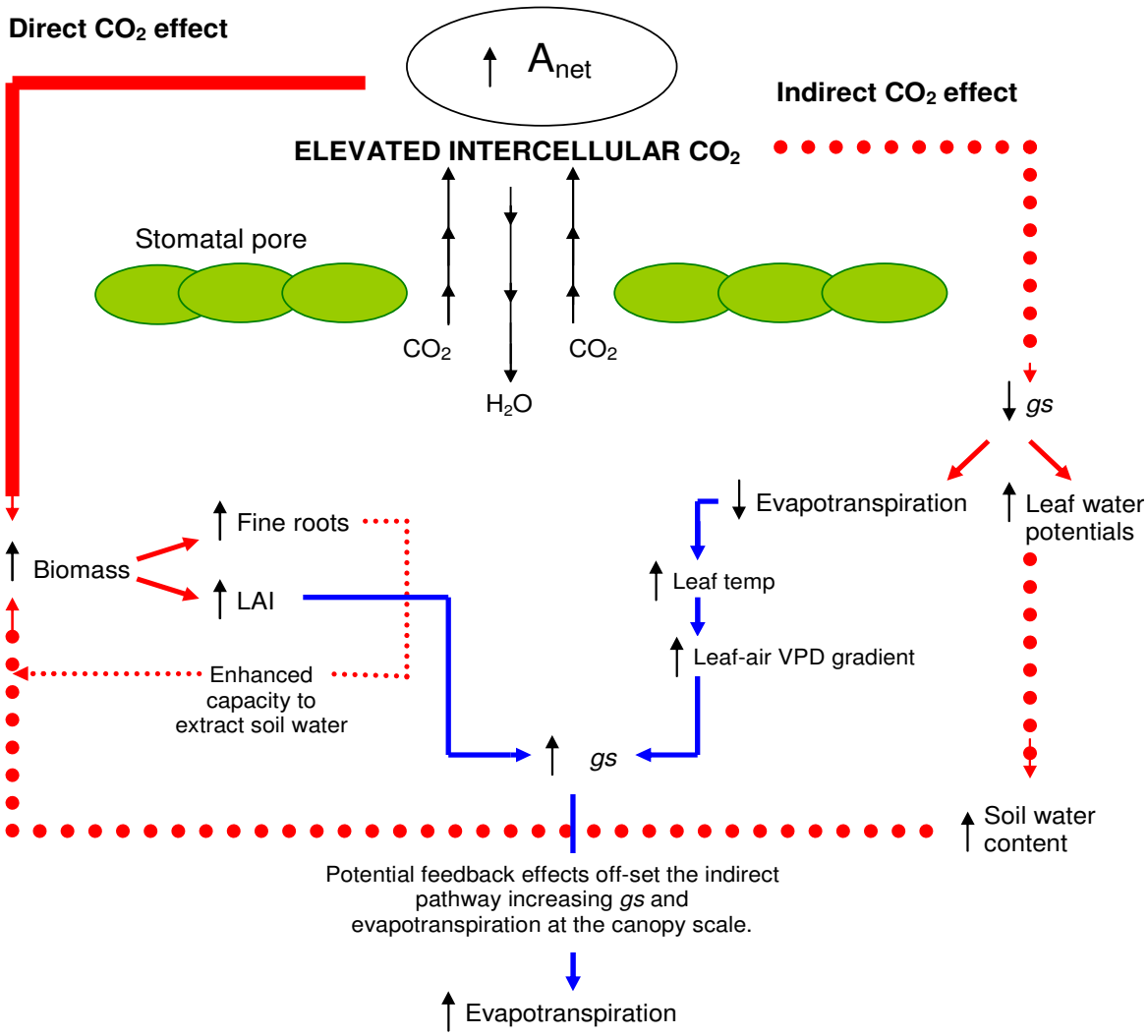

Fig. 1. The main pathways through which elevated atmospheric CO_2 affects plant biomass and water-use.

Denotes the pathway through which elevated CO_2 directly stimulates photosynthetic metabolism, increasing net carbon assimilation (A_{net}) and thus biomass. The direct stimulation of photosynthesis in C_3 plants is well documented and mechanisms understood. In C_4 plants, direct stimulation of photosynthesis is unclear, it has been observed in some studies, but proposed mechanisms are not well understood and theory suggests C_4 species would not respond to elevated CO_2.

● ● Denotes the pathway through which elevated CO_2 has an indirect effect on plant photosynthesis, thus increasing biomass. Decreased stomatal conductance (*gs*) leads to improved plant water relations. Transpirational water loss is reduced, which results in the maintenance of higher leaf water potentials and higher soil water content over the course of the growing season. Together these offset the negative effects of drought by delaying the development of water stress in the plant which may inhibit plant photosynthesis and reduce growth.

Denotes potential negative feedbacks that may off-set the beneficial effects of elevated CO_2 on plant water-use. Increased leaf area index (*LAI*) may result in higher leaf *gs*, thus evapotranspiration at the canopy scale will increase. Another potential scenario suggests decreased evapotranspiration from reduced *gs* may lead to higher leaf temperatures. This may decrease humidity within the canopy and thus increase the leaf-to-air vapour pressure gradient, ultimately increasing the driving force for transpiration within the canopy.

2.3 The direct CO_2 effect: how does elevated atmospheric CO_2 effect photosynthesis?

The response of photosynthesis to elevated atmospheric CO_2 is probably the most intensively studied plant response to growth in a changed climate. During photosynthesis, plants use CO_2 from the atmosphere to generate energy for growth. There are two different photosynthetic pathways that are dominantly used by plants, C_3 and C_4. The majority of plants, including trees use the C_3 pathway. Under cool, moist conditions with normal light intensity the C_3 pathway is dominant as it is most efficient. The C_4 pathway is an adaptation to arid conditions because it results in better water-use efficiency, and is more efficient than the C_3 pathway under high light intensity and high temperature conditions. The names are such simply because the C_3 pathway incorporates CO_2 into a 3-carbon compound, and the C_4 pathway uses a 4-carbon compound. In the C_3 pathway, RuBP (ribulose-1,5-bisphosphate) is the substrate for CO_2. Carboxylation of RuBP is catalysed by the photosynthetic enzyme Rubisco (ribulose-1,5-bisphosphate carboxylase/oxygenase), this is the first major step in carbon fixation. Carboxylation is competitively inhibited by oxygen (O_2) in a process called photorespiration. This ultimately decreases the efficiency of photosynthetic carbon assimilation. In the C_4 pathway, Rubisco is localised in the bundle sheath cell chloroplasts. The enzyme PEP carboxylase (phosphoenolpyruvate) binds to CO_2 and delivers it to Rubisco. Thus, C_4 photosynthesis manages to bypass the photorespiration pathway as Rubisco is kept isolated from atmospheric O_2, and the CO_2 concentration is 3 to 6 times higher in the bundle sheath cells than in the atmosphere (von Caemmerer & Furbank, 2003). Assumptions based on photosynthetic theory suggest that C_4 species would not benefit from increases in atmospheric CO_2 because of the "CO_2 concentrating mechanism in the bundle sheath cells" (Wand *et al.*, 1999). Conversely as C_3 plants are currently substrate limited at ambient CO_2 levels, a strong stimulation of net photosynthesis is predicted if the concentration of CO_2 is increased.

2.3.1 C_3 plants

Light-saturated photosynthesis (A_{sat}) is more responsive to elevated atmospheric CO_2 than light-limited photosynthesis (Long *et al.*, 2004). Light-saturated photosynthesis is predominantly limited by the activity of Rubisco that catalyses the carboxylation reaction between CO_2 and RuBP (Rogers & Humphries, 2000). Under current ambient CO_2 concentrations, this limitation is due to limited supply of CO_2. As the concentration of CO_2

rises, RuBP competitively binds CO_2 over O_2 which inhibits the photorespiration pathway. Consequently, carboxylation of RuBP, and therefore activity of Rubisco, is increased. Concentrations of atmospheric CO_2 below 600 µmol mol^{-1} are typically insufficient to saturate photosynthetic carboxylation (Nowak *et al.*, 2004). As ambient atmospheric CO_2 concentration is currently around 350 µmol mol^{-1}, any increase of CO_2 concentration will enhance leaf A_{net} due to increased substrate availability (Gunderson & Wullschleger, 1994). The efficiency of net CO_2 uptake is increased by decreasing photorespiratory CO_2 loss and diverting ATP (adenosine triphosphate) and NADPH (nicotinamide adenine dinucleotide) away from photorespiratory metabolism to photosynthetic assimilation, thus increasing the efficiency of A_{net} (Long *et al.*, 2004). In light-limiting conditions, photosynthesis is limited by the rate of regeneration of the CO_2 acceptor, RuBP (Gielen & Ceulemans, 2001). In this case, photosynthesis is limited by RuBP supply which is independent of CO_2 concentration.

2.3.2 C_4 plants

Greater C_4 plant photosynthesis under elevated atmospheric CO_2 has been attributed to a range of possible mechanisms:

(1) Direct effects of Rubisco CO_2 saturation: Although C_4 photosynthesis is considered to be at saturation under current ambient atmospheric CO_2 concentrations, a number of studies have found that photosynthesis is not completely saturated in many well-watered C_4 species, thus allowing A_{net} to increase with increasing atmospheric CO_2 concentration (Wand *et al.*, 1999; Watling & Press, 1997; Ziska & Bunce, 1997).

(2) Bundle sheath leakiness: Within C_4 plants is said to exist C_4 sub-types, which differ biochemically in the enzymes used for decarboxylation of the C_4 product formed (Poorter & Navas, 2003). Briefly, the three types NADP-ME (NADP-malic enzyme), PCK (phosphoenolpyruvate carboxykinase), and NAD-ME (NAD-malic enzyme) are said to exhibit increasing levels of 'leakiness' to CO_2 from the bundle sheath to the mesophyll, in the above order (Wand *et al.*, 1999). Thus the growth response to elevated atmospheric CO_2 was thought to increase with leakiness, with the NAD-ME type being most responsive to an increase in atmospheric CO_2. Ghannoum *et al*., (2000), however, suggest that because of the vast inconsistencies in results from different studies, and because bundle sheath

leakiness can only be indirectly measured, these two facts combined cast substantial doubt over the relationship between leakiness and biochemical subtype.

(3) C_3 like photosynthesis: Some young C_4 leaves have been found to have immature C_4 pathways that are C_3-like making them more sensitive to enhanced photosynthesis under elevated atmospheric CO_2 (Dai *et al.*, 1995; Ziska *et al.*, 1999). This mechanism, however, is species dependent. Young C_4 Sorghum (*Sorghum bicolor*) leaves, for example, were found to have C_3 like photosynthesis (Cousins *et al.*, 2001). In young sorghum plants, A_{net} was partially stimulated when atmospheric O_2 concentrations were reduced, i.e. suppression of photorespiration (Cousins *et al.*, 2001). However, young C_4 leaves of *Panicum antidotale* and *Panicum colotatum* investigated by Ghannoum *et al*. (1998) were not found to be C_3 like.

2.4 The photosynthetic response of C_3 and C_4 plants

It is now understood that growth in elevated atmospheric CO_2 leads to a direct increase in photosynthetic rate in C_3 species (Table 1). Curtis and Wang (1998) reported a +31% increase in A_{sat} for trees grown under concentrations of elevated atmospheric CO_2 that ranged between ~600 - 800 ppm. A meta-analyses conducted by Ainsworth and Long (2005) showed that within the C_3 functional group, trees showed the greatest photosynthetic response to elevated CO_2. A +47% increase in A_{sat} was reported for an increase in CO_2 concentration that ranged between 475 - 600 ppm. A_{sat} was enhanced more in woody species (+38%) relative to herbaceous species (+12%) as reported by Nowak *et al*. (2004) for a doubling of ambient CO_2 concentration (~550 ppm). In poplar SRC, Bernacchi *et al*. (2003) showed evidence for differences in photosynthetic stimulation as a result of elevated atmospheric CO_2 (550 ppm) between genotypes within species, and at different stages of the growth cycle. For pre-coppiced poplars in elevated atmospheric CO_2, the mean increase in A_{sat} for all 3 species (*P. alba, P. nigra and P.x euramericana*) was 38%. Post-coppice, however, during re-growth, a large down-regulation response was observed for two species (*P. nigra and P.x euramericana*), but not for the third (*P. alba*).

The effects of elevated atmospheric CO_2 on C_4 plants are not well understood. Despite photosynthetic theory that suggests C_4 plants will not be responsive to elevated atmospheric CO_2, there is vast inconsistency between experimental studies. Some observe

no response (Leakey *et al.*, 2006; Nie *et al.*, 1992), whilst others observe significant effects upon photosynthesis under roughly twice ambient CO_2 concentration (Leakey *et al.*, 2004; Wand *et al.*, 1999; Watling & Press, 1997). For example, studies on the photosynthetic response of maize (*Zea mays*) and the C_4 weed *Amaranthus retroflexus*, found that the weed species responded strongly to double current ambient concentrations of CO_2, but photosynthetic rate of the maize was much less responsive, A_{net} was stimulated by just +5% (Ziska & Bunce, 1997). In a later study, growth in elevated atmospheric CO_2 (550 ppm) was found to have no effect on photosynthesis in maize (*Zea mays*) (Leakey *et al.*, 2006).

Species	Average change in A_{sat} with elevated CO_2	Experiment	Length of study	Reference
C_3 woody species				
Populus x euramericana *P. nigra* *P. alba*	Mean for all 3 *spp.*: ↑ 38%	FACE	3 years	Bernacchi *et al.* (2003)
Liquidambar styraciflua (Sweetgum)	sun leaves: ↑ 63% shade leaves: ↑ 48%	FACE	3 years	Herrick & Thomas (2001)
Liquidambar styraciflua (Sweetgum)	↑ 44% (upper canopy)	FACE	3 years	Sholtis *et al.* (2004)
Liquidambar styraciflua (Sweetgum)	↑ 46% (upper canopy)	FACE	3 years	Gunderson *et al.* (2002)
Pinus taeda (Loblolly pine)	↑ 45% current yr needles	FACE	1 season	Rogers & Ellsworth (2002)
Pinus taeda (Loblolly pine)	↑ 50 - 60% current yr needles	FACE	400 days	Ellsworth (1999)
C_3 grasses				
Abutilon theophrasti	↑ ~ 35%	Growth chambers	1 season	Ward *et al.* (1999)
C_4 grasses				
Zea mays (maize)	No effect	FACE	1 season	Leakey *et al.* (2006)
Amaranthus retroflexus	↑ ~ 18%	Growth chambers	1 season	Ward *et al.* (1999)
Sorghum bicolor (sorghum)	↑ 9%	FACE	2 seasons	Wall *et al.* (2001)

Table 1. Average change (%) in light-saturated photosynthetic rate (A_{sat}) with elevated atmospheric CO_2 for a range of species, all are well-watered. Results were taken from the literature reported as the average of all observations, for more details refer to individual references. ↑ = increased A_{sat}; FACE = free-air CO_2 enrichment

2.4.1 Down-regulation of plant photosynthetic capacity

Evidence regarding biochemical down-regulation of photosynthetica capacity in elevated atmospheric CO_2 is very variable. Some studies show a lack of photosynthetic acclimation (Gunderson *et al.*, 2002; Herrick & Thomas, 2001; Tognetti *et al.*, 1999), whereas others present evidence of substantial photosynthetic down-regulation occurring in selected species (Ainsworth *et al.*, 2003; Bernacchi *et al.*, 2003; Huxman *et al.*, 1998; Rogers & Ellsworth, 2002). The precise mechanism of photosynthetic down-regulation at elevated atmospheric CO_2 is still undetermined. Rogers and Humphries (2000) demonstrated that biochemical down-regulation could be attributed almost entirely to a decrease in the carboxylation capacity of Rubisco. A reduction in the amount of Rubisco following growth in elevated atmospheric CO_2 could have different causes, and the mechanism through which this occurs is uncertain (Rogers & Ellsworth, 2002). Two possibilities are variably proposed:

1) Sink strength: the source-sink imbalance

It is hypothesised that the reduction in Rubisco content is selective via decreased expression of genes coding for photosynthetic apparatus; in particular *rbcS* which codes for the small subunit of Rubisco (Drake *et al.*, 1997; Long *et al.*, 2004; Moore *et al.*, 1998; Moore *et al.*, 1999). Increased levels of soluble carbohydrates in the leaf have been linked to the suppression of certain genes, suggesting down-regulation of photosynthesis in response to increased sucrose cycling, i.e. when photosynthetic carbohydrate production is in excess of what can be utilised or exported by the plant. Sucrose is the form of sugar in which excess carbohydrate is stored, and exported from the leaf. Moore *et al.* (1999) suggest that excess sucrose is hydrolysed, producing hexose sugars which, via a hexokinase-related signalling pathway, signals the source-sink imbalance leading to the repression of Rubisco gene expression. This sugar-mediated feedback controls the amount of enzyme, leading to a selective decrease in the amount of Rubisco.

There are problems with this suggested mechanism, in particularly the uncertainty surrounding the nature of the sugar signal (Stitt & Krapp, 1999). However, Rogers and Ellsworth (2002) found that photosynthetic down-regulation in *Pinus taeda* needles grown in elevated atmospheric CO_2 was not accompanied with any significant decrease in needle

nitrogen or protein content, lending support to the hypothesis that loss of Rubisco is not the consequence of a non-selective reduction in leaf N content. The apparently selective reduction of Rubisco in older needles was associated with a significantly higher carbohydrate content, which is consistent with the concept that down-regulation in elevated atmospheric CO_2 involves a sugar-mediated response (Rogers & Ellsworth, 2002), and a loss of nitrogen is actually a dilution effect from the excess soluble carbohydrates.

Experimental evidence suggests that field-grown plants do not show the same degree of downward acclimation as those grown in pots, and that developmental sinks such as fruit set affect acclimation (Arp, 1991; Curtis & Wang, 1998; Gunderson & Wullschleger, 1994; Herrick & Thomas, 2001; Norby *et al.*, 1999). The review by Arp (1991) was first to draw attention to the trend that the reduction in photosynthetic capacity at elevated atmospheric CO_2 was most pronounced when plants had a small sink size. The volume of pots in which plants were grown affected the sink size by restricting root growth. While plants grown in small pots (i.e. small sink size) had a reduced photosynthetic capacity, plants grown in the field showed no reduction or an increase in capacity. Additionally, for *Populus* species growing under SRC management in a bioenergy plantation, long-term down-regulation of photosynthesis was avoided because the trees were shown to have a large photosynthate sink capacity (Davey *et al.*, 2006).

2) Nitrogen limitation

Given that plants invest a large amount of nitrogen (N) in Rubisco, a second mechanism suggests that the reduction in the amount of Rubisco is the result of a non-selective decrease in leaf N content. It is suggested that the observed decreases in Rubisco may reflect a general decrease in leaf protein due to relocation of nitrogen within the plant (Ainsworth & Long, 2005; Rogers & Ellsworth, 2002), or earlier leaf senescence in nitrogen-limited plants. Down-regulation of photosynthesis at elevated atmospheric CO_2 has been reported to be more pronounced when plants are N-limited, and to be absent when N supply is adequate (Ainsworth *et al.*, 2003; Nowak *et al.*, 2004; Stitt & Krapp, 1999). Ainsworth and Long (2005) demonstrated that under low N conditions the down-regulation response of photosynthetic capacity (-22 %) was larger than under high N conditions (-12 %).

2.5 Is yield enhanced in elevated atmospheric CO_2?

Most studies show that growth in elevated atmospheric CO_2 leads to an increase in plant biomass above and below ground (Ainsworth & Long, 2005; Ceulemans & Mousseau, 1994; Norby *et al.*, 1995; Stulen & den Hertog, 1993). Ceulemans and Mosseau (1994) found increases in the mean biomass of +38% for conifers and +63% for deciduous trees grown in an enriched atmospheric CO_2 environment of roughly double the ambient CO_2 concentration. The review by Ainsworth and Long (2005) concluded that woody plants increased above-ground dry matter production by +28% with greater allocation to wood and structure with a raised CO_2 concentration of between 475 - 600 ppm. Similarly, Curtis and Wang (1998) reported a +29% increase in total biomass in elevated atmospheric CO_2 that ranged between 600 - 800 ppm for young or juvenile trees grown in OTC or glasshouse studies.

Poplars are fast growing species; large and varied increases in total biomass of between 22 and 90% in response to atmospheric CO_2 enrichment have been reported (Gielen & Ceulemans, 2001). Measurements on three varieties of poplar (*P. alba, P. nigra* and *P. x euramericana*) during establishment at the popFACE facility in Italy show that all three genotypes responded by enhanced growth performance under and elevated CO_2 concentration of 550 ppm. Growth at elevated atmospheric CO_2 increased stem diameter by 13 to 40% depending on species, tree height increased slightly showing a relative increase by about 10%, and the stem volume index was increased between 54 to 79% (Calfapietra *et al.,* 2001). After two growing seasons, elevated atmospheric CO_2 enhanced biomass production by up to 29% for the three *Populus* species (Liberloo *et al*., 2006). Below ground biomass was stimulated in elevated CO_2 by up to 48% (*P. euramericana*), a 28% enhancement was observed for *P. nigra* and a 19% stimulation for *P. alba* (Liberloo *et al.,* 2006). After three growing seasons, total biomass production of the poplar plantation was still responsive to elevated atmospheric CO_2 increasing by 24% compared to trees grown in ambient atmospheric CO_2 (Calfapietra *et al.,* 2003). The increase of aboveground biomass production ranged from 15% to 27% while the effect of elevated CO_2 on belowground biomass was even greater, from 22% to 38%, depending on genotype. Lukac *et al.* (2003) observed a 47-76% increase in standing root biomass in trees grown under elevated CO_2 over a 3 year period at the poplar plantation. These results suggest that in poplars, the response of growth to elevated atmospheric CO_2 is sustained but strongly

depends on genotype and also stage in the growth cycle. Of the three genotypes used at the popFACE facility in Italy, *P. nigra* displayed the greatest response to elevated atmospheric CO_2 (Calfapietra *et al.,* 2001; Calfapietra *et al.,* 2003). Each genotype has inherent morphological and physiological differences between specific growth parameters that may be responsible for this difference; *P. nigra* is a highly productive species as shown by its higher biomass accumulation and degree of branch production in control plots. This is in agreement with an earlier study by Dickson *et al.* (1998) who also observed that the largest response to elevated atmospheric CO_2 was shown by the most productive or fastest growing genotype.

2.6 The indirect pathway: The stomatal response of C_3 and C_4 plants

It has been observed that elevated atmospheric CO_2 has significant positive effects on plant water relations in both C_3 and C_4 plants as a consequence of decreased stomatal conductance (g_s) (Ainsworth & Long, 2005; Ainsworth *et al.*, 2003; Ainsworth & Rogers, 2007; Drake *et al.*, 1997; Gunderson *et al.*, 2002; Lee *et al.*, 2001; Medlyn *et al.*, 2001; Wand *et al.*, 1999). Water loss and CO_2 uptake in higher plants is tightly regulated by stomata present on the leaf epidermis (for a detailed review of stomatal pore functioning see Vavasseur & Raghavendra (2005)). Intercellular CO_2 concentration is a key variable sensed by guard cells and used to co-ordinate stomatal opening (Tricker *et al.*, 2005). The stomatal response to changes in atmospheric CO_2 concentration, however, also tightly depends on many other variables such as light intensity, plant water status, temperature and atmospheric vapour pressure deficit. These are all key abiotic factors likely to change as a result of rising atmospheric CO_2 concentrations. Due to the control exerted by stomata over transpirational water loss and net CO_2 assimilation, quantifying stomatal responses to changes in climate and CO_2 concentration are vital in order to determine the effects of climate change on plant productivity and water-use.

Table 2 summarises changes in g_s observed under elevated atmospheric CO_2 for a range of C_3 woody species, and C_3 and C_4 grasses. Interestingly, varieties of poplar growing under SRC management at the popFACE facility in Italy were found to change their stomatal response to elevated atmospheric CO_2 depending on age. Pre-coppice stages of all three genotypes measured (*P. x euramericana*, *P. alba* and *P. nigra*) showed no g_s response with FACE treatment of 550 ppm (Bernacchi *et al.*, 2003). Following coppicing however,

during the growing season, a significant decrease in stomatal response was observed only in *P. nigra*. As the bioenergy plantation matured and approached full canopy closure, g_s measured in *P. x euramericana* alone decreased in response to FACE treatment in combination with soil nitrogen concentration, a -19% decrease at low nitrogen concentration, and -24% decrease at high nitrogen concentration (Tricker *et al*., 2005). This long-term study of different genotypes over different life cycle stages highlights the difficulty of extrapolating and predicting plant responses to elevated atmospheric CO_2, and also raises awareness of the potential impacts of management regime on plant responses to environmental change. There are no FACE experimental results for the tree genus *Salix* or for the C_4 grasses switchgrass and miscanthus. The response of willow, however, is likely to be similar to the SRC poplar, both being managed by the same SRC system and sharing similar characteristics such as fast growth rates, high biomass accumulation and high water-use.

A meta-analysis of species grown in elevated atmospheric CO_2 concentrations that ranged between 475 - 600 ppm at different FACE facilities showed that g_s decreased on average by 20% in elevated atmospheric CO_2, and there was no difference in the response between C_3 and C_4 species (Ainsworth & Long 2005). This result summarising plant functional group responses to elevated atmospheric CO_2 is interesting and suggests that when grown in realistic field conditions, no differences in g_s are apparent between C_3 trees and C_4 grasses in response to atmospheric CO_2. Results in Table 2 would similarly suggest that the stomatal response of C_3 and C_4 species are comparable.

Species	Average change in *gs* with elevated CO_2	Experiment	Length of study	Reference
C_3 woody species:				
Populus x euramericana (clone I-214, poplar)	↓ 19% (low N) ↓ 24% (high N)	FACE	5 years	Tricker *et al.* (2005)
Liquidambar styraciflua L (Sweetgum)	↓ 24% (upper canopy) ↓ 14% (mid canopy)	FACE	3 years	Gunderson *et al*. (2002)
Liquidambar styraciflua L (Sweetgum)	↓ 31% (upper canopy) ↓ 25% (mid canopy)	FACE	4 years	Herrick *et al.* (2004)
Liquidambar styraciflua L (Sweetgum)	↓ 22 / 23%	FACE	1 growing season	Wullschleger *et al.* (2002)
Larrea tridentata (L. divaricata) (creosotebush)	↓ 13%	FACE	3 years	Nowak *et al.* (2001)
C_3 grasses:				
Poaceae (various, meta-anlysis) (grasses)	↓ 24%	FACE, OTC & CE	n/a	Wand *et al.* (1999)
Triticum aestivum (L. cv. 'Yecora Rojo') (spring wheat)	↓ 36%	FACE	1 growing season	Garcia *et al.* (1998)
Achnatherum hymenoides (Roemer & Schultes) (indian ricegrass)	↓ 20%	FACE	3 years	Nowak *et al.* (2001)
C_4 grasses:				
Poaceae (various, meta-anlysis) (grasses)	↓ 29%	FACE, OTC & CE	n/a	Wand *et al.* (1999)
Zea mays (maize)	↓ 34%	FACE	1 growing season	Leakey *et al.* (2006)
Sorghum bicolor (sorghum)	↓ 32% (limited soil water) ↓ 37% (ample soil water)	FACE	1 growing season	Wall *et al.* (2001)
Lolium perenne (L. cv. Bastion) (perennial ryegrass)	↓ 30%	FACE	10 years	Ainsworth *et al.* (2003)
Pleuraphis rigida (Thurber) (big galleta grass)	↓ 35%	FACE	3 years	Nowak *et al.* (2001)

Table 2. Average change (%) in stomatal conductance (g_s) with elevated atmospheric CO_2 for a range of C_3 woody species, C_3 and C_4 grasses. Results were taken from the literature reported as the average of all observations, for more details refer to individual references. ↓ = decreased g_s; N = nitrogen; FACE = free-air CO_2 enrichment; O_3 = ozone OTC = open top chamber; CE = controlled environment.

2.7 The mechanism of reduced stomatal conductance in elevated atmospheric CO_2

Original research suggested the observed decline in g_s was due to a decline in stomatal density or frequency (Woodward, 1987). Stomatal density determines the maximum g_s that a unit area of leaf can attain; therefore an acclamatory response via change in stomatal numbers is often suggested. Historical evidence across geological time from herbarium and fossil records suggested a decrease in stomatal density in trees with increasing atmospheric CO_2 (Van der Burgh *et al.*, 1993; Woodward, 1987), but this can only ever be correlative rather than causative. Beerling *et al*. (1996) analysed stomatal density of leaves grown in ambient and elevated atmospheric CO_2 covering the period AD1800-1994, which represents a change in CO_2 from 283-350ppm. The three species studied, (Beech: *Fagus sylvatica* L.; Birch: *Betula pubescens* Ehrh.; and Oak: *Quercus robur* L.), showed a

decrease in stomatal density, with the steepest decline between 1927 and 1994. Woodward (1987) attributed a 40% decrease in stomatal density in the leaves of herbarium samples of tree species collected over the last 200 years to the increase in atmospheric CO_2. Poole *et al.* (1996), however, carried out an intense survey of stomatal density from leaves of *Alnus glutinosa* from over 70 sites. They found that stomatal density differed, with considerable variation from measurements within the same tree. This decreases the reliability of historical results of those such as Beerling *et al*. (1996) and Woodward (1987). Another limitation of historical studies is also highlighted, since in the majority only stomatal density and not stomatal index was measured. Stomatal density is the number of stomata in a given area of epidermis and can be affected indirectly by the expansion of epidermal cells, which are also known to be sensitive to atmospheric CO_2 (Taylor *et al.*, 2003). Stomatal index, in contrast, is the density of stomata expressed as a percentage of the density of epidermal cells plus stomata (Poole *et al.*, 1996).

Manipulative studies using elevated atmospheric CO_2 also give variable results. Radoglou and Jarvis (1990b) showed that growth of four hybrid poplars at elevated atmospheric CO_2 did not affect stomatal density, index or length of stomatal pore. A meta-analysis of stomatal density responses to elevated CO_2 across FACE studies by Ainsworth and Rogers (2007) found no detectable decrease in stomatal density. Because stomatal density is a feature that is established during the early stages of leaf development, Radoglou and Jarvis (1990b) suggested that elevated CO_2 has no direct effects on the initiation of the number of stomata during ontogenesis, or on epidermal cell expansion at a later stage, instead g_s decreases because of the effect of CO_2 on stomatal opening. In support of this Tricker *et al.* (2005) showed that after five growing seasons the g_s of *P. x euramericana* was still responsive to FACE treatment, whereas the frequency of stomata (density and index), which had decreased during the first two years of exposure to elevated atmospheric CO_2, was not. This suggests that changes in stomatal aperture, rather than stomatal density, determine the long-term response of g_s to elevated atmospheric CO_2.

2.8 Is transpirational water loss of C_3 and C_4 plants reduced in elevated atmospheric CO_2?

A recent study analysing historical records of continental river runoff found that runoff has increased through the twentieth century. Using optimal fingerprinting statistical techniques Gedney *et al.* (2006) attributed this observation to a direct effect of increasing atmospheric CO_2 acting to suppress plant transpiration following CO_2 induced partial stomatal closure. On a smaller scale, studies of tree-canopy water-use of six deciduous tree species showed maximum reductions in tree transpiration under elevated atmospheric CO_2 (540 ppm) of -22% (marginally significant), but this only occurred at low vapour pressure deficit (VPD) (Cech *et al.*, 2003). At the same site Leuzinger and Körner (2007) reported a -14% reduction in tree water-use at an elevated atmospheric CO_2 concentration of 540 ppm over a single growing season. Reductions in tree transpiration for sweetgum (*Liquidambar styraciflua*) exposed to an elevated atmospheric CO_2 concentration of 540 - 560 ppm ranged from -13 to -25% (Schäfer *et al.*, 2002; Wullschleger & Norby, 2001). Elevated atmospheric CO_2 reduced canopy evapotranspiration by -22% for a C_4 dominated tallgrass prairie, but evapotranspiration in response to atmospheric CO_2 concentration was reduced by only -6 to -10% in elevated compared to ambient CO_2 conditions in a calcareous grassland (Owensby *et al.*, 1997; Stocker *et al.*, 1997). Ellsworth *et al.* (1995), however, measured sap flow in a *Pinus taeda* forest ecosystem exposed to FACE treatment (550 ppm) and recorded only a marginal effect of CO_2 on canopy water loss, reducing transpiration by just -6 to -7%. They surmised that there was no evidence to suggest water savings in elevated atmospheric CO_2 under drought and non-drought conditions (Ellsworth *et al*., 1999) with the response being well within measurement error. However, the observations of tree transpiration were only made for eight days. Over such a short time scale it is difficult to fully resolve the complex responses of leaf and canopy water-use and their interactions with other environmental factors. Nevertheless, in irrigated conditions, Tricker *et al.,* (2009) found whole-plant transpiration, as measured by sap flux techniques for *P. x euramericana* grown as SRC in a bioenergy plantation at the popFACE facility in Italy, increased in elevated atmospheric CO_2 (550 ppm). Similarly, a two-year study of sap flux from trees growing in stands of pure aspen (*Populus tremuloides*) and mixed aspen and paper birch (*Betula papyifera* Marsh.) at the AspenFACE facility, USA, found sap flux increased in response to elevated atmospheric CO_2 (+18% at 560 ppm) (Uddling *et al.*, 2008).

The response of canopy transpiration to elevated atmospheric CO_2 is therefore very variable, ranging from reduced transpiration (Cech *et al.*, 2003; Leuzinger & Körner, 2007; Owensby *et al.*, 1997; Schäfer *et al.*, 2002; Wullschleger & Norby, 2001), through no significant response (Cech *et al.*, 2003; Ellsworth, 1999), to a considerable increase in canopy water-use (Tricker *et al.*, 2009; Uddling *et al.*, 2008). Therefore, it is apparent that the almost universal reductions in leaf-level g_s in response to elevated atmospheric CO_2 are of greater magnitude than changes in canopy-level transpiration. Consequently, leaf-level measurements alone are not a reliable indicator of canopy water-use, and scaling results from the leaf-level to infer canopy or ecosystem water-use could lead to large errors. The reduction in canopy transpiration of -13 to -25% for a sweetgum stand exposed to elevated atmospheric CO_2 (Wullschleger & Norby, 2001) was associated with -31% reduction in g_s measured at the leaf-level for top of canopy sun leaves (Herrick *et al.*, 2004). Measurements of g_s from leaves in a 12 year-old sweetgum plantation exposed to an enriched CO_2 atmosphere were up to -44% lower at elevated than ambient CO_2, whereas canopy conductance averaged over the growing season was only -14% lower in the stands exposed to elevated atmospheric CO_2 (Wullschleger *et al.*, 2002b; Wullschleger & Norby, 2001). Both these studies show that unlike leaf g_s, canopy conductance was only marginally affected by CO_2 treatment. Consequently, it is evident that there are canopy-dependent responses to elevated atmospheric CO_2 that mediate the response at the leaf-level. This generates a more conservative effect at the whole-plant level than what is otherwise suggested by leaf-level measurements of g_s alone (Wullschleger & Norby, 2001). Such canopy-dependent factors are outlined below, and are shown in Fig. 1:

i) One documented response of growth in elevated atmospheric CO_2 is an increase in *LAI* for many species (Ferris *et al.*, 2001; Gielen *et al.*, 2001; Gielen & Ceulemans, 2001; Gielen *et al.*, 2003; Liberloo *et al.*, 2006; Taylor *et al.*, 2001a; Uddling *et al.*, 2008). It is therefore possible for transpiration and water-use on a larger scale to increase, offsetting the reductions in water-use due to partial stomatal closure at the leaf-level. Observations of droughted cherry seedlings (*Prunus avium*) showed that whilst whole-plant WUE was increased by +56 to +103% with elevated atmospheric CO_2, there was no difference in plant water-use between CO_2 treatments. Consequently there was no CO_2 induced enhancement of soil moisture content (Centritto *et al.*, 1999a). Tricker *et al.,* (2009) found whole-plant transpiration for a poplar SRC plantation

exposed to FACE treatment increased in elevated atmospheric CO_2; an average increase of +12 and +23% was observed in the first and second measurement campaigns respectively despite a -16 to -39% decline in g_s. In both these studies, leaf area was found to be higher in plants grown in elevated atmospheric CO_2, which was thought to be partly responsible for the observations. Wullschleger *et al*. (2002b) conclude that equivalent rates of water-use for plants exposed to ambient and elevated atmospheric CO_2 suggest that there are trade-offs between increases in leaf area and reductions in g_s, such that in many cases there are few, if any, effects of elevated atmospheric CO_2 on enhancing whole-plant water-use.

ii) As stomata close and cooling via transpiration decreases, leaf and consequently canopy temperature have been found to increase (Wall *et al*., 2001). This may have other micro-climatic effects within the canopy such as decreasing humidity, thus increasing the leaf-to-air vapour pressure gradient. As a result, this may feedback to increase the driving force for transpiration, negating the CO_2 effect and leading to increased water-use at the canopy scale (Wullschleger & Norby, 2001; Wall *et al*., 2001). A number of studies have shown that stomatal responses to elevated atmospheric CO_2 are only significant under high humidity (Cech *et al.*, 2003; Leuzinger & Körner, 2007; Wullschleger *et al.*, 2002b). Cech *et al*. (2003), for example, found that the reduction in mean daily sap flux density of mature deciduous trees exposed to elevated atmospheric CO_2 was almost negligible on days with high evaporative demand. It remains unclear to what extent atmospheric feedback such as this will mitigate canopy-level CO_2 effects on plant water-use (Leuzinger & Körner, 2007).

iii) The degree to which stomata exert control over transpiration is also governed by the aerodynamic conductance of the canopy. This is relevant for determining the response of plants to future global atmospheric CO_2 concentrations as in situations where this exerts stronger control on water vapour loss than stomata, any potential change in g_s induced by elevated atmospheric CO_2 will only marginally affect transpiration and stand water-use (Wullschleger *et al.*, 2002a). Dense, uniform vegetation such as grassland has a low degree of atmospheric coupling whereas a natural forest stand, for example, which is more structurally

diverse and open, allowing for greater air circulation within and above the canopy, is well coupled (Körner *et al.*, 2007). In the latter case it is thought that the canopy will have a low aerodynamic resistance, with stomatal resistance being the dominant force controlling transpiration. In the former example with a high aerodynamic resistance, a number of feedback processes may compensate for reductions in g_s such that transpiration remains unaltered (Schäfer *et al.*, 2002).

iv) Canopy dynamics can alter the magnitude of response to elevated atmospheric CO_2. Stomatal conductance has been found to vary with depth into the canopy. Leaves in the lower canopy are generally older, often possess lower nitrogen concentrations, and are therefore less physiologically active than upper-canopy leaves. Lower-canopy leaves also experience different environmental conditions in terms of radiation and humidity that can decrease maximal stomatal function. Wullschleger *et al*. (2002b), observed that g_s of mid-canopy sweetgum leaves was on average -30 to -40% lower than upper-canopy leaves, and no significant difference was observed for g_s between CO_2 treatment in lower-canopy leaves. Similarly, Gunderson *et al*. (2002) documented variation in g_s with depth into the canopy.

Canopy-dependent effects that interact with elevated atmospheric CO_2 to alter the magnitude of plant responses to an enriched CO_2 atmosphere clearly show the difficulty of predicting whole-plant and ecosystem responses to a changed climate. Bioenergy plantations will be particularly susceptible to canopy-dependent factors because they are densely planted, relatively uniform systems. At full canopy closure both grass and tree plantations will likely display a low degree of atmospheric coupling allowing atmospheric feedback processes to maintain g_s and transpiration at levels unaffected by atmospheric CO_2 concentration. Consequently, canopies are complex structures, and that structure is itself important in determining the CO_2 response.

2.9 Enhanced capability of soil water extraction in elevated atmospheric CO_2?

In water stressed conditions plants increase root biomass and architecture to extract water from the soil more efficiently and from greater depths. There is evidence for stimulated root production in elevated atmospheric CO_2, especially fine roots which are important for water uptake, but whether this is a direct effect of atmospheric CO_2 from increased carbon allocation to the roots, or that of overall enhanced growth rate in elevated atmospheric CO_2 is less clear (Körner *et al.*, 2005; Norby *et al.*, 2004; Norby *et al.*, 1999). Plant biomass (above and below ground) is found to increase under elevated atmospheric CO_2 in many species (Calfapietra *et al.*, 2003b; Ceulemans & Mousseau, 1994; Liberloo *et al.*, 2006; Lukac *et al.*, 2003). The majority of studies suggest there is no change in relative biomass allocation, i.e. the root: shoot ratio, indicating there is no greater proportion of carbon allocated to root production as opposed to above-ground biomass production (Crookshanks *et al.*, 1998; Norby *et al.*, 1995; Tissue *et al.*, 1997). Nevertheless, increased absolute root production in elevated atmospheric CO_2, especially fine-roots, would improve water extraction by plants and allow access to greater water reserves that may be inaccessible to trees grown at ambient CO_2 concentrations.

2.10 Plant responses to drought

Determining plant responses to soil water stress has always been important to our understanding of ecosystem function, and will be more so in a future climate with a predicted increase in the frequency of drought. Due to the shared stomatal pathway through which plant-water relations in response to both elevated atmospheric CO_2 and drought are controlled, it is likely the two will interact, such that the response of one is mediated by the other. The effects of drought can be devastating on plant growth and survival. Photosynthetic CO_2 fixation is suppressed under drought stress by enhanced diffusive resistances within the leaf (closure of stomata and decline of mesophyll and chloroplast conductance) and by drought-induced impairments of metabolic processes (Flexas *et al.*, 2006; Flexas *et al.*, 2004a; Gallé *et al.*, 2007; Lawlor, 2002; Tezara *et al.*, 1999; Yin *et al.*, 2006). The combined effect of these leads to reduced carbon assimilation and ultimately a decline in plant growth (Chaves, 1991; Chaves *et al.*, 2002).

Cell enlargement is particularly sensitive to water deficit. Turgor pressure provides the driving force for cell expansion in growing cells and so with decreasing turgor potentials leaf area expansion is inhibited (Jones, 1992). Stomatal closure together with leaf growth inhibition prevents further water loss, which would result in irreversible cell dehydration and xylem cavitation during drought stress (Chaves *et al.*, 2003). As a consequence of reduced transpirational water loss and reduced leaf area however, the plant capacity to assimilate CO_2 is also reduced.

Productivity of perennial bioenergy crops species, both C_3 *Salicaceae* trees and C_4 grasses, is limited predominantly by water availability (Clifton-Brown & Lewandowski, 2000; Clifton-Brown *et al.*, 2002). Even within species, different genotypes display very different sensitivities to drought, which is important in crop breeding trials (Street *et al.*, 2006). A study of three genotypes of miscanthus, for example, indicated that whilst *M. sinensis* displayed stomatal regulation of water loss by reducing leaf conductance and photosynthesis in order to retain green leaf area, even under severe water shortage, *M. sacchariflorus* and *M. x giganteus* lost leaf area under drought by senescence (Clifton-Brown *et al.*, 2002). Differences in whole-plant WUE were not detected in the three genotypes (Clifton-Brown & Lewandowski, 2000) leading the authors to suggest that the 'best' strategy for drought survival would depend on the timing, frequency and magnitude of the drought; *M. sacchariflorus* and *M. x giganteus* would be better suited when droughts are normally short, however if droughts are prolonged, *M. sinensis* may be better suited being able to maintain leaf area and continue growth after the drought period has passed. Studies of C_3 *Salicaceae* trees indicate poplar is less responsive to water stress and changes in atmospheric vapour pressure than willow (Hinckley *et al.*, 1994; Johnson *et al.*, 2002), however variable responses to drought displayed by many poplar genotypes suggests a large pool of variation from which to select varieties with improved responses (Street *et al.*, 2006). Interestingly, research conducted by Ripley *et al*., (2007) suggests inherent differences between the C_3 and C_4 photosynthetic pathways with respect to the sensitivity of drought-induced metabolic limitations of photosynthetic activity. They suggest the C_4 pathway is more sensitive to metabolic inhibition, and this mechanism may partially explain the paradox of decreasing relative C_4 species abundance along regional gradients of declining rainfall, despite high WUE in C_4 leaves (Ripley *et al.*, 2007).

The mechanism of stomatal closure in response to drought remains unclear. Stomata are observed to close in response to either a decline in leaf turgor and/or water potential, and low humidity (Chaves *et al.*, 2002). Experiments also show that stomatal closure is linked to soil moisture content. Therefore, it has been suggested that the stomatal control of transpiration in response to soil water deficit is mediated by a feed-forward signal from root to shoots, involving the chemical signal abscisic acid (ABA). For detailed reviews of plant responses to drought, readers are referred to Chaves *et al*., (2003) and Wilkinson and Davies (2002).

2.11 The interacting effects of drought and rising CO_2: Does elevated atmospheric CO_2 confer drought tolerance during periods of water stress?

Studies directly investigating the interaction between elevated atmospheric CO_2 and water stress suggest that the indirect effect of an enriched CO_2 atmosphere can improve survival of C_3 and C_4 species during periods of drought because of improved plant-water relations. In a number of studies, reduced g_s and canopy transpiration, even if not of the same magnitude, generated improved plant-water potentials and increased soil water availability (Baker *et al.*, 1997; Conley *et al.*, 2001; Hibbs *et al.*, 1995; Johnson *et al.*, 2002; Leakey *et al.*, 2004; Morse *et al.*, 1993; Ottman *et al.*, 2001; Wall *et al.*, 2001; Wall *et al.*, 2006). Coupled with increased carbon gain, plant WUE was enhanced as a result of elevated atmospheric CO_2, which was seen to be most pronounced under high soil water stress for many C_4 species. Studies of the C_4 grass *Amaranthus retroflexus* by Ward *et al.* (1999), for example, showed that in response to increasing atmospheric CO_2 concentration, g_s and transpiration were significantly reduced. During a period of induced drought, plants grown at elevated atmospheric CO_2 showed lower relative reductions in net photosynthesis by the end of the drought compared to plants grown at lower CO_2 concentrations, indicating atmospheric CO_2 enrichment enhanced drought tolerance in this species (Ward *et al.*, 1999). Reich *et al*. (2001) investigating CO_2 x N (nitrogen) interactions in C_3 and C_4 grassland monocultures, found that overall, the percentage soil water was higher under elevated atmospheric CO_2. Over the growing season, g_s responses to elevated atmospheric CO_2, measured in maize (*Zea mays*) in a field FACE experiment where ample soil moisture conditions prevailed, showed that g_s was on average -34% lower but photosynthesis was not stimulated (Leakey *et al.*, 2006). Nevertheless, this coincided with improved soil moisture availability (up to +31% higher) by midseason. In contrast, at the

same site in 2002 when episodic droughts occurred, photosynthesis was stimulated, on average, by +10% (Leakey *et al.*, 2004), which was probably a result of increased soil water conservation in elevated atmospheric CO_2 plots as found by the later study. In sugarcane plants, *Saccharum officinarum*, subjected to elevated atmospheric CO_2 and an imposed drought, g_s was reduced and A_{net} increased because of increased available soil water. Consequently, the WUE of stressed plants in elevated CO_2 was higher than the WUE of stressed plants grown at ambient CO_2 (Vu & Allen Jr, 2009). Triggs *et al.* (2004) quantified evapotranspiration of sorghum exposed to FACE treatment and different soil moisture regimes over a two-year study period. They found that whilst FACE reduced evapotranspiration from wet plots in both years, drought-stress resulted in reduced evapotranspiration from FACE plots in the first year (-8.5%) and increased evapotranspiration the following year (+10.5%). The authors suggested these plots had enhanced soil water availability for plants to continue transpiring during dry periods because the FACE-grown plants used water more slowly. This was supported by information on the sensible heat fluxes from the plots (Triggs *et al.*, 2004).

Recent literature for C_3 woody species is less abundant. Johnson *et al.* (2002) demonstrated that elevated atmospheric CO_2 mitigated the effects of water stress in willow (*Salix sagitta*), but not in poplar (*Populus trichocarpa x P. deltoides*). Centritto *et al.* (1999a; 1999b) found cherry seedlings (*Prunus avium*) subject to elevated atmospheric CO_2 and drought increased total plant dry mass and displayed reduced transpiration rate per unit leaf area which contributed to enhanced WUE, but found no difference in actual water loss from the soil between CO_2 treatments, indicating no soil water conservation as a result of elevated atmospheric CO_2. Therefore, as is apparent from the results of Centritto *et al.* (1999a; 1999b) and echoed by Wullschelger *et al.* (2002a) and Leuzinger and Körner (2007), studies that report g_s and evapotranspiration responses of plants grown in elevated atmospheric CO_2 can only infer enhanced drought tolerance. Without data on the effect of CO_2 treatment on stand soil water status, or quantitative evaluation of the significance of any soil moisture effect on plant growth and physiology during drought, our understanding of how the indirect CO_2 effect impacts on drought tolerance is little enhanced.

More recent FACE studies have measured soil water content along with canopy transpiration in some mature C_3 woody species. Results of these studies indicate that soil moisture content is enhanced in elevated atmospheric CO_2 primarily because the water

holding capacity of the soil is increased and soil evaporation reduced due to increased leaf-litter build up and fine root production, rather than a direct response to elevated atmospheric CO_2 driven through reduced g_s (Schäfer *et al.*, 2002; Uddling *et al.*, 2008). Additionally, these studies highlight different responses between species, with some saving water under elevated atmospheric CO_2 and others not (Körner *et al.*, 2007). For example, in the study by Schäfer *et al.*(2002) sweetgum trees responded by reducing overall water use by -25% over the 3.5 year study whereas *Pinus taeda*, the dominant tree species, displayed no significant response. In the study by Cech *et al.* (2003), some species e.g. *Carpinus* were highly responsive to elevated atmospheric CO_2, whereas others e.g. *Fagus* did not respond at all. Therefore, the magnitude of the CO_2 effect on stand transpiration will depend on the relative abundance of different species (Cech *et al.*, 2003), which will determine the degree to which a forest could be water-saving, if at all.

Maintenance of higher (less negative) leaf water potentials are an important aspect to drought survival (Wullschleger *et al.*, 2002a). Centritto *et al*. (1999b) suggest that higher plant water potentials in drying soils enable plants to remain turgid and thus able to maintain metabolic processes, consequently increasing their tolerance to drought. Many studies document higher leaf-water and turgor potentials of plants in response to elevated atmospheric CO_2 and under soil water stress. Tognetti *et al*. (2000) investigated field water relations of three Mediterranean shrub species under increasing seasonal drought at a natural CO_2 spring with elevated and ambient atmospheric CO_2 concentrations. They found significant effects on plant leaf-water potentials. At sites with elevated atmospheric CO_2, pre-dawn and midday water potentials were higher (less negative) than those at control sites, with differences most pronounced between June and September when drought conditions were most severe. Deciduous forest trees in central Europe exposed to a seasonal drought had less negative pre-dawn leaf water potentials when exposed to elevated atmospheric CO_2 (Leuzinger *et al.*, 2005). Johnson *et al*. (2002) found that pre-dawn leaf-water potentials of poplar and willow species were higher in elevated than ambient atmospheric CO_2, even as the imposed drought period progressed. At a given water potential, stressed trees in elevated atmospheric CO_2 could maintain a more positive turgor potential than trees in ambient CO_2. During the experiment wilting was observed (turgor potential = zero), but this only occurred in the control plots. Similarly, Hibbs *et al*. (1995), Morse *et al*. (1993) and Roden & Ball (1996), studying red alder seedlings, birch seedlings and eucalyptus species respectively, found that elevated atmospheric CO_2 grown

plants maintained high leaf-water potentials in the presence of soil water stress when compared to ambient CO_2 grown trees. Evidently, down-regulation of photosynthetic capacity as a result of poor leaf-water status during drought is avoided in many species when grown in elevated atmospheric CO_2.

2.12 Conclusions

Responses of C_3 and C_4 plant photosynthesis and g_s to elevated atmospheric CO_2 were investigated in this review and the physiological mechanisms responsible. Plant responses at the leaf-level were compared with observed responses at the larger scale of the canopy, revealing scale-dependent differences in the magnitude and direction of response to elevated atmospheric CO_2. Studies showed that observed decreases in water-use at the leaf- and canopy-level were often not of the same magnitude because of other canopy-dependent factors such as size, structure, dynamics, age-class and leaf area that can modify the CO_2 response. As a result, some studies, including a poplar SRC plantation, showed that water-use increased in elevated atmospheric CO_2. Therefore, plant responses to an enriched CO_2 environment at the canopy-scale are shown to be variable, and not easily predictable from leaf-level responses. The response of plants to the combined environmental stresses of increased atmospheric CO_2 and drought were then investigated. It was shown in many studies that although productivity of C_3 *Salicaceae* trees and C_4 grass bioenergy crop species is seriously compromised by soil water deficit, growth in an enriched atmospheric CO_2 environment can relieve the negative impacts of drought on growth. However big or small the net effect, in general, increased photosynthetic rates and reduced leaf-level water-use generated increases in soil moisture content and/or maintained leaf water- and turgor-potentials such that the onset of drought was delayed in many species. However, recent studies suggest this response of plants to these changes in their environment is more complex and not necesssarily a direct response to elevated atmospheric CO_2. These studies showed that higher soil moisture content under elevated atmospheric CO_2 was due to increased organic matter input to the soil which increased the water-holding capacity of the soil and reduced soil evaporation, allowing plants to use more water.

Evidently, although plant responses to elevated atmospheric CO_2 and drought at the leaf-level are fairly well elucidated, the impacts of this interaction between climate changes at the whole-plant scale are not. This work suggests that more large-scale FACE-type field

experiments are needed to investigate this CO_2 and drought interaction, in addition to other climate changes such as temperature, particularly in stands of large, woody vegetation. It is understood however that this is very difficult, given the cost and space required by such experiments, in addition to the strategic difficulties of imposing a controlled drought in the field.

Due to the difficulties and limitations that arise with multiple-factor field trials, it calls for a shift of focus to the integration of fieldwork and modelling. The development of models that can predict the growth of SRC for bioenergy could be used to predict growth and water-use of these crops at the whole-plant scale in response to changes in climate and atmospheric CO_2 concentration. This would provide a tool to investigate and enhance our understanding of responses of yield and water-use of dedicated bioenergy crops, such as poplar SRC, to future climate change at the landscape-scale. That is exactly what this research aims to do.

Chapter 3

Measurement of photosynthesis and stomatal conductance in poplar SRC: Assessing the impact of water-stress and internal CO_2 conductance on productivity and biochemical photosynthetic parameters

3.1 Introduction

In temperate regions, one of the candidate species for bioenergy includes poplar (*Populus*) species that can be grown as short rotation coppice (SRC). The suitability of poplar varieties for bioenergy is largely due to their fast growth rates and high yields (Bunn *et al.*, 2004; Monclus *et al.*, 2006; Nonhebel, 2002; Scarascia-Mugnozza *et al.*, 1997; Tubby & Armstrong, 2002), although this high productivity is associated with large water requirements (Hall & Allen, 1997; Hall *et al.*, 1996; Hansen, 1988; Hinckley *et al.*, 1994). Studies on both poplar and willow varieties show that they use significantly more water than agricultural crops and most broadleaved tree species, but not conifers (Lindroth & Cienciala, 1996; Lindroth *et al.*, 1994). As a consequence, productivity closely depends on water availability. Additionally, poplar species are notoriously susceptible to drought (Monclus *et al.*, 2006), with many studies showing a significant decline in growth and productivity with reduced water availability (Ibrahim *et al.*, 1997; Johnson *et al.*, 2002; Linderson *et al.*, 2007; Yin *et al.*, 2005; Zhang *et al.*, 2004). Reductions in yield and increased variability in the year-to-year supply of woody biomass as a result of reduced water supply raise significant concerns over the economic viability of poplar SRC as a reliable and sustainable energy source for the future. This is compounded by the increase in the frequency of summer drought predicted for regions of western Europe, such as the UK, with a maritime climate (IPCC, 2007; Jenkins *et al.*, 2009). Thus, within these regions, understanding the physiological and biochemical processes that lead to reduced productivity are an important input to modelling approaches that can investigate future climate change impacts on the yield and water consumption of bioenergy crops.

Land-surface schemes are large-scale models that simulate the exchange of carbon and water between the land and the atmosphere. These provide the tools to determine wide-

scale impacts of bioenergy crop growth under different climatic conditions and with a changing climate as a result of greenhouse gas forcing. Land-surface models that can be used for such applications commonly model carbon exchange using biochemical models of leaf-level photosynthesis based on the equations of Farquhar *et al*., (1980), coupled to a stomatal conductance model to simulate leaf-level fluxes of water. These are then scaled up to simulate carbon and water exchange at the canopy-level. Following the model of Farquhar *et al*., (1980) as modified by Harley and Sharkey (1991) and von Caemmerer (2000), biochemically based photosynthesis models describe photosynthesis as dependening on the rates of three potentially limiting processes; carboxylation capacity (A_c), electron transport (A_j), and triose phosphate export (A_p). The actual rate of photosynthesis (A) is determined by the minimum of these three rates, given by equation 1:

$$A = \min\{A_c, A_j, A_p\} \qquad \text{(equation 1)}$$

Photosynthesis limited by carboxylation capacity is limited by the activity of Rubisco (ribulose bisphosphate carboxylase/oxygenase), which is the enzyme that catalyses the carboxylation reaction, assuming a saturating supply of substrate, RuBP (ribulose-1,5-bisphosphate) (Sharkey *et al.*, 2007). The limitation by Rubisco is associated with low CO_2 concentration. A key photosynthetic kinetic parameter that describes the biochemical capacity for CO_2 assimilation during this stage is V_{max}, the maximum rate of carboxylation at Rubisco. Photosynthesis limited by electron transport is limited by the rate of regeneration of RuBP, the substrate for photosynthesis. The maximum rate of electron transport, J_{max}, is the parameter describing the biochemical photosynthetic capacity at this stage. Triose-phosphate use limitation, or export-limited CO_2 assimilation, occurs when the photosynthetic reactions in the chloroplast have a higher capacity than the capacity of the leaf to use those products, primarily triose-phosphate, in the synthesis of starch and sucrose (Sharkey *et al.*, 2007). The photosynthetic parameter *TPU* describes the biochemical capacity for photosynthetic carbon gain during this stage, although this process is not always included in models of photosynthesis.

V_{max} and J_{max} are two key parameters commonly used to parameterise land-surface scheme photosynthesis sub-models. The apparent quantum efficiency, (α_{app}), describes the efficiency of light utilisation in photosynthesis, and is an additional parameter used in photosynthesis models which commonly requires parameterisation in land-surface models.

Accurate simulation of rates of leaf-level carbon assimilation for specific vegetation types can be achieved through finding suitable values for these parameters. Additionally, as leaf-level rates of photosynthesis are scaled up to predict canopy-level carbon assimilation, these parameters are important for accurate simulation of net ecosystem exchange. Consequently, the parameters V_{max}, J_{max} and α_{app}, are key to land-surface models. Fortunately, these parameters can be derived relatively easily from field measurements by generating CO_2- and light-response curves using gas exchange equipment.

Accurate determination of these photosynthetic parameters is important, however recent research suggests that internal CO_2 conductance can significantly impact parameter estimates. During photosynthesis, CO_2 diffuses from the atmosphere (c_a) into the sub-stomatal cavities inside the leaf through stomatal openings on the leaf surface (c_i). From there CO_2 moves to the site of carboxylation inside the chloroplast stroma (c_c) through the leaf mesophyll (Flexas *et al.*, 2008). This passage of CO_2 inside the leaf to the actual site of carboxylation is internal CO_2 conductance (g_i). Until recently it was thought that any limitation on the transfer of CO_2 along this third pathway, i.e. c_i to c_c, was negligible and thus c_i was equal to c_c, giving rise to the assumption that there is infinite conductance to CO_2 within the leaf (Wullschleger, 1993; Epron *et al.*, 1995). Based on this assumption, most biochemical models of C_3 leaf photosynthesis do not include this transfer. Recent research, however, has shown that g_i is actually finite and can be sufficiently small as to impose significant limitation on photosynthesis (Flexas *et al.*, 2004a; Flexas *et al.*, 2008; Long & Bernacchi, 2003; Von Caemmerer, 2000), consequently introducing another diffusive limitation to A_{net} in addition to stomatal conductance (g_s). Further, it has been shown that like g_s, g_i responds to changing environmental conditions in the long- and short-term. In response to drought, for example, g_i has been shown to decrease significantly (Flexas *et al.*, 2002). It is now understood that analysing A_{net} at c_i can lead to significant underestimation of V_{max}. Comparison of A_{net} - c_c responses of stressed and non-stressed plants has shown that differences in photosynthetic capacity that were observed in A_{net} - c_i responses often disappear (Flexas *et al.*, 2006). Therefore it is suggested that under stressed conditions, g_s and g_i are co-regulated and that the sum of both (stomatal and mesophyll), and not metabolic impairment, largely sets the limit for photosynthesis (Centritto *et al.*, 2003; Flexas *et al.*, 2004a). Therefore, estimates of the key photosynthetic parameters, such as V_{max} and J_{max}, may be erroneous when determined at c_i.

This work investigated the response of photosynthesis, stomatal conductance and productivity in two genotypes of poplar SRC (*Populus nigra* and *P. x euramericana*) to drought. This information will be used in the following chapters to aid with calibration and validation of the land-surface scheme JULES. Throughout the growing season, CO_2- and light-response curves were measured to determine values for the key photosynthetic parameters required by the photosynthesis – stomatal conductance model used in JULES. This provided an opportunity to determine the impact of g_i on estimates of V_{max} and J_{max} in healthy and water-stressed *P. nigra* and *P. x euramericana* SRC, something that has not previously been done for these two genotypes. These values for the photosynthetic parameters estimated with and without g_i will be used in the following chapter to investigate the accuracy of simulated photosynthesis with and without the transfer of CO_2 from c_i to c_c included in the model. Therefore, the present study investigated these two candidate poplar genotypes for bioenergy with the following objectives: 1) what are the genotype dependent differences between the two varieties of poplar in terms of photosynthetic capacity, stomatal conductance and carbon allocation, and how do these respond to water-stress? 2) what are values for the key biochemical photosynthetic parameters for both genotypes of poplar, and how does internal conductance to CO_2 impact on estimates of these parameters?

3.2 Materials and Methods

3.2.1 Plant material and experimental setup

Cuttings of *Populus nigra* L. (genotype Jean Pourtet) and *P. x euramericana* (*P. deltoides* Bart. ex Marsh. x *P. nigra* L., genotype I-214) were grown under glasshouse conditions for three months with controlled temperature and light levels to induce bud-burst and growth. In April 2008, the cuttings were potted into 10 litre pots (300 mm diam. x 250 mm depth) using a soil-based, lime-free compost (John Innes No. 3) and transferred outside. One hundred trees (25 per genotype per treatment) were arranged in a split-plot design (Wytham, Oxfordshire, UK; 51º44’99”N, 1º18’97”W). Trees of both genotypes were randomly distributed between four blocks. Two blocks were subject to periods when water was withheld to impose a drought treatment. The remaining two blocks were watered continuously over the course of the experiment. Trees were allocated so there was roughly an equal number of each genotype in each block. A_{net} and g_s were measured over the course

of the experiment under ambient atmospheric conditions. Recordings were made from at least four, and up to ten trees per genotype, per block, per treatment at each measurement period (before, during and after each drought period). Trees were chosen at random, and measurements were made on the first fully expanded, sun-exposed leaf (i.e. one leaf per tree). Three recordings on the same leaf were made, and the average of these was used in analyses. Measurement of the response curves used three trees per genotype, per treatment, and the same trees were used over the course of the experiment. Trees had been selected at random from the blocks and curves were measured on the first fully expanded leaf of each tree. Leaf area and final stem biomass were measured destructively at the end of the experiment on fifteen trees per genotype, per treatment, these samples were randomly selected.

Before the onset of experiments all trees were fully watered. Pots were spaced at 300 mm intervals to avoid shading and allow access to the trees. Watering treatments began when leaves were completely developed and matured. Control trees were continuously watered so their soil moisture content remained near to field capacity (around 30 % volume). Stressed trees endured two periods of imposed soil water stress where they were not watered and pots were shielded from rainfall by the use of a polythene cone fitted around the base of the stem and the lip of the pot so the canopy remained exposed to the atmosphere. The protective covers could be raised and lowered as necessary to allow circulation of air beneath during dry periods, any effect of the use of these covers on soil temperature was deemed minimal when compared to the effect of reduced moisture content on soil temperature. In total, water was withheld for 25 days (2 to 26 June) during the first drought cycle; trees were then fully re-watered for eight weeks until the onset of the second drought cycle, which lasted 40 days (20 August to 28 September). In both drought cycles, plants were kept without water until net photosynthesis was almost completely inhibited during the late morning.

Fig.1. Experimental setup of poplar cuttings (*P. x euramericana* and *P. nigra*) at Wytham field station. The box in the middle contains the data logger for the soil moisture probes.

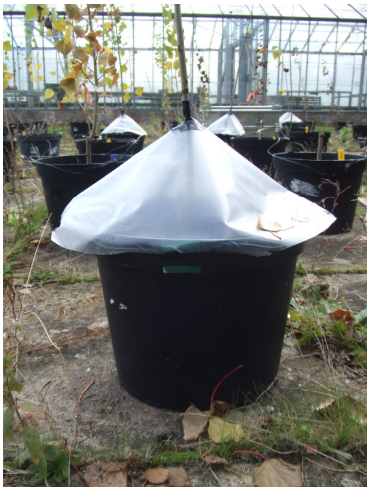

Fig. 2. Rain covers used to shield drought treatment pots from rainfall.

3.2.2 Soil moisture

Soil moisture was monitored continuously over the course of the experiment using SM200 soil moisture sensors (Delta-T Devices Ltd, Cambridge, UK). Soil moisture was recorded as % volumetric water content (% vol.). The sensors are accurate to ± 3% vol. within the range of 0 to 50% vol. Twelve sensors in total were used, allowing soil moisture of three trees per treatment per genotype to be logged continuously. Point measurements using a hand-held SM200 soil moisture sensor were also made to check the soil moisture content of pots without sensors.

3.2.3 Leaf-gas exchange measurements

Leaf-level gas exchange measurements to determine the rates of A_{net} and g_s and intercellular CO_2 concentration (c_i) were made using a portable infrared gas exchange analyser (IRGA) system (CIRAS-2, PP-systems, Hitchin, UK). For all measurements, the leaf area used was 250 mm^2 and as both *P. x euramericana* and *P. nigra* are amphistomatous, the stomatal ratio was maintained at 30% for the upper- and 70% for the lower-leaf surface. This ratio had been determined from previous measurements of the contribution of stomata on the abaxial and adaxial leaf surfaces to the rate of g_s in both genotypes (Ingmar Tulva *pers. comm.*, 2007).

3.2.4 Leaf-gas exchange under ambient atmospheric conditions

Leaf-level A_{net} and g_s over the course of the experiment were measured *in situ* under ambient atmospheric conditions using the IRGA system. Measurements were made on the first fully expanded, sun-exposed leaf of eight to ten different trees per treatment (one leaf per plant) during the hours 09:00-12:00 GMT. Net CO_2 assimilation rate (A_{net}), calculated stomatal conductance for water vapour (g_s) and calculated intercellular CO_2 concentration (c_i) were measured on successive days over the course of the growing season. Measurements were restricted to days with clear skies; temperature and relative humidity inside the leaf chamber were always close to ambient values. The CO_2 concentration inside the leaf chamber was maintained at 380 ± 5ppm using a CO_2 cartridge plugged into the CIRAS-2.

3.2.5 Response curves

3.2.5.1 CO_2 response curve

The response of A_{net} to increasing concentrations of c_i was measured *in situ* using the IRGA system before (predrought), during (drought) and after (recovery) both drought cycles. Three A_{net} - c_i curves per genotype per treatment were measured on the first fully expanded leaf of each tree. Measurements were made between the hours of 09:00 and 14:00. Leaf temperatures were set at 25 ºC for all measurements, leaves were illuminated using a red-blue LED light source attached to the gas exchange system and photosynthetic

photon flux density (PPFD) was maintained at 1500 μmol m^{-2} s^{-1}. Leaf vapour pressure deficits were maintained close to ambient. Following IRGA guidelines and protocols suggested by Long and Bernacchi (2003) and Bernacchi *et al*., (2003), leaves were incubated at a CO_2 concentration of 200 ppm for 20-30 minutes prior to measurement to maximise stomatal opening. Measurement of A_{net} in response to changing levels of c_i were made according to Bernacchi *et al.* (2003) starting at 400 ppm CO_2 , decreasing in steps of 50 ppm to 50 ppm, returning to 400 ppm, and increasing stepwise to 1800 ppm CO_2.

The A_{net} - c_i curves were fitted using the approach of Sharkey *et al*., (2007) who provide an online analytical tool to aid with curve fitting, found at http://www.blackwellpublishing.com/plantsci/pcecalculation/. This model has been developed to provide optimised estimates of the maximum carboxylation velocity (V_{max}; μmol CO_2 m^{-2} s^{-1}), the maximum rate of electron transport (J_{max}; μmol electrons m^{-2} s^{-1}), *TPU* (μmol m^{-2} s^{-1}) and g_i (μmol m^{-2} s^{-1} Pa^{-1}) at c_c, i,e. accounting for internal conductance to CO_2. This method uses the biochemically based model for photosynthesis of Farquhar *et al*., (1980) with modifications for g_i, which uses c_c instead of c_i where $c_c = c_i - A/g_i$. This model was then adapted to calculate V_{max}, J_{max}, *TPU* and R_d at c_i, where $c_c = c_i$, assuming infinite internal conductance to CO_2. For more information on this method see Sharkey *et al*., (2007) and Pons *et al*., (2009).

3.2.5.2 Light response curve

Leaves were sampled as described for A_{net} - c_i measurements above. Leaves were placed in the leaf chamber and illuminated until steady-state rates of A_{net} and g_s had been achieved. Leaf temperatures were set at 25 ºC for all measurements and CO_2 concentration was maintained at 380 ppm. A_{net} - P_{PFD} response curves were then measured starting at saturating light (2000 μmol m^{-2} s^{-1}) and decreasing stepwise to darkness.

The response of A_{net} to increasing light intensity was analysed using the software 'Photosynthesis Assistant' (Parsons & Ogston, 1998) to aid with curve fitting, which uses the equation given by Prioul & Chartier (1977) below (equation 2). The software solves the equation by iteration to give parameter values associated with the smallest error. In this study the parameter of interest was the apparent quantum efficiency (α_{app}; mol CO_2 m^{-2} s^{-1}):

$$A_{net} = \frac{\alpha_{pp} P_{PFD} + (A_{\max} - R_d) - \sqrt{\{(\alpha_{app} P_{PFD} + (A_{\max} - R_d))^2 - 4\Theta\alpha_{pp} P_{PFD}(A_{\max} - R_d)\}}}{2.\Theta} - R_d$$

(equation 2)

where, P_{PFD} (µmol m^{-2} s^{-1}) is the light intensity, A_{max} (µmol CO_2 m^{-2} s^{-1}) is the maximum assimilation rate, R_d (µmol CO_2 m^{-2} s^{-1}) is the dark respiration rate, and Θ (dimensionless) is the curvature factor.

3.2.6 Chlorophyll fluorescence

Chlorophyll *a* fluorescence was recorded using a portable pulse amplitude modulated fluorometer, the PAM-2000 (Heinz Walz GmbH, Effeltrich, Germany). The maximum potential quantum efficiency of PSII (F_v/F_m) was determined and calculated according to Maxwell & Johnson (2000). Leaves were dark-adapted for 30 minutes prior to measurement, they were then exposed to a modulated light of < 0.1 µmol m^{-2} s^{-1} to determine the minimal fluorescence level (F_o), a saturating pulse of light was then applied for 0.8 s to induce maximal fluorescence (F_m). On each day of measurement, F_v/F_m was measured on at least three trees per treatment, per genotype.

3.2.7 Growth measurements

Leaf area was measured destructively using an LI-3100 Area Meter (LI-COR, Nebraska, USA) at the end of the experimental period. Leaf area of both the whole plant and the first fully expanded leaf was assessed on fifteen plants per genotype per treatment.

Stem height and diameter were recorded over the course of the experimental period on all trees. Stem height was measured from the point where the stem sprouted out of the original cutting to the top. Stem diameter was measured 50 mm above the point where the stem sprouted from the original cutting.

Final stem biomass was determined at the end of the experimental period on fifteen trees per genotype per treatment. The stems were cut at the point they had sprouted from the

original cutting, all leaves were removed and the stems were dried at 65 °C for 72 hours and weighed to obtain their dry weight.

3.2.8 Statistical analysis

Because the experimental design was a split-plot and repeated measures were made over time, data were analysed using a linear mixed effects model, using the package *lme4* (Bates & Maechler, 2009) available in the statistical software *R2.10.1* (R2.10.1, 2009). The analysis tested main effects and interactions, with the random blocks nested within treatment levels, and day of year. An example model is shown below, specific models used and all outputs of analyses can be seen in appendix 6 Table 6-1 and Table 6-2.

V_{max}~per+gen+treat+gi+gi:treat+gen:gi+gen:treat+per:gen+(1|treat/block)+(1|DOY)

where V_{max} is the response variable, per (experimental period), gen (genotype), treat (treatment) and gi (internal CO_2 transfer) are fixed effects (":" is the notation for an interaction), and (1|treat/block) (1|DOY) are crossed random effects to handle the experimental pseudoreplication ("/" is the notation for nesting). Significance of fixed effects were tested for using likelihood ratio tests (*LRT*) that use the chi-squared (x^2) distribution and maximum likelihood estimators (*MLE*) (Faraway, 2006). Following the approach of Faraway (2006), parametric bootstrap methods were used to provide a more robust estimate of the significance of the observed test statistic.

Different models were used where necessary to describe the data, for example a non-linear regression was used to fit sigmoid curves using a four parameter logistic function (equation 3) to describe the relationship between soil moisture content and g_s and A_{net}. This type of relationship is often used to describe biological relationships. The four parameter sigmoid curve was chosen as it provided the lowest residual standard error (RSE) for both data sets (RSE=62.3 on 1,29 d.f (g_s); RSE=2.8 on 68 d.f (A_{net})) as opposed to other possible models.

$$y = a + \frac{b-a}{1+e^{c(d-x)}} \qquad \text{(equation 3)}$$

3.3 Results

3.3.1 Climatic conditions and water status

Over the experimental period of 2008 daily maximum air temperatures ranged between 26.7 ^{o}C and 12.8 ^{o}C. Daily minimum temperatures ranged between 7.2 ^{o}C and 17.0 ^{o}C. Average daily temperature recorded during the first drought period (2 - 26 June) was 14.2 ± 0.39 ^{o}C, and 14.1 ± 0.30 ^{o}C during the second drought period (20 August – 28 September). Whilst the average daily temperatures did not vary greatly between drought treatments, it is evident from Fig. 3a that the highest daily maximum temperatures were only achieved during the first drought period. Daily maximum solar radiation ranged between 149 - 919 W m^{-2}. The maximum daily solar radiation recorded during the first drought period ranged between 166.4 - 919.0 W m^{-2}, during the second drought period this range was 188.9 – 718.6 W m^{-2}. The highest levels of recorded daily maximum solar radiation were therefore only achieved during the first drought period and a notable decline in maximum daily solar radiation was recorded during the second drought treatment. Over the first drought period trees were therefore subject to higher light intensities and higher maximum air temperatures. Water was withheld and significant soil moisture stress was imposed on trees during both drought periods (Fig. 3b). The lowest soil moisture content was recorded close to 2 % vol. in the first drought period and 5 % vol. in the second drought period. In both instances, depletion of soil moisture reserves in stressed trees was fairly rapid with the onset of drought treatment. Upon recovery from soil moisture stressed conditions, stressed trees were fully re-watered so their soil moisture content was similar to that of control trees. Over the course of the experiment, the soil moisture content of control trees was maintained close to field capacity, which was within the range of 28.0 – 35.0 % vol.

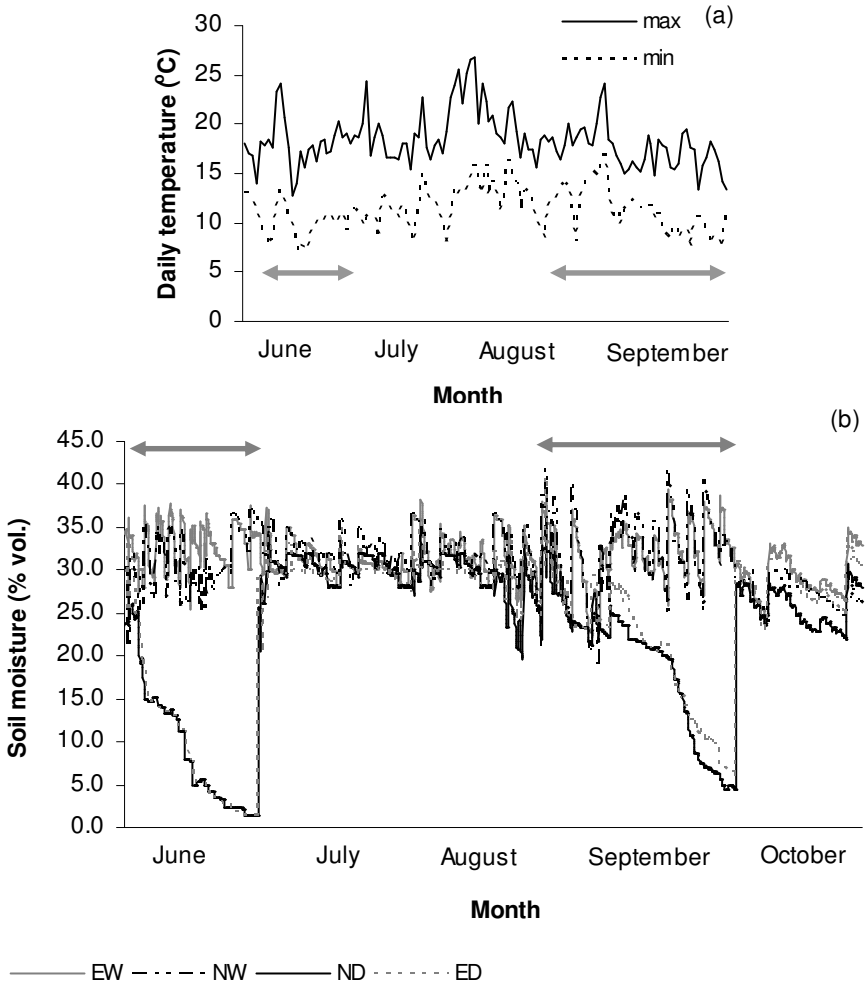

Fig. 3. Climatic variables recorded over the growing season of 2008 (2 June – 1 October). a) Daily records of maximum (solid line) and minimum (dotted line) air temperatures (°C); b) Soil moisture content (% volume) recorded hourly over the course of the experiment, where NW = control *P. nigra*; EW = control *P. x euramericana*; ED = stressed *P. x euramericana*; ND = stressed *P. nigra*. Grey arrows indicate the periods of imposed drought.

3.3.2 The response of A_{net} and g_s to soil moisture and VPD

In response to declining soil water concentration both g_s and A_{net} declined markedly, with no difference apparent between the two genotypes. Both responses were best described by a sigmoid function whereby after a threshold level of soil moisture (11 –18%), g_s and A_{net} declined rapidly (Fig. 4a & b). Non-linear regression was used to fit a four parameter logistic function (equation 3) which produced a sigmoid curve that best described the response of A_{net} and g_s to soil moisture stress ($A_{net} = 15.3/(1+e^{(0.6\,(7.9-SM))})$ and g_s =

$349.2/(1+e^{(0.6\,(10.4-SM))})$). This shape of logistic curve is used to describe many biological processes, and was appropriate here to describe the threshold response of g_s and A_{net} to soil moisture stress. Almost complete inhibition of g_s and A_{net} was reached at a soil moisture content of < 5% (g_s < 100 mmol m^{-2} s^{-1}; A_{net} < 2 µmol m^{-2} s^{-1}). Above the threshold soil moisture content, g_s ranged between 200 to 600 mmol m^{-2} s^{-1} and A_{net} ranged between 6 to 23 µmol m^{-2} s^{-1}, this suggests that soil moisture is not limiting and both g_s and A_{net} can occur at their maximum potential capacity if all other environmental conditions were optimal. Values of g_s and A_{net} in leaves of control plants averaged over the experimental period were 355 ± 11 mmol m^{-2} s^{-1} and 15 ± 0.4 µmol m^{-2} s^{-1} respectively, in stressed trees this declined to 58 ± 9 mmol m^{-2} s^{-1} and 4 ± 0.7 µmol m^{-2} s^{-1} respectively.

Analysis of the relationship between A_{net} and VPD, and g_s and VPD was carried out where A_{net} was ≥ 2.5 µmol m^{-2} s^{-1} and where g_s ≥ 50.0 mmol m^{-2} s^{-1} (Fig. 4c & d). Using a subset of the data in this way included points where A_{net} and g_s were low but not completely inhibited by lack of available soil moisture, in other words within this range stomata were still responsive to other environmental conditions. With increasing atmospheric evaporative demand, both A_{net} and g_s showed a negative correlation ($A_{net} = 19.7 + -0.5VPD$, $x^2=32.6$, $p < 0.001$, $n = 89$; $g_s = 408.5 + -7.8VPD$; $x^2=44.1$ $p < 0.001$, $n = 77$; Fig. 4c & d), with both genotypes responding in a similar manner.

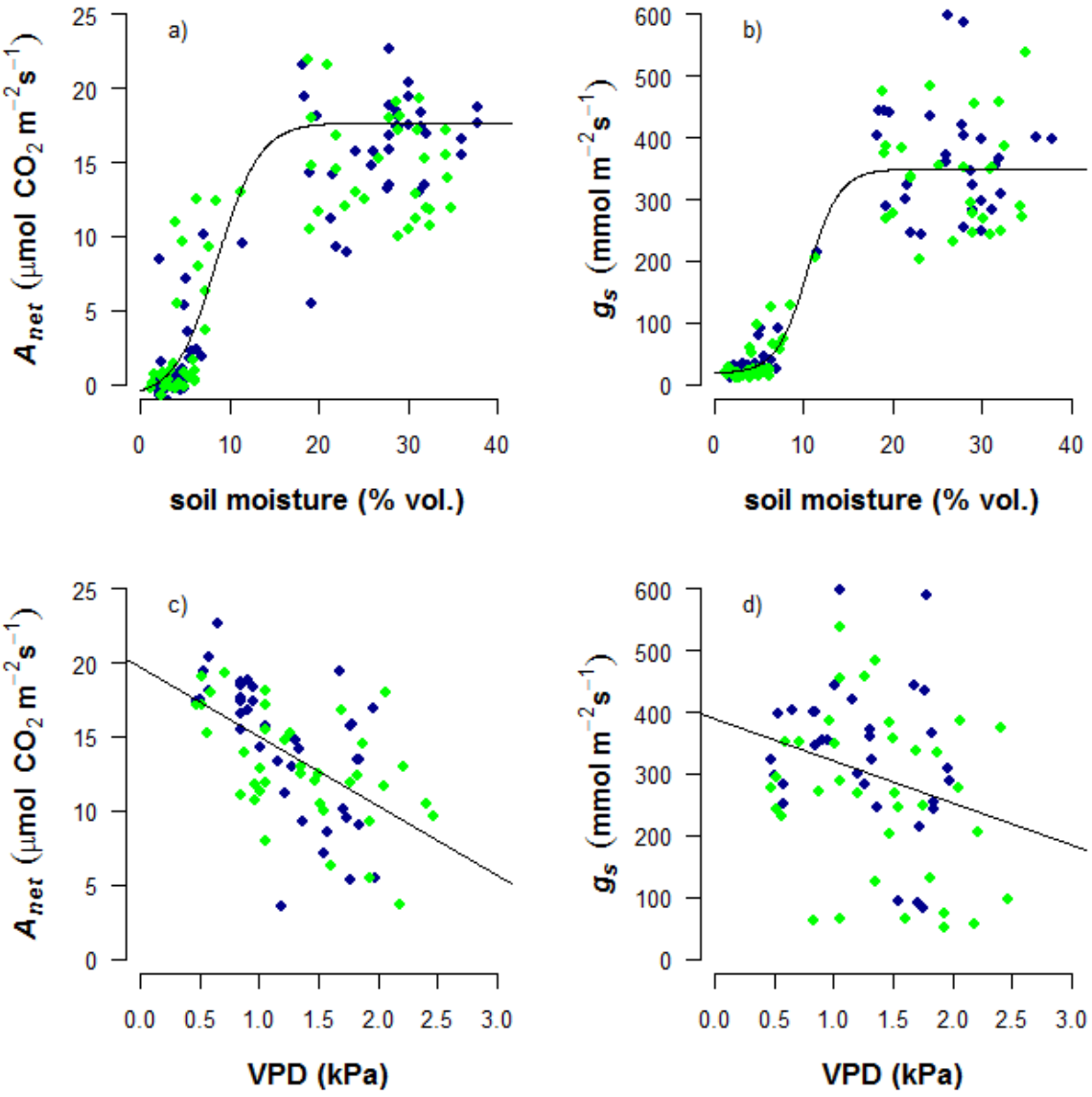

Fig. 4. a) Net photosynthesis (A_{net}) and **b)** stomatal conductance (g_s) in response to soil moisture concentration (% volume), **c)** A_{net}, and **d)** g_s in response to atmospheric vapour pressure deficit (VPD, kPa). All were measured over the course of the growing season from 2nd June to 1st October. *P. x euramericana* = blue, *P. nigra* = green.

Measured under ambient environmental conditions over the growing season, a positive relationship was found between A_{net} and g_s ($p < 0.01$, $F=1269$ *on* $1,125$ *d.f;* $r^2=0.91$) with no difference found between the two genotypes. Such a strong correlation suggests co-regulation of A_{net} and g_s, especially under stressed conditions.

3.3.3 Photosynthetic parameters

An effect of g_i on the estimate of V_{max} was detected in both genotypes ($x^2=40.05$, $p < 0.01$, $n = 120$). In well watered and drought treated trees, estimates of V_{max} made assuming finite g_i resulted in detectably higher values of V_{max}, this can clearly be seen in Fig 5a & b. The mean of V_{max} estimated for stressed trees of both genotypes was 18.25 ± 8.1 µmol CO_2 m^{-2} s^{-1} assuming finite g_i, and 12.64 ± 4.5 µmol CO_2 m^{-2} s^{-1} assuming infinite g_i during the first drought period, and 45.58 ± 5.7 µmol CO_2 m^{-2} s^{-1} assuming finite g_i, and 32.29 ± 4.0 µmol CO_2 m^{-2} s^{-1} assuming infinite g_i for the second drought period. The data clearly shows that accounting for g_i has an impact on the estimate of V_{max}, leading to higher values.

Drought led to a substantial decrease in estimated V_{max} compared to well-watered trees ($x^2=11.78$, $p < 0.01$, $n = 120$; Fig 5a & b). Estimated V_{max} differed between *P. x euramericana* and *P. nigra*, but this was also dependent on experimental period ($x^2=19.64$, $p < 0.01$, $n = 120$). Fig 5a & b shows that early season, (predrought.1), values of V_{max} were significantly higher in *P.x euramericana* trees than *P. nigra* trees, particularly for the data that accounts for g_i. The reduction in V_{max} as a result of drought was noticeably less during the second drought period compared to the first, and was also not as extreme in *P. nigra* as *P. x euramericana* during the first drought period. As trees of both genotype were re-watered following the first drought period, it was evident that V_{max} estimated in recovering trees was significantly higher than the control trees, whose soil moisture content had remained near to field capacity over the course of the experimental period. This effect was greatest in *P. nigra* (Fig 5a & b). V_{max} measured over the rest of the growing season was comparable between the genotypes, especially in control trees.

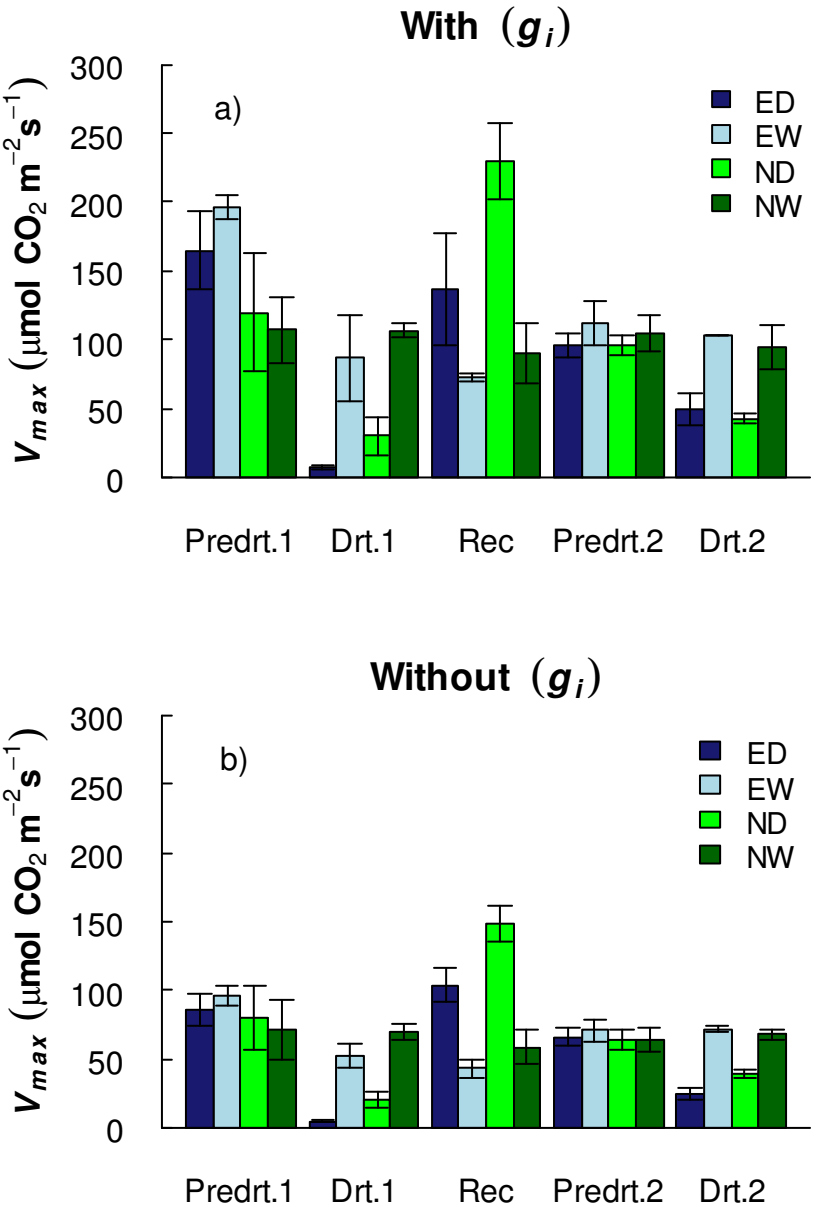

Fig. 5 Values of **a)** the maximum carboxylation velocity (V_{max}) estimated assuming finite g_i, and **b)** V_{max} estimated assuming infinite g_i. For each measurement period, the mean is shown ± s.e. EW and NW are control *P. x euramericana* and *P. nigra* respectively; ED and ND are stressed *P. x euramericana* and *P. nigra* respectively. The legend on the x axis refers to the measurement period, Predrt.1 = before the first drought treatment, Drt.1 = during the first drought treatment, Rec = recovery/ re-watering, Predrt.2 = before the second drought treatment, Drt.2 = during the second drought treatment.

There was no detectable effect of g_i on the estimate of J_{max} in both genotypes. As seen in Fig. 6a & b, estimates of J_{max} both with and without g_i were similar. In both genotypes, J_{max} declined with drought ($x^2=14.15$, $p < 0.05$, $n = 120$). Differences in estimated J_{max} between the two genotypes were detected, but was dependent the measurement period ($x^2=23.33$, $p < 0.05$, $n = 120$). Early in the growing season (Predrt.1), values of J_{max} determined for both

genotypes were higher than at most other points in the season (Fig. 6a & b), with the exception of J_{max} measured in recovering drought treated trees. J_{max} measured in *P. x euramericana* trees at this early stage in the growing season was higher than *P. nigra*. The reduction in J_{max} with drought was noticeably less in both genotypes during the second drought period, and was also not as severe in *P. nigra* during the first drought period as *P. x euramericana*. As stressed trees were re-watered following the first drought, values of J_{max} in these trees were significantly higher compared to control trees, with the effect greatest in *P. nigra*.

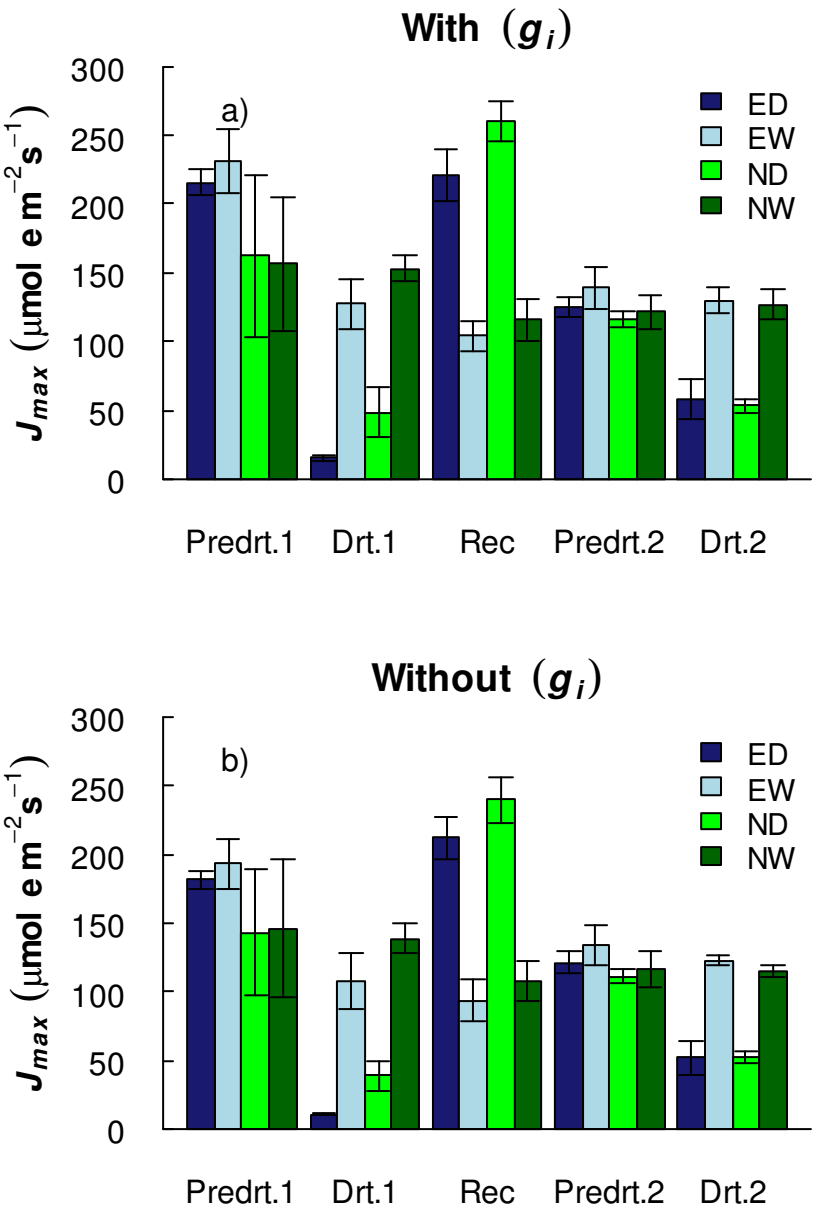

Fig. 6. Values of **a)** the maximum rate of electron transport (J_{max}) estimated assuming finite g_i, and **b)** J_{max} estimated assuming infinite g_i. For each measurement period, the mean is shown ± s.e. EW and NW are control *P. x euramericana* and *P. nigra* respectively; ED and ND are stressed *P. x euramericana* and *P. nigra* respectively. The legend on the x axis refers to the measurement period, Predrt.1 = before the first drought treatment, Drt.1 = during the first drought treatment, Rec = recovery/ re-watering, Predrt.2 = before the second drought treatment, Drt.2 = during the second drought treatment.

Internal conductance to CO_2 (g_i) declined with water-stress ($x^2=18.43$, $p < 0.05$, $n = 60$; Fig. 7). Down-regulation was greater for *P. x euramericana* during the first drought period than *P. nigra*, and vice -versa during the second drought period. Detectable differences between genotypes of estimated values of g_i were found only at certain times through the growing season ($x^2=12.95$, $p < 0.05$, $n = 60$). The most noticeable differences were the

low mean value of g_i determined for control *P. x euramericana* trees during the recovery period, and the high mean g_i estimated for control *P. nigra* trees during the second drought (Fig. 7). In control trees, values of g_i over the remaining growing season were comparable between genotypes.

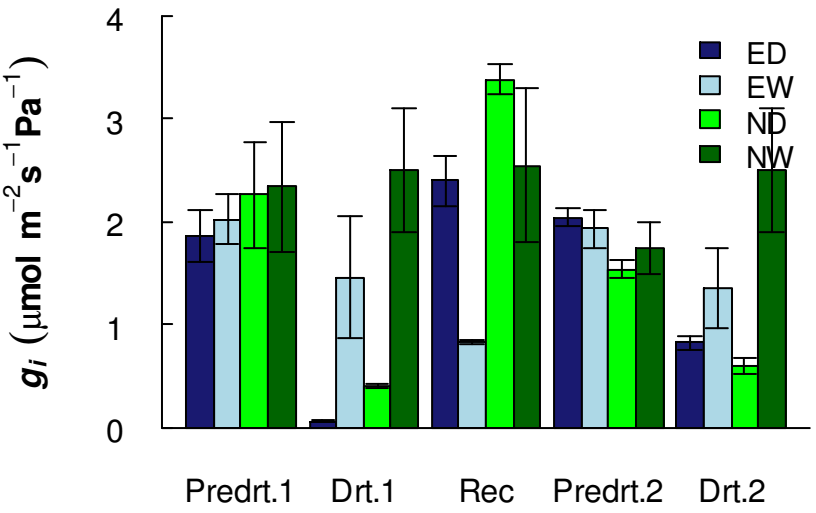

Fig. 7. Values of the internal conductance to CO_2 (g_i) determined for each genotype over the growing season. For each measurement period, the mean is shown ± the s.e. EW and NW are control *P. x euramericana* and *P. nigra* respectively; ED and ND are stressed *P. x euramericana* and *P. nigra* respectively. The legend on the x axis refers to the measurement period, Predrt.1 = before the first drought treatment, Drt.1 = during the first drought treatment, Rec = recovery/ re-watering, Predrt.2 = before the second drought treatment, Drt.2 = during the second drought treatment.

The apparent quantum efficiency (α_{app}) did not differ between genotypes and varied little over the course of the growing season, ranging between 0.03 to 0.05 mol CO_2 mol^{-1} PAR (Fig. 8). During the first drought period, α_{app} declined in stressed trees as a result of water stress, ranging between 0.012 to 0.011 mol CO_2 mol^{-1} PAR depending on genotype ($x^2=10.1$, $p < 0.05$, $n = 60$). During the second drought period however, α_{app} was not affected by water-stress. Values ranged between 0.034 to 0.039 mol CO_2 mol^{-1} PAR during this second drought period, and were well within values measured in control trees over the rest of the growing season.

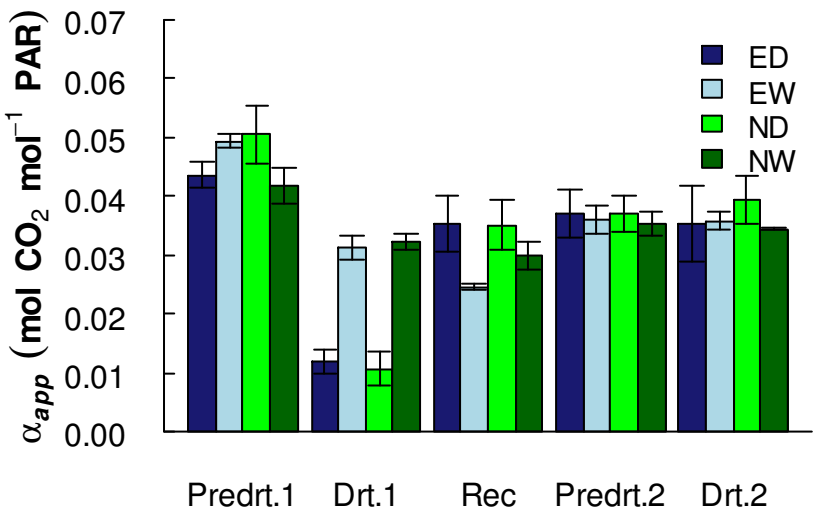

Fig. 8. Values of the apparent quantum efficiency (α_{app}) determined for each genotype over the growing season. For each measurement period, the mean is shown ± the s.e. EW and NW are control *P. x euramericana* and *P. nigra* respectively; ED and ND are stressed *P. x euramericana* and *P. nigra* respectively. The legend on the x axis refers to the measurement period, Predrt.1 = before the first drought treatment, Drt.1 = during the first drought treatment, Rec = recovery/ re-watering, Predrt.2 = before the second drought treatment, Drt.2 = during the second drought treatment.

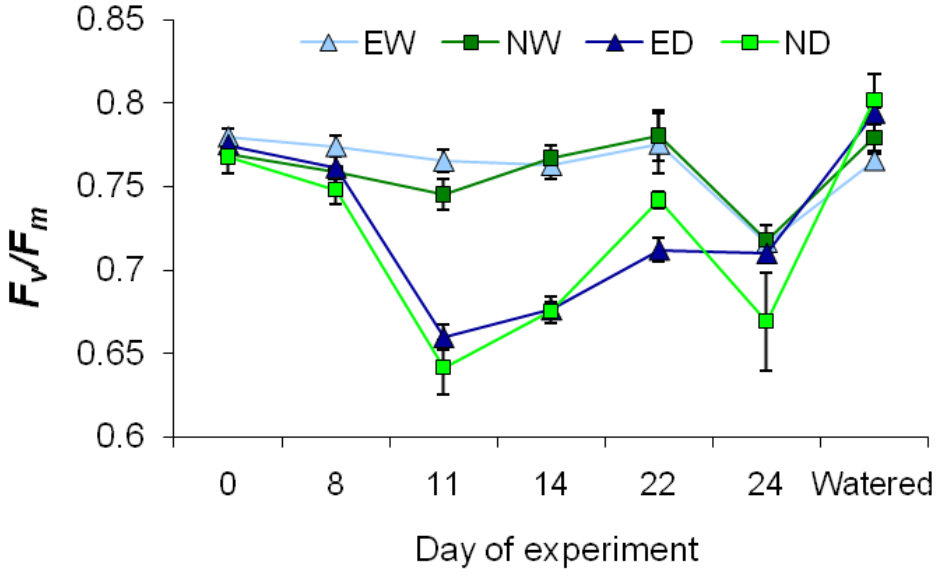

Fig. 9. Maximum potential quantum efficiency of PSII (F_v/F_m) measured by chlorophyll fluorescence over the course of the first drought period and during re-watering of stressed trees. EW and NW, control *P. x euramericana* and *P. nigra* respectively; ED and ND, stressed *P. x euramericana* and *P. nigra* respectively.

Measurement of the maximum potential quantum efficiency of PSII (F_v/F_m) over the first experimental drought period and upon re-watering showed a substantial decline in F_v/F_m from day eleven of the imposed drought (Fig. 9). As water-stress was relieved by re-watering, the efficiency of PSII was fully restored (Fig. 9).

3.3.4 Growth of *P. nigra* and *P. x euramericana*

Water deficit had a significant impact on growth and biomass accumulation in both genotypes. After two successive drought periods in one growing season, growth of stressed trees was substantially impaired, as shown by the lower final dry stem biomass ($x^2=5.08$, $p < 0.05$, $n = 58$), reduced stem height ($x^2=9.47$, $p < 0.05$, $n = 58$) and diameter ($x^2=4.72$, $p < 0.05$, $n = 58$), and lower total leaf area ($x^2=12.43$, $p < 0.05$, $n = 31$) (Fig. 10a - d). The impact of water deficit on growth did not differ between genotypes. The final dry stem weight achieved by *P. x euramericana* (22.85 ± 2.5g) was not significantly different to that achieved by *P. nigra* (22.31 ± 1.4g). There were no detectable differences between the two genotypes regarding final total leaf area, final stem diameter or final stem height. Nevertheless, growth in water stressed conditions led to a 30.9 % reduction in above-ground harvestable dry biomass in *P. x euramericana* and a 48.7 % reduction in *P. nigra*.

Interestingly, the control trees revealed genotype differences in growth strategies and biomass accumulation. The data suggested that partitioning of assimilated carbon is dominantly to the stem or 'woody parts' in *P. nigra* as seen from the higher dry stem biomass (43.52 ± 2.9g as opposed to 33.07 ± 2.5g in *P. x euramericana*; $x^2=5.08$, $p < 0.05$, $n = 58$) and stem diameter ($x^2=4.72$, $p < 0.05$, $n = 58$). *P. x euramericana* on the other hand appears to partition carbon dominantly to leaves, as seen from the higher leaf area it produces (1657.7 ± 55.2 cm^2, as opposed to 1353.7 ± 70.9 cm^2 in *P. nigra*; $x^2=12.43$, $p < 0.05$, $n = 31$). These contrasting patterns of carbon allocation generate a 31.6 % increase in above-ground harvestable dry biomass in well-watered *P. nigra* trees compared to *P. x euramericana*.

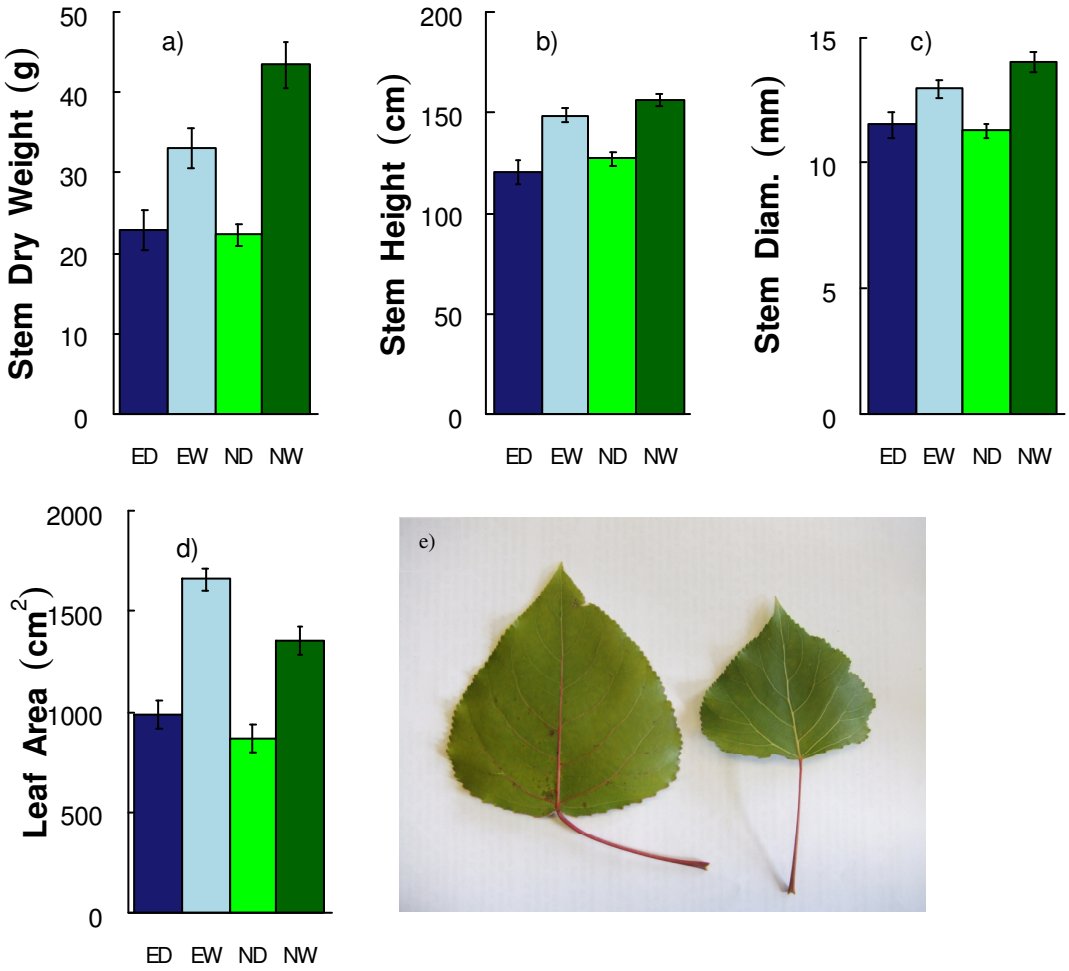

Fig. 10. a) Final dry stem weight, **b)** stem height, **c)** stem diameter and **d)** total leaf area of control and drought treated poplars as measured at the end of the experiment. EW, control *P. x euramericana*; NW, control *P. nigra*; ED, stressed *P. x euramericana*; ND, stressed *P. nigra*. The picture, **e)**, shows examples of the difference in size of top of canopy leaves from healthy *P. x euramericana* (left) and *P. nigra* (right).

3.4 Discussion

3.4.1 Response of A_{net} and g_s to environmental variables

In response to increasing soil water deficit and increased atmospheric evaporative demand, net CO_2 assimilation and g_s in leaves of potted poplars decreased. As soil moisture content declined, trees of both genotypes responded in parallel showing a 'threshold' response, whereby below an apparent critical threshold of soil water deficit (11-18 % vol.), stressed plants closed stomata. In response to increasing atmospheric VPD, A_{net} and g_s of *P. x euramericana* and *P. nigra* displayed a strong negative correlation. Reduced stomatal

conductance is one of the earliest responses to drought stress (Jones, 1992). Stomatal closure protects against further water loss, loss of turgor and irreversible cell dehydration under progressing drought (Gallé *et al.*, 2007). Closure of stomata in response to increasing evaporative demand is a well documented response (Lange, 1971). By avoiding high transpiration rates that would otherwise be caused by increasing gradients of water vapour between leaf and air, stomatal closure avoids the corresponding decline in plant water potential that can lead to cell dehydration and physiological damage (Oren *et al.*, 1999; Saliendra *et al.*, 1995). Indeed, both *P. x euramericana* and *P. nigra* displayed a strong relationship between A_{net} and g_s, which is indicative of the regulative function of the stomata which minimise excessive water loss that could be physiologically damaging, at the expense of photosynthetic carbon gain.

The sensitivities of both poplar genotypes to these two environmental stresses were very similar. The threshold response of the poplars to soil moisture content showed they have a limited sensitivity to this environmental stress in particular. A threshold response is commonly used to describe the response of plant transpiration to available soil moisture content in other studies (Sinclair, 2005). However, in this study, the critical threshold of soil moisture content was low before leaves responded by closing stomata. This is possibly indicative of the inherent growth strategy of poplars in the natural environment as pioneer species.

3.4.2 The response of key photosynthetic parameters to internal CO_2 conductance and drought stress

Estimates of V_{max} made under the assumption of infinite g_i were found to be lower in well-watered and drought treated trees of both genotypes. This work shows that in these fast growing poplar genotypes, the assumption that internal CO_2 transfer is infinitely large as to have a negligible impact on the drawdown of CO_2 from c_i to c_c is invalid. Under well-watered conditions, values of V_{max} calculated from A_{net} - c_c curves were, on average, 64 % and 52 % higher than values calculated from A_{net} - c_i curves in *P. x euramericana* and *P. nigra* SRC trees respectively. The differences between c_i and c_c based estimates of V_{max} in these poplar genotypes are large. There are no comparable studies of poplars in the literature, but Niinemets *et al*., (2009) reported V_{max} calculated on a c_c basis was 25 % higher than on a c_i basis in young fully mature leaves of field-grown olive trees. Bown *et*

al., (2009) found mean values of V_{max} calculated on a c_c basis were 15.4 % higher in pot grown *Pinus radiata* trees. Both these studies show smaller differences than in this study. Manter and Kerrigan (2004), however, reported differences in c_i versus c_c based estimates of V_{max} for 19 woody tree species that were very wide ranging, from -1.6% (*Quercus garryana*) to +92.1% (*Abies concolor*). The results from this study fall within the mid range of these values. Therefore, this work highlights the impact g_i has on estimates of this important photosynthetic parameter, V_{max}, measured in these two genotypes of poplar SRC. This parameter is regarded as a good indicator of photosynthetic capacity and is generally considered a directly transferable parameter to calibrate models of ecosystem carbon exchange. Measured at c_i however, evidently V_{max} is no longer the pure biochemical parameter on which models of photosynthesis, such as Farquhar *et al*., (1980) are founded, since it contains information about the internal conductance of CO_2.

Internal conductance to CO_2 has been found to vary greatly among and within species (Ethier & Livingston, 2004; Flexas *et al.*, 2008; Niinemets *et al.*, 2009; Warren, 2008). In this study, g_i was only found to be marginally different between genotypes at certain points in the growing season. Besides this, g_i remained fairly constant throughout the growing season in control trees, ranging between 0.83 - 2.55 µmol m^{-2} s^{-1} Pa^{-1}. Flexas *et al*., (2008) report a range of g_i from literature measured in *Populus* species of between 0.4 to 5.0 µmol m^{-2} s^{-1} Pa^{-1}, whilst this range is very large, it at least confirms that g_i measured in well watered trees of both genotypes in this study falls well within this. The drought induced decline in g_i was significant, indicating a substantial contribution of this diffusive limitation to photosynthetic carbon gain during the two periods of water-stress. During drought, g_i declined to range between 0.06 - 0.4 µmol m^{-2} s^{-1} Pa^{-1} and 0.82 - 0.6 µmol m^{-2} s^{-1} Pa^{-1} in the first and second drought period respectively depending on genotype. The potential importance of g_i in models of photosynthesis having only recently received attention, values of g_i reported in the literature are relatively few and for a limited number of species and genotypes. Therefore, these measurements contribute to expanding this knowledge base. Additionally, although values of g_i reported in this study are relatively high for these two well-watered genotypes of poplar SRC, there is noticeable variation in the measurements. Consequently, at times it is possible g_i may be limiting to photosynthesis even under well-watered conditions. This identifies a potential target for breeding programmes to improve yields and WUE.

Differences between the estimates of V_{max} and J_{max} and genotype were only apparent at certain times during the growing season. Both V_{max} and J_{max} were lower in *P. nigra* at the start of the growing season. After this, values of V_{max} were comparable between genotypes and measurement period for control trees as estimated both with and without g_i. V_{max} and J_{max} measured in this study were somewhat lower than the range of values measured for irrigated SRC *P. x euramericana* and *P. nigra* growing in a bioenergy plantation free-air CO_2 enrichment (FACE) experiment in Italy at ambient CO_2 concentration (Bernacchi *et al.*, 2003; Hovenden, 2003; Liberloo *et al.*, 2006a). However, this is probably because of the higher growth temperatures the poplars in Italy were acclimated to, and temperature is known to affect the kinetic properties of Rubisco and increase V_{max} (Hikosaka *et al.*, 2006).

During the recovery period following the first imposed drought, V_{max} and J_{max} were 'up-regulated' to values well above those measured in control trees. Seven weeks later, photosynthetic capacity of the drought treated trees had declined again to match that of control trees. This highlights the 'plasticity' of these photosynthetic kinetic parameters that can be modified by the plant to adapt to changing environmental conditions. With drought, the reduction in photosynthetic capacity (V_{max} and J_{max}) is necessary to allow photosynthesis to continue operating near the break-point between the RuBP- and CO_2-limited reactions (Lambers *et al.*, 2008). Therefore, drought-acclimated plants can maximise the effectiveness of both light and dark reactions of photosynthesis under dry conditions. Upon re-watering, it is possible V_{max} and J_{max} increased so the poplar trees could capitalise on optimal environmental conditions. α_{app} was less variable over the growing season and is evidently an inherent property of the leaf that is fairly well conserved unless exposed to extreme environmental conditions, as was seen during the first drought period that caused a significant decline in α_{app}.

In response to drought, V_{max}, J_{max} and g_i in both genotypes declined. Analysis of the key biochemical photosynthetic parameters both with and without g_i showed a similar response to water-stress. Whilst it is well known that one of the first responses to drought is closure of stomata (Chaves *et al.*, 2002), there is still much debate over prevailing factors that limit photosynthesis as water stress progresses (metabolic or diffusive) (Flexas *et al.*, 2002; Lawlor & Cornic, 2002; Tezara *et al.*, 1999). Nevertheless, V_{max} is the photosynthetic parameter most sensitive to g_i ,and in this study, the differences observed in carboxylation capacity between stressed and non-stressed trees determined at c_i did not disappear when

determined at c_c, as has been found in previous studies (Flexas *et al.*, 2006). This suggests that the decline in V_{max} with water stress was significant and not an artefact of the method used to estimate the parameter. Therefore, it is likely that concurrent with significant diffusive limitations, (stomatal and mesophyll), during the first drought period trees also experienced some degree of metabolic limitation to photosynthetic carbon gain. Flexas *et al*., (2004a) compiled data from various studies looking at photosynthetic metabolism impairment under drought and salinity stress and concluded that below a g_s threshold of about 0.1 mol H_2O m^{-2} s^{-1}, metabolic components of photosynthesis became increasingly impaired. These included initial Rubisco activity, nitrate reductase activity, RuBP content, ATP content, total soluble protein content and PSII activity (F_v/F_m). In this study, g_s was at or below this threshold during the imposed periods of water stress, in line with the suggestion of Flexas *et al*., (2004b; 2004a) that metabolic impairment of A_{net} may be significant. Indeed, in this study, α_{app} and the activity of PSII were reduced during the first drought period. This was probably due to the higher temperatures and irradiance experienced by the poplars during this time, which likely required the activation of photo-protective mechanisms to prevent photo-inhibition and irreversible damage to the photosynthetic machinery occurring during this drought period. Indeed, after four days of re-watering following the imposed drought, photosynthetic capacity was shown to be fully restored in stressed trees. Consequently, as a result of the down-regulation of α_{app} and F_v/F_m, full functionality of the photosynthetic machinery was preserved. Gallé and Feller (2007) saw a similar response with regards to down-regulation of F_v/F_m during periods of water stress in beech trees. This resulted in increased thermal dissipation of excess excitation energy in the PSII antennae to protect the photochemistry apparatus against the deleterious effects of high light, in addition to the increased activation of xanthophyll cycle pigments. It is likely that similar mechanisms were invoked in the poplar leaves in this study to prevent severe photo-inhibition.

3.4.3 Productivity of *P. x euramericana* and *P.nigra*

Aboveground, 'woody' biomass accumulation was reduced by the occurrence of drought stress in both *P. x euramericana* and *P. nigra*. Reduced growth is a common response to limited water availability and is observed in many other studies using different poplar varieties (Ibrahim *et al.*, 1997; Yin *et al.*, 2005; Zhang *et al.*, 2004). A decrease in both stem height and stem diameter were equally responsible for the decreased plant dry weight

in both poplar genotypes, causing an overall 30.9 % and 48.7 % decrease in above-ground harvestable woody biomass in *P. x euramericana* and *P. nigra* respectively. Total tree leaf area was also reduced in stressed plants as a result of decreased total leaf number rather than decreased individual leaf area (results not shown).

In control plants, *P. nigra* achieved a higher harvestable plant dry biomass at the end of the experiment compared to *P. x euramericana* (+ 31.6 %). This is in agreement with other studies that found *P. nigra* grown as SRC to be more productive than *P. x euramericana* in both ambient and elevated atmospheric CO_2 concentrations, generating greater above- and below-ground biomass (Calfapietra *et al.*, 2003b; Calfapietra *et al.*, 2001; Liberloo *et al.*, 2006). Higher biomass achieved in *P. nigra* was as a result of thicker stems. *P. x euramericana* in contrast had higher total leaf area. These results suggest *P. nigra* allocates assimilated carbon primarily to structural, woody biomass, whereas *P. x euramericana* allocates carbon dominantly to leaves. It is known that differences in growth patterns can result in response to environmental conditions, but also as a result of genotypic differences in carbon partitioning (Pregitzer *et al.*, 1990), as appears to be the case with these two poplar genotypes. As regards species grown for bioenergy, because maximising yield gain per hectare of crop grown is central to the success of the bioenergy industry, maximum allocation of carbon to aboveground structural carbon pools (e.g. cellulose, hemi-cellulose and lignin) is desirable in order to increase yield (Luo *et al.*, 2006). Therefore, based purely on harvestable yield with growth under optimal soil water conditions, our study would suggest *P. nigra* is a more suitable bioenergy crop species. However, this study would also suggest that the impact of drought on productivity would be greatest in *P. nigra*.

3.4.3 Limitations

Analysis of data obtained as a result of gas exchange relies on the assumption of reliable determination of c_i measurements, which consequently affects computation of key photosynthetic parameters, such as V_{max} and J_{max}. Stomatal patchiness (heterogenous stomatal closure) and cuticular conductance (i.e. when stomata close there is a larger conductance to water vapour than CO_2 across the cuticle leading to overestimations of the water-based calculations of c_i), introduce two potential errors in the estimation of c_i (Boyer *et al.*, 1997; Buckley *et al.*, 1997; Flexas *et al.*, 2004a; Grassi & Magnani, 2005; Sanchez-

Rodriguez *et al.*, 1999). They pose a particular problem under water limited conditions, which may lead to an overestimate of c_i under drought and consequent erroneous determination of the kinetics of photosynthesis under stressed conditions. Lawlor and Cornic (2002) however conclude that 'patchiness is probably much less important than once thought'.

Secondly, in this work, the curve-fitting method is used to determine estimates of g_i (Ethier & Livingston, 2004; Sharkey *et al.*, 2007). Limitations of this method may lead to errors in the determination of g_i. Firstly, the method necessitates that the data points be allocated, before analysis, to the two limiting portions (Rubisco activity, and regeneration of RuBP) of the A_{net} - c_i curve. Manter and Kerrigan (2004), for example, show that estimates of V_{max} from A_{net} - c_i curves may be erroneous when preliminary estimates of where the Rubisco- and electron-transport portions of the curve intersect are set either too high or too low. Secondly, this method requires values for additional parameters (i.e. K_c and K_o) which are Rubsico kinetic constants, measured at c_c. There are few estimates of these values made in a limited number of species. Therefore the values of K_c and K_o used may result in unknown errors in the estimates of g_i, and also in V_{max} and J_{max}. Thirdly, the generation of $A_{net} - c_i$ curves involves rapid changes in CO_2 concentration around leaves, and g_i has been shown to respond quite strongly to changes in CO_2 concentration (During, 2003; Flexas *et al.*, 2007). Consequently, this method gives an estimate of the 'average' g_i over a given CO_2 range (Flexas *et al.*, 2008), which may reduced the accuracy of the estimate. Nevertheless, in comparison with other methods, the curve-fitting method has be found to provide comparable estimates of g_i (Pons *et al.*, 2009), suggesting similar results would have been achieved had g_i been estimated by alternative methods.

3.5 Conclusions

Estimates of V_{max}, J_{max}, α_{app} and g_i displayed limited variation between genotypes and over the course of the growing season. Estimates of V_{max} based on the assumption of infinite internal conductance to CO_2 were lower than those determined assuming finite g_i. With severe drought, V_{max}, J_{max}, g_i, α_{pp} and F_v/F_m declined in both genotypes. V_{max} is the photosynthetic parameter most sensitive to g_i, however the decline in carboxylation capacity inferred from measurements assuming infinite g_i remained present when the same data were analysed assuming finite g_i. Therefore, the reduced carboxylation capacity was

significant and not an artefact of the method used to estimate V_{max}. This suggests that with severe water stress and high temperatures and light intensities, as were experienced during the first drought period, metabolic impairment of photosynthesis occurred in addition to diffusive (stomata and mesophyll) limitations and down-regulation of photochemistry. This down-regulation of photosynthetic capacity was reversible, and four days after re-watering full functionality of PSII was restored and V_{max}, J_{max} and g_i were up-regulated in trees that had been water-stressed.

As a result of diffusive and metabolic limitations to photosynthetic carbon gain, water stress significantly impeded growth of *P. x euramericana* and *P. nigra*. Stem height, diameter and total leaf area were reduced under drought. In contrast, well-watered *P. nigra* trees achieved a higher harvestable biomass at the end of the growing season compared to *P. x euramericana*, despite *P. x euramericana* having a greater total leaf area.

This work has characterised the response of two candidate species of poplar for bioenergy to water-stress. It provides information on the physiological responses of both *P. x euramericana* and *P. nigra* to water-stress and key photosynthetic parameters, including the impact of internal CO_2 conductance on parameter estimation. This information will be used in the next chapter to inform, calibrate and validate the leaf-level photosynthesis – stomatal conductance model used in the land-surface scheme JULES. It is anticipated that this will improve the accuracy of simulated leaf-level photosynthesis and stomatal conductance for poplar SRC, and when scaled-up in JULES, it will increase the accuracy of predicted plant yield and water-use. This is important for the final objective of this thesis which is to predict the yield and water-use of poplar SRC under the current and future climate scenarios.

Chapter 4

Modelling photosynthesis and stomatal conductance in poplar SRC: Assessing the impact of internal CO_2 conductance on the accuracy of simulations at the leaf-level

4.1 Introduction

From the gains and losses of carbon through photosynthesis and respiration, and the passage of water through plant stomata, vegetation plays a major role in both the global carbon and water cycles. For land-surface schemes to correctly simulate carbon and water budgets, they must accurately represent the processes of carbon and water exchange from vegetated surfaces. The works of Hughes *et al*. (2010) and Vanloocke *et al*. (2010) both use land-surface schemes to determine the carbon- and water-balances respectively of extensive plantings of *Miscanthus x giganteus*, a C_4 perennial grass bioenergy crop. Used in this application, it is imperative that such models are parameterised appropriately and that model simplifications used to describe key processes are adequate. Land-surface schemes commonly model carbon exchange of vegetation using biochemical models of leaf-level photosynthesis based on the equations of Farquhar *et al*., (1980), coupled to a stomatal conductance model to simulate leaf-level fluxes of water. These are then scaled up to simulate carbon and water exchanges at the canopy-level. Therefore, correct parameterisation of these models at the leaf-level is central to correct predictions of vegetation water-use and productivity at the larger-scale.

Using values for the photosynthetic parameters determined in the previous chapter, the main objective of this chapter was to test and validate, against leaf-level measurements of photosynthesis and stomatal conductance (also measured in the previous chapter), a coupled model for leaf-level net photosynthesis (A_{net}) and stomatal conductance (g_s) used in a land-surface scheme JULES, (hereafter referred to as the JULES A_{net} - g_s model). The JULES A_{net} - g_s model uses the biochemical model for leaf-level photosynthesis of Collatz *et al*., (1991; 1992), and uses the stomatal closure described by Jacobs (1994). Similar to the JULES model, other land-surface schemes include photosynthesis sub-models that

incorporate the equations of Collatz *et al*., (1991; 1992) or Farquhar *et al*., (1980), e.g. ORCHIDEE, IBIS, LPJ.

Until recently, photosynthesis in plants was considered to be limited dominantly by two factors; g_s, which regulates the CO_2 supply into the leaf, and leaf biochemistry, which is the basic photochemistry, carboxylation and Calvin cycle reactions that regulate the CO_2 demand (Flexas *et al.*, 2008). Consequently, models of photosynthesis, such as Farquhar *et al*., (1980) and Collatz *et al*., (1991; 1992), were founded on the assumption that differences in the CO_2 concentration in the sub-stomatal cavities and at the site of carboxylation in the chloroplast stroma inside mesophyll cells was negligible. In other words, c_i (the intercellular CO_2 concentration) was equal to c_c (the chloroplastic CO_2 concentration). Recent research, however, identified the important role of internal CO_2 conductance (g_i) in regulating photosynthesis, i.e. the transfer of CO_2 across mesophyll cells from c_i to c_c. There is increasing evidence suggesting that g_i is actually finite and can itself respond to changing environmental conditions, such that it can impose a significant limitation on photosynthesis (Centritto *et al.*, 2003; During, 2003; Flexas *et al.*, 2007; Flexas *et al.*, 2002; Grassi & Magnani, 2005; Warren *et al.*, 2004). Current research suggests that g_i is of similar quantitative importance to stomata and Rubisco in terms of limiting/regulating photosynthesis (Ethier & Livingston, 2004; Flexas *et al.*, 2008; Warren, 2008). Indeed, work in Chapter 3 showed that estimates of V_{max} were significantly higher when assuming finite g_i. Therefore, it is suggested that it may be necessary to re-formulate photosynthesis models to include this process in order to improve predictions of leaf-level carbon assimilation (Ethier & Livingston, 2004; Flexas *et al.*, 2008; Niinemets *et al.*, 2009).

The JULES A_{net} - g_s model does not currently include the transfer of c_i to c_c. Therefore, this work addressed the following: 1) does the inclusion of g_i in the JULES A_{net} - g_s sub-model improve the accuracy of simulated photosynthesis? 2) is the accuracy of simulated photosynthesis and stomatal conductance improved by using calibrated parameters as opposed to default values? These questions were addressed specifically for two genotypes of poplar, *Populus. x euramericana* and *P. nigra*.

4.2 Materials and Methods

4.2.1 Overview

This work used A_{net} - c_i and A_{net} - P_{PFD} response curve data, described in Chapter 3, from *Populus. x euramericana* and *P. nigra* trees to calibrate the JULES A_{net} - g_s sub-model for these two poplar genotypes. The JULES A_{net} - g_s model was used in the following configurations; 1) the original configuration 2) modified to include the transfer of c_i to c_c and 3) modified to use the photosynthesis model of Farquhar *et al*., (1980) and include internal CO_2 conductance. The accuracy of simulated A_{net} and g_s was compared in these three different model configurations. Model testing, parameterisation and evaluation occurred in three steps:

i) The performance of each model configuration was tested after being parameterised with individual values for the photosynthetic parameters (V_{max}, α, g_i and where applicable J_{max}) taken from separate A_{net} - c_i and A_{net} - P_{PFD} response curves. The accuracy of simulated A_{net} in response to increasing concentrations of atmospheric CO_2 was compared with the observed A_{net} - c_i response curve data.

ii) When used in the land-surface scheme, the JULES A_{net} - g_s sub-model requires a single value for each of the photosynthetic parameters. The aim of this study was equally to calibrate the JULES A_{net} - g_s sub-model for these two genotypes of poplar for use in the land-surface scheme. Therefore, the average value of each photosynthetic parameter derived from the A_{net} - c_i and A_{net} - P_{PFD} response curves, measured in well-watered trees in Chapter 3, was used to calibrate the model, and model performance was assessed again.

iii) Using the single calibration performed in step ii, the model configurations were validated against an independent data set of leaf-level A_{net} and g_s measured across the growing season under ambient atmospheric conditions, in healthy and water-stressed top of canopy leaves of *P. x euramericana* and *P. nigra*. These data are described in Chapter 3.

4.2.2 Model

4.2.2.1 The coupled model for leaf-level photosynthesis and stomatal conductance

The JULES A_{net} - g_s model used in this work is taken from the land-surface scheme JULES (Joint UK Land Environment Simulator). This sub-model calculates the leaf-level exchanges of carbon and water. These are described as depending on a number of

environmental variables and as well as the internal CO_2 concentration (c_i), with an additional direct dependence on soil moisture status. This sub-model is based on the photosynthesis model of Collatz *et al.*, (1991) for C_3 plants and Collatz *et al.*, (1992) for C_4 plants, and uses the stomatal closure described by Jacobs (1994). Elements of the model important to this work are outlined below, but more detail can be found in Cox *et al.*, (1998) and Cox (2001).

The leaf-level stomatal conductance, g_s (m s^{-1}) and net leaf photosynthesis, A_{net} (µmol CO_2 m^{-2} s^{-1}) are related in the following equations:

$$g_s = 1.6RT_l \frac{A_{net}}{c_a - c_i} \qquad \text{(equation 1)}$$

$$A_{net} = \beta(W - R_d) \qquad \text{(equation 2)}$$

where R is the universal gas constant (J K^{-1} mol^{-1}), T_l is the leaf surface temperature (K), c_a and c_i (both Pa) are the leaf surface and internal CO_2 partial pressures respectively, and the factor 1.6 accounts for g_s being the conductance for water vapour rather than CO_2. β is the soil moisture stress factor, W is the potential (non-moisture stressed) leaf-level gross photosynthesis (µmol CO_2 m^{-2} s^{-1}) and R_d is the dark respiration rate (µmol CO_2 m^{-2} s^{-1}). W and R_d are calculated using the physiologically-based photosynthesis model of Collatz *et al.,* (1991) described in the section below. Leaf-level gross photosynthesis (W) is determined as a function of environmental conditions and leaf parameters:

$$W = W\left(\vec{X}, c_i\right) \qquad \text{(equation 3)}$$

where $\vec{X}$ is general vector of environmental variables including light, humidity, temperature and atmospheric pressure.

Both g_s and W depend on unknown c_i, which is calculated according to the closure defined by Jacobs (1994).

$$\left\{\frac{c_i - \Gamma}{c_a - \Gamma}\right\} = F_0\left\{1 - \frac{D_Q}{D_c}\right\} \qquad \text{(equation 4)}$$

where Γ (Pa) is the CO_2 photorespiration compensation point (the internal partial pressure of CO_2 at which photosynthesis just balances photorespiration), D_Q is the humidity deficit

at the leaf surface (kg kg^{-1}), and F_0 (unit-less) and D_c (kg kg^{-1}) are vegetation specific parameters (see Cox, 2001). F_0 is the c_i/c_a for specific humidity deficit in canopy, and D_c is the critical humidity deficit. Equation 4 is consistent with the observations of Morison and Gifford (1983) which suggests that c_i/c_a decreases approximately linearly with humidity deficit, and only weakly depends on other environmental variables (Cox *et al.*, 1998). The soil moisture stress factor, β is given by:

$$\beta = \begin{cases} 1 & \text{for } \theta > \theta_c \\ \dfrac{\theta - \theta_w}{\theta_c - \theta_w} & \text{for } \theta_w < \theta \le \theta_c \\ 0 & \text{for } \theta \le \theta_w \end{cases} \qquad \text{(equation 5)}$$

where θ is the volumetric soil moisture concentration within the root zone (m^3 m^{-3}), θ_c is the volumetric soil moisture concentration at the 'critical point', above which plants are not water limited, and θ_w is the volumetric soil moisture concentration at the 'wilting point', below which transpiration ceases (Cox, 2001).

4.2.2.2 The physiologically based photosynthesis model

The leaf photosynthesis model is based on the work of Collatz *et al.,* (1991; 1992). Presented here are the key equations used to calculate non-moisture stressed net leaf C_3 photosynthesis, A_p. Firstly, the rate of gross leaf photosynthesis (W) is calculated in terms of the minimum of three potentially limiting rates:

1. W_{carb} represents the rate of gross photosynthesis when CO_2 is limiting:

$$W_{carb} = V_{\max}\left\{\frac{c_i - \Gamma}{c_i + K_c\left(1 + O_a / K_o\right)}\right\} \qquad \text{(equation 6)}$$

where V_{max} (μmol CO_2 m^{-2} s^{-1}) is the maximum rate of carboxylation of Rubisco adjusted for temperature, O_a (kPa) is the partial pressure of atmospheric oxygen, K_c (Pa) and K_o (kPa) are Michaelis-Menton constants for CO_2 and O_2 respectively, Γ (Pa) is the CO_2 photorespiration compensation point, and c_i (Pa) is the internal CO_2 partial pressure.

2. W_{lite} is the light-limited rate of gross photosynthesis:

$$W_{lite} = \alpha_{\text{int}} \omega I_{par} \left\{ \frac{c_i - \Gamma}{c_i + 2\Gamma} \right\} \qquad \text{(equation 7)}$$

where I_{par} (μmol m^{-2} s^{-1}) is the photosynthetically active radiation, ω is the leaf scattering coefficient for PAR (0.15) taken from Cox (2001), and α_{int} is the intrinsic quantum efficiency (mol CO_2 mol^{-1} quanta).

3. W_{exp} is the limitation associated with transport of the photosynthetic products:

$$W_{\text{exp}} = 0.5 V_{\text{max}} \qquad \text{(equation 8)}$$

The actual gross rate of photosynthesis, W, is calculated as the smoothed minimum of these three limiting rates:

$$\beta_1 W_p^2 - W_p \{W_c + W_l\} + W_c W_l = 0$$
$$\beta_2 W^2 - W \{W_p + W_e\} + W_p W_e = 0 \qquad \text{(equations 9a \& b)}$$

where W_p is the smoothed minimum of W_{carb} and W_{lite}, and $\beta_1 = 0.83$ and $\beta_2 = 0.93$ are "co-limitation" coefficients. The smallest root of each quadratic is selected (Cox, 2001). Finally (non-moisture stressed) net leaf photosynthesis, A_p, is calculated by subtracting the rate of dark respiration, R_d, from the gross photosynthetic rate, W:

$$A_p = W - R_d \qquad \text{(equation 10)}$$

where R_d (μmol CO_2 m^{-2} s^{-1}) is scaled to V_{max} as (Cox, 2001):

$$R_d = 0.015 V_{\text{max}} \qquad \text{(equation 11)}$$

The parameters R_d, V_{max}, K_o, K_c and Γ are all temperature dependent parameters taken from Collatz *et al*., (1991), who use a Q_{10} temperature function. The temperature dependence of V_{max} is described by equation 12:

$$V_{\max} = \frac{V_{max25} f_T(2.0)}{\left[1+\exp\{0.3(T_c - T_{upp})\}\right]\left[1+\exp\{0.3(T_{low} - T_c)\}\right]} \qquad \text{(equation 12)}$$

where, V_{max25} (μmol CO_2 m^{-2} s^{-1}) is the maximum rate of Rubisco carboxylation at 25°C, T_c (°C) is the leaf temperature, T_{upp} and T_{low} (both °C) are the plant dependent parameters for the upper and lower temperature limits of photosynthesis, and f_T is the Q_{10} temperature dependence:

$$f_T = f_{T25} Q_{10}^{0.1(T_c - 25)} \qquad \text{(equation 13)}$$

where, f_{T25} is the parameter value at 25 °C and Q_{10} is the relative change in the parameter for a 10 °C change in temperature (Collatz *et al*., 1991). The dependence of K_o, K_c, Γ and R_d on temperature is described by the 'standard' Q_{10} function shown in equation 13. Values for the parameters and respective Q_{10} are given in Table 2. The photorespiration CO_2 compensation point, Γ (Pa), is calculated as:

$$\Gamma = \frac{O_a}{2\tau} \qquad \text{(equation 14)}$$

where τ is the Rubisco specificity factor for CO_2 relative to O_2.

4.2.3 Model configurations

The impact of including g_i on modelled net photosynthesis (A_{net}) was assessed using three different configurations of the JULES A_{net} - g_s model. These are summarised in Table 1. Model 1 is the photosynthesis sub-model currently used in JULES, which is based on the photosynthesis model described by Collatz *et al*., (1991). Model 2 is equivalent to Model 1, but the transfer of c_i to c_c has been included, according to Ethier & Livingston (2004), to represent g_i. Model 3 uses the configuration of the more common Farquhar *et al*., (1980) photosynthesis model, that has been modified in the same manner as Model 2 to include the transfer of c_i to c_c. The main differences between the basic configuration of the Collatz *et al.,* (1991) model (Model 1 and Model 2) and the Farquhar *et al*., (1980) model (Model 3) is the description of the dependence of photosynthetic rate on light. The Farquhar *et al*., (1980) model uses an additional parameter, J_{max} (the maximum rate of electron transport), which is used to determine the light limited rate of photosynthesis. Model 3 also uses more common exponential temperature response functions for key temperature dependent

parameters (K_o, K_c, Γ/ Γ*,V_{max}, J_{max}, R_d, g_i; equations 21 & 22), also used in Sharkey *et al*., (2007), as opposed to the Q_{10} temperature response functions used in the Collatz *et al*., (1991) model (equation 13). In each case, the temperature response functions and coefficients correct the value of each parameter to the leaf temperature. As a result, Model 3 uses alternative Rubisco kinetic constants (K_o, K_c, Γ/ Γ*) to the Q_{10} temperature coefficients specified in Collatz *et al*., (1991). The Rubisco kinetic constants are a set of parameters used in biochemical models of leaf photosynthesis that describe the kinetics of the enzyme-mediated reaction, and are commonly taken from previously published estimates. In this instance, the values used in Model 3 are taken from Sharkey *et al*., (2007) that have been determined *in vivo* at c_c (Table 2). Model 2 uses a Q_{10} temperature response function for g_i with a coefficient of 2.0 as suggested by Niinemets *et al*., (2009). Because both Model 2 and Model 3 include g_i, they will be parameterised with values of V_{max} estimated at c_c instead of c_i. The temperature coefficients used for all models are shown in Table 2. For all three models, calculation of the dark respiration rate and the triose-phosphate export limited rate of photosynthesis were the same, and followed the approach used in the Collatz *et al*., (1991) model, (equation 8 and equation 11 respectively).

	Model 1	Model 2	Model 3
V_{max}	x	x	x
α (int/app)	x (int)	x (int)	x (app)
g_i	n/a	x	x
J_{max}	n/a	n/a	x
F_0	x	x	x
D_c	x	x	x
Temperature Dependencies	Q_{10} function (see Collatz *et al*., 1991)	Q_{10} function (see Collatz *et al*., 1991)	Exponential function (see Sharkey *et al*., 2007)
Rubisco kinetic constants	Q_{10} temp. Coefficients (see Collatz *et al*., 1991)	Q_{10} temp. Coefficients (see Collatz *et al*., 1991 and Niinemets *et al*., 2009)	Values determined *in vivo* at c_c (see Sharkey *et al*., 2007)

Table 1. Differences between the three model configurations: V_{max} (μmol CO_2 m^{-2} s^{-1}), maximum carboxylation rate of Rubisco; $\alpha_{int/app}$ (mol CO_2 mol^{-1} quanta; mol e^- mol^{-1} quanta respectively), intrinsic/apparent quantum efficiency; g_i (μmol CO_2 m^{-2} s^{-1} Pa^{-1}), the internal conductance to CO_2; J_{max} (μmol e^- m^{-2} s^{-1}), maximum rate of electron transport; F_0, c_i/c_a ratio for specific humidity deficit in canopy; D_c (kg kg^{-1}), the critical humidity deficit. Paremeters each model configuration requires are indicated by 'x'.

	Exponential function					Q_{10} function	
	Value at 25 °C	c	ΔH_a	ΔH_d	ΔS	Value at 25 °C	Q_{10}
Parameters used for fitting							
K_o (Pa)	16582	12.3772	23.72			30000	1.20
K_c (Pa)	27.238	35.9774	80.99			30	2.10
Γ/Γ^* (Pa)	3.743	11.187	24.46			2.6	0.57
Used for normalising							
R_d (µmol CO_2 m^{-2} s^{-1})		18.7145	46.39				2.00
V_{max} (µmol CO_2 m^{-2} s^{-1})		26.355	65.33				2.00
J_{max} (µmol e^- m^{-2} s^{-1})		17.71	43.9				*n/a*
g_i (µmol CO_2 m^{-2} s^{-1} Pa^{-1})		20.01	49.6	437.4	1.4		2.00

Table 2. Exponential and Q_{10} temperature response functions for photosynthetic parameters and Rubisco enzyme kinetic parameters (plus values at 25 °C for model fitting). Values are taken from Bernacchi *et al*., (2002; 2001) and Bernacchi *et al*., (2003) for the exponential functions. Values are from Collatz *et al*., (1991) and Niinemets *et al*., (2009) for the Q_{10} response functions: *c,* scaling constant; ΔH_a, enthalpy of activation; ΔH_d enthalpy of deactivation; ΔS, entropy; K_o, Michaelis-Menton constant of Rubisco for O_2; K_c, Michaelis-Menton constant of Rubisco for CO_2; Γ, CO_2 photorespiration compensation point Γ^*, chloroplastic CO_2 photorespiration compensation point; R_d, dark respiration; V_{max}, maximum carboxylation rate of Rubisco; J_{max}, maximum rate of electron transport; g_i the internal conductance to CO_2. This table is partly reproduced from Sharkey *et al*., (2007).

4.2.4 Calculating internal conductance to CO_2

Models 2 and 3 were modified to include the transfer of CO_2 from intercellular air spaces across the mesophyll cell wall and into the chloroplast. Ethier & Livingston (2004) modified the biochemically based photosynthesis model of Farquhar *et al*., (1980) to include this transfer. They developed a non-rectangular hyperbola version of the model that includes g_i to calculate both the CO_2- and light-limited rates of photosynthesis at the CO_2 concentration inside the chloroplast (c_c). This approach was taken in both Model 2 and Model 3. Under Rubsico limited conditions, the rate of photosynthesis can be determined at c_c (W_{carbc}) by equation 15. This is identical to the calculation of W_{carb} at c_i in the Collatz *et al*., (1991) model (equation 6):

$$W_{carbc} = \frac{(c_c - \Gamma^*)V_{\max}}{c_c + K_c(1 + O_a / K_o)} - R_d \qquad \text{(equation 15)}$$

where W_{carbc} (µmol CO_2 m^{-2} s^{-1}) is the CO_2 - limited (or RuBP - saturated) CO_2 assimilation rate determined at c_c, c_c (Pa) is the chloroplastic CO_2 concentration and Γ^* (Pa) is the chloroplastic CO_2 compensation point. Substituting c_c with equation 16, where g_i (µmol CO_2 m^{-2} s^{-1} Pa^{-1}) is the internal CO_2 conductance transfer, gives a quadratic equation the solution of which is the positive root (equation 17; Ethier & Livingston, 2004).

$$c_c = c_i - \frac{W_{carbc}}{g_i} \qquad \text{(equation16)}$$

$$W_{carbc} = \frac{-b + \sqrt{b^2 - 4ac}}{2a}$$

where: $a = -1/g_i$

$$b = (V_{\max} - R_d)/g_i + c_i + K_c(1 + O_a / K_o)$$

$$c = R_d(c_i + K_c(1 + O_a / K_o)) - V_{\max}(c_i - \Gamma^*)$$

(equation 17)

The light-limited rate of photosynthesis at c_c, W_{litec}, can be derived in a similar manner. Using the Farquhar *et al*., (1980) model (Model 3), W_{litec} is determined following equation 18:

$$W_{litec} = \frac{J/4(c_c - \Gamma^*)}{c_c + 2\Gamma^*} - R_d \qquad \text{(equation 18)}$$

where J (µmol e^- m^{-2} s^{-1}) is the rate of electron transport dependent on irradiance (I_{par}), given in equation 19 after Harley *et al*., (1992):

$$J = \frac{\alpha_{app} I_{par}}{\sqrt{1 + \left(\frac{\alpha_{app} I_{par}}{J_{\max}}\right)^2}} \qquad \text{(equation 19)}$$

where J_{max} (µmol e^- m^{-2} s^{-1}) is the maximum electron transport rate, α_{app} (mol e^- mol^{-1} quanta) is the apparent quantum efficiency, and I_{par} (µmol m^{-2} s^{-1}) is the photosynthetically active radiation. In the Collatz *et al*., (1991) model (Model 2), the description of the

dependence of photosynthetic rate on light is slightly different and is repeated again here from equation 7 for determination at c_c (equation 20):

$$W_{litec} = \frac{\alpha_{\text{int}} \omega I_{par} \left(c_c - \Gamma^*\right)}{c_c + 2\Gamma^*} - R_d \qquad \text{(equation 20)}$$

where I_{par} (µmol m^{-2} s^{-1}) is the photosynthetically active radiation, ω is the leaf scattering coefficient for PAR (0.15) and α_{int} is the intrinsic quantum efficiency (mol CO_2 mol^{-1} quanta). For simplicity we will call the first three terms on the top of equation 20 $J_{collatz}$ which describes the dependency of photosynthetic rate on available light in the Collatz *et al*., (1991) model. Consequently, like W_{carbc}, the light-limited CO_2 assimilation rate, W_{litec}, can be derived as outlined in equations 15 to 17 for Model 2 and Model 3 by replacing V_{max} with $J_{collatz}$ (Model 2) or with $J/4$ (Model 3), and $K_c(1 + O_a/K_o)$ with $2\Gamma^*$. The factor of four used in the Farquhar *et al*., (1980) model accounts for four electrons being required per carboxylation/oxygenation reaction, and it is noted that the apparent quantum efficiency (α_{app}) is used in this version of the model with the units of mol e^- mol^{-1} quanta, whereas in the Collatz *et al*., (1991) version of the model the intrinsic quantum efficiency (α_{int}) is used with the units of mol CO_2 mol^{-1} quanta.

4.2.5 Adjusting for temperature

In Model 1 and Model 2, temperature dependencies of the following parameters, R_d, V_{max}, g_i, K_o, K_c and Γ / Γ^*, are described using the Q_{10} function shown in equation 13. Alternative temperature response functions are exponential functions. These were used in Model 3, which uses the Farquhar *et al*., (1980) model configuration. In this version of the model, the temperature dependence of V_{max}, J_{max}, R_d, K_c, K_o and Γ^* were each described by equation 21, (Harley *et al.*, 1992; Sharkey *et al.*, 2007);

$$Parameter = \exp\left(c - \frac{\Delta H_a}{RT_c}\right) \qquad \text{(equation 21)}$$

where c is a scaling constant, ΔH_a is an enthalpy of activation, R is the perfect gas constant (8.314 J mol^{-1} K^{-1}) and T_c is leaf temperature (^oC). The temperature dependence for g_i used in Model 3 follows equation 22 (Sharkey *et al.*, 2007):

$$Parameter = \frac{\exp\left(c - \frac{\Delta H_a}{RT_c}\right)}{1 + \exp\left(\Delta ST_c \frac{\Delta H_d}{RT_c}\right)} \quad \text{(equation 22)}$$

where ΔH_d is an enthalpy of deactivation and ΔS is entropy. The parameter values used in these and the Q_{10} functions are shown in Table 2.

4.2.6 Data

4.2.6.1 Model testing

Key parameters required by the three model configurations (see Table 1 for requirements of the different configurations) include; V_{max}, (µmol CO_2 m^{-2} s^{-1}) the maximum rate of Rubisco carboxylation, J_{max}, (µmol e^- m^{-2} s^{-1}) the maximum rate of electron transport, and g_i, (µmol CO_2 m^{-2} s^{-1} Pa^{-1}) the internal transfer of CO_2 from c_i to c_c. Values for these parameters had previously been derived from $A_{net} - c_i$ response curves measured from leaves of *P. x euramericana* and *P. nigra* across the growing season of 2008 on healthy and water-stressed trees (see Chapter 3 for details). α_{app}, (mol e^- mol^{-1} quanta) the apparent quantum efficiency, describes the efficiency of light utilisation in photosynthesis, and is another key parameter that had previously been derived from measured $A_{net} - P_{PFD}$ response curves from leaves of *P. x euramericana* and *P. nigra* (see Chapter 3 for details). α_{int}, (mol CO_2 mol^{-1} quanta) the intrinsic quantum efficiency, is similar to α_{app} but takes into account reflected and transmitted light, therefore it is thought to be highly conserved across C_3 species (Long *et al.*, 1993), with typical values ranging between 0.06 to 0.125 mol CO_2 mol^{-1} quanta (Collatz *et al.*, 1991; Farquhar *et al.*, 1980; Laisk *et al.*, 2002; Lambers *et al.*, 2008; Long *et al.*, 1993). It is also suggested that there is a close relationship between α_{int} and F_v/F_m (the maximum potential quantum efficiency of photosystem II) as measured by chlorophyll fluorescence (Kao & Forseth, 1992). F_v/F_m was also measured in well-watered *P. x euramericana* and *P. nigra* trees over the same experimental period (May – October 2008). F_v/F_m varied little over the course of the growing season, ranging between 0.072 - 0.08 mol CO_2 mol^{-1} quanta (see Chapter 3 for details). The average of this range (0.076 mol CO_2 mol^{-1}quanta) was chosen as the value of α_{int} to use in both Model 1 and Model 2. F_0 (unit-less) and D_c (kg kg^{-1}) are additional plant-

specific parameters. F_0 is the c_i/c_a for specific humidity deficit in the canopy, and D_c is the critical humidity deficit. These parameters were not as readily measured or commonly available in the literature, so it was necessary to tune these parameters to find suitable values. The value of F_0 used was taken from literature (Cox, 2001; Finch *et al.*, 2004). D_c was found by running each model in a Monte-Carlo simulation for 5000 loops to find the parameter value that minimised the RMSD (root mean squared deviation) between modelled and observed A_{net}. It was observed that there was minimal sensitivity to this parameter. The same value was used for all models which was close to the default value for C_3 plants specified in the JULES documentation (Cox, 2001) and that used in a study by Cox *et al*., (1998).

Using the values of V_{max}, J_{max}, $\alpha_{int/app}$, and g_i inferred from each measured A_{net} - c_i and A_{net} - P_{PFD} data set, each model was assessed on its ability to predict leaf-level rates of A_{net}. Parameter values used for testing the three model versions are shown in Table 3 for *P. x euramericana* and Table 4 for *P. nigra*. V_{max} estimated without g_i (i.e. at c_i), was used in Model 1 that does not include the transfer of c_i to c_c. Whereas V_{max} estimated with g_i (i.e. at c_c) was used in Models 2 and 3. Additionally, Model 3 used values of J_{max} determined at c_c and α_{app} instead of α_{int}. At this stage, model testing was only performed with parameters from well-watered trees, therefore the soil moisture stress factor (β; equation 5) was set to one (i.e. no soil moisture stress).

4.2.6.2 Model parameterisation

The leaf-level A_{net} - g_s model tested is integral to a land-surface scheme, which requires just one value for each parameter (V_{max}, J_{max}, g_i, α, F_0 and D_c). As values of the measured parameters (V_{max}, J_{max}, g_i and α) were seen to vary across the growing season, it was decided to use the mean of these values from well-watered trees for parameterisation. These values are shown highlighted in bold at the bottom of Table 3 and Table 4. Simulated A_{net} was assessed against the observed data (all A_{net}-c_i response curve data from well-watered trees aggregated) to determine the performance of each model and its calibrated parameter set. These initial evaluations of model performance served as a benchmark for comparisons with independent data in the final stages of this work. Model 1 was also used with a default parameter set for a C_3 broadleaf tree PFT used in the JULES model (Cox, 2001: JULES_def; V_{max} = 32.00, α_{int} = 0.08, F_0 = 0.875, D_c = 0.09). These were the default parameter values in the JULES model for a broadleaf tree. This was to assess

the accuracy of modelled A_{net} when using default parameter values as opposed to calibrated parameters. This could not be done to compare the performance of Model 2 or Model 3 as default values for J_{max} and g_i were unknown.

4.2.6.3 Model validation

Model validation was performed against an independent data set of observed, leaf-level rates of A_{net} and g_s measured across the growing season under ambient environmental conditions and with imposed soil moisture stress (described in Chapter 3). The soil moisture stress factor was calculated according to equation 5. Having tested the ability of the three model versions to accurately simulate A_{net}, the two best performing parameterised models were selected for validation. Model validation was based on the accuracy of predicted leaf-level rates of A_{net} and g_s compared against observations.

P. x euramericana							
without g_i	with g_i						
♦	**Δ †**	†	**Δ †**	†	**♦ Δ**	**♦ Δ †**	**♦ Δ †**
V_{max}	V_{max}	J_{max}	g_i	α_{app}	α_{int}	F_0	D_c
80.48	211.52	186.18	2.55	0.20	0.076	0.875	0.07
68.39	108.28	197.69	2.08	0.20	0.076	0.875	0.07
103.75	182.63	261.11	1.43	0.20	0.076	0.875	0.07
82.85	188.93	231.82	1.86	0.20	0.076	0.875	0.07
102.65	194.80	247.06	2.42	0.22	0.076	0.875	0.07
107.00	196.62	218.08	2.29	0.19	0.076	0.875	0.07
55.65	57.73	120.22	0.83	0.14	0.076	0.875	0.07
66.21	148.69	162.78	1.31	0.13	0.076	0.875	0.07
39.22	77.38	99.82	1.60	0.11	0.076	0.875	0.07
55.00	68.38	124.91	0.88	0.20	0.076	0.875	0.07
54.83	83.18	109.54	1.57	0.24	0.076	0.875	0.07
79.48	136.84	158.41	2.23	0.09	0.076	0.875	0.07
78.41	115.21	150.10	1.98	0.24	0.076	0.875	0.07
75.20	103.08	124.53	2.02	0.24	0.076	0.875	0.07
68.79	102.51	116.46	1.95	0.30	0.076	0.875	0.07
71.53	70.08	147.64	1.62	0.24	0.076	0.875	0.07
74.34 ± 4.73	**122.31 ± 12.71**	**166.02 ± 12.95**	**1.74 ± 0.12**	**0.20 ± 0.01**	**0.076**	**0.875**	**0.07**

Table 3. Parameter values from each individual A_{net} - c_i and A_{net} - P_{PFD} response curve measured for *P. x euramericana*. Values in bold show the mean ± S.E. The symbols indicate which model the parameter values were used in: ♦ Model 1, **Δ** Model 2, † Model 3. V_{max} (µmol CO_2 m^{-2} s^{-1}), maximum carboxylation rate of Rubisco estimated with and without g_i; J_{max} (µmol e^- m^{-2} s^{-1}), maximum rate of electron transport; g_i (µmol CO_2 m^{-2} s^{-1} Pa^{-1}), the internal conductance to CO_2; $\alpha_{int/app}$ (mol CO_2 mol^{-1} quanta; mol e^- mol^{-1} quanta respectively), intrinsic/apparent quantum efficiency; F_0, c_i/c_a ratio for specific humidity deficit in canopy; D_c (kg kg^{-1}), the critical humidity deficit.

P. nigra							
without g_i	with g_i						
♦	**Δ †**	†	**Δ †**	†	**♦ Δ**	**♦ Δ †**	**♦ Δ †**
V_{max}	V_{max}	J_{max}	g_i	α_{app}	α_{int}	F_0	D_c
27.92	59.11	61.12	1.12	0.11	0.076	0.875	0.07
100.73	120.69	220.23	3.01	0.18	0.076	0.875	0.07
96.91	38.41	56.25	1.27	0.24	0.076	0.875	0.07
110.00	186.54	259.96	2.70	0.19	0.076	0.875	0.07
81.93	114.39	171.27	3.70	0.14	0.076	0.875	0.07
63.71	97.62	144.62	2.07	0.09	0.076	0.875	0.07
64.26	107.24	143.76	1.73	0.14	0.076	0.875	0.07
82.43	126.00	143.66	3.74	0.22	0.076	0.875	0.07
42.70	51.04	90.61	1.85	0.11	0.076	0.875	0.07
50.41	92.80	114.01	1.17	0.15	0.076	0.875	0.07
47.88	80.50	97.47	1.27	0.14	0.076	0.875	0.07
67.34	109.41	130.07	2.73	0.20	0.076	0.875	0.07
77.07	124.77	137.99	2.13	0.20	0.076	0.875	0.07
60.59	63.45	105.74	3.70	0.20	0.076	0.875	0.07
70.48	109.75	136.23	2.07	0.20	0.076	0.875	0.07
73.05	109.75	139.58	1.73	0.21	0.076	0.875	0.07
69.84 ± 5.47	**99.47 ± 8.99**	**134.54 ± 13.04**	**2.25 ± 0.23**	**0.17 ± 0.01**	**0.076**	**0.875**	**0.07**

Table 4. Parameter values from each individual A_{net} - c_i and A_{net} - P_{PFD} response curve measured for *P. nigra*. Values in bold show the mean ± S.E. The symbols indicate which model the parameter values were used in: ♦ Model 1, **Δ** Model 2, † Model 3. V_{max} (µmol CO_2 m^{-2} s^{-1}), maximum carboxylation rate of Rubisco estimated with and without g_i; J_{max} (µmol e^- m^{-2} s^{-1}), maximum rate of electron transport; g_i (µmol CO_2 m^{-2} s^{-1} Pa^{-1}), the internal conductance to CO_2; $\alpha_{int/app}$ (mol CO_2 mol^{-1} quanta; mol e^- mol^{-1} quanta respectively), intrinsic/apparent quantum efficiency; F_0, c_i/c_a ratio for specific humidity deficit in canopy; D_c (kg kg^{-1}), the critical humidity deficit.

4.2.7 Model assessment

Observed data were plotted against their corresponding model-predicted values, model bias and goodness of fit was assessed based on the intercept, slope and coefficient of determination (r^2) of the optimal least squares regression line. The r^2 shows the proportion of the total variance explained by the regression model (and also the proportion of the variance in observed values that is explained by predicted values), the slope describes the model bias and the intercept the model consistency (Piñeiro *et al.*, 2008). Based on the recommendation of Piñeiro *et al*., (2008) all model assessments used regressions of observed (in the y-axis) vs. predicted (in the x-axis). The root mean squared deviation (RMSD) was also estimated, which represents the mean deviation of predicted values with respect to the observed ones, in the same units as the model variable under evaluation (Piñeiro *et al.*, 2008), and is calculated as:

$$RMSD = \sqrt{\frac{1}{n-1}\sum_{i=1}^{n}\left(Y_i - X_i\right)^2} \qquad \text{(equation 23)}$$

where Y is observed data and X is modelled data.

4.2.8 Model driving data

Required meteorological driving variables were; leaf temperature (K), air pressure (Pa), PAR (W m^{-2}) and specific humidity (Q; kg kg^{-1}). Leaf temperature, air pressure and PAR were measured and recorded by the IRGA (infra-red gas analyser) at the time the measurements were made. Specific humidity (Q; kg kg^{-1}) was calculated using equation 24:

$$Q = 0.622 e_a 0.01 \qquad \text{(equation 24)}$$

Where, e_a is the actual vapour pressure (kPa) as measured by the IRGA.

4.3 Results

4.3.1 Testing different configurations of the photosynthesis model

4.3.1.1 Model 1

The JULES model in its original configuration simulated observed rates of A_{net} with a high degree of accuracy for both *P. x euramericana* and *P. nigra* (Fig. 1a and Fig. 2a respectively). The coefficient of determination (r^2) was high for both *P. x euramericana* and *P. nigra*, 0.96 and 0.98 respectively. For both genotypes a positive correlation between observed and predicted data was detected (Table 5). Bias in the model was detected however, as both the intercept and slope of the regression model line were different from zero and one respectively for both genotypes. Although the 95% confidence interval (CI) surrounding the slope and intercept were lower for *P. nigra* suggesting reduced bias in the model compared to *P. x euramericana* (Table 5). The model over predicted A_{net} at low values and under predicted at high rates of A_{net}. The root mean squared deviation (RMSD) was low for both genotypes, 2.55µmol CO_2 m^{-2} s^{-1} for *P. x euramericana* and 1.68µmol CO_2 m^{-2} s^{-1} for *P. nigra* (Table 5).

4.3.1.2 Model 2

This version of the JULES model was modified to include the CO_2 transfer from c_i to c_c. Minimal differences in model accuracy were detected (Fig. 1b and Fig. 2b respectively). For *P. x euramericana*, the r^2 marginally increased to 0.97. A positive correlation between observed and modelled data was detected, however bias in the model was also detected as both the intercept and slope were different from zero and one respectively (Table 5). Similar to Model 1, rates of A_{net} were over predicted at low values and under predicted at high values of A_{net}. The RMSD however, slightly decreased to 2.24µmol CO_2 m^{-2} s^{-1} also indicating an improved fit between modelled and observed data (Table 8). In *P. nigra*, the r^2 slightly declined to 0.96. Similar to *P. x euramericana,* a positive relationship between observed and modelled data was detected, however bias in the model was also detected as both the intercept and slope were different from zero and one respectively (Table 5). The RMSD increased to 2.7 µmol CO_2 m^{-2} s^{-1} (Table 8). The increase in RMSD from Model 1 is relatively large and suggests a signifincant loss of accuracy compared to Model 1.

4.3.1.3 Model 3

This model used the configuration of the Farquhar *et al*., (1980) model modified to include g_i. For *P.x euramericana*, Model 3 marginally improved the accuracy of simulated A_{net} compared to both Model 1 and Model 2. The r^2 was increased to 0.98 and the RMSD minimised to 1.84 µmol CO_2 m^{-2} s^{-1} (Fig. 1c, Table 5). Additionally, neither the intercept or slope of the regression line were significantly different from the 1:1 line (Table 5). The CI surrounding both the slope and intercept were much reduced compared to the other two model configurations, together suggesting minimal bias in Model 3. For *P. nigra*, no significant improvement in modelled A_{net} was seen using Model 3 compared to Model 1, although improvement in accuracy was seen in comparison to Model 2. Identical to Model 1, the r^2 remained high at 0.98. However, Model 3 also generated a marginal increase in the RMSD (1.71µmol CO_2 m^{-2} s^{-1}) compared to Model 1 (1.68µmol CO_2 m^{-2} s^{-1}), but a substantial decrease in RMSD compared to Model 2. Model 3 showed a similar bias in predicted A_{net} to both Model 1 and Model 2, over predicting at low values and under predicting at high values of A_{net}. Both the regression model intercept and slope were significantly different to zero and one respectively (Table 5). The CI surrounding the slope and intercept were similar to Model 1, but much reduced compared to Model 2. These results suggest although the accuracy of simulated A_{net} by Model 3 is high, Model 1 performs marginally better than Model 3.

Fig. 3a and Fig. 4a further show the minimal difference between the three models, and highlight the ability of all three to predict rates of A_{net} with reasonable accuracy. It can be seen that for all three models, certainly where $c_a > 20$ Pa, they predict A_{net} within the error of the observations, which is well below current ambient atmospheric CO_2 concentrations.

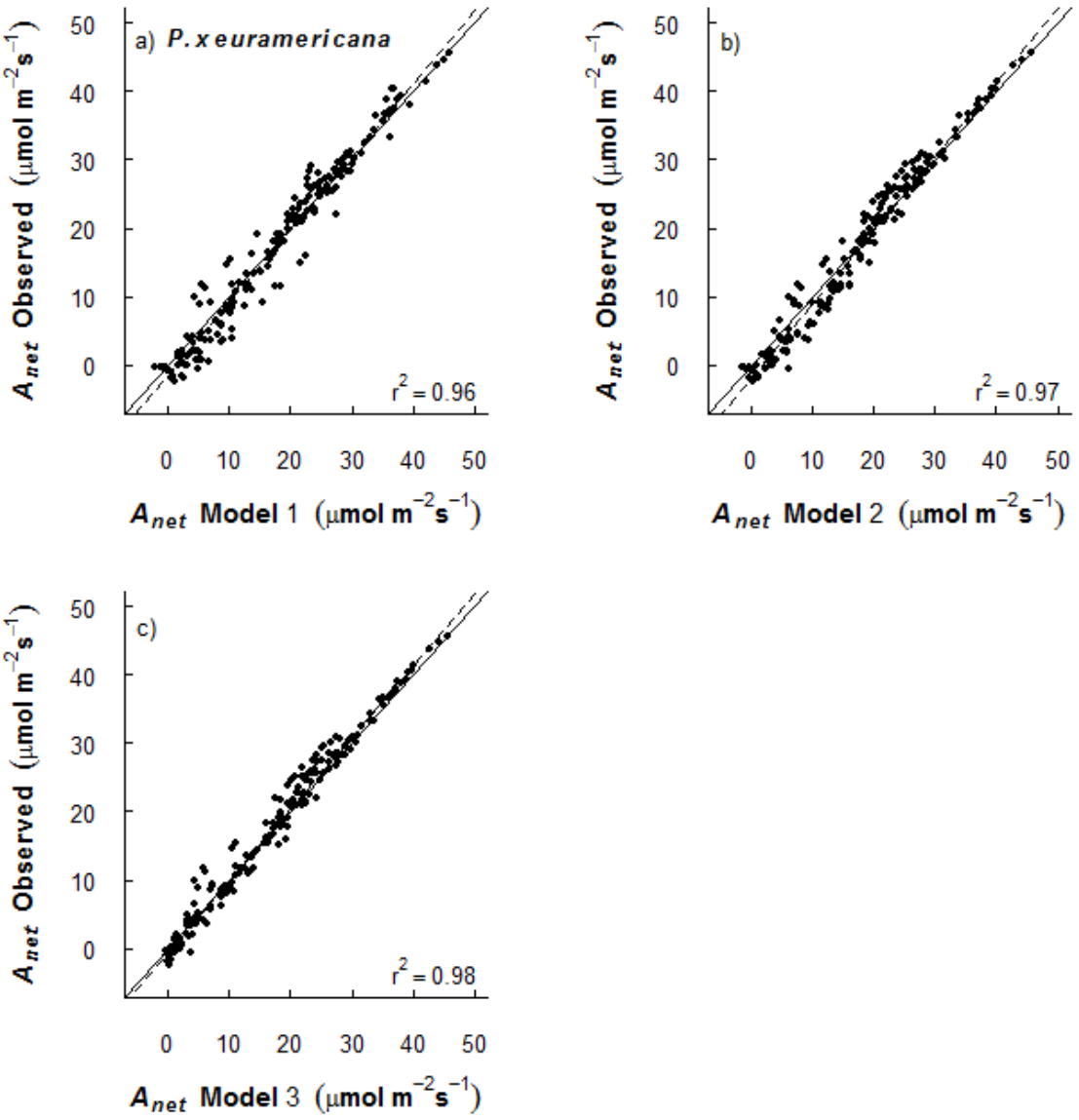

Fig. 1. Model testing, observed vs. predicted A_{net} shown for *P. x euramericana*: a) Model 1, b) Model 2, c) Model 3. The regression line (dotted line) and r^2 are shown, along with the 1:1 line (solid line).

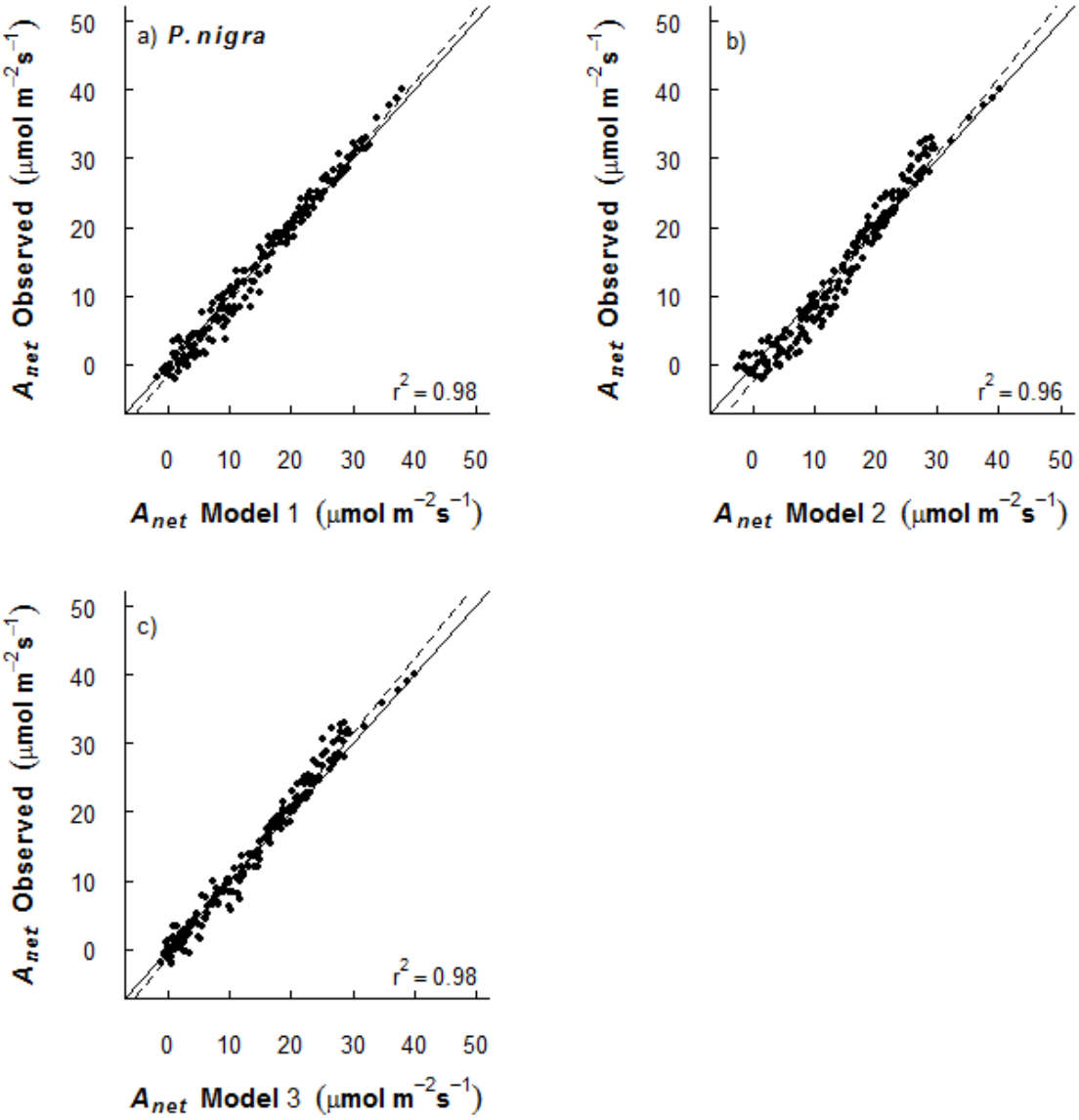

Fig. 2. Model testing, observed vs. predicted A_{net} shown for *P. nigra*: a) Model 1, b) Model 2, c) Model 3. The regression line (dotted line) and r^2 are shown, along with the 1:1 line (solid line).

	Regression line	r^2	95 % CI Intercept	95 % CI Slope	Correlation *F* (1, 190 *d.f*)	Correlation *P*	RMSD
***P. x euramericana*: Model Testing**							
Model 1	y = -1.47 - 1.06*x*	0.96	0.62 ***	0.03 ***	4877	< 0.001	2.55
Model 2	y = -1.77 - 1.08*x*	0.97	0.52 ***	0.03 ***	7064	< 0.001	2.24
Model 3	y = -0.38 - 1.04*x*	0.98	0.42	0.02	9655	< 0.001	1.84
***P. x euramericana*: Model Parameterisation**							
Model 1	y = -1.05 - 1.06*x*	0.76	1.69	0.09 ***	595.7	< 0.001	6.15
Model 2	y = -3.37 - 1.08*x*	0.80	1.62***	0.08 ***	786.3	< 0.001	5.85
Model 3	y = -2.33 - 1.02*x*	0.84	1.39 **	0.07 **	996.2	< 0.001	5.13
Model1$_{_def}$	y = -1.14 - 2.42*x*	0.76	1.65	0.19 ***	630.3	< 0.001	12.86
***P. nigra*: Model Testing**							
Model 1	y = -1.26 - 1.06*x*	0.98	0.38 ***	0.02 ***	9412	< 0.001	1.68
Model 2	y = -2.17 - 1.10*x*	0.96	0.56 ***	0.03 ***	4643	< 0.001	2.7
Model 3	y = -0.97 - 1.08*x*	0.98	0.37 ***	0.02 ***	9678	< 0.001	1.71
***P. nigra*: Model Parameterisation**							
Model 1	y = -1.16 - 1.00*x*	0.76	1.41	0.08	614.3	< 0.001	5.34
Model 2	y = -1.73 - 1.05*x*	0.69	1.69 *	0.1 *	442	< 0.001	5.99
Model 3	y = -1.44 - 1.09*x*	0.76	1.45	0.09	594.9	< 0.001	5.35
Model1$_{_def}$	y = 1.12 - 1.71*x*	0.71	1.43	0.16 ***	463.1	< 0.001	9.42

Table 5. Quantitative measures of the ability of the models to predict observed rates of A_{net} during model testing and model parameterisation. Results are show for *P. x euramericana* and *P. nigra*. The units of RMSD are (µmol CO_2 m^{-2} s^{-1}). CI refers to the 95 % confidence interval surrounding the estimate of the regression line intercept/slope. The stars indicate whether the intercept/slope is significantly different to zero/one respectively: *** $p < 0.001$, ** $p < 0.01$, * $p < 0.05$.

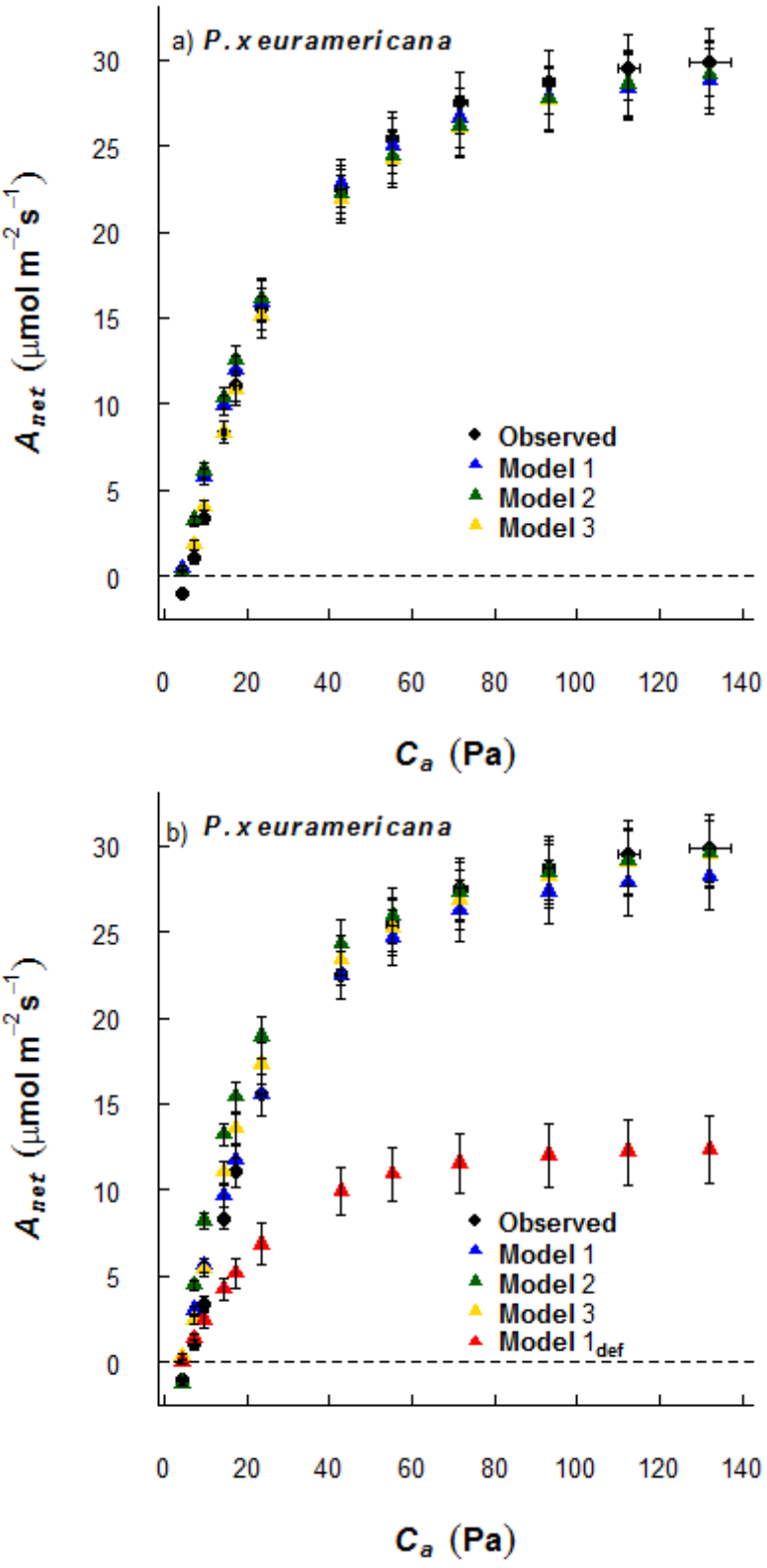

Fig. 3. Mean A_{net} ± s.e versus atmospheric CO_2 concentration (c_a) at measurement for *P. x euramericana*; observed data: black diamond, Model 1: blue triangle, Model 2: green triangle, Model 3: yellow triangle, and Model 1_{def}: red triangle, Fig. 3b only; a) model testing, b) model calibration (single value).

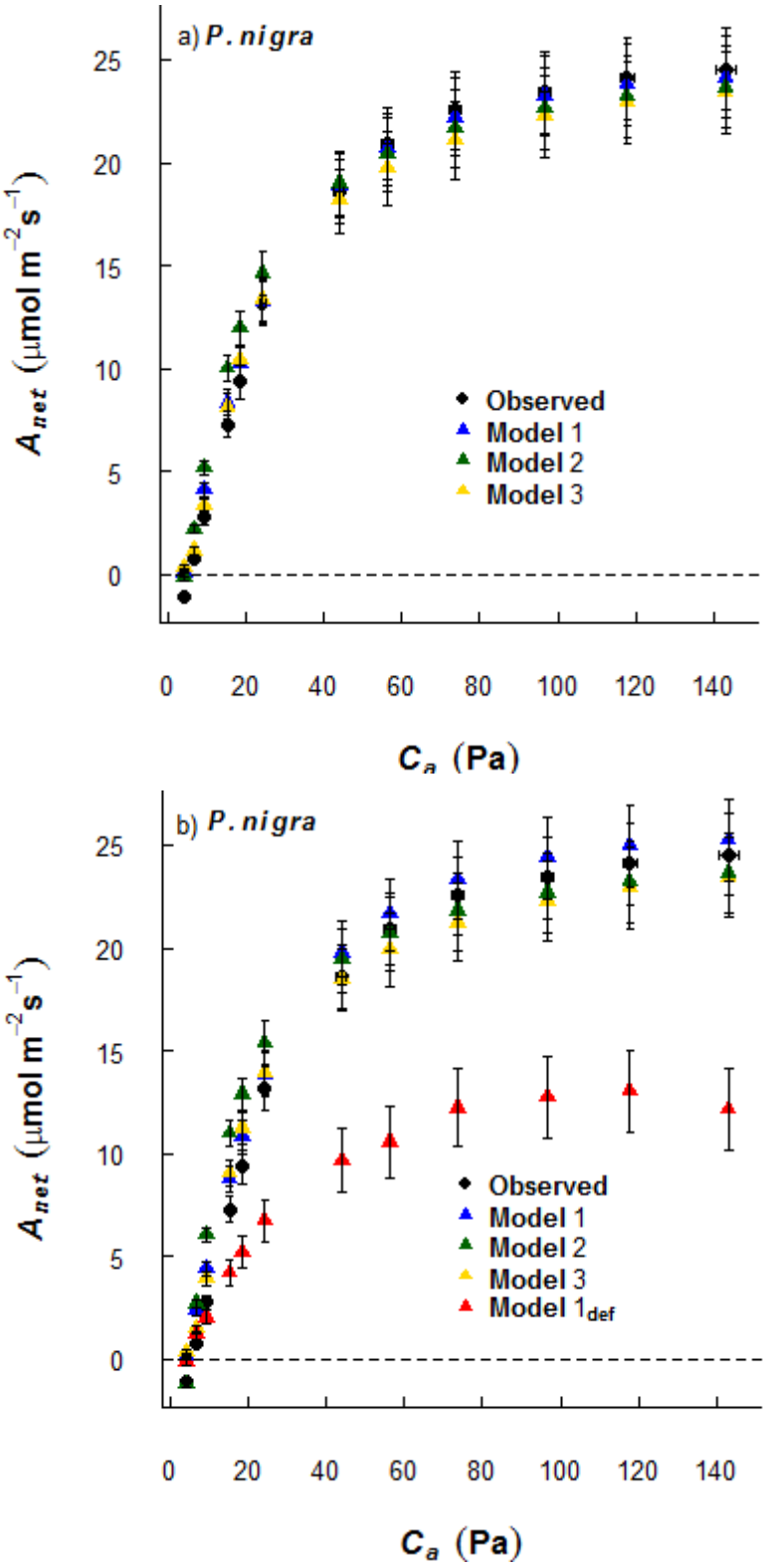

Fig. 4. Mean A_{net} ± s.e versus atmospheric CO_2 concentration (c_a) at measurement for *P. nigra*; observed data: black diamond, Model 1: blue triangle, Model 2: green triangle, Model 3: yellow triangle, and Model 1_{def}: red triangle, Fig. 4b only. a) model testing, b) model calibration (single value).

4.3.2 Parameterising the photosynthesis model

4.3.2.1 Model 1

Parameterisation of Model 1 with a single set of calibrated parameter values maintained a reasonable fit to the observed data. For both genotypes the r^2 was 0.76 (Fig. 5a and Fig. 6a). The RMSD was 6.15µmol CO_2 m^{-2} s^{-1} and 5.34µmol CO_2 m^{-2} s^{-1} for *P. x euramericana* and *P. nigra* respectively (Table 5). For both genotypes, the bias in the model was minimal. For *P. nigra*, the regression model line was not detectably different to the 1:1 line. For *P. x euramericana*, the intercept of the regression model line was not different to zero, but the slope was detectably different to one, suggesting a tendency to under predict A_{net} at higher values. For both genotypes, however, the CI surrounding both the slope and intercept were larger than the CI's reported during the model testing stage, suggesting increased uncertainty of the values of the regression parameters. It is clearly evident that calibration of the model's with a single set of parameters reduces the ability of the model's to simulate the observations. Nevertheless, given the apparent sensitivity of each of the model configurations to parameter values, the accuracy of the model's remains reasonably high.

4.3.2.2 Model 2

Compared to Model 1, simulated A_{net} was improved in *P. x euramericana*, but not in *P. nigra* (Fig. 5b and Fig. 6b). In the former, r^2 was increased to 0.80 and RMSD decreased to 5.85µmol CO_2 m^{-2} s^{-1}, but there was evidence of bias in the model predictions with both the intercept and slope of the regression model line significantly different to the 1:1 line (Table 5). In the latter, the r^2 decreased to 0.69, RMSD increased to 5.99µmol CO_2 m^{-2} s^{-1}, and there was bias in the model predictions which was not present in Model 1(Table 5). Both genotypes showed the same tendency to over predicted A_{net}, which was most noticeable at values within the lower range of A_{net}.

4.3.2.3 Model 3

A_{net} predicted by Model 3 maintained a high level of accuracy (Fig. 5c and Fig. 6c). For *P. x euramericana*, the r^2 increased to 0.84 and RMSD decreased to 5.13µmol CO_2 m^{-2} s^{-1} compared to both Model 1 and Model 2 (Table 8). Bias in the model predictions were

detected as both the slope and intercept were significantly different to the 1:1 line, although the CI surrounding the slope and intercept were smallest in this model configuration. For *P. nigra*, the r^2 was 0.76, which was identical to Model 1, but an increase in fit compared to Model 2. The RMSD of Model 3 marginally increased compared to Model 1, from 5.34µmol CO_2 m^{-2} s^{-1} to 5.35µmol CO_2 m^{-2} s^{-1} (Table 5), but this increase in RMSD was minimal. Similar to Model 1, in Model 3 neither the regression model intercept or slope were found to be significantly different from the 1:1 line, although the CI surrounding the slope and intercept were marginally increased.

4.3.2.4 Model 1_{def}: Calibrated vs. default parameters

Comparison of Model 1 and Model 1_{def} (Fig. 5a & d; Fig. 6a & d) showed the substantial improvement in accuracy gained by using calibrated parameters as opposed to default model parameter values. Use of the default parameter values led to substantial under prediction of A_{net} in both genotypes. For *P. x euramericana*, the RMSD was increased from 6.15µmol CO_2 m^{-2} s^{-1} to 12.86µmol CO_2 m^{-2} s^{-1} (Table 5). For *P. nigra* the RMSD was increased from 5.34µmol CO_2 m^{-2} s^{-1} to 9.42µmol CO_2 m^{-2} s^{-1} (Table 5).

Fig. 3b and Fig. 4b also show the improved accuracy of simulated A_{net} using a calibrated parameter set as opposed to a default model parameter set. The single parameter set clearly maintains a high level of accuracy of simulated A_{net} for all three models, although greater variation surrounding the predicted values is evident, compared to the use of 'curve-specific' parameters. Nevertheless, for Model 1 and Model 3, simulated A_{net} was within the error of the observations for $c_a > 20$ Pa. These calibrated parameter sets therefore do well at capturing much of the within season variation. It is evident that simulated A_{net} is very sensitive to the photosynthetic parameter V_{max}. Values of α_{int}, F_0 and D_c changed margnially between the default values and calibrated parameter sets. Additionally, in a previous Monte Carlo experiment to determine a suitable value for D_c, it was seen that A_{net} displayed little sensitivity to this parameter. V_{max}, however, changed substantially between simulations, with the calibrated values being more than double the default value. Therefore, correct calibration of V_{max} in particular is key to improving predictions of leaf-level A_{net}.

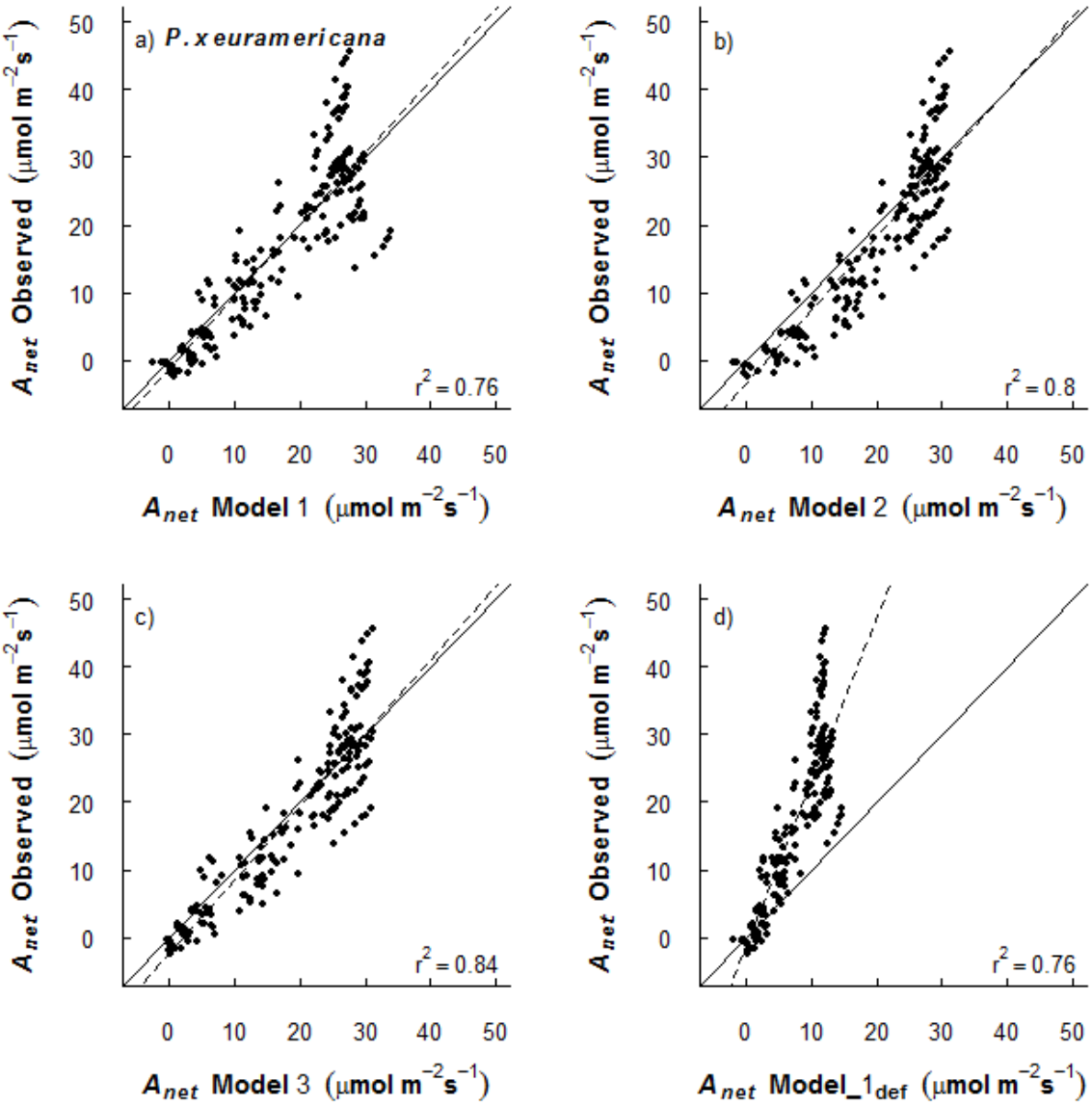

Fig. 5. Model parameterisation, observed vs. predicted A_{net} shown for *P. x euramericana*: a) Model 1, b) Model 2, c) Model 3, d) Model_1$_{def}$. The regression line (dotted line) and r^2 are shown, along with the 1:1 line (solid line).

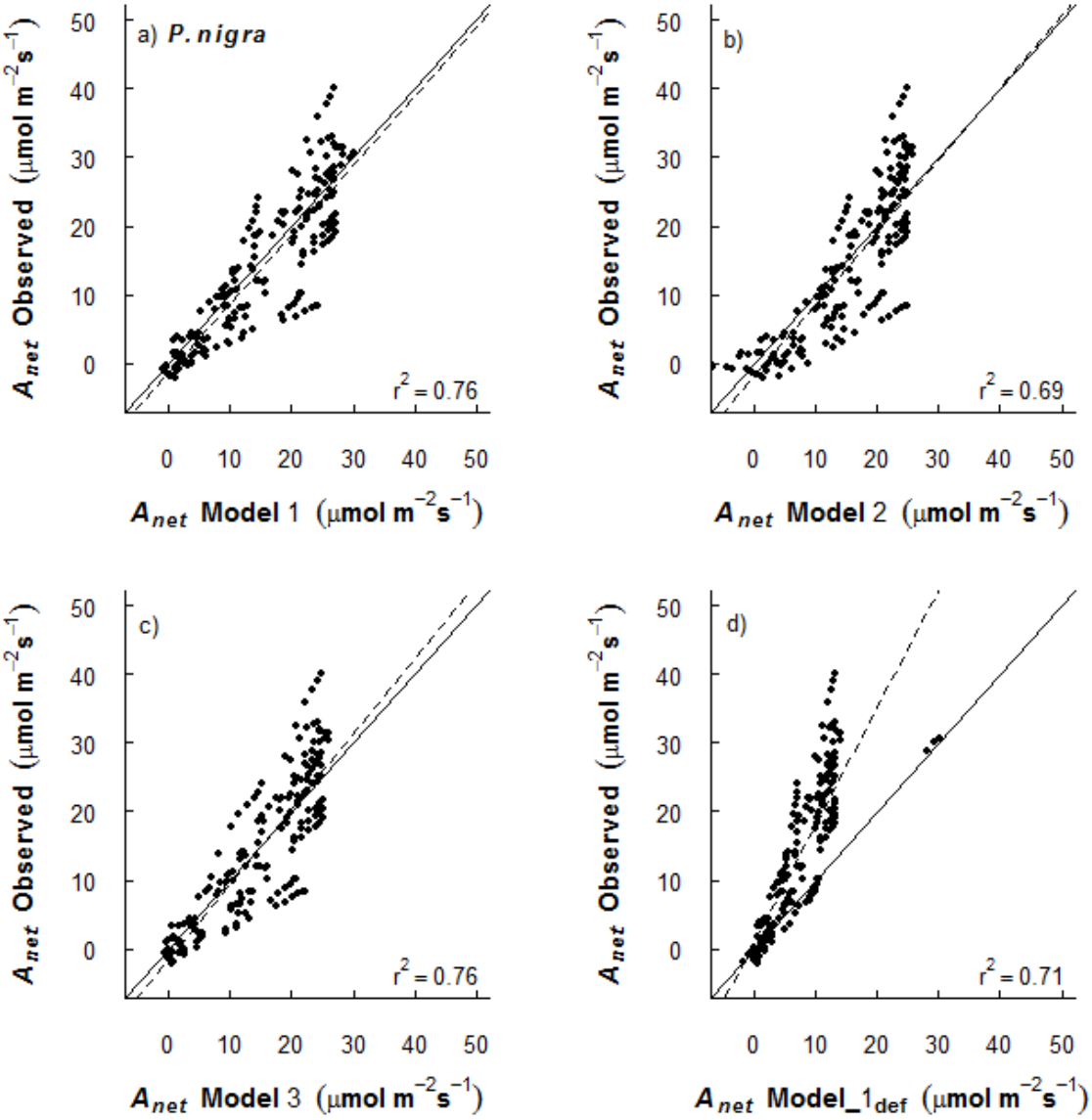

Fig. 6. Model parameterisation, observed vs. predicted A_{net} shown for *P. nigra*: a) Model 1, b) Model 2, c) Model 3, d) Model_1$_{def}$. The regression line (dotted line) and r^2 are shown, along with the 1:1 line (solid line).

4.3.3 Model validation

The accuracy of Model 1, the simplest model, and Model 3, the best performing 'alternative' model, was validated in this section.

4.3.3.1 Photosynthesis

In both genotypes, the accuracy of simulated A_{net} was greatest in Model 1 compared to Model 3 (Fig. 7a & c, Fig. 8a & c). Model 1 is the JULES model in its original configuration and is the simplest model. The improvement in accuracy seen with Model 1 was slight, nevertheless, r^2 increased from 0.78 (Model 3) to 0.83 (Model 1) in *P. x euramericana*, and from 0.72 (Model 3) to 0.77 (Model 1) in *P. nigra*. The RMSD decreased from 4.65µmol CO_2 m^{-2} s^{-1} (Model 3) to 3.26µmol CO_2 m^{-2} s^{-1} (Model 1) in *P. x euramericana*, and from 3.91µmol CO_2 m^{-2} s^{-1} (Model 3) to 3.36µmol CO_2 m^{-2} s^{-1} (Model 1) in *P. nigra* (Table 6). Both models suggested bias in model predictions, in all models the regression line slope was significantly lower than one suggesting a tendency to over predict A_{net} at higher values (Table 6).

4.3.3.2 Stomatal conductance

Validation of the two models based on rates of g_s showed inconsistencies in model performance between the two genotypes. In *P. x euramericana*, r^2 was higher in Model 3 (0.82) than Model 1 (0.79), conversely the RMSD was higher in Model 3 (87.16mmol H_2O m^{-2} s^{-1}) than Model 1 (78.97mmol H_2O m^{-2} s^{-1}) (Table 6). In both models the regression line intercepts were not found to be different to zero, but both slopes were significantly lower than one, suggesting a consistent trend to over-predict rates of g_s that increased with increasing g_s, the same bias was observed for *P. nigra* also (Fig. 7b & d, Fig. 8b & d). Validation of the two models for *P. nigra* showed the accuracy of simulated g_s was marginally improved in Model 3. The r^2 was higher in Model 3 (0.86) than Model 1 (0.82), and the RMSD was lower in Model 3 (58.23mmol H_2O m^{-2} s^{-1}) than Model 1 (65.45mmol H_2O m^{-2} s^{-1}) (Table 6).

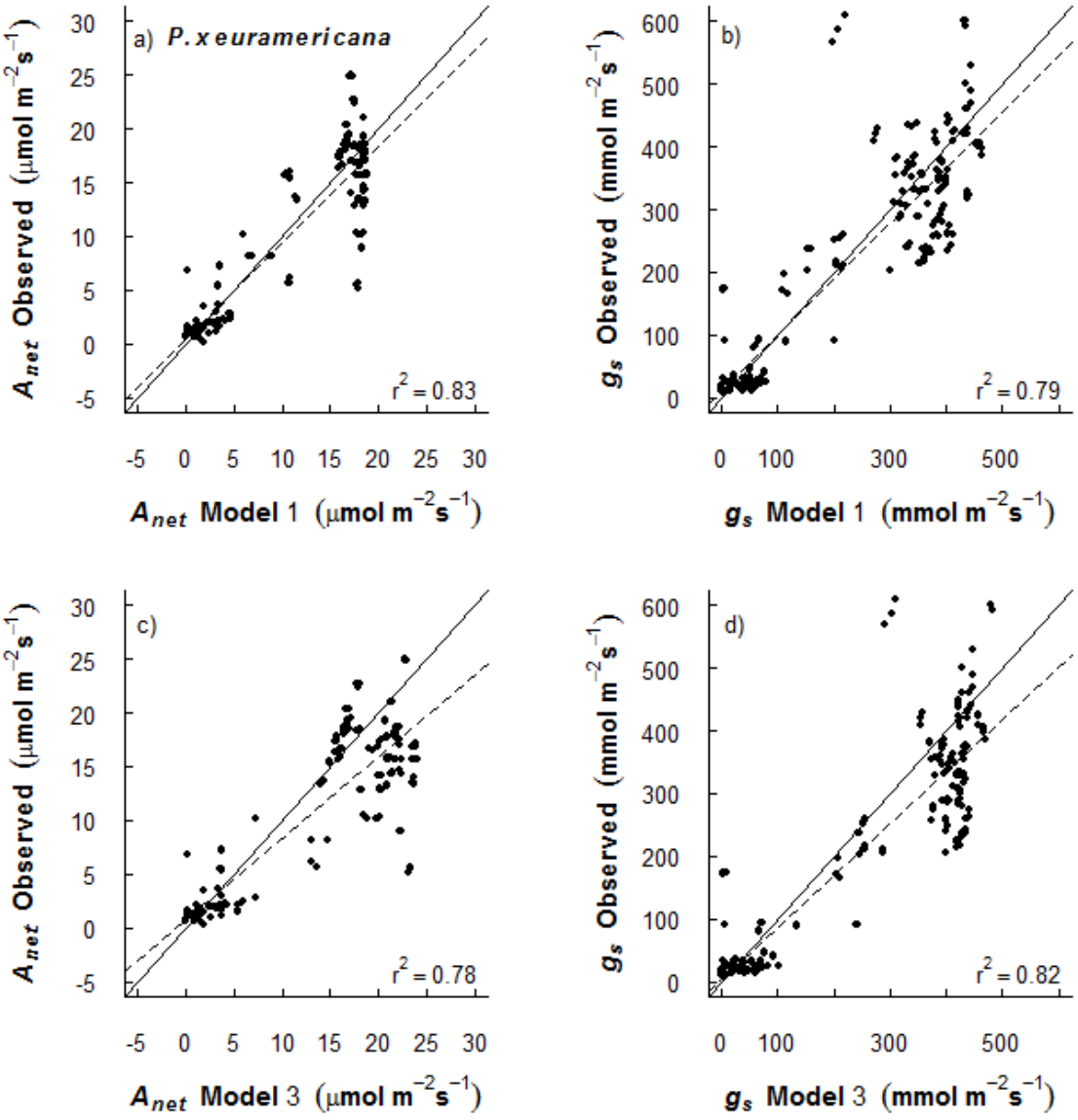

Fig. 7. Model validation, observed vs. predicted A_{net} and g_s shown for *P. x eurameriana*: a & b) Model 1, c & d) Model 3. The regression line (dotted line) and r^2 are shown, along with the 1:1 line (solid line).

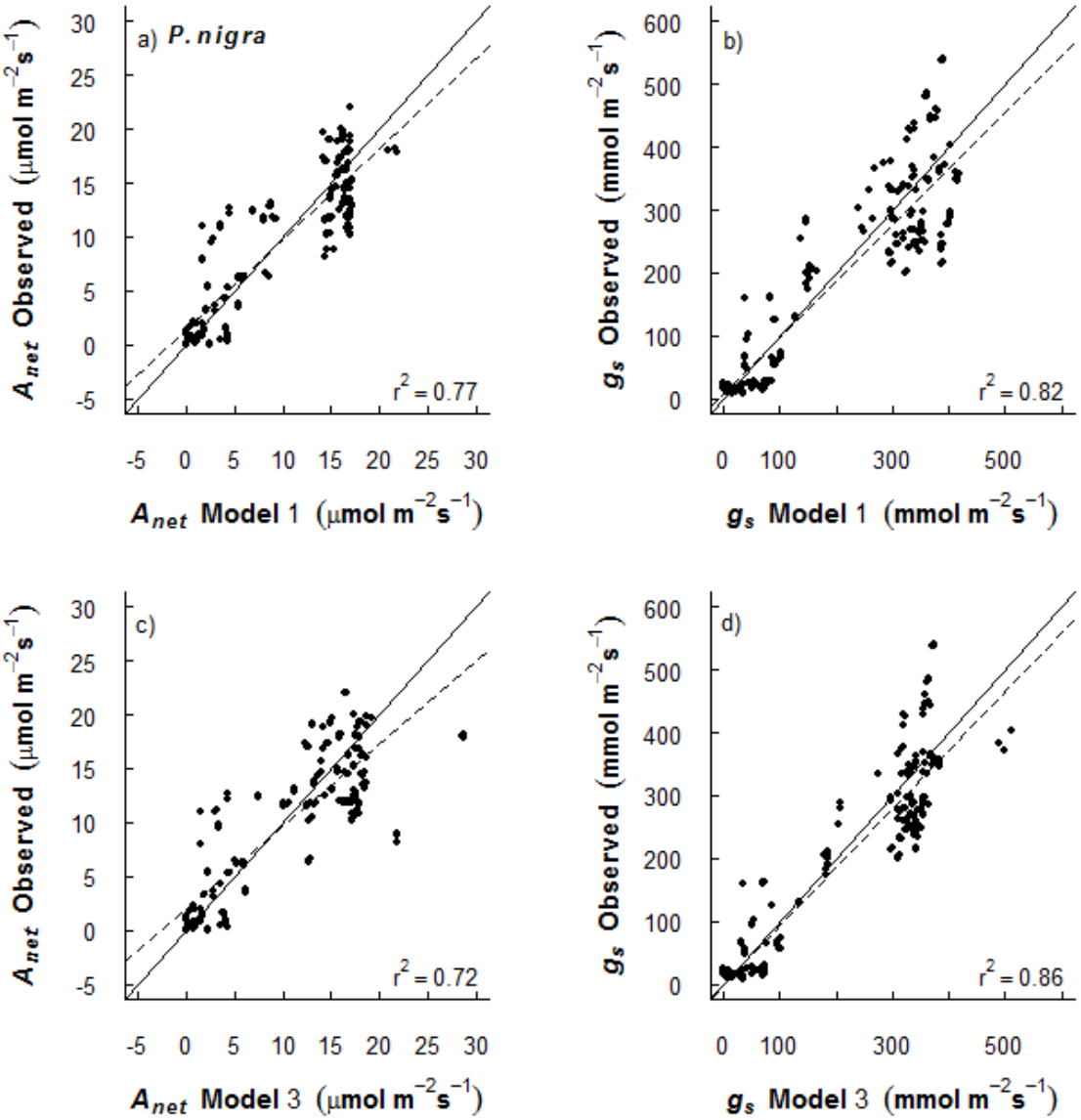

Fig. 8. Model validation, observed vs. predicted A_{net} and g_s shown for *P. nigra*: a & b) Model 1, c & d) Model 3. The regression line (dotted line) and r^2 are shown, along with the 1:1 line (solid line).

	Regression fit	r^2	95 % CI Intercept	95 % CI Slope	Correlation F †	Correlation P	RMSD
***P. x euramericana*: A_{net}**							
Model 1	$y = 0.56 - 0.89x$	0.83	0.66	0.05 ***	1169	< 0.001	3.26
Model 3	$y = 0.79 - 0.75x$	0.78	0.75 *	0.05 ***	865.3	< 0.001	4.65
***P. x euramericana*: g_s**							
Model 1	$y = 12.61 - 0.89x$	0.79	15.60	0.06 ***	941.8	< 0.001	78.97
Model 3	$y = 3.01 - 0.83x$	0.82	15.03	0.05 ***	1091	< 0.001	87.16
***P. nigra*: A_{net}**							
Model 1	$y = 1.45 - 0.84x$	0.77	0.72 ***	0.06 ***	763.4	< 0.001	3.36
Model 3	$y = 1.96 - 0.77x$	0.72	0.78 ***	0.06 ***	589.2	< 0.001	3.91
***P. nigra*: g_s**							
Model 1	$y = 8.50 - 0.90x$	0.82	13.61	0.05 ***	1083	< 0.001	65.45
Model 3	$y = 1.89 - 0.93x$	0.86	12.32	0.05 ***	1403	< 0.001	58.23

Table 6. Quantitative measures of the ability of the models to predict observed rates of A_{net} and g_s during validation. Results are show for *P. x euramericana* and *P. nigra*. The units of RMSD are (μmol CO_2 m^{-2} s^{-1}) for A_{net} and (mmol H_2O m^{-2} s^{-1}) for g_s. CI refers to the 95 % confidence interval surrounding the estimate of the regression line intercept/slope. The stars indicate whether the intercept/slope is significantly different to zero/one respectively: *** $p < 0.001$, ** $p < 0.01$, * $p < 0.05$. † indicates *P. x euramericana* is analysed on 1, 242 *d.f.* (degrees of freedom); *P. nigra* is analysed on 1, 230 *d.f.*

4.4 Discussion

4.4.1 Modelling A_{net} and g_s to include g_i

These results suggest there is no significant improvement in the accuracy of modelled A_{net} to warrant the addition of complexity to the model by including further processes and parameters. Testing, parameterisation and validation of the three model configurations showed the performance of Model 1 (the simplest model) and Model 3 (the most complex model) were very similar. Initial model testing with 'curve-specific' parameters produced highly accurate predictions of leaf-level A_{net} in all three models. In *P. x euramericana*, Model 3 performed marginally better than Model 1 and Model 2 having the highest r^2, lowest RMSD, and no detectable bias in predicted A_{net}. Simulated A_{net} by Model 2 was marginally improved compared to Model 1, but the differences between all three models were minimal. In *P. nigra*, the performance of Model 1 and Model 3 were such that it was difficult to distinguish between them. Both Model 1 and Model 3 had equally high r^2

values, but the RMSD was marginally lower in Model 1 compared to Model 3, suggesting a slight improvement in fit. Both models showed similar bias in predicted A_{net}. Model 2 did not perform as well. The goodness of fit of the data was only slightly reduced, but the RMSD was increased quite substantially compared to the other two models. Further confirmation of the high performance of all three models was seen in plots of A_{net} versus c_a where, certainly for c_a > 20 Pa, all three models predicted A_{net} within the error of the observations. Atmospheric CO_2 concentrations of between 20 to 40 Pa are currently relevant concentrations, and the models were shown to perform well over this range. A high performance was maintained above this, the full curve was measured up to an atmospheric CO_2 concentration of 180 Pa, suggesting necessary accuracy would be maintained in climate change studies with rising concentrations of atmospheric CO_2.

Each model was parameterised with a single set of parameter values. Each model calibrated with a single set of parameter values maintained a high level of accuracy of simulated leaf-level A_{net}. Similar results, in terms of the performance of each model relative to each other, were produced to the previous model testing stage. In *P. x euramericana*, the models followed the same hierarchy whereby simulated A_{net} was most accurate in Model 3 and least accurate in Model 1, although these differences were minimal. In addition, Model 1suggested reduced bias in predicted A_{net} as the regression line intercept was not different to zero. In *P. nigra*, model performance was marginally better in Model 1 compared to Model 3 (same r^2, marginally lower RMSD), although no bias was detected in A_{net} simulated by Model 3. Model 2 performed least well out of all three. In both *P. x euramericana* and *P. nigra*, simulated A_{net} using default parameter values ($JULES\_{def}$) was seen to substantially reduce the accuracy of predicted A_{net}. This highlighted the importance of finding appropriate parameter values in order to correctly simulate the observed processes. In addition, these results demonstrated the large sensitivity of the JULES A_{net} - g_s model is its original configuration to the photosynthetic parameter V_{max}.

The r^2 of the models calibrated with a single set of parameter values ranged between 0.69 to 0.84, this is compared to 0.96 to 0.98 during model testing with 'curve-specific' parameters. Therefore, some loss of accuracy was seen. This is to be expected, however, as each model was simulating observations from across the growing season with the use of a single calibrated parameter set, and it was seen that values inferred from each A_{net} - c_i and

A_{net} - P_{PFD} curve varied across the growing season. Given the sensitivity of modelled A_{net} to parameter values, as seen for the sensitivity of Model 1 to V_{max}, an exact match between the observed and modelled data can never be expected, given the large within season variation.

Comparison of Model 2 and Model 3 during both model testing and parameterisation suggested that using different temperature response functions (Q_{10} vs. exponential functions) and Rubisco kinetic constants, and changing the description of the dependence of photosynthetic rate on light does not generate any substantial improvements in the accuracy of simulated A_{net}. Temperature response functions are crucial to allow accurate simulation of rates of photosynthesis at the leaf temperature. This is particularly important for global land-surface schemes that need to predict carbon uptake in terrestrial ecosystems under wide ranging and highly variable atmospheric conditions. This work indicates both sets of parameterisations for the temperature responses of photosynthesis perform well. However, no firm conclusions can be drawn. During model testing and parameterisation, the A_{net} - c_i data used had been recorded under relatively controlled conditions (i.e. close to 25^{o}C). Deviations in measurement temperature occurred, but were nowhere near the large range needed to fully test the performance of different temperature response functions (e.g. 10 to 40^{o}C).

Validation of parameterised Model 1 and Model 3 using an independent data set revealed that leaf-level A_{net} was simulated more accurately by Model 1 in both genotypes. The r^2 were higher in Model 1 and RMSD marginally lower. The increased accuracy seen in modelled A_{net} with Model 1 as opposed to Model 3 was greatest in *P. x euramericana*. In *P. x euramericana*, there was also less bias in simulated A_{net} in Model 1 compared to Model 3. In *P. nigra*, both models displayed bias in predictions, showing a trend to over-predict rates of A_{net}, however this trend was less pronounced in Model 1 compared to Model 3. Conflicting results were obtained for simulated g_s. In both genotypes, the r^2 were increased using Model 3. However, in *P. x euramericna* the RMSD was also increased using Model 3, whereas in *P. nigra* it decreased, nevertheless, the accuracy of simulated g_s by both models was still comparably high, and models displayed similar bias in predicted rates of g_s. Given the high accuracy of simulated leaf-level A_{net} and g_s by both Model 1 and Model 3, it was concluded that accounting for g_i in the JULES A_{net} - g_s sub-model, for

incorporation into a large-scale, land-surface scheme does not lead to improvements that are significant enough to justify its inclusion.

Field measurements made in chapter 3 showed that estimating V_{max} under the assumption of infinite CO_2 conductance from c_i to c_c led to significant underestimation of V_{max}. Therefore, it was suggested that V_{max} is not such a straightforward biochemical parameter it was always considered to be, and that it is not directly transferable from measurements to model, since it is significantly different when measured at either c_i or c_c. Consequently, including the internal transfer of CO_2 from c_i to c_c was not seen to impact the accuracy of modelled A_{net} and g_s in the A_{net} - g_s model since the value of V_{max} used in each model configuration compensated for the presence/absence of this additional pathway. Therefore, for photosynthesis models used within land-surface schemes, whose primary role is to predict ecosystem gains and losses of NPP, we suggest that the calibration of V_{max} with an appropriate value is the most important step to generate accurate simulations of rates of A_{net} and g_s, rather than inclusion of the additional CO_2 transfer pathway itself in the model. Given the high sensitivity of modelled A_{net} to V_{max}, using a value of V_{max} derived from a model assuming finite g_i in a model that assumes infinite g_i would likely lead to overestimation of leaf-level A_{net} and canopy productivity, and vice versa. Therefore, with the universal importance of V_{max} in models of photosynthesis within land-surface schemes and global circulation models, it is essential to understand the impact of g_i on parameter estimation to ensure V_{max} is applied appropriately in these models. It may be beneficial to modify the use of the term V_{max} in future to reflect the importance of g_i in this parameter value.

4.4.2 Limitations

Some limitations were identified in this study that may affect model performance. Values of g_i were estimated from $A_{net} – c_i$ measurements by the curve-fitting procedure of Sharkey *et al*., (2007). Performing $A_{net} – c_i$ curves requires rapid changes in CO_2 concentration around leaves, and g_i has been shown to respond quite strongly to changes in CO_2 concentration (During, 2003; Flexas *et al.*, 2007). Consequently, this method gives an estimate of the 'average' g_i over a given CO_2 range (Flexas *et al.*, 2008) which may not be optimal for model parameterisation. Nevertheless, studies that have compared different

methods of g_i determination show that they generally agree well (Pons *et al.*, 2009), suggesting other methods of determining g_i would generate similar results.
In Model 2 and Model 3, g_i was included as a constant. Few models simulating whole-pant carbon exchange consider the internal transfer of CO_2 as part of their parameterisation. The ISBA-Ags (Interactions Between Soil, Biosphere and Atmosphere) land-surface model (Calvet *et al.*, 1998), C-TESSEL (Tiled ECMWF Scheme for Surface Exchanges over Land) surface exchange scheme (Voogt *et al.*, 2005), which is based on the ISBA-Ags scheme, and the SPA (Soil-Plant Atmosphere) model (Williams *et al.*, 1996) include the transfer of CO_2 from c_i to c_c. In these three examples, g_i is also parameterised as a constant value. This may not be the most accurate representation of the process, because similar to g_s, g_i is known to respond to changing environmental conditions in the long (days/weeks) and short (minutes) term (Flexas *et al.*, 2008; Warren, 2008). Therefore, its implementation as a process that has the capacity to change with environmental variables may be more appropriate. Currently, however, there are significant research gaps that would make this difficult. For example, the variation in g_i with temperature, and the response of g_i to light and vapour pressure deficit are areas that require more attention (Bernacchi *et al.*, 2002; Flexas *et al.*, 2008; Niinemets *et al.*, 2006; Warren, 2008; Warren & Adams, 2006; Warren & Dreyer, 2006). Further issues that would need to be considered include an appropriate way to scale g_i within the canopy. It is understood that g_i is finite and variable, but that variability is difficult to predict. For example, recent work suggests that g_i does not necessarily scale with photosynthetic capacity and that c_i differs from c_c within and between species in a manner that is not easily predictable (Bernacchi *et al.*, 2001; Flexas *et al.*, 2008; Warren & Adams, 2006). Additionally, g_i shows relationships with leaf age and illumination within canopies which makes the issue of scaling within the canopy even more complex (Niinemets *et al.*, 2006).

4.5 Conclusions

Previous work in Chapter 3 had shown that estimates of the key photosynthetic parameter, V_{max}, were significantly higher when estimated under the assumption of finite internal conductance to CO_2. It is also understood that g_i is of similar quantitative importance to stomata and Rubisco in regulating photosynthesis. In light of this, this work modified a coupled model of leaf-level $A_{net} - g_s$ integral to a land-surface scheme to include the transfer of CO_2 from c_i to c_c. Different model configurations were tested to determine whether including g_i improved the accuracy of simulated leaf-level A_{net} in a photosynthesis

model applied in this way. Parameterisation and validation of model configurations assessed the ability of the models to simulate observed rates of A_{net} and g_s for the most productive, (top of canopy), leaves of *Populus x euramericana* and *P. nigra*. Results showed that including g_i in the $A_{net} - g_s$ model did not significantly improve predicted A_{net}. Model validation of the parameterised $A_{net} - g_s$ model revealed that including g_i actually marginally reduced the accuracy of simulated A_{net}. Simulated g_s was marginally improved when g_i was accounted for, however g_s was simulated to a high level of accuracy in both model configurations. Consequently, no justification was found for adding complexity, (additional processes and parameters), to the existing $A_{net} - g_s$ model. Validation of the calibrated parameter sets used in each model showed the suitability and transferability of these parameter values, as the accuracy of predicted A_{net} and g_s remained high. Additionally, comparison of predicted A_{net} simulated using calibrated parameter values to A_{net} simulated using default parameter values showed the degree of accuracy lost when using default values.

This work not only highlighted the impact of g_i on estimation of V_{max}, but also the sensitivity of modelled A_{net} to V_{max}. V_{max} is generally considered a directly transferable parameter from measurement to models, and between models, and is universally used to calibrate models of ecosystem carbon exchange. This work suggests, however, that V_{max} is more complex than the straightforward, transferable biochemical parameter it was always considered to be, since estimated values for this parameter are significantly different depending on whether it is measured at c_i or c_c. Consequently, including the internal transfer of CO_2 from c_i to c_c was not seen to impact the accuracy of modelled A_{net} and g_s in the A_{net} - g_s model since the value of V_{max} used in each model configuration compensated for the presence/absence of this additional pathway. Therefore, it was concluded that, for application within a land-surface scheme, whilst including g_i in the photosynthesis model had no impact on the accuracy of modelled A_{net} and g_s, accurate calibration of V_{max} with an appropriate value, i.e. derived at c_i or c_c as appropriate for the model, is vital. Given the importance of V_{max} in models of photosynthesis within land-surface schemes and global circulation models, it is essential modellers understand the impact of g_i on parameter estimation to ensure V_{max} is applied appropriately in these models.

Further work will continue with Model 1, the JULES $A_{net} - g_s$ model in its current configuration. The calibrated parameter sets validated in this work will be used in

following chapter, where predicted leaf-level A_{net} and g_s are scaled-up in JULES to simulate the growth and water-use of poplar SRC at the canopy-level.

Chapter 5

Simulating the growth and transpiration of poplar SRC: scaling up from the leaf-level

5.1 Introduction

With growing commitments in the UK to generate more energy from renewable sources, the proportion of land committed to growing dedicated bioenergy crops, such as poplar short rotation coppice (SRC), has the potential to significantly increase (DEFRA, 2007; Haughton *et al.*, 2009). Bioenergy crops are not currently represented in land-surface schemes. In the land-surface scheme JULES (Joint UK Land Environment Simulator), five vegetation types are recognised; broadleaf tree, coniferous tree, C_3 grass, C_4 grass and shrub. Poplar SRC, however, is very different to any of these vegetation types; firstly, poplar SRC is managed, secondly, it has a rapid growth rate, typically achieving full canopy closure in less than two years, and thirdly, poplar SRC has been shown to have very high rates of water-use. For land-surface schemes to realistically simulate exchanges of water, carbon and energy at the landscape scale, the representation of dedicated bioenergy crops, such as poplar SRC, in these models is imperative.

This is a new application for JULES, which is predominantly used to simulate the growth of natural vegetation in an "equilibrium" vegetation state. This will build on work from the previous chapter that calibrated parameter values for *P. x euramericana* and *P. nigra* for the leaf-level photosynthesis - stomatal conductance model integral to JULES. In this chapter, leaf-level fluxes are scaled to the whole plant. Modifications to JULES will be necessary to simulate the managed coppice rotation of poplar SRC for the two genotypes of poplar. In addition, changes to the allometric constants that determine the partitioning of carbon to different plant stores will be needed, and new values for the plant-specific parameters that control the growth and water-use will be required. Model performance with the new parameterisations will then be tested against observations of poplar growth and water-use under ambient and elevated atmospheric CO_2 concentrations. Observations

used to inform and constrain the model in this study are from a free-air CO_2 enrichment (FACE) experiment located in Italy, where both *P. x euramericana* and *P. nigra* were grown and managed as SRC. The desired output is a fully modified and parameterised model that can simulate the growth of *P. x euramericana* and *P. nigra*, so that it can be used in further work to explore how yield and water-use of this managed bioenergy crop respond to future climate change.

The JULES model was used as it contains the necessary processes required to simulate fluxes of carbon, water, and energy at the landscape scale, with the added advantage that the model can ultimately be run globally. Additionally, JULES is a community model, so changes made will contribute to the wider JULES modeling community. Therefore, the following objectives were addressed: 1) can the JULES model be modified to simulate the growth cycle of *P. x euramericana* and *P. nigra* SRC? 2) what are suitable values for the allometric constants and plant-specific parameters for *P. x euramericana* and *P. nigra*? 3) how well does the fully modified and parameterised model perform against observations?

5.2 Methods

5.2.1 Sites and data

Observations to aid in calibration and validation of the model were from one primary site located in central Italy, near the city of Tuscania (Viterbo, latitude 42°37'04"N, longitude 11°80'87"E, elevation 150m). Both *Populus x euramericana* (*P. deltoides* Bart. ex Marsh. x *P. nigra* L., I-214) and *P. nigra* L. (Jean Pourtet) trees were grown at this site which included free–air CO_2 enrichment (FACE) allowing detailed growth and physiological measurements to be made under both elevated and ambient atmospheric CO_2 concentrations. Trees were managed as SRC on a three-year rotation.

The site was planted in spring 1999 and six experimental plots (30 m x 30 m) were established within the plantation. Three plots represented control plots where trees were exposed to ambient concentrations of atmospheric CO_2. The remaining three plots were fitted with FACE technology so trees were exposed to concentrations of atmospheric CO_2 predicted for the middle of this century (around 550ppm). To avoid cross contamination between control and FACE plots, the minimum distance between plots was 120 m. Within

each experimental plot three genotypes of poplar were established; *P. x euramericana, P. nigra* and *P. alba* (2AS-11), although this work is only concerned with *P. x euramericana* and *P. nigra,* these two genotypes having being identified as suitable candidate species for bioenergy. The plantation was fully irrigated. Arrangement of trees in the FACE facility, application of nitrogen fertilizer and the method for elevating the concentration of atmospheric CO_2 are described in more detail in the following papers (Calfapietra *et al.*, 2001; Miglietta *et al.*, 2001; Tricker *et al.*, 2009; Tricker *et al.*, 2005).

Observations of the growth of poplar SRC (canopy height, *h*; leaf area index, *LAI*; total carbon content of the vegetation, C_v; and carbon content of the leaves, *L*, and the above- and belowground biomass, *W* and *R* respectively) that are relevant to this work and used to inform and validate the model, are reported in Table 1 and Table 2. Table 1 reports the carbon contents of the component parts of the total biomass (*L*, *W* and *R*) measured at the poplar free-air CO_2 enrichment (popFACE) site for both *P. x euramericana, P. nigra*. The total biomass (C_v) is the sum of all the three component parts. Values typically represent the biomass recorded by destructive sampling at the end of each growing season, for more details, readers are referred to the individual references. Where not recorded as actual carbon content, the biomass has been converted assuming a mean carbon (C) concentration of 48% according to Gielen *et al*., (2005). The leaf biomass was not commonly recorded in each year, Gielen *et al*., (2005) reported the leaf carbon content measured in 2000 and 2001. Consequently these values were used to infer the leaf biomass in the second rotation based on *LAI*. Table 2 shows the yearly maximum value of stem height and *LAI* recorded in each genotype over two rotations at the popFACE site. Significant differences in height and *LAI* between genotypes are indicated (with values that are not significantly different highlight in bold). The value of maximum *LAI* achieved each year is significantly higher in *P. nigra* over the course of both rotations. Interestingly height is generally higher in *P. x euramericana*, although for much of the first rotation there were no significant differences between the two genotypes. The relative differences between elevated and ambient CO_2 treatments (%) is calculated as ((FACE-control)/control) and is shown in Table 2 for years where the FACE treatment has a statistically significant effect only. It is shown that FACE treatment has a positive effect on height, ranging between + 2.4 % to + 14 % depending on year and genotype. The FACE effect on *LAI* ranges between + 1.5 % to + 84 % depending on year and genotype. However, a significant effect of FACE treatment is not apparent in all years.

		1st rotation				2nd rotation						
		2000		2001		2002		2003		2004		
		Control	FACE	Control	FACE	Control	FACE	Control	FACE	Control	FACE	Ref.
P. nigra	Aboveground biomass (kg C m^{-2})	1.13 (0.17)	1.30 (0.19)	2.57 (0.14)	2.96 (0.14)	0.97 (0.08)	1.08 (0.07)	1.48 (0.07)	1.66 (0.17)	3.36 (0.24)	4.27 (0.29)	a, b, c
	Belowground biomass (kg C m^{-2})	0.11 (0.02)	0.16 (0.04)	0.41 (0.13)	0.49 (0.1)	0.32 (0.06)	0.38 (0.1)	0.31 (0.05)	0.34 (0.1)	0.48 (0.03)	0.53 (0.05)	a, b, c, d
	Leaf biomass (kg C m^{-2})	0.25 (0.01)	0.28 (0.01)	0.52 (0.02)	0.57 (0.02)	0.25 (0.01)	0.28 (0.01)	0.52 (0.02)	0.57 (0.02)	0.52 (0.02)	0.57 (0.02)	e
	Total biomass (kg C m^{-2})	**1.49**	**1.74**	**3.49**	**4.02**	**1.54**	**1.74**	**2.30**	**2.57**	**4.36**	**5.37**	
P. x euramericana	Aboveground biomass (kg C m^{-2})	0.79 (0.12)	1.09 (0.2)	1.83 (0.14)	2.32 (0.15)	0.69 (0.12)	0.69 (0.14)	1.34 (0.16)	1.34 (0.13)	3.74 (0.24)	4.32 (0.38)	a, b, c
	Belowground biomass (kg C m^{-2})	0.17 (0.04)	0.35 (0.09)	0.38 (0.1)	0.49 (0.12)	0.31 (0.09)	0.45 (0.09)	0.30 (0.08)	0.45 (0.1)	0.43 (0.04)	0.67 (0.14)	a, b, c, d
	Leaf biomass (kg C m^{-2})	0.25 (0.01)	0.26 (0.022)	0.49 (0.007)	0.52 (0.02)	0.25 (0.01)	0.26 (0.02)	0.49 (0.007)	0.52 (0.02)	0.49 (0.007)	0.52 (0.02)	e
	Total biomass (kg C m^{-2})	**1.21**	**1.70**	**2.70**	**3.33**	**1.26**	**1.40**	**2.14**	**2.31**	**4.67**	**5.51**	

Table 1. Carbon (C) contents of the component parts of biomass (aboveground, *W*; belowground, *R*, and leaf biomass, *L*) measured at the popFACE SRC plantation in both *Populus* genotypes. Control refers to an ambient CO_2 concentration of ~380 ppm; FACE refers to an elevated CO_2 concentration of ~550 ppm. The total biomass (total carbon content; C_v) is the sum of all the three component parts. Where not recorded as actual carbon content, the biomass has been converted assuming a mean C concentration of 48% according to Gielen *et al*., (2005). Values are shown ± their standard error, they typically represent the biomass recorded at the end of the growing season, for more information, please refer to individual references; a = Calfapietra *et al*., (2003b); b = Liberloo *et al*., (2006); c = Liberloo *et al*., (2005); d = Lukac *pers comm*. (2007); e = Gielen *et al*., (2005).

		1st rotation									2nd rotation						
		1999			2000			2001			2002			2003			
		Control		FACE	Control		FACE	Control		FACE	Control		FACE	Control		FACE	Ref.
P. nigra	Height (m)	1.68 (0.03)	+11%	1.86 (0.03)	**5.87 (0.08)**	ns	**6.06 (0.06)**	**8.73 (0.14)**	+6%	**9.28 (0.10)**	4.22 (0.02)	ns	4.32 (0.02)	6.20 (0.1)	+2.4%	6.35 (0.05)	a, b, c, d
	LAI (m^{-2} m^{-2})	0.95 (0.02)	+80%	1.71 (0.13)	5.93 (0.20)	ns	6.32 (0.41)	7.24 (0.16)	ns	7.55 (0.21)	5.13 (0.20)	+7%	5.50 (0.25)	6.70 (0.67)	+1.5%	6.80 (0.14)	b, c, e, f, i
P. x eur.	Height (m)	1.41 (0.04)	+11%	1.56 (0.03)	**5.76 (0.05)**	ns	**5.92 (0.14)**	**8.45 (0.12)**	+7%	**9.01 (0.15)**	4.23 (0.02)	ns	4.33 (0.02)	6.20 (0.18)	+14%	7.20 (0.05)	a, b, c, d
	LAI (m^{-2} m^{-2})	0.44 (0.02)	+84%	0.81 (0.04)	3.68 (0.10)	ns	3.95 (0.16)	4.53 (0.31)	ns	4.57 (0.23)	3.90 (0.15)	+13%	4.40 (0.25)	5.60 (0.27)	+18%	6.60 (0.27)	b, c, e, f

Table 2. Maximum stem height (*h*) and leaf area index (*LAI*) recorded in each genotype over two rotations at the popFACE facility in Italy. Control refers to an ambient CO_2 concentration of ~380 ppm; FACE refers to an elevated CO_2 concentration of ~550 ppm. Values are shown ± their standard error. Values in bold indicate no significant difference between genotypes ($p > 0.05$), for more information please refer to the individual references. The relative differences between FACE and control treatments (%) and is calculated as ((FACE-control)/control) and is shown only where FACE treatment has a significant effect, ($p < 0.05$), otherwise, ns (not significant), is shown. For more information, please refer to the individual references, a = Calfapietra *et al*., (2003a); b = Liberloo *et al*., (2004); c = Liberloo *et al*.,(2005); d = Calfapietra *et al*., (2001); e = Gielen *et al*., (2001); f = Gielen *et al*., (2003); g = Liberloo *et al*., (2004); h = Liberloo *et al*., (2005); i = Liberloo *et al*., (2006).

5.2.2 Driving data

Meteorological data required to drive the model were downward longwave radiation (W m^{-2}), downward shortwave radiation (W m^{-2}), precipitation rate (kg m^{-2} s^{-1}), specific humidity (kg kg^{-1}), air pressure (Pa), air temperature (K), and total wind speed (m s^{-1}). These were collected at the popFACE site by an automatic weather station (AWS) for the periods 01 Jan 1999 to 31st Dec 2000, 25th April to 24th to Sept 2003, 28th Oct 27th to Nov 2003, and 11th May to 31st Aug 2004. A continuous data set is needed to drive the land-surface scheme, therefore where meteorological data were not collected or missing due to instrument failure, (i.e. all of 2001 and 2002, and periods during 2003 and 2004), data were in-filled using meteorological data recorded at a 'FLUXNET' site with an established AWS (www.fluxnet.ornl.gov). The two nearest FLUXNET sites were considered; 1) Collelongo, latitude 41^{o}52'N, longitude 13^{o}38'E, elevation 1550 m, and 2) San Rossore, latitude 43^{o}43'N, longitude 10^{o}17'E, elevation 4 m. It was decided to use data from San Rossore as this was closest in elevation to the popFACE site, with 146 m vs. 1400 m difference in elevation between the popFACE and San Rossore/Collelongo sites respectively. Although complete data sets from the FLUXNET site were required for all of 2001 and 2002, fortunately in 2003 and 2004 data were available from the popFACE AWS for much of the growing season. Therefore, in these years data only needed gap-filling for periods of autumn and winter when the trees were not actively growing.

Linear regression was used to assess the relationship between meteorological variables at the San Rossore site and popFACE site for periods where data existed for both sites. For all the variables assessed, the slope and intercept were considered close enough to one and zero respectively to warrant using the San Rossore data without alteration (shortwave radiation, slope = 0.88, intercept = 3.5, r^2 = 0.94; longwave radiation, slope = 0.95, intercept = 59.7, r^2 = 0.78; air temperature, slope = 0.81, intercept = 22.3, r^2 = 0.91; specific humidity, slope = 0.85, intercept = 0.003, r^2 = 0.84). As the popFACE site was irrigated, the precipitation was modified using an artificial data set of precipitation that essentially added rainfall at regular intervals over the main growing season (April - October), so as to avoid the development of water stress at the site.

5.2.3 Model

5.2.3.1 JULES: Joint UK Land Environment Simulator

The land-surface scheme used in this study is the Joint UK Land Environment Simulator (JULES). It originated from the land-surface model MOSES (Met Office Surface Exchange Scheme), used in the UK Met Office Hadley Centre climate model. Elements of the model important to this work are outlined here, but for a more comprehensive description readers are referred to Cox (2001) and Essery *et al*., (2001).

5.2.3.2 Energy fluxes

JULES calculates the surface exchange of energy, mass and momentum for nine surface types (five vegetation and four non-vegetation) under the same near-surface forcing. The surface energy balance is calculated separately for each surface type as the sum of the three turbulent energy fluxes at the atmospheric boundary layer (equation 1); H (W m^{-2}) the sensible heat flux, λE (W m^{-2}) the latent heat flux, and G (W m^{-2}) the ground heat flux. R_n (W m^{-2}) is net radiation at the surface.

$$R_n = \lambda E + H + G \qquad \text{(equation 1)}$$

The sensible heat flux, H, is the turbulent transfer of heat that is not associated with phase changes of water, i.e. dry convection. The latent heat flux, λE, is the transference of heat energy from the surface to the atmosphere as a result of a change of state of water from liquid to gaseous phase, i.e. evaporation. The ground heat flux, G, is the transference of heat energy into the soil, which occurs mainly by conduction. Under dense vegetation , G can be negligible. The G also depends on soil thermal properties which are a function of soil composition, bulk density and soil moisture content.

The surface net radiation balance of each surface type at temperature T_* is determined as the sum of incoming and outgoing shortwave and longwave radiation fluxes, given by equation 2:

$$R_n = S_W(1-\alpha) + L_W - \varepsilon\sigma T_*^4 \qquad \text{(equation 2)}$$

where S_W (W m^{-2}) is the insolation (direct and diffuse), α is the surface albedo, L_W (W m^{-2}) is the downward long-wave flux, ε is the emissivity of the surface, σ is the Stefan-Boltzmann constant and T_* (K) is the land surface temperature. The core calculation in the scheme ensures the downwelling fluxes (S and L_W) are balanced by the outgoing fluxes of H, λE, G, reflected shortwave radiation and upwelling thermal energy (σT_*^4) as in equation 3 (Alton *et al.*, 2007).

$$S_W(1-\alpha)+L_W = \sigma T_*^4 + \lambda E + H + G \qquad \text{(equation 3)}$$

The heat fluxes are directly determined from the available energy, the gradients in surface and near-surface properties (temperature or humidity) and resistances (aerodynamic, r_a, and/or stomatal, r_s) (equations 4 to 6). The total evaporation, E (equation 4), is made up of three components; evaporation from the canopy store, transpiration by vegetation, and bare soil evaporation. The factor ψ (equation 4) accounts for (potential rate) evaporation from a wet canopy store and plant limited transpiration through stomatal conductance. The total evaporation and other heat fluxes are defined as:

$$E = \frac{\rho\psi}{r_a}\left[q_*^s - q_1\right] \qquad \text{(equation 4)}$$

$$H = \frac{\rho c_p}{r_a}\left[T_* - T_1\right] \qquad \text{(equation 5)}$$

$$G = \frac{2\lambda_{dry}}{\Delta z}\left[T_* - T_{s1}\right] \qquad \text{(equation 6)}$$

where, r_a (m s^{-1}) is the aerodynamic resistance, q_*^s and q_1 (both kg kg^{-1}) are saturated and unsaturated specific humidities at the surface and reference level, T_*, T_1 and T_{s1} (all K) are the surface, reference level and top soil layer temperatures respectively, ρ (kg m^{-3}) is the density of air, c_p (J kg^{-1} K^{-1}) is the specific heat capacity of air, λ_{dry} (W m^{-1} K^{-1}) is the soil thermal conductivity, and Δz is the thickness of the top soil layer. r_a and r_s are both functions of the surface characteristics, wind speed and stability of the atmosphere. r_s is the bulk stomatal resistance of the canopy, and it controls the resistance to water loss from transpiring vegetation. r_a controls the rate of turbulent diffusion of water and heat away from a surface. It is inversely proportional to wind speed and changes with the height of the vegetation (Monteith & Unsworth, 1990).

5.2.3.3 Carbon fluxes

Leaf-level carbon fluxes (described in chapter 4) are scaled to the canopy-level following the method of Sellers *et al*., (1992). Top-of-canopy leaf-level values are multiplied by a function of canopy leaf area index, *LAI*, to yield canopy-level values of conductance, g_c, photosynthesis, W_c, and dark respiration, R_{dc}:

$$g_c = g_s f_{par} \quad \text{(equation 7)}$$

$$W_c = W f_{par} \quad \text{(equation 8)}$$

$$R_{dc} = R_d f_{par} \quad \text{(equation 9)}$$

$$f_{par} = \frac{1-\exp\{-kLAI\}}{k} \quad \text{(equation10)}$$

where, k is the PAR extinction coefficient, $k = 0.65$ for poplar SRC canopies (Gielen *et al.*, 2003). The vegetation canopy-level surface carbon balance is calculated as:

$$NPP = GPP - R_P \quad \text{(equation 11)}$$

where *NPP* (kg C m^{-2} s^{-1}) is net primary productivity, *GPP* (kg C m^{-2} s^{-1}) is the gross primary productivity, and R_p (kg C m^{-2} s^{-1}) is the total autotrophic (plant) respiration. R_p is the sum of maintenance and growth respiration. The latter is assumed to be a fixed fraction, r_g, of the *NPP*. The maintenance respiration is a simple function of the canopy dark respiration, R_{dc}. This yields the following equations for canopy-level *GPP* and *NPP*:

$$GPP = 0.012\{W_c + \beta R_{dc}\} \quad \text{(equation12)}$$

$$NPP = 0.012(1-r_g)\left\{W_c - \beta R_{dc}\left(\beta + \frac{N_r + N_s}{N_l}\right)\right\} \quad \text{(equation 13)}$$

where W_c is the canopy photosynthesis, β is the soil moisture stress factor, 0.012 converts from units of mol CO_2 m^{-2} s^{-1} to kg C m^{-2} s^{-1}, N_r, N_s and N_l (all kg N kg C^{-1}) are the nitrogen contents of the root, stem and leaves respectively.

5.2.3.4 Vegetation growth

In JULES, vegetation growth is controlled by the dynamic global vegetation model (DGVM) TRIFFID (top-down representation of interactive foliage and flora including dynamics). The plant distribution and soil carbon are updated in the model based on climate sensitive CO_2 fluxes at the land-atmosphere interface (Cox, 2001). The net flux of carbon (plant photosynthesis and respiration), calculated on an hourly/sub-hourly time step, is used to update leaf area index (*LAI*) and canopy height of the vegetation, and the soil carbon store on a daily time step. The rates of photosynthesis and plant respiration calculated depend on both climate and atmospheric CO_2 concentration, as are the changes in vegetation dynamics and soil carbon. In its standard configuration, JULES recognises five plant functional types; broadleaf tree, coniferous tree, C_3 grass, C_4 grass and shrub. In this work JULES is developed to model a managed SRC bioenergy crop of *Populus spp*.. JULES models natural vegetation dynamics through two processes, growth and competition, which are described by two first order differential equations (see Cox, 2001; equations 1 & 2). As this work aims to simulate a managed SRC crop, the competition element of the model is not required and is essentially switched off.

The allocation of carbon in the vegetation is described by equation 14. The vegetation carbon density, C_v, is related allometrically to changes in the balanced *LAI*, L_b, which is the potential achievable *LAI* if the plant was in full leaf. C_v is calculated as the total contribution of carbon from three vegetation pools; leaf, *L*, root, *R*, and stem, *W*, carbon, which are determined as follows:

$$C_v = L + R + W \qquad \text{(equation 14)}$$

$$L = \sigma_l L_b \qquad \text{(equation 15)}$$

$$R = L \qquad \text{(equation 16)}$$

$$W = a_{wl} L_b^{\,b_{wl}} \qquad \text{(equation 17)}$$

where, σ_l is the specific leaf carbon density (kg C m^{-2} LAI^{1}) of the PFT, and both a_{wl} and b_{wl} are PFT-dependent parameters in the power law relating *LAI* and total stem biomass.
Equation 17 describes carbon allocation to the stem. This allometric relationship is a function of the balanced *LAI*, L_b, allowing the stem carbon density to change in a realistic manner with the growth cycle of the vegetation, i.e. accumulation of more carbon when the vegetation is in full leaf and generating carbohydrates for growth. Equation 18 describes the ratio of total stem

carbon to respiring stem carbon, *S*. The respiring stem carbon is calculated using a "pipemodel" approach in which live stem-wood is proportional to leaf area and canopy height (equation 19).

$$W = a_{ws} S \qquad \text{(equation 18)}$$

$$S = \eta_{sl} h L_{AI} \qquad \text{(equation 19)}$$

where a_{ws} is a PFT-dependent parameter relating the woody biomass to the live stem biomass, η_{sl} is a live stem-wood coefficient (kg C m^{-2} LAI^{-1}) which also depends on PFT, h is canopy height (m) and L_{AI} is the actual *LAI* of the canopy, which is determined as the L_b modified by the phenological status of the vegetation. Through combining equations 17, 18 and 19, canopy height is then diagnosed from the total stem biomass using equation 20:

$$h = \frac{W}{a_{ws}\eta_{sl}} \left\{ \frac{a_{wl}}{W} \right\}^{\frac{1}{b_{wl}}} \qquad \text{(equation 20)}$$

5.2.4 Model parameters

5.2.4.1 Leaf-level carbon and water-exchange

Parameters required by the photosynthesis - stomatal conductance sub-model to determine leaf-level fluxes of carbon and water are V_{max} (the maximum carboxylation rate of Rubisco), α_{int} (the intrinsic quantum efficiency), F_0 (the c_i/c_a ratio for specific humidity deficit in canopy) and D_c (the critical humidity deficit at the leaf surface). Values for these parameters were determined in the previous chapter (Chapter 4) for both *P. x euramericana* and *P. nigra*, but are shown again here for clarity (Table 3).

	V_{max} (μmol CO_2 m^{-2} s^{-1})	α_{int} (mol CO_2 mol^{-1} quanta)	F_0	D_c (kg kg^{-1})
P. x euramericana	74.34	0.076	0.875	0.07
P. nigra	69.84	0.076	0.875	0.07

Table 3. Calibrated parameter values required by the photosynthesis - stomatal conductance sub-model.

5.2.4.2 Soil

JULES has four soil layers extending down to a maximum depth of 3 m. The modelled root-depth for poplar SRC is set at 3 m and root density decreases exponentially with depth. Soil hydraulic parameters for the van Genuchten model and soil thermal parameters (Essery *et al.*, 2001) were obtained from Dharssi (2010). Dharssi (2010) has created a new high resolution soil texture map with parameter values required by the model for six recognised soil types that merges data from three separate sources; Harmonised World Soil Database (FAO/IIASA/ISRIC/ISS-CAS/JRC, 2008), State Soil Geographic Database (United States region,(Miller & White, 1998)) and point observations of soil sand, silt and clay fractions. The van Genuchten parameters for the six soil types are from Wosten *et al*.,(1999). These parameter values are used in the Met Office Unified Model. The soil texture map and associated parameters are on a grid of 25 km and values used in this work were taken from the grid box closest in latitude and longitude to the popFACE site. These parameter values are shown in Table 4. The soil parameters are therefore not site local as this information was not available, however the Met Office soil ancillary files, provide a suitable alternative.

$1/(n\text{-}1)$ and $1/\alpha$ (m) are both parameters of the van Genuchten model. k_s (kg m^{-2} s^{-1}) is the hydraulic conductivity at saturation. θ_{sat} (m^3 m^{-3}) is the volumetric soil moisture content at saturation, at which point transpiration is not limited by soil moisture, θ. θ_{crit} (m^3 m^{-3}) is the volumetric soil moisture concentration at the critical point, below which the limit on transpiration increases linearly with decreasing θ. θ_{crit} corresponds to a matric potential greater than –33 kPa, where $\beta = 1.0$. θ_{wilt} (m^3 m^{-3}) is the volumetric soil moisture concentration at wilting point when transpiration ceases, this corresponds to a matric potential of less than –1500 kPa, where $\beta = 0$ (see equation 5 in chapter 4). C_{dry} (J m^{-3} K^{-1}) is the dry soil heat capacity and λ_{dry} (W m^{-1} K^{-1}) is the dry soil thermal conductivity.

$1/(n-1)$	$1/\alpha$ (m)	k_s (kg m^{-2} s^{-1})	θ_{sat} (m^3 m^{-3})	θ_{crit} (m^3 m^{-3})	θ_{wilt} (m^3 m^{-3})	C_{dry} (J m^{-3} K^{-1})	λ_{dry} (W m^{-1} K^{-1})
7.1356	0.2683	0.0035	0.4435	0.3112	0.1823	1222180.0	0.2394

Table 4. Soil hydraulic and thermal parameters required by the van Genuchten model used in JULES and their values used in this work. These parameters do not vary with soil depth. The parameters were obtained from Dharssi (2010). Where, $1/(n-1)$ is an exponent used in the van Genuchten model; $1/\alpha$ is a parameter of the van Genuchten model; k_s is the hydraulic conductivity at saturation; θ_{sat} is the volumetric soil moisture content at saturation; θ_{crit} is the volumetric soil moisture concentration at the critical point; θ_{wilt} is the volumetric soil moisture concentration at the wilting point; C_{dry} is the dry soil heat capacity and λ_{dry} is the dry soil heat conductivity.

5.2.4.3 Surface properties

The aerodynamic resistance, r_a, depends on roughness length, z_o, wind speed and atmospheric stability. For vegetated surfaces, z_o is parameterised through two plant-functional type (PFT)-dependent parameters; i) the roughness length for momentum (z_{om}) as a fixed fraction of the vegetation height (h) (dz_{om}/d_h), and ii) the roughness length for heat (z_{oh}) as a fixed fraction of the roughness length for momentum (z_{oh}_ z_{om}). Poplar species are well known for large stomatal conductances (low stomatal resistance, r_s) (Hall, 2002). With r_s small or of the same magnitude as r_a in poplar *spp*., transpiration is inevitably more sensitive to r_a and so it has a strong effect on the canopy water-use. It was therefore likely that these two PFT-dependent parameters (dz_{om}/d_h and z_{oh}_ z_{om}) would impact on predictions of canopy transpiration. The structure of a poplar SRC canopy is much smoother and more uniform compared to a mature forest, therefore it was hypothesised that the default parameter values for a broadleaf tree, dz_{om}/d_h and z_{oh}_ z_{om}, would be unsuitable for simulating the water-use of poplar SRC. Two sets of parameter values were investigated for both PFT-dependent parameters; default values for a C_3 broadleaf PFT in JULES (Cox, 2001), and values reduced from the default to reflect the change in structure to a smoother canopy. dz_{om}/d_h was reduced by a factor of five (default value = 0.05, new value = 0.01) and z_{oh}_ z_{om} by a factor of 2 (default value = 0.1, new value = 0.05). The values used in simulations were selected based on their ability to reasonably model the water balance of poplar SRC.

5.3 Sensitivity analysis of growth parameters and model modifications

5.3.1 Identifying the key growth parameters

Finding accurate parameterisations for the PFT-dependent parameters that determine the growth was a key objective of this work. The first step was to identify the key 'growth' parameters central to the model and understand their interaction with each other and their relationship with model diagnostics such as h, LAI and C_v. The allocation of carbon in the vegetation is described by equations 14 to 20.

When equation 20 is written in full (equation 21.1), it is seen how the modelled canopy height depends on the balanced LAI, L_b, in addition to many of the PFT-dependent parameters. Further, as is seen in steps from equation 21.1 through to equation 21.6, the inverse of equation 20 is used to calculate L_b:

$$h = \frac{a_{wl} L_b^{\,b_{wl}}}{a_{ws}\eta_{sl}} \left\{ \frac{a_{wl}}{a_{wl} L_b^{\,b_{wl}}} \right\}^{\frac{1}{b_{wl}}} \qquad \text{(equation 21.1)}$$

$$h = \frac{a_{wl} L_b^{\,b_{wl}}}{a_{ws}\eta_{sl}} \left\{ \frac{1}{L_b^{\,b_{wl}}} \right\}^{\frac{1}{b_{wl}}} \qquad \text{(equation 21.2)}$$

$$h = \frac{a_{wl} L_b^{\,b_{wl}}}{a_{ws}\eta_{sl}} \left\{ \frac{1}{L_b} \right\} \qquad \text{(equation 21.3)}$$

$$h = \frac{a_{wl} L_b^{\,(b_{wl}-1)}}{a_{ws}\eta_{sl}} \qquad \text{(equation 21.4)}$$

$$L_b^{\,(b_{wl}-1)} = \frac{a_{ws}\eta_{sl} h}{a_{wl}} \qquad \text{(equation 21.5)}$$

$$L_b = \left(\frac{a_{ws}\eta_{sl} h}{a_{wl}} \right)^{\frac{1}{b_{wl}-1}} \qquad \text{(equation 21.6)}$$

These equations demonstrate the close relationship between h and LAI. The h is updated through LAI, and vice versa, and determination of both involves the key PFT-dependent growth parameters a_{wl}, b_{wl}, a_{ws} and η_{sl}. h and LAI are therefore very strongly linked and both are sensitive to the key growth parameters. This makes it very difficult to separate the sensitivity and dependence of h and L_b on each parameter. The total vegetation carbon density, C_v, is also sensitive to these growth parameters through equation 17, and σ_l is identified as an additional important PFT-dependent growth parameter through equations 15 and 16, where it is key in determining the carbon allocation to leaf and root pools. Therefore, in total, five key PFT-dependent parameters (a_{wl}, b_{wl}, a_{ws}, η_{sl} and σ_l) are identified as central to determining vegetation growth (h, LAI and C_v). Finding the right parameter values for these key growth and allocation parameters is very important yet difficult because many of them are not easily found in the literature. Even if available in the literature, it is often necessary to tune parameter values to allow a reasonable performance of the model. Additionally, the equations to calculate C_v, h and L_b indicate that many of the parameters may be correlated with behaviours that are very sensitive to each other.

The closest PFT approximation to poplar SRC currently in JULES is a broadleaf tree or shrub, however the growth strategies of these are fundamentally different to that of poplar SRC. In contrast to a mature broadleaf tree or shrub, SRC poplar achieves full canopy closure (maximum LAI) at considerably lower h whilst maximising the allocation of carbon to the stem. This is likely to upset the growth dynamics in the model, and will therefore require different values of the PFT growth parameters to the default parameters in order to achieve this alternative growth strategy.

5.3.2 Sensitivity analysis using Monte-Carlo simulation

A Monte-Carlo approach was taken to investigate the sensitivity of h, LAI and C_v to the key growth parameters. This was also used to identify suitable 'parameter space' for the key growth parameters based on observations of the h, LAI and C_v of *P. x euramericana* and *P. nigra* in the field. Usually in a Monte-Carlo experiment, all parameters vary randomly across a wide bound. For this work, however, using this method it was found that the signal of dependency of the output on the parameters was lost and no discernable relationships could be seen. Therefore, it was decided to narrow the bounds of the interacting parameters to their default value ± 25 % (Table 5). This would then demonstrate the general trend of the dependency plus the uncertainty due to the use of unknown parameters. Therefore, this unique

Monte-Carlo method allowed assessment of the sensitivity of model output to changes in each parameter while allowing for interactions with other linked parameters.

Using this approach a_{wl}, η_{sl} and σ_l were varied randomly between specified bounds (Table 5) for 5000 simulations. Each parameter could be plotted against each response variable whilst interacting parameters were maintained within ± 25 % of the default value to investigate their relationships and dependencies. The parameters a_{ws} and b_{wl} were excluded from the Monte-Carlo simulation as these parameters were directly correlated with other parameters. a_{ws} is a multiplier in the relationship between woody and live-stem biomass, and b_{wl} is an allometric exponent. According to Guan (2000) estimated sensitivity of strongly correlated parameters such as these is not meaningful. Therefore, values of a_{ws} and b_{wl} used default parameter values for a broadleaf tree already in the model (Table 6). The value of b_{wl} was taken from work by Enquist *et al*., (1998) who have determined allometric relationships for plant communities.

	a_{wl}	η_{sl}	σ_l
Default value	0.65	0.010	0.038
+ 25%	0.81	0.013	0.047
- 25%	0.49	0.008	0.028
MC upper bound	1.00	0.020	0.100
MC lower bound	0.10	0.001	0.001

Table 5. Default PFT-dependent parameter values in JULES for a broadleaf tree PFT for a_{wl}, η_{sl} and σ_l, ± 25% of their default value, and the upper and lower bounds specified in the Monte-Carlo simulation; a_{wl} (kg C m^{-2}) is the allometric coefficient relating the target woody biomass to the leaf area index; η_{sl} (kg C m^{-2}) is the live stemwood coefficient; σ_l (kg C m^{-2} leaf) is the specific density of leaf carbon.

Suitable parameter space for individual parameters was identified from the plots of model output (Figs. 1 & 2), primarily of *h, LAI,* C_v, versus parameter range, based on the observed growth of each poplar genotype in year three of the first rotation (data shown in Table 1 and Table 2). Once suitable parameter space had been identified, specific parameter values were tuned in simulations to generate the parameter set that best simulated the observations of growth in Table 1 and Table 2. The observed data used are therefore considered partially dependent, because some of the data were used to inform and constrain the model during parameterisation, i.e. observations of growth in 2001. The remaining data were used to validate the model. Unfortunately there was no completely independent data available with which to validate model performance. Additionally, it is stressed here that an exact calibration of every parameter was not possible with this model; complex interactions and tipping points meant that finding parameters that gave reasonable overall model performance were the best outcome.

5.3.3 Results: parameter sensitivity and values

Figures 1 and 2 show how the model output vary with each parameter, while all the interacting parameters are constrained at default ± 25%. A weak positive trend is evident between h and a_{wl} ($r^2 = 0.59$; Fig. 1a). A strong negative relationship is seen between a_{wl} and LAI (Fig. 1b). This is to be expected from equation 21.6 as a_{wl} is the denominator in the equation, suggesting as a_{wl} gets smaller, LAI will get bigger. This relationship between LAI and a_{wl} drives the negative relationship seen between W and a_{wl} (Fig. 2c). LAI and a_{wl} co-vary in equation 17, and LAI is involved in the power law in equation 17, which is responsible for increasing the magnitude of the decline. L and R are not directly determined by a_{wl}, but they are causally linked and display a negative trend when plotted against a_{wl} (Fig. 2a & b). Consequently, because the total carbon content of the vegetation, C_v, is determined by the contributions from L, R and W, and these are additive, there is a strong negative relationship between C_v and a_{wl} ($r^2 = 0.96$; Fig1.c). η_{sl} displays a strong negative trend with h, and to a lesser extent maximum LAI (Fig. 1d & e). It is clear that η_{sl} has a threshold point (~ 0.003 kg C m^{-2} LAI^{-1}) above which a reasonable performance of the model can be expected in terms of h and LAI, and below which predictions have a tendency to go out of reasonable bounds and become excessively large. η_{sl} does not display a significant relationship with C_v, L, R or W (Fig. 1f; Fig. 2d, e & f). σ_l shows a strong positive relationship with both L and R ($r^2 = 0.79$ for L and R; Fig. 2g &h), which is to be expected from equations 15 and 16 that indicate L and R are linear and proportional to σ_l. A negative trend between LAI and σ_l is evident (Fig. 1h), however this is very weak ($r^2 = 0.49$), so does not change the sign of the relationship between L/R and σ_l. σ_l does not directly determine W, however as it is causally linked it shows a strong negative relationship with W ($r^2 = 0.84$; Fig. 2i) because of the dominant effect of the power law in the calculation of W (equation 17), which also explains the negative trend between C_v and σ_l ($r^2 = 0.75$; Fig. 1i). This Monte-Carlo approach clearly shows the complex interactions between parameters, and highlights the importance of such methods to increase understanding of the behaviour of parameters in a complex, non-linear system such as this.

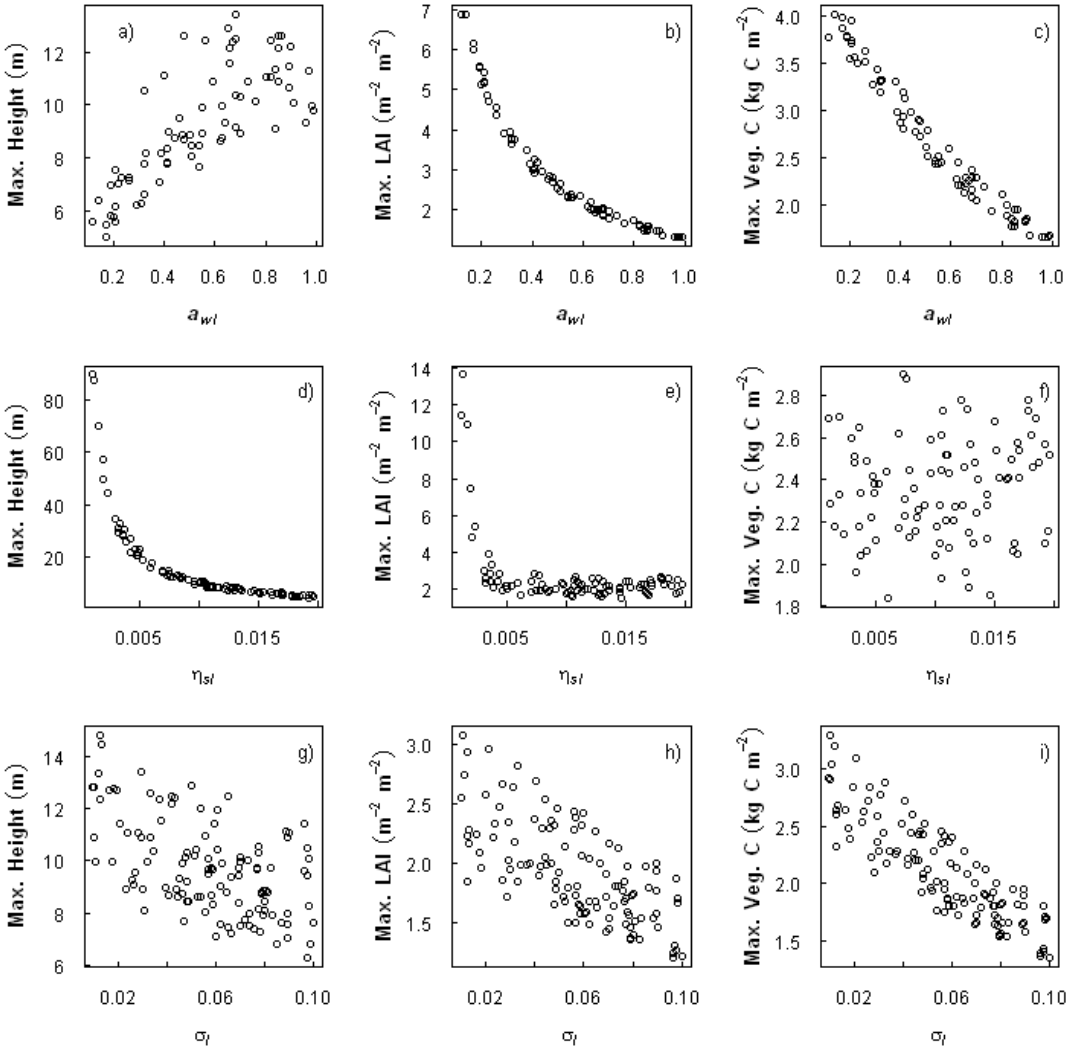

Fig. 1. The relationship between key growth parameters (a_{wl}, η_{sl} and σ_l) and maximum canopy height, *h*, maximum *LAI* and maximum total carbon content of the vegetation, C_v. Each parameter plotted on the x axis is allowed to vary over its full range specified in the Monte-Carlo simulation, and the other parameters are constrained to ± 25% of their default value (Table 5). a_{wl} (kg C m^{-2}) is the allometric coefficient relating the target woody biomass to the leaf area index; η_{sl} (kg C m^{-2}) is the live stemwood coefficient; σ_l (kg C m^{-2} leaf) is the specific density of leaf carbon.

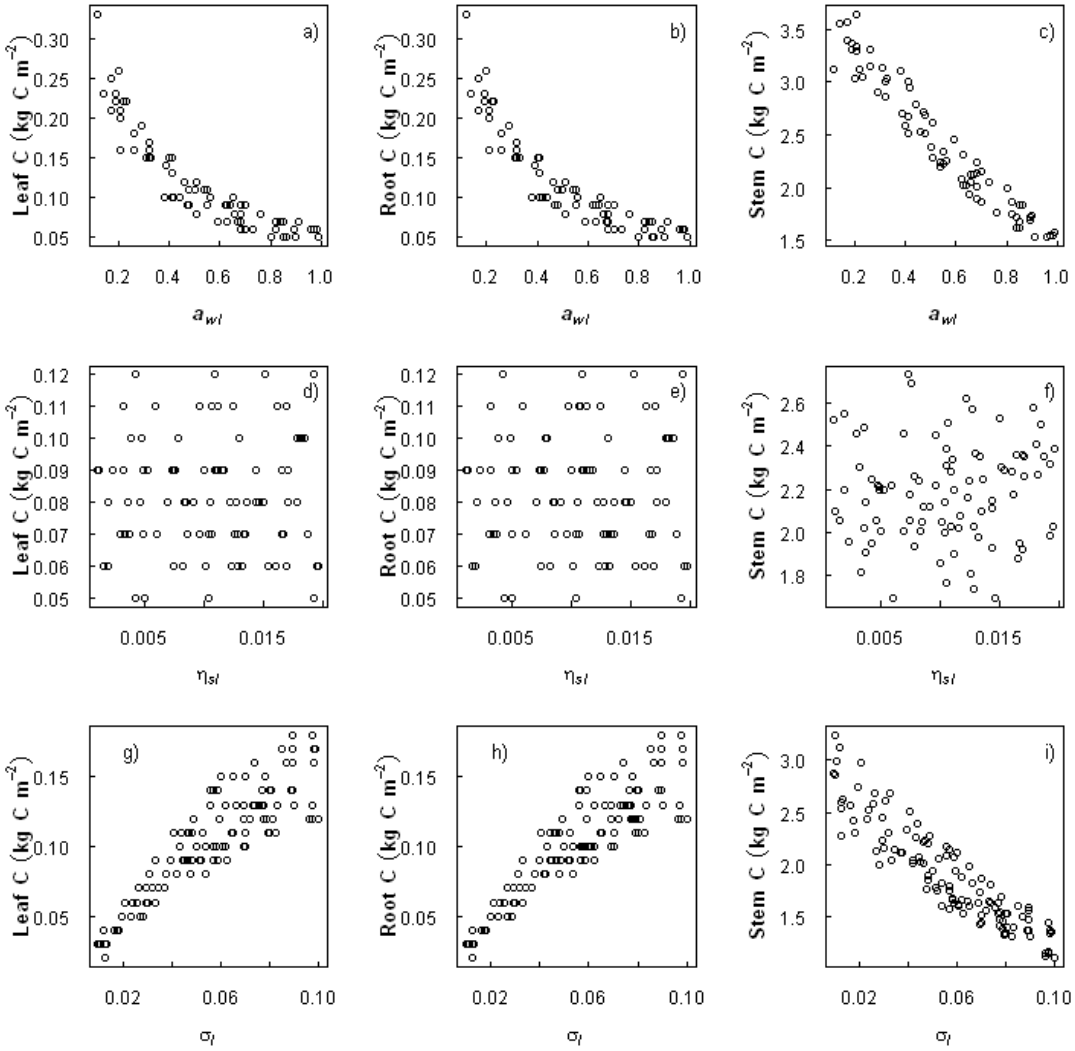

Fig. 2. The relationship between key growth parameters (a_{wl}, η_{sl} and σ_l) and maximum leaf carbon content, *L*, maximum root carbon content, *R,* and maximum stem carbon content, *W*. Each parameter plotted on the x axis is allowed to vary over its full range specified in the Monte-Carlo simulation, and the other parameters are constrained to ± 25% of their default value (Table 5). a_{wl} (kg C m^{-2}) is the allometric coefficient relating the target woody biomass to the leaf area index; η_{sl} (kg C m^{-2}) is the live stemwood coefficient; σ_l (kg C m^{-2} leaf) is the specific density of leaf carbon.

Canopy height is most sensitive to η_{sl} (Fig. 1d). When η_{sl} is not constrained to ± 25% of its default value, model predictions of maximum *h* span a very wide range, achieving heights in excess of 80 m. Despite η_{sl} having a 'threshold' value (~ 0.003 kg C m^{-2} *LAI*$^{-1}$) below which model predictions tend to go outside of reasonable bounds, even above this threshold, predictions of *h* are still larger (maximum achievable ~ 25 m) than when η_{sl} is constrained. *LAI* is most sensitive to a_{wl} (Fig. 1b). *LAI* is fairly insensitive to η_{sl}, no trend between η_{sl} and *LAI* is evident above the threshold value (Fig. 1e). The increase in *LAI* below the threshold value of

η_{sl} would suggest at this point the relationship becomes unstable and predictions can be tipped out of reasonable bounds. *LAI* also shows sensitivity to σ_l, although there is a lot of variation in this relationship (Fig. 1h). C_v is most sensitive to a_{wl}, spanning a wider range of predicted values when a_{wl} is not constrained and displaying a strong negative relationship (Fig. 1c). C_v is not sensitive to η_{sl} and shows some sensitivity to σ_l, however there is greater variation in this relationship (Figs. 1f & 1i respectively).

Suitable parameter space for each parameter was identified from Figures 1 and 2. The ranges of parameter values were identified primarily from Fig. 1a - i, based on values of the observed maximum *h*, *LAI* and C_v achieved in ambient CO_2-grown trees in year three of the first rotation at the FACE experiment in Italy (2001; Table 1 and Table 2). Therefore, the desired growth characteristics for *P. nigra* were; maximum *h* of 8.73 m ± 0.14, maximum *LAI* of 7.24 m^2 m^{-2} ± 0.16, and maximum C_v of 4.02 kg C m^{-2}. The desired growth characteristics for *P. x euramericana* were; maximum *h* of 8.45 m ± 0.12, maximum *LAI* of 4.53 m^2 m^{-2} ± 0.31, and maximum C_v of 3.33 kg C m^{-2}. The results of the Monte-Carlo suggest a much lower value of a_{wl} than the default (0.65 kg C m^{-2}; Table 6) value is needed to achieve this desired combination of *h*, *LAI* and C_v for both genotypes (Fig. 1a - c). Somewhere in the range of 0.15 to 0.30 kg C m^{-2} would be more appropriate to achieve the desired growth of both *P. nigra* and *P. x euramericana* according to observations. η_{sl} does not need to deviate far from the default value (0.01 kg C m^{-2} LAI^{-1}) to reasonably simulate observations of *h* (Fig.1d). However, a value of σ_l lower than the default value (0.0375 kg C m^{-2} LAI^{-1}) is necessary to improve predictions of C_v (< = 0.02 kg C m^{-2} LAI^{-1}) (Fig. 1i). Once suitable parameter space was identified, specific parameter values were tuned in model simulations to generate the parameter set that best simulated the observations, these are shown in Table 6.

	P. x euramericana	*P. nigra*	Default
a_{wl}	0.300	0.150	0.650
a_{ws}	10.000	10.000	10.000
b_{wl}	1.667	1.667	1.667
η_{sl}	0.010	0.007	0.010
σ_l	0.020	0.020	0.038

Table 6. Key growth parameter values used in JULES to determine growth and carbon allocation to stem, leaf and root pools in the vegetation. Values are shown for *P. x euramericana* and *P. nigra* following the Monte-Carlo simulation method and parameter tuning to find the parameter set that best simulates the observed growth. These are compared to the default values used in JULES to simulate growth of a broadleaf tree. a_{wl} is the allometric coefficient relating the target woody biomass to the leaf area index (kg C m^{-2}); a_{ws} relates the woody biomass to the live stem biomass; b_{wl} is the allometric exponent relating the target woody biomass to the leaf area index; η_{sl} is the live stemwood coefficient (kg C m^{-2}); σ_l is the specific density of leaf carbon (kg C m^{-2} leaf).

5.3.4 Modifications to the model

The standard application of JULES is to model shifts in natural vegetation cover and associated carbon and water cycles in response to climate. Simulations are usually "spun-up" from bare ground conditions to reach an established, "equilibrium" vegetation state. In this work, however, we want to simulate a managed bioenergy crop grown on a three-year rotation, starting with initial planting and/or re-growth after coppicing, through to harvesting at the end of each rotation. This requires significant modifications to JULES to grow trees under a managed system, instead of allowing JULES to essentially determine its own vegetation type and cover. Modifications were made to the code to introduce a harvesting subroutine, and change the allocation of carbon to different plant pools within the model. These steps are described below.

5.3.4.1 Harvesting

Harvesting of poplar SRC was introduced based on a three-year rotation from initial planting of the crop to harvesting, or re-growth through to harvesting. The harvesting is an enforced management regime based on date; the crop is harvested every February of the fourth year. In the model, this is simulated by re-setting all pools of vegetation carbon (above- and below-ground) to a minimum value (0.0001 kg C m^{-2}) along with the canopy height. This approach is very simplistic, yet, with constraints due to the structure of the model, provides an adequate simulation of the SRC cycle. A more realistic representation of the SRC cycle within the

model would require TRIFFID to recognise a separate carbon 'store' for above- and below-ground carbon. In which case the aboveground carbon could be removed, leaving the root carbon in the ground. With the root mass already in place, more carbon could be allocated to aboveground growth to simulate the rapid re-growth observed after coppicing. However, in its current configuration, TRIFFID does not have a separate above- and belowground carbon store; every call to TRIFFID re-calculates and updates the carbon content of the vegetation based on the allometric equations. It was beyond the scope of this work to re-configure TRIFFID in such a major way so as to introduce a carbon store.

5.3.4.2 Changing the allocation of carbon

The original configuration of TRIFFID allocates carbon equally to root and leaf pools (see equations 15 and 16). Used in simulations this ratio did not produce appropriate allocations of carbon to root and leaf pools as suggested by the observations (Table 1), with too much carbon being allocated to the root pool. To ensure the model could track the carbon content of the different vegetation pools in a more realistic way, the allometric constants were modified based on the ratios of carbon in the roots and leaves reported in the literature for poplar SRC (see Table 1). Using the data from Table 1, ratios of root:leaf carbon contents ranged from 0.44 to 1.28 for ambient CO_2 grown trees of both genotypes, this range is quite large because it includes all the growth cycle stages of poplar SRC which vary quite considerably with respect to their carbon allocation strategy. An average of these values was taken, excluding data from 2002 after the trees had just been coppiced, giving a root:leaf carbon content ratio of 0.71 (~1:1.41) for poplar SRC, however, in simulations a ratio of 0.67 (~ 1:1.5) produced more accurate allocation of carbon between root and leaf pools. This ratio was used to modify the distribution of carbon to root and leaf pools to improve simulations of the total carbon contents of the vegetation in addition to the carbon contents of the individual pools.

5.3.5 Results: influence of changing model structure

The influence of changing the model structure and key PFT-dependent growth parameters on model output is shown in Fig. 3a - c. The yellow line in Fig. 3a - c shows simulations of h, LAI and C_v under the original configuration of JULES using default broadleaf tree values for the PFT-dependent growth parameters. For this simulation, default values for the initial conditions for growth of a broadleaf tree were used : h = 19.0 m; LAI = 5.0 m^2 m^{-2}; maximum LAI = 9.0 m^2 m^{-2}; minimum LAI = 3.0 m^2 m^{-2}. From Fig. 3a - c, it is evident that rather than simulating

the growth of the vegetation from bare ground conditions, the model uses the bounds set in the initial conditions to simulate an established cover of relatively mature trees, given the available NPP. The year-to-year growth thereafter is very slow with minimal gain in h, LAI and C_v. This growth is indicative of a slow growing, mature tree in a steady-state of growth. Therefore, it is clear these initial conditions and PFT-dependent growth parameters are unsuitable for simulating growth of a managed SRC bioenergy crop from planting.

The red line in Fig. 3a - c shows the effect of changing the model structure to introduce a three-year coppicing cycle and modifying the ratio of carbon allocation to the leaves and roots. The harvesting in the third year is clearly apparent, and changing the ratio of carbon allocation to the roots and leaves generates a marginally more defined pattern of year-to-year growth that is particularly evident in C_v (Fig. 3c), but less so in the simulated h and LAI. Evidently, although modifications to the structure of the model improve simulation of the management regime, the initial conditions for growth and default parameter values are not representative of a fast-growing poplar SRC crop.

For comparison, the blue line (Fig. 3a - c) shows the influence of modifying the model structure, using calibrated parameter values and initial conditions (h = 0.43 m; LAI = 0.1 m^2 m^{-2}; maximum LAI = 9.0 m^2 m^{-2}, minimum LAI min = 0.1 m^2 m^{-2}). The calibrated PFT - dependent growth parameters used are those for *P. x euramericana* (Table 6), section 5.3.2 describes how these values were determined. Vast improvements are clearly seen in the model's ability to simulate the managed growth cycle of poplar SRC. Changing the initial conditions reduced the initial growth accordingly, which effectively simulated the growth of poplar SRC from bare ground conditions. Thereafter, the year-to-year growth is fairly well defined, and the model shows capacity to capture differences in growth as a result of the different stages in the growth cycle. For example, the model captures the slower growth in the first year during an 'establishment' phase, then the exponential growth seen in years two and three, this is particularly evident in LAI and C_v. The imposed harvest at the end of year three is effective at simulating removal of the vegetation, dropping C_v , h and LAI back to zero.

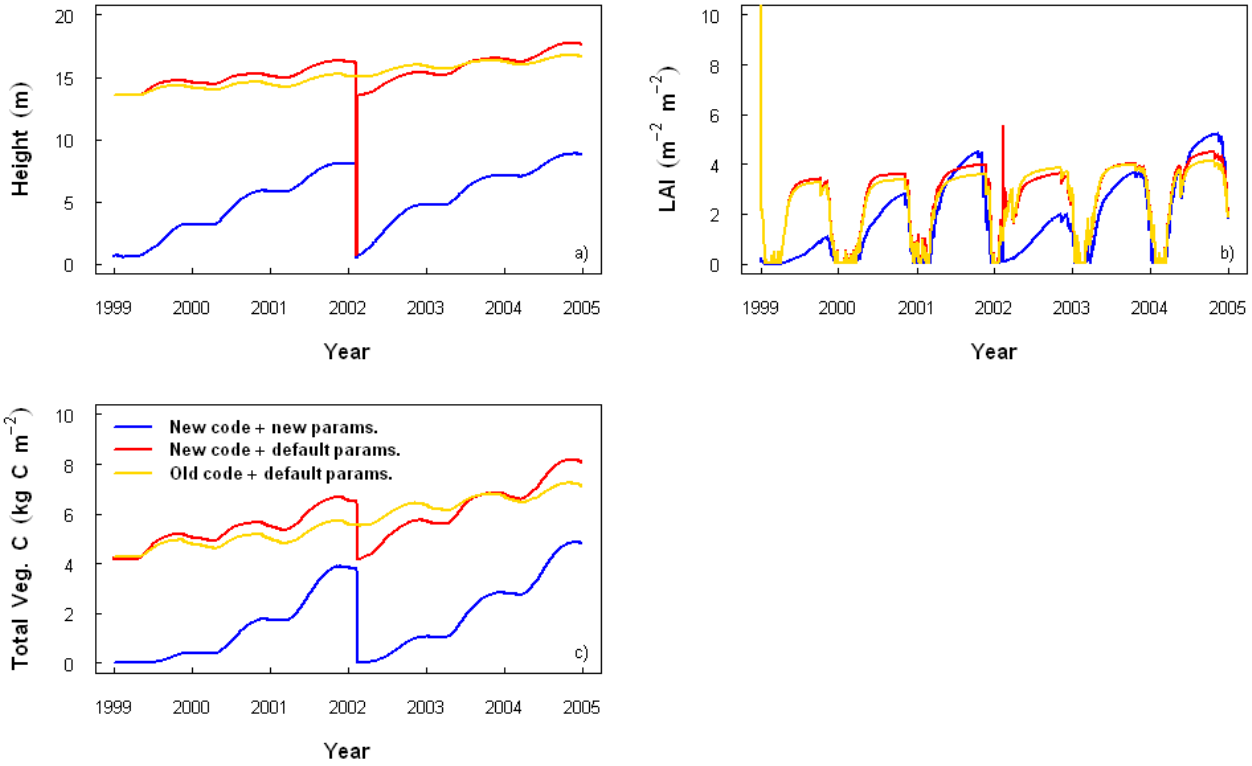

Fig. 3. Performance of the JULES model simulating: a) canopy height, b) *LAI* and c) total vegetation carbon content. Three model configurations are compared: 1) the original configuration of JULES and default PFT growth parameters (yellow line), 2) modifications made to the JULES code to include a harvest and altered carbon allocation to the roots and leaves, and default PFT growth parameters (red line), 3) as 2) but with new values for the PFT growth parameters identified by the Monte-Carlo sensitivity analysis and tuned based on observations of poplar SRC growth (blues line).

5.4 Results: performance of the modified and parameterised model

5.4.1 Growth of poplar SRC under ambient atmospheric CO_2 concentrations

Modelled poplar SRC growth under ambient atmospheric CO_2 concentration (380 ppm) is shown in Fig. 4 (blue line = modelled *P. x euamericana*; green line = modelled *P. nigra*). This is plotted with observed values of the maximum growth (*h*, *LAI*, C_v, *L*, *R* and *W*) achieved each year (data in Tables 1 and 2; blue circle = observed *P. x euamericana*; green circle = observed *P. nigra*). The observations in year three of the first rotation (2001) were used to inform and constrain the model during model parameterisation, therefore these data are considered partially dependent, but the complete data set of growth over two rotations is useful to validate the model performance over a longer time-scale. Additionally, it is noted that with only one data point per year and with considerable variation in the number of replicates used to generate

each point, the observations and their standard errors are only a rough guide to the accuracy and performance of the model.

For both genotypes, overall, the model simulates growth over two rotations of an SRC cycle reasonably well. Canopy height (*h*) is well simulated in the model, achieving maximum heights close to observed values in all years (Fig. 4a; Table 7). The exception is year one, where the model grossly over-predicts *h* by up to 96 % in *P. nigra* and 127 % in *P. x euramericana* (Table 7). Simulated *h* in the second year of the first rotation (2000) is within the error of the observations for both genotypes (Table 7). Predicted *h* during re-growth following harvesting is underestimated by the model by between -13 to -4 % depending on genotype (Table 7). Thereafter, the model slightly over-predicts the maximum *h* achieved each year, which ranges between +12 to + 28 % depending on genotype (Table 7). *LAI* is reasonably well simulated by the model, although there is a lot of variation between years and predicted *LAI* is more accurate for *P. nigra* than *P. x euramericana* (Fig. 4b; Table 7). Inaccuracies in simulated *LAI* are particularly noticeable in the first year of both rotations (1999 and 2002). During establishment, the model over-predicts *LAI* by 108 % in *P. nigra* and 150 % in *P. x euramericana*. During re-growth following harvesting, the model under-predicts *LAI* by 28 % in *P. nigra* and 49 % in *P. x euramericana*. In the remaining years, the model performs reasonably well, but simulated *LAI* is always under-predicted. The percentage difference between modelled and observed maximum *LAI* in these years ranges between -21 to -2 % in *P. nigra* and -34 to 0 % in *P. x euramericana* (Table 7). In all years the clear difference in *LAI* between the two genotypes is captured by the model. Unfortunately there are no observations for year three of the second rotation. The difference between the modelled and observed *LAI* in the first year of the second rotation is probably because of the lack of a separate above- and below-ground 'carbon store' in the model. In the model, after coppicing, the crop is essentially re-growing from nothing i.e. there is no carbon reserve in the root pool, whereas in the real world, the rootstock remains in the ground and only the aboveground biomass is removed. With this reserve of carbon already in place the crop shows accelerated growth. Nevertheless, although this appears to be an issue in the simulation of *LAI*, it does not appear to be an issue for model predictions of *h*, C_v or *W*. Simulated C_v is reasonable for both genotypes, although this is variable between years, and in all years the difference between the two genotypes is captured by the model (Fig. 4c). The breakdown of simulated C_v into the individual pools of stem, *W* (Fig. 4d), leaf, *L* (Fig. 4e) and root, *R* (Fig. 4f), carbon shows that although the simulation of *W* is fairly good, simulation of *L* and *R* is less so. Nevertheless, for this work, the pool of stem carbon, *W*, is the most important pool for the model to predict with reasonable

accuracy, as this represents the harvestable biomass, or yield, of the bioenergy crop. The simulation of *W* is reasonable (Fig. 4d; Table 7). Simulated *W* is more accurate for *P. nigra* than *P. x euramericana*. For both genotypes, *W* is over-predicted in year two of the first rotation (2000), although this is much larger for *P. x euramericana* (+41 %) than *P. nigra* (+15 %) (Table 7). In the third year of the first rotation (2001), simulated *W* is within the error of the observations for *P. nigra*, but is over-estimated for *P. x euramericana* (+ 35 %). During year one of the second rotation, simulated *W* is within the error of the observations for both genotypes. Thereafter, the model over-predicts *W* in year two of the second rotation in both genotypes, and under predicts in year three, although this is marginal for *P. nigra* (Table 7). The model correctly captures differences between the two genotypes, i.e. in most years *P.nigra* achieves a higher *W*.

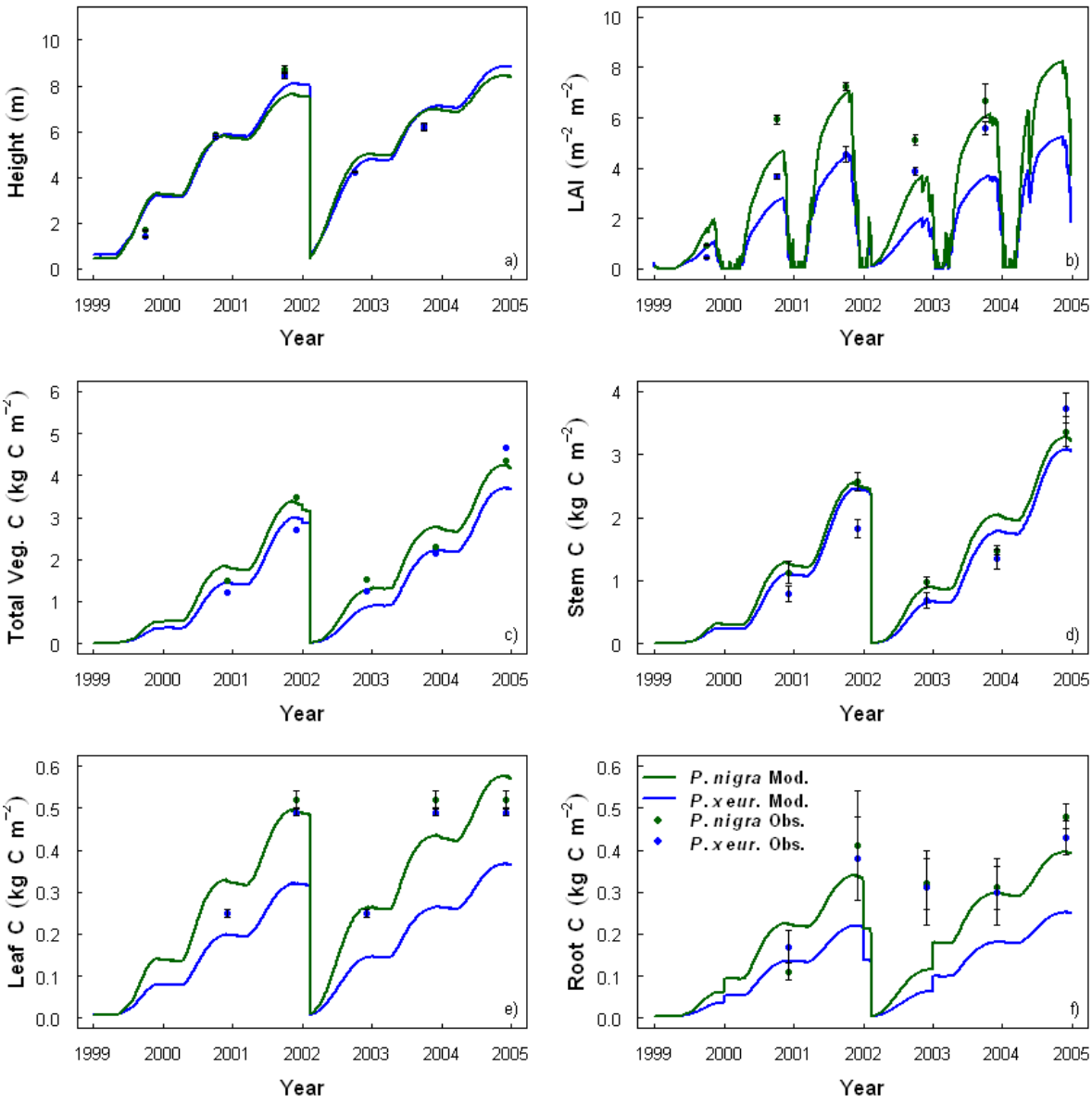

Fig. 4. Simulated growth of *P.x euamericana* (blue line) and *P. nigra* (green line) over two rotations of a three-year SRC cycle grown in ambient atmospheric CO_2; a) canopy height (m), *h*, b) *LAI* (m^2 m^{-2}), c) total vegetation carbon content (kg C m^{-2}), C_v, d) carbon content of the stem (kg C m^{-2}), *W*, e) carbon content of the leaves, (kg C m^{-2}), *L*, f) carbon content of the roots (kg C m^{-2}), *R*. Observations of growth of *P.x euamericana* (blue dot) and *P. nigra* (green dot) from the popFACE site in Italy, ± their s.e. where available, are also plotted.

	P. nigra			*P. x euramericana*		
	Mod.	**% diff.**	**Obs.**	**Mod.**	**% diff.**	**Obs.**
			Max. Height (m)			
1999	3.29	95.83	1.68 ± 0.03	3.19	126.24	1.41 ± 0.04
2000	5.87	0.00	5.87 ± 0.08	5.80	0.69	5.76 ± 0.05
2001	7.64	-12.49	8.73 ± 0.14	8.08	-4.38	8.45 ± 0.12
2002	5.37	27.25	4.22 ± 0.02	5.25	24.11	4.23 ± 0.02
2003	6.98	12.58	6.20 ± 0.1	7.11	14.68	6.20 ± 0.18
			Max. *LAI* (m^2 m^{-2})			
1999	1.97	107.37	0.95 ± 0.02	1.10	150.00	0.44 ± 0.02
2000	4.69	-20.91	5.93 ± 0.20	2.82	-23.37	3.68 ± 0.10
2001	7.04	-2.76	7.24 ± 0.16	4.52	-0.22	4.53 ± 0.31
2002	3.70	-27.88	5.13 ± 0.20	2.02	-48.21	3.90 ± 0.15
2003	6.15	-8.21	6.70 ± 0.67	3.71	-33.75	5.60 ± 0.27
			Max. Stem C content (kg C m^{-2})			
2000	1.29	14.16	1.13 ± 0.17	1.11	40.51	0.79 ± 0.12
2001	2.56	-0.39	2.57 ± 0.14	2.46	34.43	1.83 ± 0.14
2002	0.92	-5.15	0.97 ± 0.08	0.63	-8.70	0.69 ± 0.12
2003	2.05	38.51	1.48 ± 0.07	1.78	32.84	1.34 ± 0.16
2004	3.27	-2.68	3.36 ± 0.24	3.08	-17.65	3.74 ± 0.24

Table 7. Modelled (ambient CO_2) and observed ± s.e. maximum canopy height (*h*), maximum *LAI* and maximum stem carbon content (*W*) achieved in each year for *P. nigra* and *P. x euramericana*. The observed data are reproduced from Table 1 and Table 2. The percentage difference between the modelled and observed data are shown calculated as (((mod. – obs.)/obs.)*100).

5.4.2 Growth of poplar SRC under elevated atmospheric CO_2 concentrations

Using the same set of model parameters, model simulations of the growth of *P. nigra* (Fig. 5) and *P. x euramericana* (Fig. 6) under elevated atmospheric CO_2 (~ 550 ppm; broken line) are shown compared to ambient CO_2 simulations (solid line), and observations (data from Tables 1 and 2). Note that the only difference between simulations is the change in atmospheric CO_2 concentration, assessing the model's ability to simulate poplar SRC growth in response to an elevated concentration of atmospheric CO_2. In both genotypes there is a reasonable change in the model outputs. Although the observations and the simulations do not always match perfectly, the behaviour of the model captures the increased growth response seen under elevated atmospheric CO_2. Canopy height, *h*, is predicted reasonably well (Fig. 5a & 6a; Table 8) for both genotypes of poplar. This is with the exception of the establishment year, where the model struggles to capture the low growth and largely over predicts *h* by +127 % for *P. nigra* and 161 % for *P. x euramericana* (Table 8). Thereafter, the relative difference between

modelled and observed *h* ranges between -10 to +37 % for *P. nigra*, and between -2 to +30 % for *P. x euramericana*. This suggests simulated *h* is marginally more accurate for *P. x euramericana.* The model over-predicts *h* in all years except the third year of the first rotation where *h* is under-predicted, although this is marginal, particularly for *P. x euramericana* (Table 8). Simulated *LAI* is reasonable in both genotypes, certainly during years two and three of the first rotation (Fig. 5b & 6b; Table 8). During the second rotation simulated *LAI* is reasonable for *P. nigra*, the percentage difference between observed and modelled data ranges between -22 to +3 %, but is largely under-predicted for *P. x euramericana,* -46 to -35 %. The model struggles to capture the minimal growth in year one of the first rotation in both genotypes, over-predicting *LAI* by 69 % in *P. nigra* and 98 % in *P. x euramericana*. The model largely over-predicts C_v (Fig. 5c & 6c) in both genotypes, however differences in C_v as a result of the CO_2 fertilisation effect are apparent. Breaking down C_v into its component parts of *W* (Fig. 5d), *L* (Fig. 5e) and *R* (Fig. 5f) shows the model's ability to simulate each carbon pool. In both genotypes simulation of carbon content in the root pool is not very accurate, especially for *P. x euramericana*. The observations however, are surrounded by a large amount of variation, which reflects the difficulty of measuring below-ground biomass. Simulation of the carbon content in the leaf pool is reasonable for *P. nigra*, but the model largely under-predicts for *P. x euramericana*. Simulation of the carbon content of the stem is reasonably accurate for both genotypes, and for this work it is the main carbon pool of interest, representing the harvestable biomass. Simulated *W* is more accurate for *P. nigra* than *P. x euramericana*, with differences between modelled and observed *W* ranging between -11 to 53 % for *P. nigra*, and between -12 to 69 % for P. *x euramericana* (Table 8). During year one of the first rotation, *W* is largely over-predicted in both genotypes. Thereafter, simulated *W* is good for *P. nigra*, with marginal differences between observed and modelled data of +8 % in 2001 and 0 % in 2002, for P. *x euramericana* the differences are larger, +33 % in 2001 and +32 % in 2002. In year two of the second rotation, *W* is over –predicted in both genotypes, and is marginally under-predicted the following year.

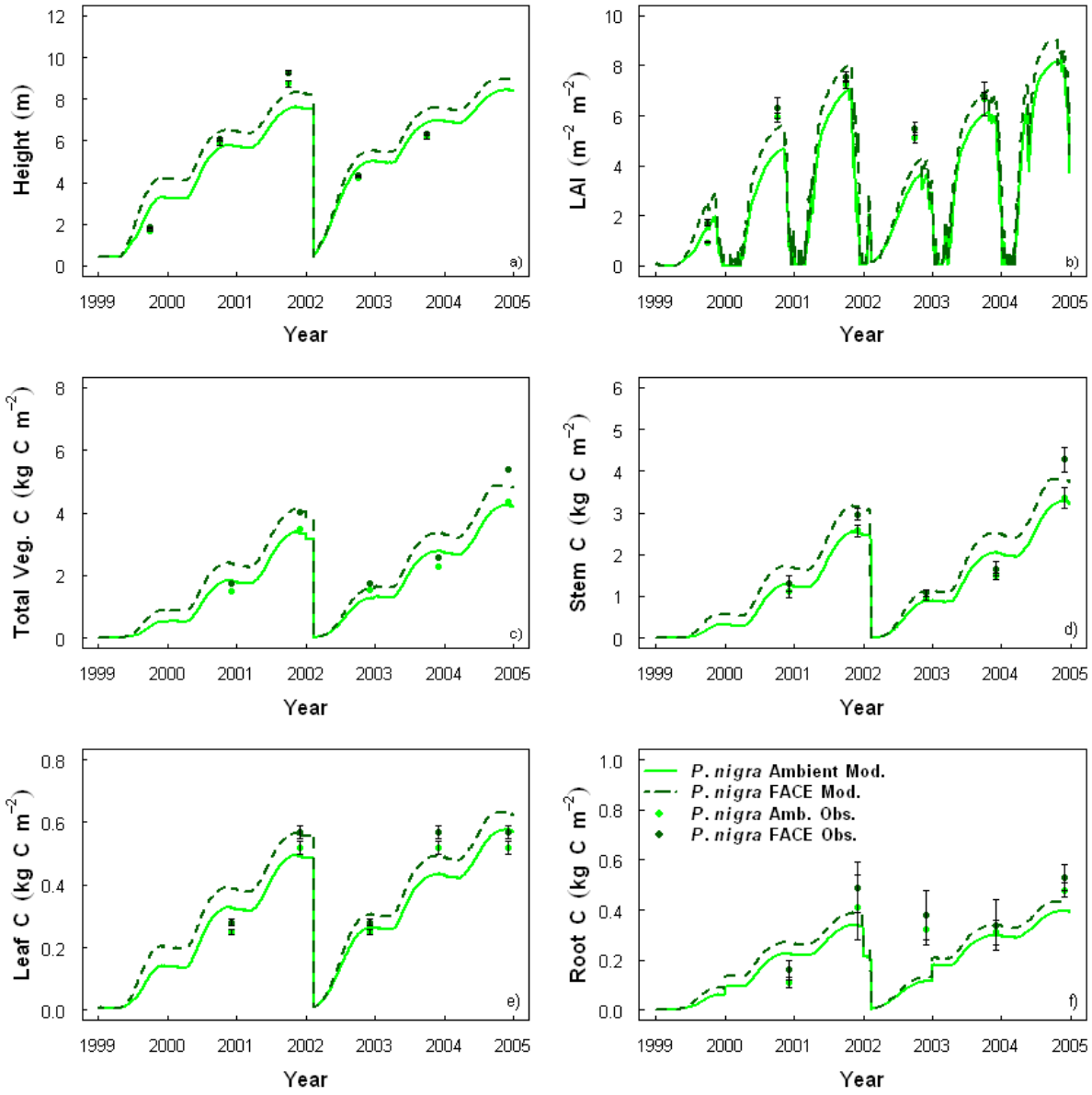

Fig. 5. Simulated growth of *P. nigra* in ambient atmospheric CO_2 (light green line) and *P. nigra* in elevated atmospheric CO_2 (dark green broken line) over two rotations of a three-year SRC cycle; a) canopy height (m), *h*, b) *LAI* (m^2 m^{-2}), c) total vegetation carbon content (kg C m^{-2}), C_v, d) carbon content of the stem (kg C m^{-2}), *W*, e) carbon content of the leaves, (kg C m^{-2}), *L*, f) carbon content of the roots (kg C m^{-2}), *R*. Observations of growth of *P. nigra* in ambient atmospheric CO_2 (light green dot) and *P. nigra* in elevated atmospheric CO_2 (dark green dot) from the popFACE site in Italy, ± their s.e. where available, are also plotted.

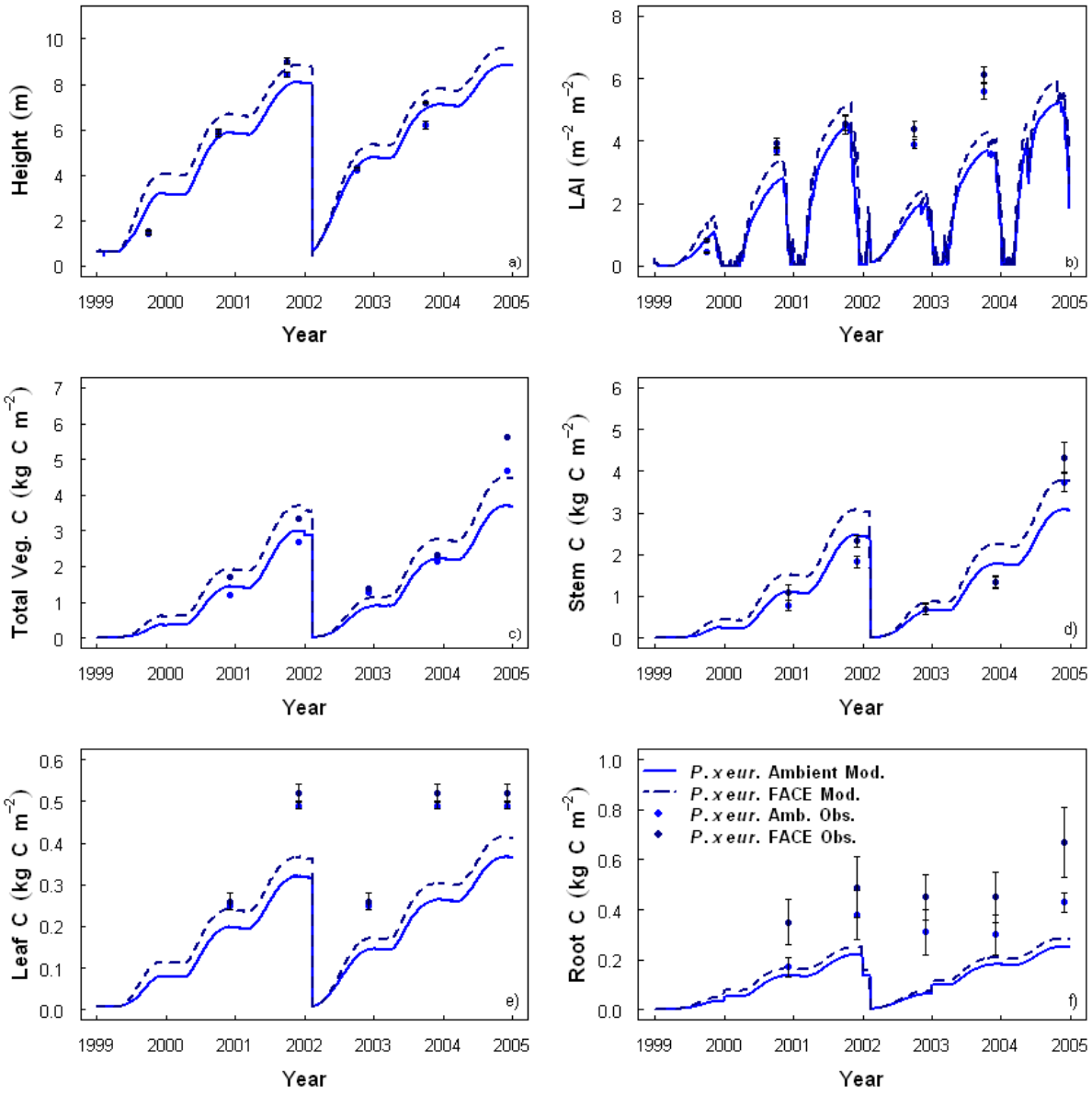

Fig. 6. Simulated growth of *P. x euramericana* in ambient atmospheric CO_2 (light blue line) and *P. x euramericana* in elevated atmospheric CO_2 (dark blue broken line) over two rotations of a three-year SRC cycle; a) canopy height (m), *h*, b) *LAI* (m^2 m^{-2}), c) total vegetation carbon content (kg C m^{-2}), C_v, d) carbon content of the stem (kg C m^{-2}), *W*, e) carbon content of the leaves, (kg C m^{-2}), *L*, f) carbon content of the roots (kg C m^{-2}), *R*. Observations of growth of *P. x euramericana* in ambient atmospheric CO_2 (light blue dot) and *P. x euramericana* in elevated atmospheric CO_2 (dark blue dot) from the popFACE site in Italy, ± their s.e. where available, are also plotted.

	P. nigra			*P. x euramericana*		
	Mod.	**% diff.**	**Obs.**	**Mod.**	**% diff.**	**Obs.**
			Max. Height (m)			
1999	4.21	126.34	1.86 ± 0.03	4.07	160.90	1.56 ± 0.03
2000	6.55	8.09	6.06 ± 0.06	6.69	13.01	5.92 ± 0.14
2001	8.33	-10.24	9.28 ± 0.10	8.84	-1.89	9.01 ± 0.15
2002	5.89	36.34	4.32 ± 0.02	5.61	29.56	4.33 ± 0.02
2003	7.60	19.69	6.35 ± 0.05	7.81	8.47	7.20 ± 0.05
			Max. *LAI* (m^2 m^{-2})			
1999	2.88	68.42	1.71 ± 0.13	1.60	97.53	0.81 ± 0.04
2000	5.63	-10.92	6.32 ± 0.41	3.43	-13.16	3.95 ± 0.16
2001	8.08	7.02	7.55 ± 0.21	5.23	14.44	4.57 ± 0.23
2002	4.31	-21.64	5.50 ± 0.25	2.39	-45.68	4.40 ± 0.25
2003	6.99	2.79	6.80 ± 0.14	4.29	-35.00	6.60 ± 0.27
			Max. Stem C content (kg C m^{-2})			
2000	1.74	33.85	1.30 ± 0.19	1.53	40.37	1.09 ± 0.20
2001	3.18	7.43	2.96 ± 0.14	3.07	32.33	2.32 ± 0.15
2002	1.08	0.00	1.08 ± 0.07	0.91	31.88	0.69 ± 0.14
2003	2.53	52.41	1.66 ± 0.17	2.26	68.66	1.34 ± 0.13
2004	3.80	-11.01	4.27 ± 0.29	3.79	-12.27	4.32 ± 0.38

Table 8. Modelled (elevated atmospheric CO_2) and observed ± s.e. maximum canopy height (h), maximum *LAI* and maximum stem carbon content (W) achieved in each year for *P. nigra* and *P. x euramericana*. The observed data are reproduced from Table 1 and Table 2. The percentage difference between the modelled and observed data are shown calculated as (((mod. – obs.)/obs.)*100).

5.4.3 Water-use of poplar SRC

Having parameterised the model to simulate the growth of poplar SRC, Fig. 7 shows the modelled canopy transpiration produced as a result of these parameterisations for *P. x euramericana* under ambient CO_2. Unfortunately observed data for *P. nigra* were not available. Hourly modelled and observed canopy transpiration measured by sap flow technique for *P. x euramericana* trees in ambient atmospheric CO_2 are plotted for seven days during the growing season in 2000. The observed data are taken from Tricker *et al*., (2009) where more details can be found on the experimental setup. Simulated water-use is shown using the default parameter values for dz_{om}/d_h and z_{oh}_ z_{om} and using modified values (see section 5.2.4.3). Plotted as a diurnal cycle on an hourly time-step, Fig. 7 suggests the model has a tendency to over-predict water-use of *P. x euramericana* trees, particularly in the middle of the day. Modifying dz_{om}/d_h and z_{oh}_ z_{om} is shown to significantly improve the accuracy of simulated water-use, the model tendency to over-predict water-use, especially in the peak of the day, is

still present, but much reduced. Further, when calculated as a daily total of canopy transpiration (Table 9), the observed and modelled data, using the modified parameter values for dz_{om}/d_h and $z_{oh}\_ z_{om}$, compare well. The cumulative four-day total of transpirational water loss from measurements was 17.09 mm day^{-1}, and the modelled total was 17.49 mm day^{-1}.

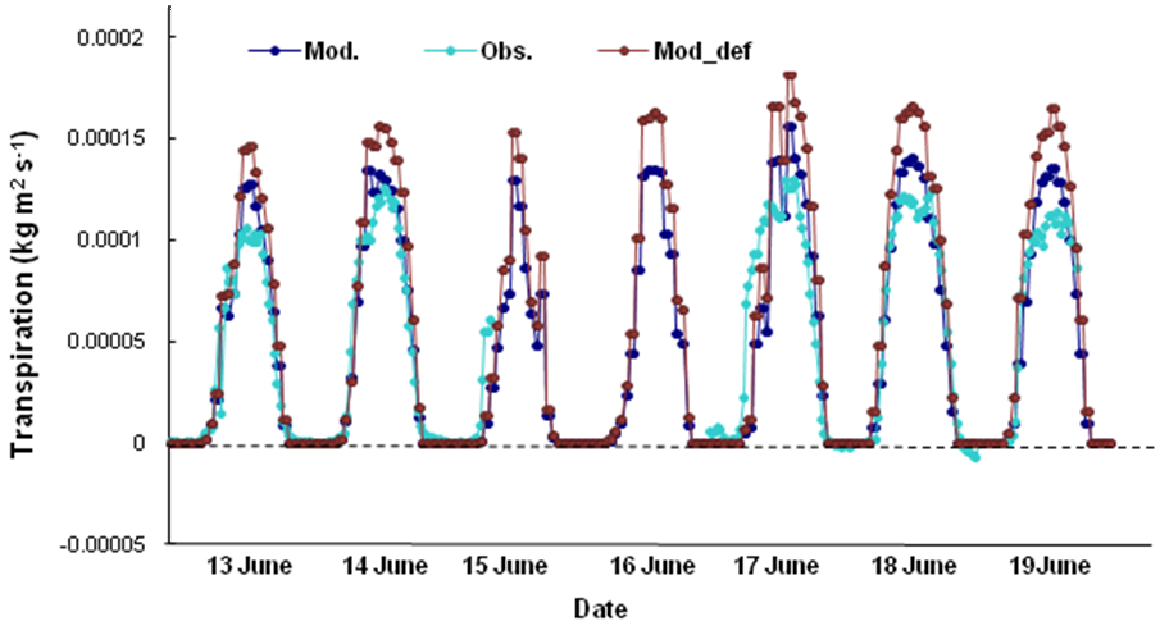

Fig. 7. Modelled transpiration (kg m^{-2} s^{-1}) of *P.x euramericana* trees over the course of seven days in June 2000 plotted with observed transpiration of *P. x euramericana* trees over the same period measured by sap flow technique (stem heat balance), and scaled to the whole plant on a ground area basis. The observed data is from Tricker *et al*., (2009). Sap flow reported as W m^{-2} (latent heat: *LE*) was converted to kg m^{-2} s^{-1} for the purpose of this work by dividing *LE* (W m^{-2}, also equivalent to J s^{-1} m^{-2}) by the latent heat of vapourization of water (taken as 2450000 J kg^{-1} as used in Tricker *et al*., 2009). Modelled results using the default (Mod_def) and modified (Mod.) parameter values for dz_{om}/d_h and $z_{oh}\_ z_{om}$ (see section 5.2.4.3).

	Observed (mm day^{-1})	Modelled (mm day^{-1})
13-Jun	3.33	3.66
14-Jun	4.16	4.34
17-Jun	4.95	4.67
18-Jun	4.66	4.82
Total	**17.09**	**17.49**

Table 9. Daily totals of transpiration for *P. x euramericana* in June 2000. Data used are only where a full set of measurements were available for the observed data. The total shows the sum of transpiration over the four-day period. Modelled results use modified parameter values for dz_{om}/d_h and $z_{oh}\_ z_{om}$ as opposed to default values (see section 5.2.4.3).

5.5 Discussion

The goal of this work was to modify the land-surface scheme JULES, to simulate the growth of *Populus x euamericana* and *P. nigra* managed as short-rotation coppice (SRC) on a three year rotation. The growth cycle of this bioenergy SRC crop is unique. It is a fast-growing, woody crop achieving full canopy closure and accumulating large amounts of biomass in a relatively short time period (~ three years). No suitable parameterisation existed in the model in its original configuration to simulate this vegetation type. Additionally, this crop is grown in a managed system. Consequently, modifications to the model were required as this was an application for which the model was not designed and had not previously been used. It was decided to use JULES as it contains the appropriate processes to model the exchanges of carbon and water between the vegetation and the atmosphere, with the added benefit that it can ultimately be run on a global scale. Further, it is a community model, so changes to the model's parameterisation in this manner would contribute to understanding in the wider JULES modelling community.

5.5.1 Parameter sensitivity and model structure

Understanding the complex behaviour and sensitivity of model predictions of poplar SRC growth to the PFT-dependent growth parameters was key to this work. The key PFT-dependent growth parameters were identified as; a_{wl}, a_{ws}, b_{wl}, η_{sl} and, σ_l. Together, these primarily determined the allocation of carbon to the three vegetation pools (L, R and W), the LAI and h. The equations that derive the LAI and h and partitioning of carbon revealed a great deal of interaction between parameters. A Monte-Carlo sensitivity analysis was used to investigate the sensitivity of modelled output to each parameter, accounting for uncertainty due to the effect of other interacting parameters whose values were also unknown. This novel Monte-Carlo approach generated a greater understanding of the model processes and parameter sensitivities, and highlighted the value of such methods. It was found that h was most sensitive to η_{sl}, whereas LAI and C_v were most sensitive to a_{wl}. Nevertheless, many of the parameters displayed relationships with different growth diagnostics even if they were not directly involved in their calculation, for example, the relationship between L/R and a_{wl}, or W and σ_l. This showed that although they were not directly related, many parameters were causally linked and thus sensitive to the behaviour of other parameters. This causal, indirect behaviour is not apparent when analysing the equations alone. Additionally, for η_{sl}, for example, a 'threshold' value (~ 0.003 kg C m^{-2} LAI^{-1}) was identified below which predictions of h and LAI were observed to

often be in excess of reasonable bounds. This is often the case with model parameters, even if values are obtained from literature. Consequently it is often necessary to 'tune' values to produce sensible model behaviour. These tipping points and complex interactions highlight the difficulty of undertaking an exact calibration of individual parameters, and is why the Monte-Carlo method was used in this work to find an optimal 'parameter set'.

A suitable range for parameter values was identified by the Monte-Carlo sensitivity analysis. Further model simulations were performed to tune and calibrate the parameter values based on observations of poplar SRC growth to determine a set of growth parameters that best simulated the observations. In order to achieve the desired growth for poplar SRC, i.e. high *LAI*, C_v and *W* relative to *h*, different PFT-dependent growth parameters were required compared to the default, broadleaf tree values (Table 6).

Modification of the original code to introduce harvesting on a three-year cycle was achieved by re-initialising all pools of vegetation carbon to a minimum value (0.0001 kg C m^{-2}) and re-setting *h* to its initial condition. This was prescribed by date every three years, and provided an adequate approximation of harvesting in an SRC cycle for this work. A big limitation identified in the model was the lack of a separate above- and below-ground 'carbon store'. Given the available NPP, the model re-calculated the carbon balance according to the allometric relationships. Including a carbon store in the model would have allowed a more realistic representation of the SRC harvest and re-growth. The model could then simulate the rootstock that remained in the ground when the crop was harvested, and the accelerated re-growth following coppicing because of the existing pool of stored carbohydrates for growth. This would involve extensive modification of the model, and was beyond the scope of this work; however it would be a priority for further work.

The allocation of carbon to the roots and leaves was also modified from 1:1 to 1:1.5 to improve simulation of the distribution of carbon to the different pools, based on observations (Table 2). The growth produced by these parameterisations is reported in Fig. 4 for trees in ambient CO_2, and Fig. 5 and Fig. 6 for trees in elevated atmospheric CO_2. Compared to the original ratio of 1:1, the ratio of 1:1.5 improved the distribution of carbon; however it was still not perfect. The simulated allocation of carbon to roots and leaves was noticeably better in *P. nigra* than *P. x euramericana*, suggesting that alternative allocation ratios may be more suitable for *P. x euramericana*.

5.5.2 Simulating growth and water-use of poplar SRC in ambient and elevated CO_2

Overall it was seen that these modifications to the code and parameterisations were adequate to simulate the growth of *P. x euramericana* and *P. nigra* managed as SRC. The simulated growth was commonly within range of each observation and its surrounding error. The behaviour of the model captured the differences between the two genotypes, and the differences between ambient and elevated CO_2 grown trees. Inconsistencies between the modelled output and observed date were evident. The significance of these, however, was difficult to judge given that model performance was judged using one observation of growth per year. In addition, the observed data set were partially dependent as data from year three of the first rotation had been used to aid in constraining and calibrating suitable values for the growth parameters. Whilst this is a known pitfall in modelling methods that may result in 'circular reasoning' (Knutti, 2008), it is sometimes unavoidable due to limited data availability, as was the case in this study. The small number of observations used to assess model performance did not allow for more robust methods of assessment, such as minimising the root mean square error over a large time series of data. Other limitations were identified with the observations used to benchmark the model performance. Many of the observations, particularly *h* and *LAI*, had small standard errors, however in many cases the replication within each observation was low. Certainly for *h*, *LAI*, *L* and *R*, replication was not greater than $n = 3$ (see individual refs. in Tables 1 and 2). This small sample size is unlikely to capture all the variation within the stand. Therefore, the observations are unlikely to be truly representative. Another source of error comes from the output of simulated carbon contents of the vegetation pools, where the model outputs actual carbon content in kg C m^{-2}. More commonly reported in literature was the dry biomass, from which the carbon content was derived by assuming it is 48% carbon by mass as suggested by Gielen *et al.*, (2005). This assumption of the carbon content itself may be erroneous due to possible errors in its measurement. Further, the assumption that all vegetation pools (leaf, root and stem) have the same carbon composition may be wrong. Additionally, data on the biomass of each vegetation pool was not available in all years, so some observations were derived from interpolation between years. In the light of this, a degree of deviation between the modelled and observed results was considered acceptable, so long as the model behaviour was sensible.

Limitations in the model structure also contributed to reduced model performance. Most significant was the lack of a separate above- and below-ground ‘carbon store’. This inadequacy was likely responsible for the errors in simulated growth, particularly *LAI*, that were most

apparent in both genotypes in the first year of the second rotation. It was evident from these simulations that the allocation of carbon to the leaf and root pools, whilst reasonable for *P. nigra*, was not adequate for *P. x euramericana* regardless of the similar ratios determined from literature of root:leaf carbon contents (i.e. 1:1.5). Nevertheless, for both genotypes, the simulation of carbon allocated to the stem was good. For this work this was of most importance, as this represents the harvestable biomass. However, it is important to be aware that incorrect allocation of carbon could impact on other processes in the model. For example, under-estimating the root biomass may lead to NPP being over-estimated because the root respiration is too low. However, without measurements of NPP at the popFACE site it is difficult to test this indirect effect. The model also consistently over-predicted canopy height and *LAI* in the first year, or 'establishment' year, suggesting the description of carbon allocation was inadequate to simulate this initial growth. A more sophisticated approach may include having a seasonally- and annually-varying pattern of carbon allocation, i.e. allowing different rates of carbon assimilation to the various pools with time of year in addition to year in the growth cycle

The diurnal plots of water-use over seven days showed the improvement in modelled water-use using the modified parameters as opposed to the default values. These were compared to observations of plant-water use measured by sap flow in *P. x euramericana* at the popFACE site (see Tricker *et al.*, 2009). In both cases, however, the modelled water-use was slightly under-predicted in the early morning and late afternoon, but was largely over-predicted in the middle of the day. The observed data would therefore suggest that on many days stomatal resistance increased in the middle of the day to regulate plant-water loss, which evidently did not occur in the model. The daily total water-use, however, compared well to observed daily totals. Modelled daily totals of plant transpiration ranged from 3.66 – 4.82 mm day^{-1} and observed daily totals ranged from 3.33 – 4.95 mm day^{-1} (Table 6). It was unfortunate that more data were not available for both genotypes in ambient and elevated atmospheric CO_2. Nevertheless, this result gave confidence in the model parameterisations used, especially in the absence of a completely independent data set for model validation of the growth.

Using the Monte-Carlo sensitivity analysis to identify suitable parameter values, and understanding potential errors in the measurements and constraints of the model has allowed a reasoned approach to parameterise the model and assess its performance. Consequently, the modifications made to JULES, and the new PFT-parameter values adequately simulated the growth of *P. x euramericana* and *P. nigra* managed as SRC. With the development of

strategies to reduce emissions and minimise the impacts of climate change, there is an increasing focus on renewable energy sources. Therefore, in the UK, and globally, bioenergy crops, such as poplar SRC, are likely to become an increasing feature of the landscape. As such, their representation in model simulations is paramount. Further, models of this type provide a means to investigate large scale impacts of climate change on these crops, which is essential, both economically and environmentally. The work presented in this chapter provides a tool to do so. This modified version of the JULES model will be used in the next chapter to investigate the variation in yield and water-use of *P. x euramericana* and *P. nigra* SRC in the UK under the current climate and in response to climate change.

5.6 Conclusions

The objective of this work was to modify the land-surface scheme JULES, to simulate the growth of poplar (*Populus x euramericana* and *P. nigra*) managed as SRC. A Monte-Carlo experiment was used to investigate the sensitivity of simulated growth to key PFT-dependent growth parameters. Through this process, suitable 'parameter space' for values of these growth parameters was identified. Parameter values were tuned in model simulations to generate a parameter set for *P. x euramericana* and *P. nigra* that best simulated observations. Modifications were made to the model to simulate harvesting on a three year rotation, and the allocation of carbon to the different vegetation pools was modified.

The modified and parameterised JULES model simulated the growth and water-use of both genotypes of poplar SRC in ambient and elevated atmospheric CO_2 well. The behaviour of the model captured differences in growth between genotypes and atmospheric CO_2 concentrations. However, inconsistencies between modelled output and observations were apparent and were attributed to: i) limitations in the measurements, and/or ii) constraints in the model. Key limitations in the measurements were due to the small number of observations and low replication at the tree and site scale. Therefore, it was possible the observations did not capture significant variation between trees or may have been subject to site-specific artefacts, and thereby may not have fully captured variation in the growth of poplar SRC. Additionally the observations were considered partially dependent as some were used to inform and constrain parameterisation of the model. Given this, a margin of disagreement between the model and observations was allowed for, so long as the model behaviour was sensible. Key constraints in the model structure were identified as the lack of a separate above- and below-ground 'carbon store', the inclusion of which was identified as a priority for future work. This would allow a

more realistic representation of the post-coppice re-growth phase of the SRC cycle. Additionally, it was evident that further improvements to the allocation of carbon to the different vegetation pools was needed to improve simulation of carbon in the different plant pools, especially for *P. x euramericana*, and during the initial establishment year.

This work has successfully modified and parameterised JULES to simulate the growth and water-use of *P. x euramericana* and *P. nigra* managed as SRC. Until now, representation of this vegetation type in the JULES land-surface scheme was lacking. Its inclusion will contribute to studies by allowing for a more realistic representation of the land cover both in the UK and globally. Additionally it provides a tool to investigate the variability of the growth of these crops and their responses to changes in environmental conditions, which are important both economically and environmentally. This modified version of the model will therefore be used in the following chapter to investigate the variation in yield and water-use of *P. x euramericana* and *P. nigra* SRC in the UK, and how this is affected by climate change.

Chapter 6

Impact Modelling: The response of yield and transpiration of poplar SRC to changes in climate and atmospheric CO_2

6.1 Introduction

As atmospheric CO_2 concentrations continue to rise and the impacts of climate change are increasingly observed globally (IPCC, 2007), alternative energy sources to fossil fuels are being sought to satisfy high energy demands whilst minimising emissions of carbon. Bioenergy from dedicated bioenergy crops is recognised as an alternative, sustainable energy source with significantly lower emissions of carbon compared to conventional fossil fuels. Species of poplar (*Populus spp.*) managed as short rotation coppice (SRC) are one example of a dedicated bioenergy crop. The suitability of poplar varieties for bioenergy is largely due to their fast growth rates and high yields (Bunn *et al.*, 2004; Monclus *et al.*, 2006; Nonhebel, 2002; Scarascia-Mugnozza *et al.*, 1997; Tubby & Armstrong, 2002), although this is generally associated with large water requirements (Hall & Allen, 1997; Hall *et al.*, 1996; Hansen, 1988; Hinckley *et al.*, 1994). Additionally, poplar species are notoriously susceptible to drought (Monclus *et al.*, 2006). Therefore, a fundamental problem with poplar SRC arises, with the necessity to maintain high yields that are economically viable in large-scale plantings across a wide variety of climatic, topographic and edaphic conditions, without significantly compromising water resources in the area.

Changes in climate predicted by GCMs (global circulation models) suggest changes in the frequency and intensity of climate extremes such as heat waves, heavy precipitation and drought. In the UK, for example, warmer, wetter winters and drier summers are predicted, with an increase in the variability and intensity of rainfall and drought (Jenkins *et al.*, 2009). However, this is variable from region to region (Jenkins *et al.*, 2009). Given the importance of site and climatic factors in determining yield and water-use of poplar SRC,

and that the climate is likely to significantly change over the coming decades, this work investigated the variability of poplar SRC responses to changes in climate and atmospheric CO_2 concentration across the UK. To do this, the land-surface scheme JULES was used. In chapters 4 and 5 the JULES model was modified and parameterised to simulate the growth and water-use of two genotypes of poplar SRC. Here I will use this model to address key scientific questions outlined below.

Predictions of the climate response to rising levels of greenhouse gases vary between GCMs and are surrounded by uncertainty. Uncertainty arises from many sources, for example, model structure (i.e. because of incomplete understanding of Earth system processes and their imperfect representation in climate models), parameter uncertainty, natural climate variability (Knutti, 2008; Stainforth *et al.*, 2005; Stott & Kettleborough, 2002), and uncertainty surrounding emissions scenarios used to generate trajectories for atmospheric CO_2 and other greenhouse gases into the future. These inherent uncertainties in projections of future climate change limit the precision with which impacts can be assessed, therefore multiple climate simulations, known as ensembles, are used to help sample these uncertainties (Challinor *et al.*, 2009). Using an ensemble of climate projections from different GCMs will sample uncertainty due to climate simulation resulting from differences in model structure. This is important in impact studies to determine the full range of possible responses to climate change (Murphy *et al.*, 2004). Therefore, an ensemble approach was taken in this work in which atmospheric forcing from multiple GCMs was used to simulate a changed climate in order to determine the response of yield and transpiration of poplar SRC.

Yield and transpiration responses of poplar SRC were assessed at four climatologically different locations across the UK, and for three different soil types. Climate change was simulated using monthly climate anomalies from an ensemble of GCMs applied to a baseline climate. The anomalies were derived from GCM outputs forced with a 'medium' emissions scenario. A step by step approach was taken to disaggregate and quantify the responses of yield and transpiration to each change independently (i.e. elevated atmospheric CO_2 and a changed climate) and then together, to gain better understanding of the interaction between the two. Therefore, this work addressed the following objectives: 1) How does poplar SRC yield and transpiration differ at four locations in the UK under current climatic conditions, and how does this change under a future climate scenario? 2)

Does soil type significantly impact on yield and transpiration and their response to changes in climate and atmospheric CO_2? 3) Are the responses of yield and transpiration to atmospheric CO_2 significantly modified by interaction with the climate? 4) Does elevated atmospheric CO_2 offset the negative impacts of drought?

6.2 Methods and materials

6.2.1 Atmospheric forcing

The land-surface scheme JULES was used to simulate the response of yield and transpiration of *P. x euramericana* and *P. nigra* at four locations in the UK to perturbations in climate and atmospheric CO_2 concentration, summarised in Table 1. In the previous chapters, the JULES model has been parameterised to simulate the growth and transpiration of both *P. x euramericana* and *P. nigra* SRC. In this chapter, the model was first run to simulate the yield (kg C m^{-2}) and transpiration (mm day^{-1}) of both poplar genotypes under the current climate scenario. This used a baseline data set of observed climatology on an hourly time step over a 30 year period from 1972 to 2002. A thirty year period was used as this is considered the standard time period over which to define a baseline climate (IPCC-TGICA, 2007). With the exception of rainfall, the baseline climate had been derived from the Met Office Rainfall and Evaporation Calculation System (MORECS). This provided a historic data set of observed climatology at 40 km resolution with which to drive the model. Derivation of the meteorological variables necessary for driving JULES from this data set was performed by Dr Jon Finch of the Centre for Ecology and Hydrology and is outlined below.

MORECS is a daily data set of observations from meteorological stations on a 40 x 40 km grid. Recorded observations include air temperature, vapour pressure, total sunshine hours and wind speed. Driving variables required by JULES are air temperature, vapour pressure, downward solar radiation, downward longwave radiation, wind speed, rainfall and specific humidity. Thompson *et al*. (1981) describe the spatial interpolation of observations from the station locations to the MORECS grid. Observed air temperature and vapour pressure were corrected for altitude using a lapse rate correction according to Hough and Jones (1997), using the average topographic elevation within a given grid cell. Downward global solar radiation was calculated from the daily total sunshine hours for each grid cell using

the Ångström - Prescott equation (Ångström, 1918; Prescott, 1940), incorporating coefficients calculated by Cowley (1978). A cloud cover factor was calculated as the number of sunshine hours / total number of sunshine hours. These then determined the proportion of diffuse versus direct beam solar radiation. The calculation of solar angle used the equations given by Iqbal (1983). Downward longwave radiation was calculated from the air temperature, vapour pressure and cloud cover of each grid cell. The downward longwave radiation for clear sky conditions was calculated using the method of Dilley and O'Brien (1998) and the additional component due to clouds was calculated using the equations of Kimball *et al*.(1982). The rainfall data used were derived from measurements of the UK rain gauge network for the period 1961 to 2008. This provided daily totals of rainfall on a 1 km^2 grid for the UK that had been derived for a previous project (Continuous Estimation of River Flows; CERF), these were then aggregated to a 40 km^2 grid. Details of the spatial interpolation and corrections for topographic elevation are given in Keller *et al*.(2006). Altogether, these data sets provided daily values of the required driving variables for JULES. JULES however runs on a sub-daily time step, and consequently incorporates code to disaggregate the data to an hourly time step.

To simulate a changed climate, monthly climate anomalies resulting from simulations by ten different GCMs used in The Intergovernmental Panel on Climate Change (IPCC) Fourth Assessment Report were applied to the baseline climate data (Table 2). Reported as both the absolute and relative anomaly (relative to the control run), the anomalies were derived for each GCM and climate variable respectively by subtracting the monthly average generated by a future climate run from the monthly average resulting from the control run of the same GCM, and in the case of the relative anomaly, this was divided through by the control run monthly average. The anomalies are described in more detail in the next section. Each GCM was forced with the same emissions scenario for the control run (20C3M; http://www.ipcc-data.org/ar4/scenario-20C3M.html), which depicts greenhouse gases increasing as observed through the twentieth century. For this work, the anomalies were derived from the future run of each GCM forced under the IPCC SRES (Special Report on Emissions Scenarios) emissions scenario A1B (Nakicenovic & Swart, 2000). The IPCC SRES emissions scenarios were developed to explore future changes in the global environment with special reference to the production of greenhouse gases and aerosol precursor emissions, depending on different interactions between energy, economy, demography and land-use changes (IPCC-DDC, 2009a). The A1B scenario depicts a future

world of very rapid economic growth, global population that peaks in the mid-century and declines thereafter, and rapid introduction of new and more efficient technologies that are balanced across all energy sources (fossil and non-fossil) (IPCC-DDC, 2009a). The A1B scenario was used as it represents the medium trajectory for greenhouse gas emissions. The IPCC SRES scenarios therefore describe a range of potential pathways for atmospheric CO_2 and other greenhouse gas emissions to 2100, and allow investigation into changes in the climate resulting from these emissions trajectories.

Ambient atmospheric CO_2 concentration was prescribed in the model as the mean CO_2 concentration over the period 1970 to 2000, equivalent to 345.63 ppm. This information was taken as the mean CO_2 concentration from the two carbon cycle models (BERN and ISAMS) used to generate the pathway for atmospheric CO_2 to 2100 used as forcing in the IPCC AR4 GCMs (IPCC-DDC, 2009b). Elevated atmospheric CO_2 concentration was prescribed in the model as the mean from the two carbon cycle models over the period 2070 to 2099, which was 659.88 ppm.

Experiment name	**Experiment Description**	**Emissions Scenario**	**Atmospheric CO_2 (ppm)**
Current climate	Baseline climate for the period 1972 -2002, ambient CO_2 concentration	A1B	345.63
Elevated CO_2	Baseline climate for the period 1972 -2002, elevated CO_2 concentration	A1B	659.88
Changed climate	Climate change anomalies applied to the thirty year period of baseline climate data to simulate a changed climate with natural climate variability, ambient CO_2 concentration	A1B	345.63
Future climate	Climate change anomalies applied to the baseline climate as above, elevated CO_2 concentration	A1B	659.88

Table 1. Summary of the experiments in this chapter.

Model I.D.	Year	Country	Model name	Horizontal resolution	T*	Vertical resolution
BCM2	2005	Norway	Bergen Climate Model version 2.0	1.9^{o} x 1.9^{o}	T63	L31
GIEH	2004	USA	Model E-H	4.0^{o} x 5.0^{o}	-	L20
NCCCSM	2005	USA	Community Climate System Model version 3	1.4^{o} x 1.4^{o}	T85	L26
INCM3	2004	Russia	Coupled Model version 3.0	4.0^{o} x 5.0^{o}	-	L21
MIMR	2004	Japan	Model for Interdisciplinary Research on Climate version 3.2 medium resolution	2.8^{o} x 2.8^{o}	T42	L20
CNCM3	2004	France	ARPEGE Climate Model version 3	1.9^{o} x 1.9^{o}	T63	L45
FGOALS	2004	China	Flexible Global coupled Ocean-Atmosphere-Land System model version g1.0	2.8^{o} x 2.8^{o}	T42	L26
GIAOM	2004	USA	Atmosphere-Ocean Model	3.0^{o} x 4.0^{o}	-	L12
IPCM4	2005	France	Coupled Model version 4.0	2.5^{o} x 3.75^{o}	-	L19
HADCM3	1997	UK	Hadley centre Coupled Model version 3	2.5^{o} x 3.75^{o}	-	L19

Table 2. The ten GCMs from which climate anomalies were derived under the SRES A1B emissions scenario predicted for the period 2070 to 2099. Horizontal resolution is expressed as degrees latitude by longitude or as a triangular (T*) spectral truncation, in the latter case the translation to degrees latitude and longitude is a rough estimate. Vertical resolution is the number of vertical levels. For more information readers are referred to (IPCC, 2007).

6.2.2 Climate anomalies

From each GCM, monthly anomalies for the following climatic variables were applied to the thirty year period of baseline climate data; precipitation (kg m^{-2} s^{-1}), temperature (K), downward solar radiation (W m^{-2}), humidity (kg kg^{-1}) and total wind speed (m s^{-1}). This allowed simulation of a changed climate accounting for natural climate variability. The anomalies used were changes in climate predicted by ten different GCMs under the SRES A1B emissions scenario for the period 2070 to 2099. As with the baseline meteorological driving data, the climate anomalies were region specific. The GCM anomalies had been previously derived and were available from the Climate Change Data Portal developed at the Centre for Ecology and Hydrology (Prudhomme & Lafon, 2008). The choice of GCMs

was essentially random, the only selection criteria was to include different models rather than different versions of the same model (Table 2).

Atmospheric forcing to simulate a changed climate used the relative anomaly for climatic variables. This was used, as opposed to the absolute anomaly, to prevent negative values of, for example, precipitation and wind, that are not physically realistic. The changes were applied to the baseline hourly meteorological data through the application of the monthly percentage change to each hour of baseline data, according to the month. Unfortunately this method does not allow for more complex changes, such as changes in the frequency and distribution of rainfall. Additionally, this method does not distinguish between day time and night time, so, for example, changes in temperature and solar radiation were applied to night time values. Nevertheless, this method was sufficient for the purpose of this work, giving the direction and magnitude of climatic change predicted by different GCMs under the IPCC SRES A1B emissions scenario.

6.2.3 Sites

Four locations were chosen within the UK to investigate the response of poplar SRC to changes in climate and atmospheric CO_2 concentration, listed in Table 3 and shown on Fig. 1. These locations were chosen to represent different climatic zones within the UK based on climatic zones suggested by Gregory (1976). Additionally, observed trends in regional changes in temperature and precipitation over the period 1961 to 2006 from the UKCIP 2009 report (Jenkins *et al.*, 2009) were assessed to help pick areas that differed in their climatic regimes and showed either different patterns or magnitudes of change with a shift in climate.

Site	Lat.^{o}	Lon.^{o}
East England	52.55	0.92
South west England	51.06	-2.89
West Scotland	55.26	-3.98
Wales	52.30	-3.19

Table 3. Sites around the UK used with latitude and longitude.

Fig. 1. Map of the UK with the location of each site.

6.2.4 Climate data

The baseline climate, and the mean change in climate resulting from addition of the climate anomalies prescribed under the SRES A1B emissions scenario from the ensemble of GCMs is described below for the four UK sites. For all meteorological variables, additional plots of the monthly mean, maximum and minimum for each site are shown in Appendix 6A Figs. 6A1-5 for the baseline and future climate scenario.

Plotted as the annual mean for the period 1972 to 2002, Fig. 2a clearly shows the difference in temperatures between the sites. The East and South West of England were warmer than Scotland and Wales. Winter temperatures were different between all sites (Table 4). The coldest site was Wales, although this site had the largest range of mean winter temperature. The next coldest site was Scotland showing only a marginal increase in mean winter temperature from the Welsh site. Mean winter temperature in the East of England was higher than in Scotland or Wales, but overall, the South West of England was the warmest site during the winter (Table 4). Through the rest of the year, the East of England was the warmest site, especially during the spring and summer months, where average monthly temperatures were higher than those at the other three sites (Table 4). The South West was the next warmest site, followed by Wales and Scotland, which was the

coldest site during spring, summer and autumn (Table 4). With climate change, mean seasonal temperature increased at all sites (Table 4). The differences in mean temperature between the sites remained the same, however the East of England experienced the greatest warming under a changed climate in all seasons except during the winter, where the Scottish site experienced the greatest mean warming. The change in seasonal mean temperature as a result of climate change was lowest at the Welsh site in all seasons except during the summer, where it was lowest at the Scottish site (Table 4).

The annual mean precipitation rate for the period 1972 to 2002 clearly showed that rates of precipitation were highest in Scotland and lowest in the East of England (Fig. 2b). The South West and Wales showed similar patterns of precipitation in terms of yearly average (Fig. 2a). The difference in precipitation rate between the wettest and driest sites (Scotland and the East respectively) was extremely large, with the Scottish site receiving more than double the rainfall than the East in all seasons except the summer (Table 4). In Scotland, the South West and Wales it was noticeable that mean rates of precipitation were higher in the autumn and winter than in the spring and summer, whereas in the East mean rates of precipitation were consistently low throughout the year (Table 4). With climate change, at all sites the trend of wetter winters and drier summers was clearly evident. The seasonal mean precipitation was increased at all sites during the winter and spring. Across all sites, the increase in mean winter precipitation relative to the baseline climate ranged from +13.8% in the East of England to +17.8% in Wales. During the summer and autumn months however, the mean precipitation decreased relative to the baseline rate, except in Scotland where the mean rate of precipitation increased again during the autumn (Table 4). During winter and spring, the increase in mean precipitation was greatest in Wales and Scotland respectively, and lowest in the East of England. Mean seasonal precipitation decreased at all sites during the summer, this decrease was smallest in Scotland (-7.7%), and largest at the Welsh site (-21.1%).

The annual mean shortwave radiation was highest in the South West of England, lowest in Scotland, and similar in the East of England and Wales (Fig. 2c). The seasonal mean shortwave radiation was also consistently highest in the South West and lowest in Scotland throughout the year (Table 4). The seasonal mean shortwave radiation was similar in the East of England and Wales, but was marginally higher at the Welsh site during winter and spring, and in the East during summer and autumn (Table 4). With climate change, the

trend of seasonal mean shortwave radiation between sites remained the same, however, during the winter all sites experienced a decrease in mean shortwave radiation ranging from -7.0% at the Scottish site to -2.5% in the South West relative to the baseline climate (Table 4). During the rest of the year, the mean shortwave radiation increased at all sites, except in Scotland during the spring where mean shortwave radiation was decreased by -2.1% relative to the baseline climate. During the summer and autumn months, large increases in mean shortwave radiation were shown at all sites, and these were largest at the Welsh site. This was with the exception of the Scottish site, where mean seasonal shortwave radiation increased over this period, but was minimal.

Trends of the annual mean specific humidity were similar in the South West and East of England, and in Scotland and Wales, but were detectably higher in the former (Fig. 2d). The seasonal means suggest the specific humidity was highest in the South West in the winter and spring, and highest in both the East and South West during the summer and autumn (Table 4). The seasonal mean specific humidity was similar in Wales and Scotland, however the spread of data (range and s.e.) was noticeably larger at the Welsh site (Table 4). The change in the seasonal mean of specific humidity with a change in climate was more difficult to assess, however with climate change the range of mean seasonal specific humidity increased at all sites and in all seasons (Table 4). Additionally, the plots of monthly means (see Appendix 6A Fig. 6A-4) suggested in many months the mean specific humidity was higher under a changed climate.

Mean annual wind speed was highest in the East of England over the period 1972 to 2002 (Fig. 2e). At the remaining three sites up to 1990 the yearly average wind speed was similar, after 1990 however, the means diverged with a significant increase in windiness in the South West. In 2000 a similar trend was found in Scotland where the mean annual wind speed increased (Fig. 2e). The seasonal means show the wind speed was highest in the East of England , followed by the South West, Scotland and Wales, and this trend was consistent throughout the year (Table 4). With climate change, the pattern of difference in seasonal mean wind speed between sites remained the same, i.e. the East of England was the windiest site, and Wales the least windy. The East experienced a decrease in mean wind speed throughout the year that ranged between -1.7% to -3.3% relative to the baseline climate. Mean wind speed also decreased marginally in the South West of England in all

seasons except spring. With a changed climate, both Scotland and Wales saw an increase in the mean wind speed throughout the year, this was greatest at the Scottish site.

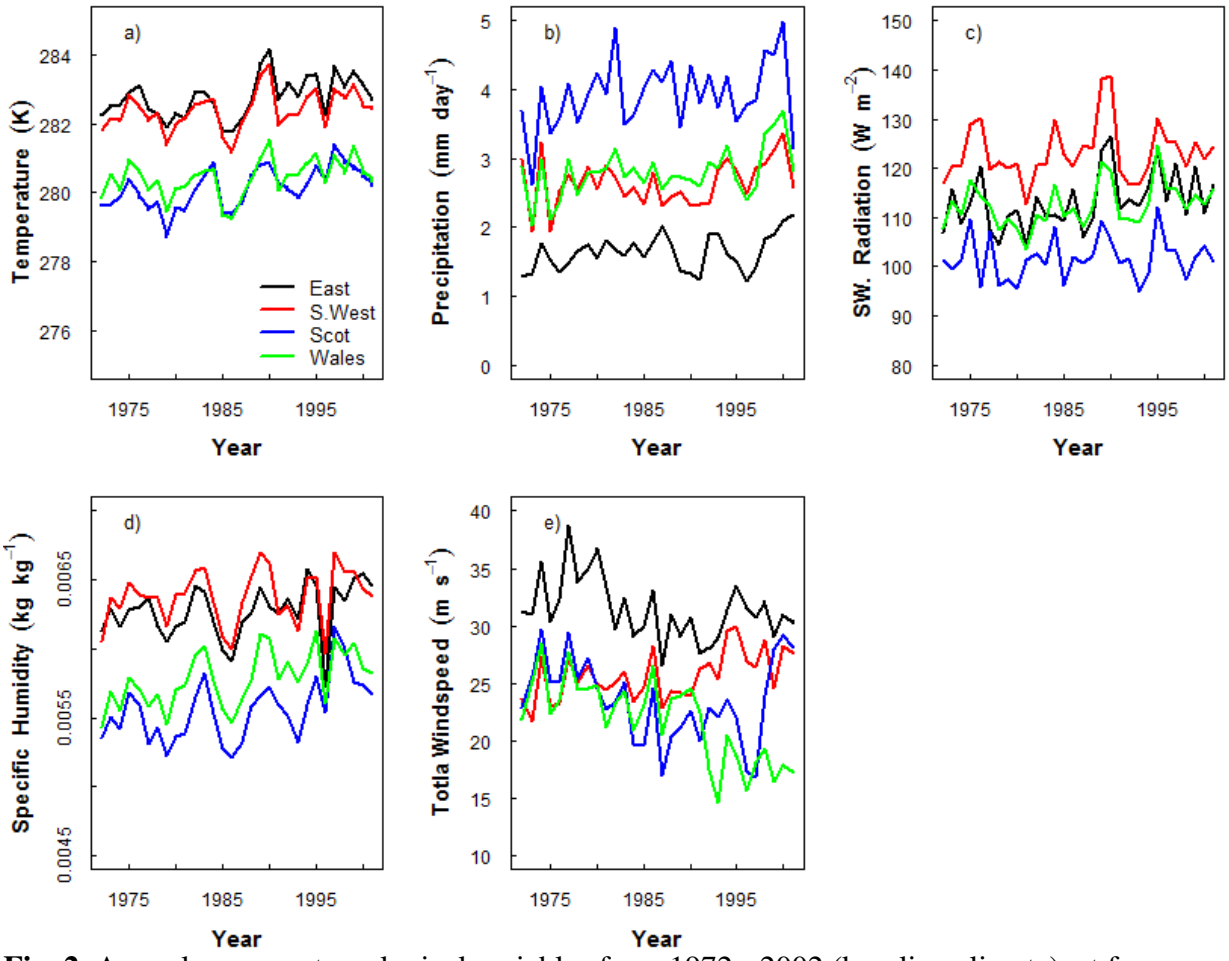

Fig. 2. Annual mean meteorological variables from 1972 - 2002 (baseline climate), at four locations around the UK; East of England (black), South West England (red), Scotland (blue) and Wales (green). **a)** temperature (K), **b)** precipitation (mm day^{-1}), **c)** downward shortwave radiation (W m^{-2}), **d)** specific humidity (kg kg^{-1}), and **e)** wind speed (m s^{-1}).

	Ambient Climate				Future Climate			
	Temperature (K)				Temperature (K)			
	DJF	**MAM**	**JJA**	**SON**	**DJF**	**MAM**	**JJA**	**SON**
East	276.92 ± 0.06	281.36 ± 0.07	288.86 ± 0.06	283.38 ± 0.08	279.82 ± 0.02	283.81 ± 0.02	291.66 ± 0.02	286.13 ± 0.03
	21.89	22.13	19.84	24.29	27.55	25.44	23.48	27.99
Scot.	275.20 ± 0.06	279.06 ± 0.06	285.57 ± 0.05	280.56 ± 0.07	278.18 ± 0.02	281.41 ± 0.02	287.79 ± 0.02	283.10 ± 0.02
	21.22	20.37	17.26	24.65	30.11	23.67	20.38	28.20
S.West	277.48 ± 0.06	280.88 ± 0.06	287.72 ± 0.05	283.06 ± 0.07	279.88 ± 0.02	283.00 ± 0.02	290.27 ± 0.02	285.53 ± 0.02
	20.66	22.11	16.87	20.96	22.80	25.01	19.96	23.87
Wales	275.02 ± 0.07	279.14 ± 0.06	286.00 ± 0.05	280.64 ± 0.07	277.34 ± 0.02	281.17 ± 0.02	288.61 ± 0.02	283.10 ± 0.02
	26.70	21.32	18.45	23.95	28.15	23.10	21.29	27.01
	Precipitation (mm day^{-1})				Precipitation (mm day^{-1})			
	DJF	**MAM**	**JJA**	**SON**	**DJF**	**MAM**	**JJA**	**SON**
East	1.60 ± 0.05	1.46 ± 0.05	1.60 ± 0.07	1.88 ± 0.07	1.82 ± 0.02	1.53 ± 0.02	1.38 ± 0.02	1.77 ± 0.02
	25.20	26.14	35.65	35.50	33.99	34.94	42.51	37.82
Scot.	4.99 ± 0.14	3.05 ± 0.10	2.85 ± 0.10	4.86 ± 0.15	5.82 ± 0.05	3.26 ± 0.04	2.63 ± 0.03	4.98 ± 0.05
	53.82	44.99	42.11	79.13	72.63	66.82	48.87	91.53
S.West	3.42 ± 0.11	2.25 ± 0.08	1.88 ± 0.08	3.05 ± 0.11	3.92 ± 0.04	2.37 ± 0.03	1.56 ± 0.02	2.86 ± 0.03
	45.25	33.72	52.40	67.99	60.07	45.86	57.58	73.31
Wales	3.54 ± 0.10	2.38 ± 0.08	2.04 ± 0.08	3.24 ± 0.11	4.17 ± 0.04	2.51 ± 0.03	1.61 ± 0.02	3.10 ± 0.03
	44.59	32.17	51.9	64.83	58.79	47.99	57.04	69.91
	SW radiation (W m^{-2})				SW radiation (W m^{-2})			
	DJF	**MAM**	**JJA**	**SON**	**DJF**	**MAM**	**JJA**	**SON**
East	32.85 ± 0.43	150.05 ± 1.47	195.26 ± 1.3	73.02 ± 0.88	31.74 ± 0.13	150.89 ± 0.48	204.35 ± 0.42	77.38 ± 0.31
	113.66	327.71	303.01	206.52	123.79	380.08	340.42	251.40
Scot.	26.47 ± 0.40	140.94 ± 1.45	177.33 ± 1.32	60.24 ± 0.80	24.62 ± 0.12	138.00 ± 0.46	178.89 ± 0.42	61.05 ± 0.27
	120.94	360.66	345.19	216.48	129.37	392.18	395.60	254.48

S.West	40.50 ± 0.51	164.06 ± 1.50	206.27 ± 1.32	80.25 ± 0.92	39.50 ± 0.16	164.17 ± 0.49	217.06 ± 0.44	84.12 ± 0.32
	149.1	341.17	339.57	222.47	159.97	396.73	392.51	270.48
Wales	34.68 ± 0.40	152.36 ± 1.29	189.53 ± 1.10	71.61 ± 0.82	33.08 ± 0.12	152.88 ± 0.42	200.35 ± 0.37	76.67 ± 0.29
	119.01	315.04	294.36	213.66	128.72	362.36	342.00	256.16
	Specific humidity (kg kg^{-1})				**Specific humidity (kg kg^{-1})**			
	DJF	**MAM**	**JJA**	**SON**	**DJF**	**MAM**	**JJA**	**SON**
East	0.004 ± 2.1e-05	0.005 ± 2.6e-05	0.009 ± 3.1e-05	0.007 ± 3.5e-05	0.004 ± 7.3e-06	0.006 ± 8.5e-06	0.009 ± 1.0e-05	0.007 ± 1.1e-05
	0.006	0.008	0.010	0.010	0.007	0.009	0.010	0.010
Scot.	0.004 ± 2.0e-05	0.005 ± 2.2e-05	0.008 ± 2.6e-05	0.006 ± 2.9e-05	0.004 ± 6.8e-06	0.005 ± 7.5e-06	0.008 ± 8.7e-06	0.006 ± 1.0e-05
	0.007	0.007	0.009	0.008	0.008	0.009	0.010	0.009
S.West	0.005 ± 2.3e-05	0.006 ± 2.5e-05	0.009 ± 2.6e-05	0.007 ± 3.2e-05	0.005 ± 7.8e-06	0.006 ± 8.2e-06	0.009 ± 8.8e-06	0.007 ± 1.1e-05
	0.007	0.009	0.009	0.009	0.008	0.010	0.009	0.010
Wales	0.004 ± 2.0e-05	0.005 ± 2.4e-05	0.008 ± 2.7e-05	0.006 ± 3.0e-05	0.004 ± 6.9e-06	0.005 ± 8.0e-06	0.008 ± 9.3e-06	0.006 ± 1.0e-05
	0.007	0.009	0.011	0.009	0.007	0.010	0.012	0.010
	Wind speed (m s^{-1})				**Wind speed (m s^{-1})**			
	DJF	**MAM**	**JJA**	**SON**	**DJF**	**MAM**	**JJA**	**SON**
East	35.25 ± 0.30	32.03 ± 0.24	27.18 ± 0.18	31.53 ± 0.25	34.19 ± 0.09	31.49 ± 0.07	26.58 ± 0.06	30.53 ± 0.08
	92.53	75.85	62.84	83.58	90.71	79.07	64.63	82.19
Scot.	26.86 ± 0.32	23.35 ± 0.23	19.72 ± 0.18	24.13 ± 0.27	27.12 ± 0.10	23.66 ± 0.07	20.15 ± 0.06	24.33 ± 0.09
	96.20	73.44	59.19	91.18	97.48	75.06	66.71	94.11
S.West	29.68 ± 0.28	25.95 ± 0.22	21.77 ± 0.16	25.39 ± 0.24	29.47 ± 0.09	25.99 ± 0.07	21.75 ± 0.05	25.20 ± 0.07
	83.75	77.19	57.41	86.76	83.07	77.86	57.05	87.65
Wales	25.38 ± 0.26	21.83 ± 0.20	18.24 ± 0.16	21.72 ± 0.22	25.58 ± 0.08	22.09 ± 0.06	18.48 ± 0.05	21.85 ± 0.07
	72.18	64.99	57.82	71.15	74.14	65.56	60.92	72.09

Table 4. Seasonal mean ± s.e and range of climate variables at four locations in the UK for ambient (baseline climate) and future (baseline + anomalies) climate conditions; DJF = December, January, February; MAM = March, April, May; JJA = June, July, August; SON = September, October, November. The mean and range for the future climate is the mean of the ensemble of GCM anomalies.

6.2.5 Model parameters

The land-surface scheme JULES had been modified in the previous chapter (Chapter 5) to simulate the growth, carbon allocation and harvesting of poplar SRC. This involved changes to the model code and finding suitable parameter values to improve simulation of the growth and transpiration. The parameter values used are shown again for clarity in Table 5. Suitable parameterisations for leaf-level photosynthesis and stomatal conductance for both *P. x euramericana* and *P. nigra* were determined in Chapter 4. The parameters are used in this work and are also shown in Table 5.

	P. x euramericana	*P. nigra*
a_{wl} (kg C m^{-2})	0.300	0.150
a_{ws}	10.000	10.000
b_{wl}	1.667	1.667
η_{sl} (kg C m^{-2})	0.010	0.007
σ_l (kg C m^{-2} leaf)	0.020	0.020
V_{max} (μmol CO_2 m^{-2} s^{-1})	74.340	69.840
α_{int} (mol mol^{-1})	0.076	0.076
F_0	0.875	0.875
D_c (kg kg^{-1})	0.070	0.070

Table 5. Growth parameter values used in JULES to determine growth and carbon allocation to stem, leaf and root pools in the vegetation, and the rates of leaf-level photosynthesis and stomatal conductance. Values are shown for *P. x euramericana* and *P. nigra* as determined in Chapter 5 and Chapter 4 respectively: a_{wl} is the allometric coefficient relating the target woody biomass to the leaf area index; a_{ws} relates the woody biomass to the live stem biomass; b_{wl} is the allometric exponent relating the target woody biomass to the leaf area index; η_{sl} is the live stemwood coefficient; σ_l is the specific density of leaf carbon; V_{max} is the maximum rate of carboxylation; α_{int} is the intrinsic quantum efficiency; F_0 is c_i/c_a ratio for specific humidity deficit in canopy; D_c is the critical humidity deficit.

Three different sets of soil parameterisations were used to investigate the impact of soil type on the growth and water use of *P. x euramericana* and *P. nigra*, these are listed in Table 6. Sand, silt and clay soil types were used as these contrast in their textural

properties and water holding capacities. Using a soil texture triangle, the three soil types were defined by their textural properties (% sand, % silt, % clay). A sand soil was defined as one containing roughly 80 to 90 % sand, a silt soil was classified as containing roughly 80 % silt, 10 % sand and 10 % clay, and a clay soil was classified as comprising roughly 70 % clay. Physical properties for these three soil textural classes were then determined using the NSRI (National Soil Resource Institute) soil series data for England and Wales, and the MLURI (Macaulay Land Use Research Institute) for Scotland. Fortunately these data were readily available having previously been collated by Dr Jon Finch of the Centre for Ecology and Hydrology, providing the necessary hydraulic, thermal and van Genuchten parameters required for the model (Table 6). Additionally, where properties were found to vary with depth, the necessary scaling to the different soil layers within the model had already been conducted. Where soil properties varied with depth, the parameters for the dominant soil layer for the depth interval of the JULES soil model layer were used (*Finch pers. comm., 2009*). Additionally, the maximum depth to which values for the soil parameters are present in the NSRI data set is 1 m and for the MLURI data set it is 1.5 m. Therefore, the soil parameters were extrapolated to the full depth required by the JULES model (3 m) by assuming that the parameters for the deepest soil layer applied down to a depth of 3 m (*Finch pers. comm., 2009*).

Soil	JULES soil layer	van Genuchten parameter (m^{-1})	van Genuchten parameter	Heat capacity of dry soil ($J\ m^{-3}\ k^{-1}$)	Thermal conductivity of dry soil ($W\ m^{-3}\ K^{-1}$)	Hydrualic conductivity at saturation ($kg\ m^{-2}\ s^{-1}$)
		$1/\alpha$	$1/(n-1)$	C_{dry}	λ_{dry}	k_s
Clay	1	0.266	4.6555	8.00×10^5	0.58446	0.00892
	2	0.266	4.6555	8.00×10^5	0.58446	0.00892
	3	0.266	4.6555	8.00×10^5	0.58446	0.00892
	4	0.266	4.6555	8.00×10^5	0.58446	0.00892
Silt	1	0.254	4.0371	7.26×10^5	0.27066	0.01747
	2	0.227	3.6832	9.87×10^5	0.35496	0.01387
	3	0.207	3.7286	1.04×10^5	0.36942	0.01068
	4	0.167	3.4602	1.06×10^5	0.34476	0.01777
Sand	1 to 4	0.103	2.8498	9.13×10^5	0.30516	0.04771

Soil	JULES soil layer	Volumetric water content at critical point ($m^3\ m^{-3}$)	Volumetric water content at saturation ($m^3\ m^{-3}$)	Volumetric water content at wilting point ($m^3\ m^{-3}$)
		θ_c	θ_s	θ_w
Clay	1	0.21056	0.3809	0.09727
	2	0.21056	0.3809	0.09728
	3	0.21056	0.3809	0.09729
	4	0.21056	0.3809	0.0973
Silt	1	0.2426	0.4856	0.09945
	2	0.14215	0.313	0.05342
	3	0.12692	0.2835	0.04824
	4	0.10671	0.2697	0.03757
Sand	1 to 4	0.09671	0.3518	0.02716

Table 6. Physical soil properties.

6.2.5 Statistical analysis

The yield was analysed using the mean of the final yield achieved in year three of each rotation over the thirty year period of driving data. The transpiration was analysed using the mean of the annual mean transpiration rate of the poplar SRC trees over the thirty year period of driving data. The soil moisture content and soil moisture stress factor (β factor or *fsmc*) were both analysed using the monthly mean over the thirty year period of driving data.

Statistical analysis of the model results was performed because of the variation arising from the different genotypes, soil types and GCM anomalies. As a result of the experimental design, the model results included both temporal and spatial pseudoreplication. Spatial pseudoreplication arose between sites as a result of the simulations being run over the same thirty year time period. Correlation between sites would therefore exist as a result of the driving data, for example, if it was a hot year, it would likely be a hot year at all sites. Temporal pseudoreplication arose as a result of repeated simulations at each site and combination of factor levels (i.e. site, soil, genotype, GCM, CO_2 concentration and climate scenario) over same the thirty year period. Therefore, output from each simulation (i.e. each unique combination of factor levels) was not independent. The model output were therefore analysed using a linear mixed-effects model, using the package *lme4* (Bates & Maechler, 2009) available in the statistical software *R2.10.1* (R2.10.1, 2009). To account for the pseudoreplication arising from the experimental design (i.e. repeated measures at each unique combination of factor levels) a random effect termed "block" is included in the statistical model. The categorical variable 'block' comprises a unique code to identify each unique combination of factor levels, effectively treating them as crossed factors (Faraway 2006). An example of the statistical model used is shown below, specific models used in each analysis are shown in Appendix 6C-1 and 6C-2:

yield~site+soil+gen+co_2+climate+co_2:climate+(1|block)+(1|year)

Where, yield is the response variable, site, soil, gen, co_2 and climate are fixed effects (":" is the notation for an interaction), and (1|block) (1|year) are random effects to handle the experimental pseudoreplication. Model residuals were checked for assumptions of normaility. Significance of fixed effects were tested for using likelihood ratio tests (*LRT*) that use the chi-squared (x^2) distribution and maximum likelihood estimators (*MLE*) (Faraway, 2006). Following the approach of Faraway (2006), parametric bootstrap methods were also used to provide a more robust estimate of the significance of the test statistic. In all boxplots shown, the black horizontal line in the coloured bar represents the median, the 'x' represents the mean, the top and bottom of the coloured bar represent the 75th and 25th percentiles respectively, and the extended dashed lines represent the maximum and minimum values.

6.3 Results

6.3.1 Experiment 1: Current climate

6.3.1.1 Yield

The mean of the maximum predicted yield achieved at the end of each three year rotation was different between the four sites ($x^2 = 86.56, p < 0.001, n = 240$). Additionally, at all sites the harvestable yield was consistently higher in *P. nigra* (Fig. 3; Table 7) ($x^2 = 32.46, p < 0.001, n = 240$). Soil type, however, had no impact on the final harvestable yield. The same variation in yield with site was observed in both genotypes. Yield was highest in the South West (*P. x euramericana*: $x^2 = 42.85, p < 0.001, n = 120$; *P. nigra*: $x^2 = 36.49, p < 0.001, n = 120$), lowest in the East (*P. x euramericana*: $x^2 = 30.16, p < 0.001, n = 120$; *P. nigra*: $x^2 = 34.70, p < 0.001, n = 120$), and no differences were detected between the Scottish and Welsh sites. All the sites suggested that there was a large range in mean predicted yield over the thirty year period, and the magnitude of this was greatest in *P. nigra*. Nevertheless, at all sites and in both genotypes the middle 50% of the data were fairly tightly distributed around the mean (Table 7; Fig. 3), although there was a slight skew towards predicted values in the lower range which was most noticeable at the Welsh site. A degree of variability in the yield is to be expected in line with natural variability that occurs in the climate from year to year. This initial modelling experiment under the baseline climate goes some way to assess the variation in yield as a result of this, and provide a point of comparison for the further experiments. Additionally, however, these results include the mean across all three soil types, and although no impact of soil type on mean predicted yield was detected, it will inevitably contribute variation to the results.

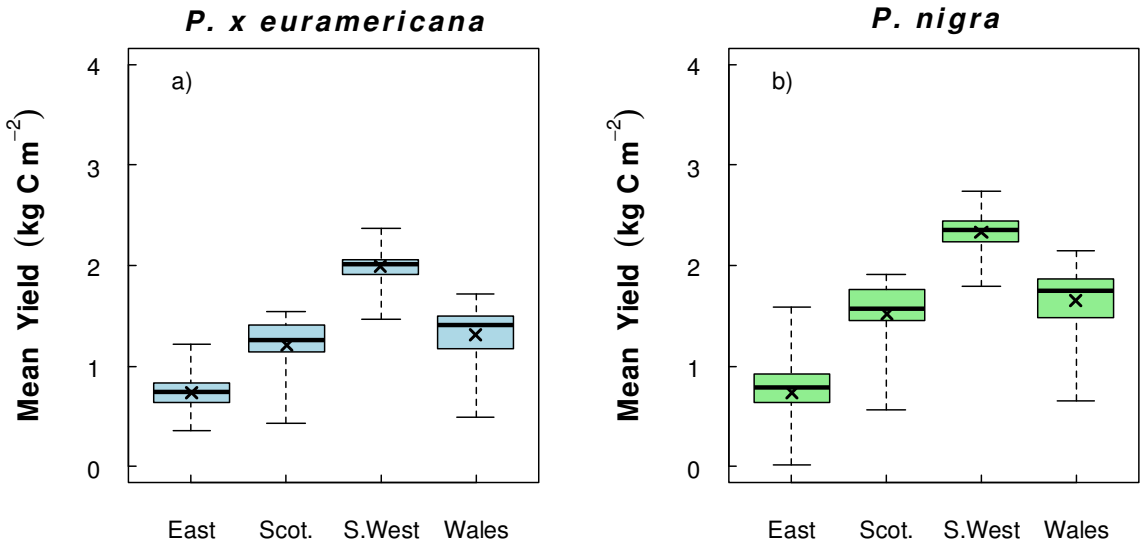

Fig. 3. Mean maximum yield (kg C m^{-2}) predicted at each site in the final year of the rotation under ambient climatic conditions over the thirty year period of baseline climate, and all three soil types. The black horizontal line in the coloured bar represents the median, the 'x' represents the mean, the top and bottom of the coloured bar represent the 75th and 25th percentiles respectively, and the extended dashed lines represent the maximum and minimum values.

	Yield (kg C m^{-2}) or *(dry t ha^{-1} yr^{-1})							
	P. x euramericana				*P. nigra*			
	East	Scotland	S. West	Wales	East	Scotland	S. West	Wales
Exp. 1: Baseline climate & ambient CO_2								
Mean ± s.e	0.74 ± 0.04	1.20 ± 0.05	1.99 ± 0.04	1.31 ± 0.06	0.73 ± 0.08	1.52 ± 0.06	2.33 ± 0.04	1.65 ± 0.07
Range	0.86	1.12	0.89	1.22	1.56	1.35	0.95	1.49
Mean* ± s.e	5.14 ± 0.28	8.33 ± 0.35	13.82 ± 0.28	9.10 ± 0.42	5.07 ± 0.56	10.55 ± 0.42	16.18 ± 0.28	11.46 ± 0.49
Exp. 2: Baseline climate & elevated CO_2								
Mean ± s.e	1.42 ± 0.06	1.60 ± 0.05	2.76 ± 0.05	1.77 ± 0.07	1.58 ± 0.07	1.95 ± 0.07	3.18 ± 0.05	2.17 ± 0.08
Range	1.48	1.32	1.12	1.45	1.69	1.52	1.16	1.68
Mean* ± s.e	9.86 ± 0.42	11.11 ± 0.35	19.16 ± 0.35	12.29 ± 0.49	10.97 ± 0.49	13.54 ± 0.49	22.08 ± 0.35	15.07 ± 0.56
% diff.	**100.00**	**33.33**	**38.69**	**35.11**	**116.44**	**22.05**	**36.48**	**23.96**
Exp.3: Changed climate & ambient CO_2								
Mean ± s.e	0.30 ± 0.01	1.86 ± 0.03	1.69 ± 0.02	1.81 ± 0.02	0.28 ± 0.02	2.18 ± 0.03	1.84 ± 0.03	2.07 ± 0.02
Range	1.05	2.61	1.8	1.53	1.14	2.89	2.02	1.99
Mean* ± s.e	2.08 ± 0.07	12.91 ± 0.21	11.73 ± 0.14	12.57 ± 0.14	1.94 ± 0.14	15.14 ± 0.21	12.78 ± 0.21	14.37 ± 0.14
% diff.	**-59.46**	**55.00**	**-15.08**	**38.17**	**-61.64**	**33.85**	**-21.03**	**19.35**
Exp. 4: Changed climate & elevated CO_2								
Mean ± s.e	0.70 ± 0.02	2.56 ± 0.04	3.07 ± 0.03	2.72 ± 0.02	0.74 ± 0.02	2.94 ± 0.04	3.43 ± 0.03	3.09 ± 0.02
Range	1.79	3.31	2.51	2.13	1.94	3.32	2.70	2.17
Mean* ± s.e	4.86 ± 0.14	17.77 ± 0.28	21.32 ± 0.21	18.89 ± 0.14	5.14 ± 0.14	20.41 ± 0.28	23.82 ± 0.21	21.45 ± 0.14
% diff.	**-5.41**	**113.33**	**54.27**	**107.63**	**1.37**	**72.82**	**47.21**	**66.36**
% diff.	133.33	37.63	81.66	50.28	164.29	34.86	86.41	49.28

Table 7. Mean ± s.e and range of predicted harvestable yield at each site in *P. x euramericana* and *P. nigra*. The mean includes the yield at the end of each three year rotation over the thirty year period of driving data, and all three soil types. In each case, the percentage difference shows the difference in yield relative to the baseline climate and ambient CO_2 (experiment 1), calculated as ((future-baseline)/baseline)*100. This is with the exception of the final row (% diff. not in bold), which shows the percentage difference resulting from elevated CO_2 under the changed climate, relative to the changed climate. The yield is shown in modelled units of kg C m^{-2} and then converted into more conventional units of dry tons ha^{-1} yr^{-1}, indicated by an asterisk.

6.3.1.2 Transpiration

The rate of predicted transpiration was analysed as the mean of the yearly mean transpiration rate for the period 1972 to 2002. The mean predicted transpiration was found to differ between sites ($x^2 = 100.27, p < 0.001, n = 720$; Fig. 4; Table 8). In *P. x euramericana*, the predicted transpiration of poplar SRC was highest in the South West ($x^2 = 53.54, p < 0.001, n = 360$), but was not found to differ between the East, Scotland or Wales (Fig. 4; Table 8). In *P. nigra* trees, predicted poplar SRC transpiration was highest in the South West ($x^2 = 49.21, p < 0.001, n = 720$), and although it was not found to differ between Scotland and Wales, it was significantly lower in the East ($x^2 = 15.74, p < 0.001, n = 720$) than at any of the other sites (Fig. 4; Table 8). Soil type had no impact on the mean rate of predicted transpiration, and at all sites, the mean transpiration of the poplars was higher in *P. nigra* compared to *P. x euramericana* ($x^2 = 53.17, p < 0.001, n = 720$). The mean predicted transpiration rate at each site was surrounded by a relatively large range, and compared to the predicted yield, there was a noticeably larger distribution of the middle 50% of the data, suggesting more variability in the prediction of transpiration rate by the model. Plots of the monthly mean transpiration for the period of baseline climate data in both genotypes (Fig. 5a-h) show the monthly variation in transpiration for the different sites. In general, transpiration rates were highest from June to August. Over these months, the data showed a large spread in rates of transpiration for both genotypes, especially in Scotland and the South West. At the site with the highest predicted mean transpiration rates, the South West, maximum rates of transpiration were in excess of 6 mm day^{-1} for *P. x euramericana* and 7 mm day^{-1} for *P. nigra*.

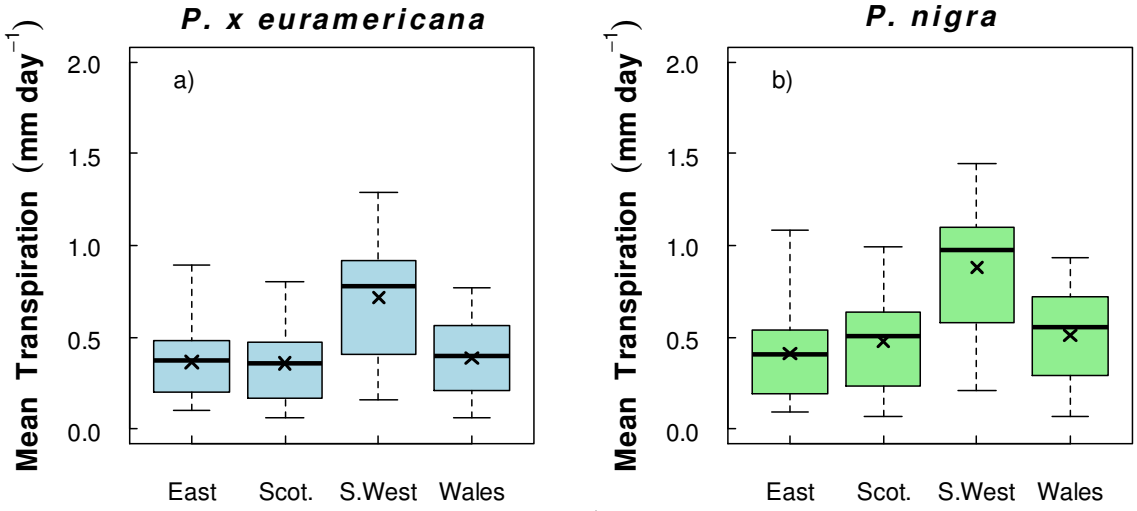

Fig. 4. Mean predicted transpiration (mm day^{-1}) at each site under ambient climatic conditions over the thirty year period of baseline climate, and all three soil types.

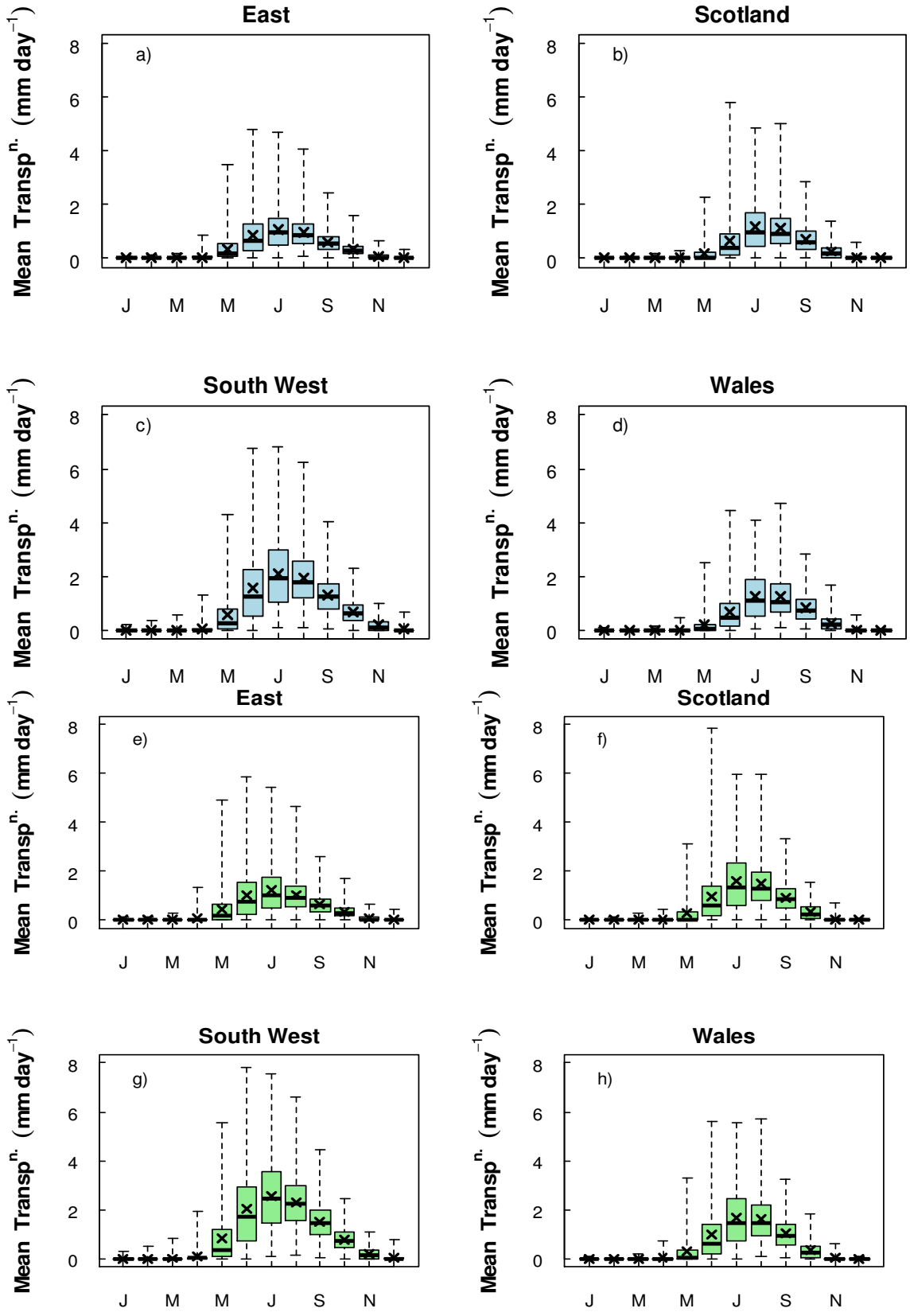

Fig. 5. The monthly mean transpiration under the baseline climate for all sites and both genotypes, the means include all three soil types; panels a - d: *P. x euramericana* (lightblue), panels e - h: *P. nigra* (lightgreen).

	Transpiration (mm day^{-1})							
	P. x euramericana				*P. nigra*			
	East	Scotland	S. West	Wales	East	Scotland	S. West	Wales
	Exp. 1: Baseline climate & ambient CO_2							
Mean ± S.E	0.36 ± 0.02	0.36 ± 0.02	0.72 ± 0.03	0.38 ± 0.02	0.41 ± 0.02	0.48 ± 0.03	0.88 ± 0.03	0.51 ± 0.03
Range	**0.79**	**0.74**	**1.13**	**0.71**	**0.99**	**0.92**	**1.24**	**0.87**
	Exp. 2: Baseline climate & elevated CO_2							
Mean ± S.E	0.36 ± 0.02	0.26 ± 0.02	0.55 ± 0.02	0.29 ± 0.02	0.43 ± 0.02	0.35 ± 0.02	0.67 ± 0.03	0.38 ± 0.02
Range	0.71	0.56	0.92	0.56	0.8	0.69	1.01	0.68
% diff.	**0.00**	**-27.78**	**-23.61**	**-23.68**	**4.88**	**-27.08**	**-31.34**	**-25.49**
	Exp.3: Changed climate & ambient CO_2							
Mean ± S.E	0.24 ± 0.01	0.77 ± 0.01	0.89 ± 0.01	0.77 ± 0.01	0.27 ± 0.01	0.95 ± 0.01	1.04 ± 0.01	0.92 ± 0.01
Range	0.81	2.03	1.37	1.4	0.97	2.23	1.52	1.54
% diff.	**-33.33**	**113.89**	**23.61**	**102.63**	**-34.15**	**97.92**	**18.18**	**80.39**
	Exp. 4: Changed climate & elevated CO_2							
Mean ± S.E	0.25 ± 0.01	0.58 ± 0.01	0.84 ± 0.01	0.63 ± 0.01	0.29 ± 0.01	0.71 ± 0.01	1.00 ± 0.01	0.76 ± 0.01
Range	0.75	1.58	1.35	1.16	0.89	1.68	1.5	1.28
% diff.	**-30.56**	**61.11**	**16.67**	**65.79**	**-29.27**	**47.92**	**13.64**	**49.02**
% diff.	4.17	-24.68	-5.62	-18.18	7.41	-25.26	-3.85	-17.39

Table 8. Mean ± s.e and range of predicted mean transpiration rate at each site in *P. x euramericana* and *P. nigra*. The mean is calculated as the yearly mean transpiration rate over the thirty year period of driving data, and includes all three soil types. In each case, the percentage difference shows the difference in transpiration relative to the historic climate and ambient CO_2, calculated as ((future-baseline)/baseline)*100. This is with the exception of the final row (% diff. not in bold), which shows the percentage difference resulting from elevated CO_2 under the changed climate, relative to the changed climate.

6.3.1.3 Soil moisture and water stress

Differences in mean predicted soil moisture content through the year, taken as the mean of all three soil types, were clearly evident between sites. Similar trends in modelled soil moisture content were seen in both genotypes (Fig. 6a - h). Most striking was the low soil moisture content in the East. During most months, the mean soil moisture content in the East was roughly half that of the wettest site, Scotland. Further, in the South West, Scotland and Wales a decline in soil moisture content during the peak summer months was clearly evident when plant transpiration was highest. However, this was followed by a distinct increase in mean predicted soil moisture content over the following winter months, as the soil moisture content of the soil column was restored. In the East however, this trend was not apparent, suggesting significant soil moisture stress at this site throughout the year.

These differences in mean soil moisture content were reflected in the mean monthly soil moisture stress factor (the β factor; Fig. 7a-h) calculated for the thirty year baseline period. This is the modelled soil moisture stress as experienced by the plant roots, and is calculated as a function of θ, θ_c and θ_w. The β factor ranges between one (no stress) and zero (stressed, transpiration ceases). In Scotland and Wales, the mean soil moisture stress experienced by the poplar SRC trees was minimal across the year. In some months the minimum value of the calculated mean β factor dropped below one suggesting the occurrence of slight soil moisture stress in some years. In the South West, it was evident that the reduced soil moisture content during the growing season was sufficient to cause soil moisture stress, and in some years this may result in a significant stress on the plants. However, these were extreme years as both the mean and the median of the β factor remained above 0.8 during the summer months. In the East, however, there was substantial soil moisture stress throughout the year. Even in winter months the β factor was close to 0.6, and there was a noticeable decline in summer months.

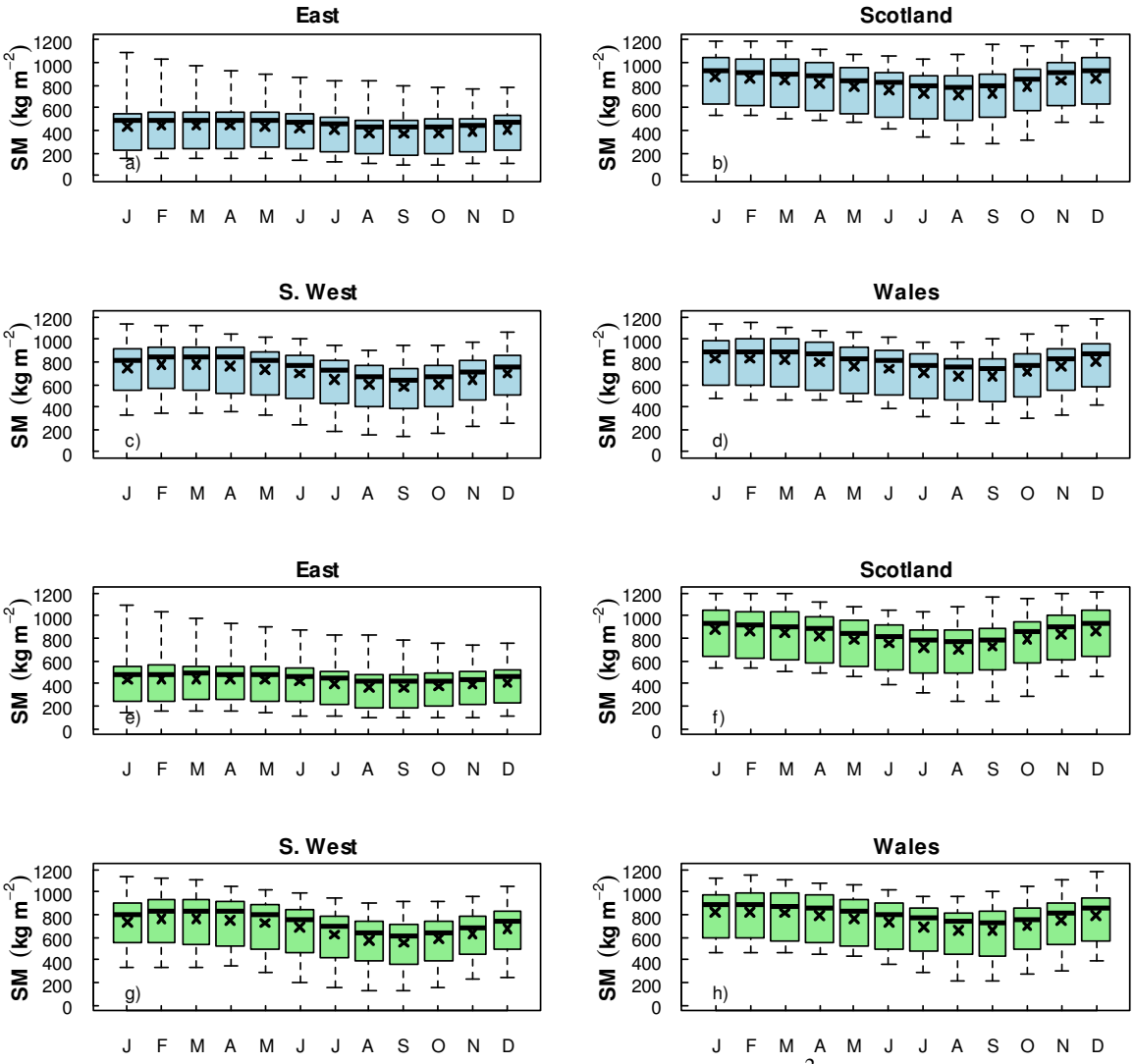

Fig. 6. Monthly mean predicted soil moisture content (SM; kg m^{-2}) of the soil column for the period 1972 to 2002, the mean includes all three soil types; panels a - d: *P. x euramericana*, panels e - h: *P. nigra*.

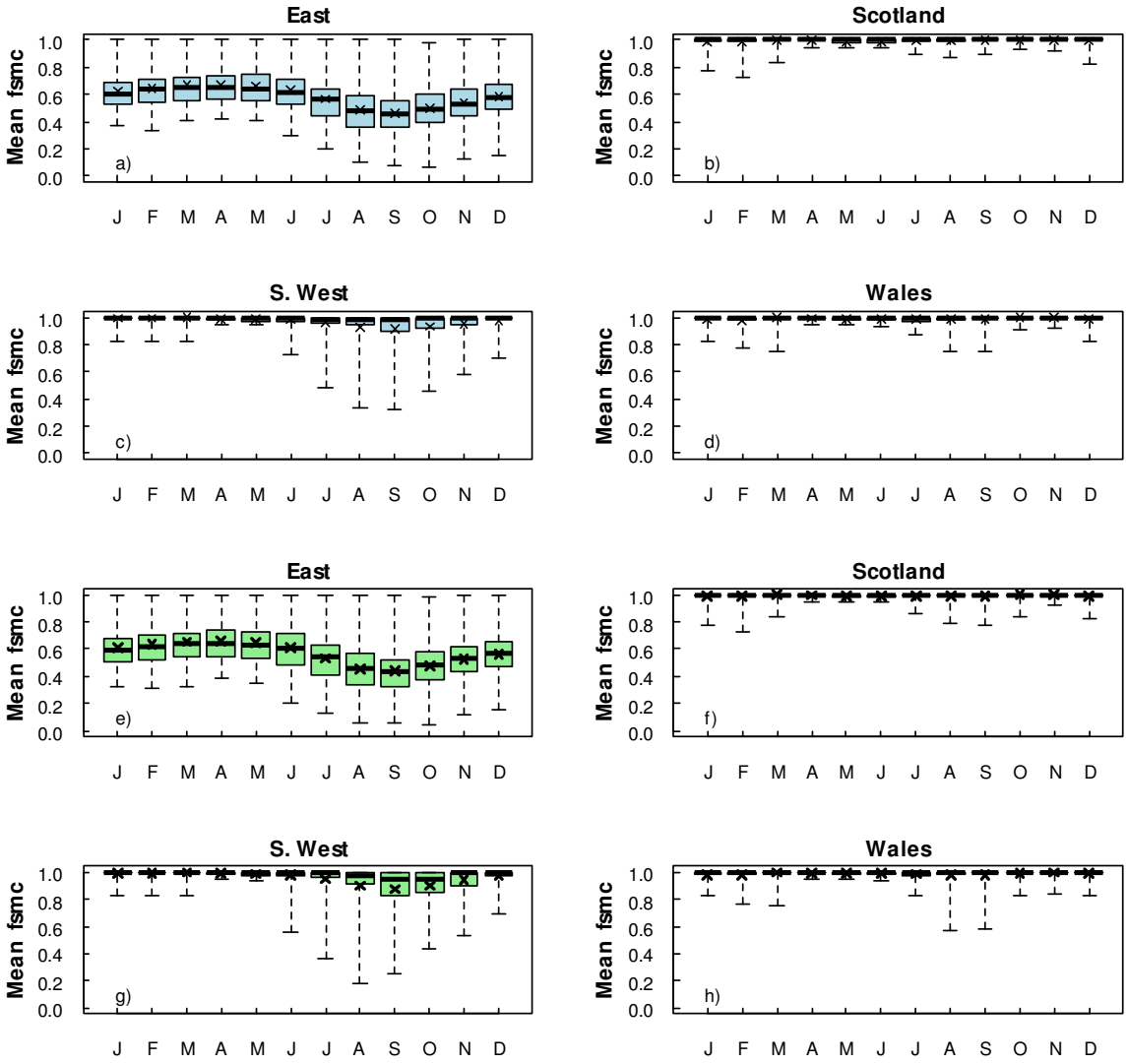

Fig. 7. Monthly mean simulated β factor (*fsmc*) for the period 1972 to 2002, the mean includes all three soil types; panels a - d: *P. x euramericana*, panels e - h: *P. nigra*.

6.3.2 Experiment 2: Elevated CO_2

6.3.2.1 Yield

Growth in an enriched CO_2 atmosphere positively enhanced mean predicted yield at all sites and in both genotypes (Fig. 8; Table 7). Soil type, however, had no impact. The mean predicted yield was higher in *P. nigra* than *P. x euramericana* at all sites ($x^2 = 89.7$, $p < 0.001$, $n = 480$), however the response of yield to elevated atmospheric CO_2 concentration differed dramatically between sites ($x^2 = 48.3$, $p < 0.001$, $n = 480$). Although the East of England remained the lowest yielding site, it saw the greatest enhancement of yield as a

result of the CO_2 fertilisation effect (Table 7). At this site, the percentage increase in yield relative to the baseline climate (ambient CO_2 concentration) was +100.0% and +116.4% for *P. x euramericana* and *P.nigra* respectively. The relative difference between mean predicted yield in the South West was +38.7% and +36.4% for *P. x euramericana* and *P.nigra* respectively. Compared to the relative difference between predicted yields with and without elevated atmospheric CO_2 for Scotland and Wales (Table 7), these results suggest that drought prone sites benefit more from the CO_2 fertilisation effect on yield. Additionally, it is evident that in the East the minimum mean predicted yields were also sunstantially reduced (Fig. 8; Table 7).

Elevated atmospheric CO_2 generated differences in mean predicted yield between sites compared to the baseline climate. In an enriched CO_2 atmosphere, mean predicted yield remained highest in the South West of England (*P. x euramericana*: $x^2 = 38.9$, $p < 0.01$, $n = 120$; *P. nigra*: $x^2 = 36.1$, $p < 0.001$, $n = 120$). The mean yield was marginally higher at the Welsh site than the Scottish site (*P. x euramericana*: $x^2 = 17.5$, $p < 0.01$, $n = 120$; *P. nigra*: $x^2 = 7.8$, $p < 0.01$, $n = 120$; Fig. 8; Table 7). Mean predicted yield was lowest in the East of England (*P. x euramericana*: $x^2 = 7.6$, $p < 0.01$, $n = 120$; *P. nigra*: $x^2 = 15.5$, $p < 0.001$, $n = 120$; Fig. 8; Table 7).

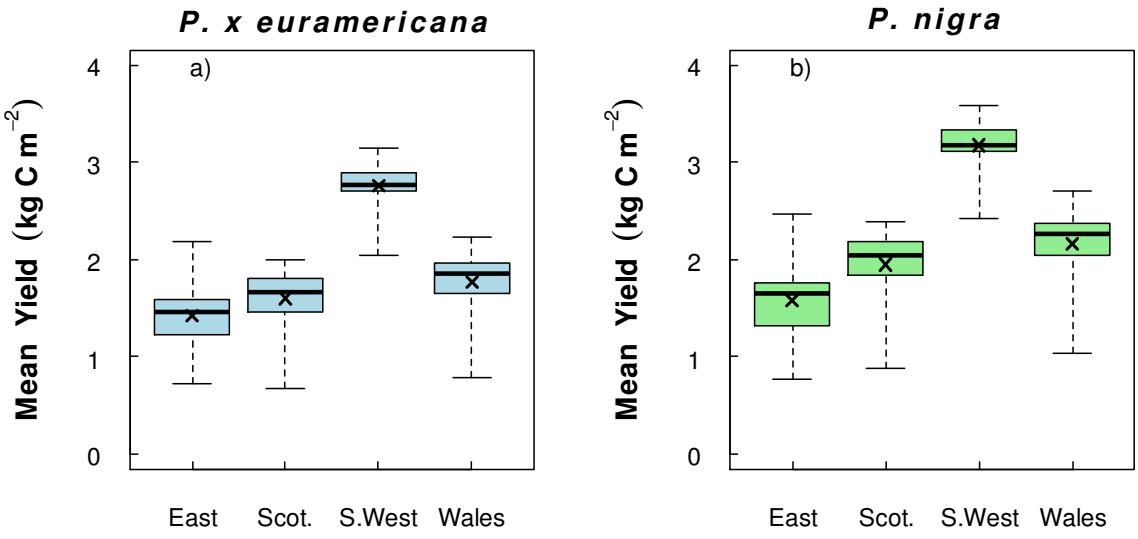

Fig. 8. Mean maximum yield (kg C m^{-2}) predicted at each site in the final year of each three year rotation under the ambient baseline climate and elevated atmospheric CO_2. The mean includes all three soil types.

6.3.2.2 Transpiration

With elevated atmospheric CO_2, predicted mean rates of transpiration decreased at most sites, with the SRC trees displaying a strong CO_2 anti-transpiration response ($x^2 = 65.21$, $p < 0.05$, $n = 1440$; Fig. 9; Table 8). This was with the exception, however, of the East of England. At this site, there was no change in the rate of transpiration with elevated atmospheric CO_2 in *P. x euramericana* trees. In *P. nigra* trees, however, mean predicted transpiration slightly increased in response to elevated atmospheric CO_2 (Table 8). At the other sites, the mean transpiration decreased under elevated atmospheric CO_2, with percentage differences ranging from -23.7 % to -31.3 % depending on site and genotype (Table 8). In *P. x euramericana*, the change in mean predicted transpiration with increased atmospheric CO_2 was greatest at the Scottish site, in *P. nigra* SRC it was greatest in the South West of England. Therefore, the response of transpiration to elevated atmospheric CO_2 is shown to be variable and strongly influenced by site, as driven through the climate, and to some extent genotype.

Mean predicted rates of transpiration by the poplars was higher in *P. nigra* at all sites ($x^2 = 116.28$, $p < 0.05$, $n = 1140$); however, soil type had no detectable impact on the transpiration. The variable CO_2 effect on transpiration at each site generated differences in mean predicted transpiration between sites compared to the baseline climate. As a result, predicted mean transpiration was lowest in Scotland (Fig. 9). This was followed by the Welsh site, with marginally higher rates of transpiration (*P. x euramericana*: $x^2 = 4.47$, $p < 0.01$, $n = 360$; *P. nigra*: $x^2 = 4.08$, $p < 0.001$, $n = 360$; Fig. 9; Table 8). Predicted mean transpiration in the East was higher than at either the Scottish or Welsh sites (*P. x euramericana*: $x^2 = 15.54$, $p < 0.01$, $n = 360$; *P. nigra*: $x^2 = 7.11$, $p < 0.01$, $n = 360$; Fig. 9; Table 8). However, transpiration remained highest in the South West of England (*P. x euramericana*: $x^2 = 37.33$, $p < 0.001$, $n = 360$; *P. nigra*: $x^2 = 37.03$, $p < 0.001$, $n = 360$; Fig. 9; Table 8).

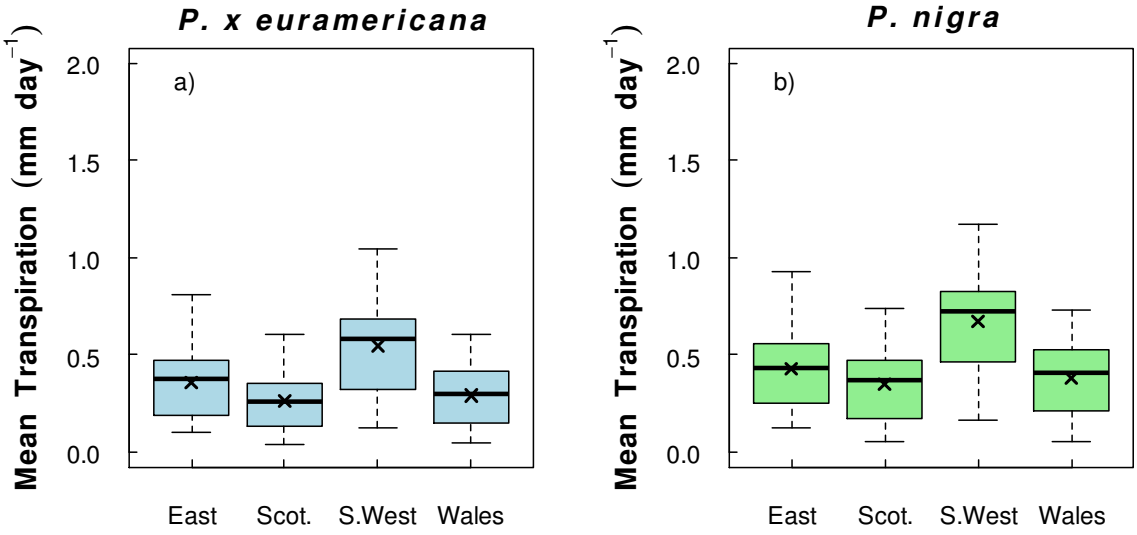

Fig. 9. Mean predicted transpiration (mm day^{-1}) at each site under ambient climatic conditions and elevated atmospheric CO_2. The mean is calculated over the thirty year period of baseline climate data, and all three soil types.

6.3.2.3 Soil moisture and water stress

Plots of the monthly predicted soil moisture content at each site under elevated atmospheric CO_2 are shown in Appendix 6B Fig. 6B-1. It is evident that there is an effect of atmospheric CO_2 concentration soil moisture content, but this is variable between sites. In the East of England mean monthly soil moisture content for both *P. x euramericana* and *P. nigra* SRC increased throughout the year under elevated atmospheric CO_2. The percentage change with increased CO_2 relative to the baseline climate ranged between +7.72 % to +10.70 % for *P. x euramericana* and +6.99 % to +10.27 % for *P. nigra*. This small increase in mean monthly predicted soil moisture content translated into a decrease in soil moisture stress seen by the trees, and this effect was consistent throughout the year in both genotypes (Fig. 10). The mean monthly β factor was increased (less stress), with a percentage difference ranging from +11.41 % to +23.23 % in *P. x euramericana* and from +10.19 % to +21.67 % in *P. nigra*. The minimum monthly value of β was also increased under elevated atmospheric CO_2.

In Scotland, mean monthly predicted soil moisture content marginally decreased compared to ambient atmospheric CO_2 during the first few months of the year (Jan to Apr; see Appendix 6B Fig. 6B-1). This decline was minimal, however, and the percentage difference in soil moisture content ranged from -0.0013 % to -0.019 % for *P. x*

euramericana and from -0.0032 % to -0.024 % for *P. nigra*. Over the remaining months, soil moisture content was marginally increased in elevated atmospheric CO_2, but again the effect was minimal. The percentage increase in soil moisture content was greatest in September for both genotypes, +2.70 % *P. x euramericana* and +3.93 % *P. nigra*. Changes in the β factor as a result of changes in the soil moisture content with elevated atmospheric CO_2 were minimal for both genotypes (Fig. 10). Percentage changes, relative to the baseline climate, ranged from -0.00032 % to +0.29 % for *P. x euramericana* and from -0.015 % to +0.61 % for *P. nigra*.

Mean monthly predicted soil moisture content in the South West increased with elevated atmospheric CO_2 throughout the year and in both genotypes (Appendix 6B Fig. 6B-1). The percentage increase simulated ranged from +1.35 % to +9.15 % for *P. x euramericana* and from +1.95 % to +12.43 % for *P. nigra*. Increases in the β factor resulted for both genotypes, ranging from +0.003 % to +5.61 % for *P. x euramericana* and +0.006 % to +9.25 % for *P. nigra* (Fig. 10).

In Wales, the mean monthly predicted soil moisture content marginally increased with elevated atmospheric CO_2 compared to the baseline climate (see Appendix 6B Fig. 6B-1). The percentage increase ranged from +0.0009 % to +3.46 % in *P. x euramericana* and from +0.09 % to +5.00 % in *P. nigra*. This translated into minimal percentage changes in the mean monthly β factor ranging between -0.006 % to +0.55 % for *P. x euramericana* and -0.002 % to +1.26 % for *P. nigra* (Fig. 10).

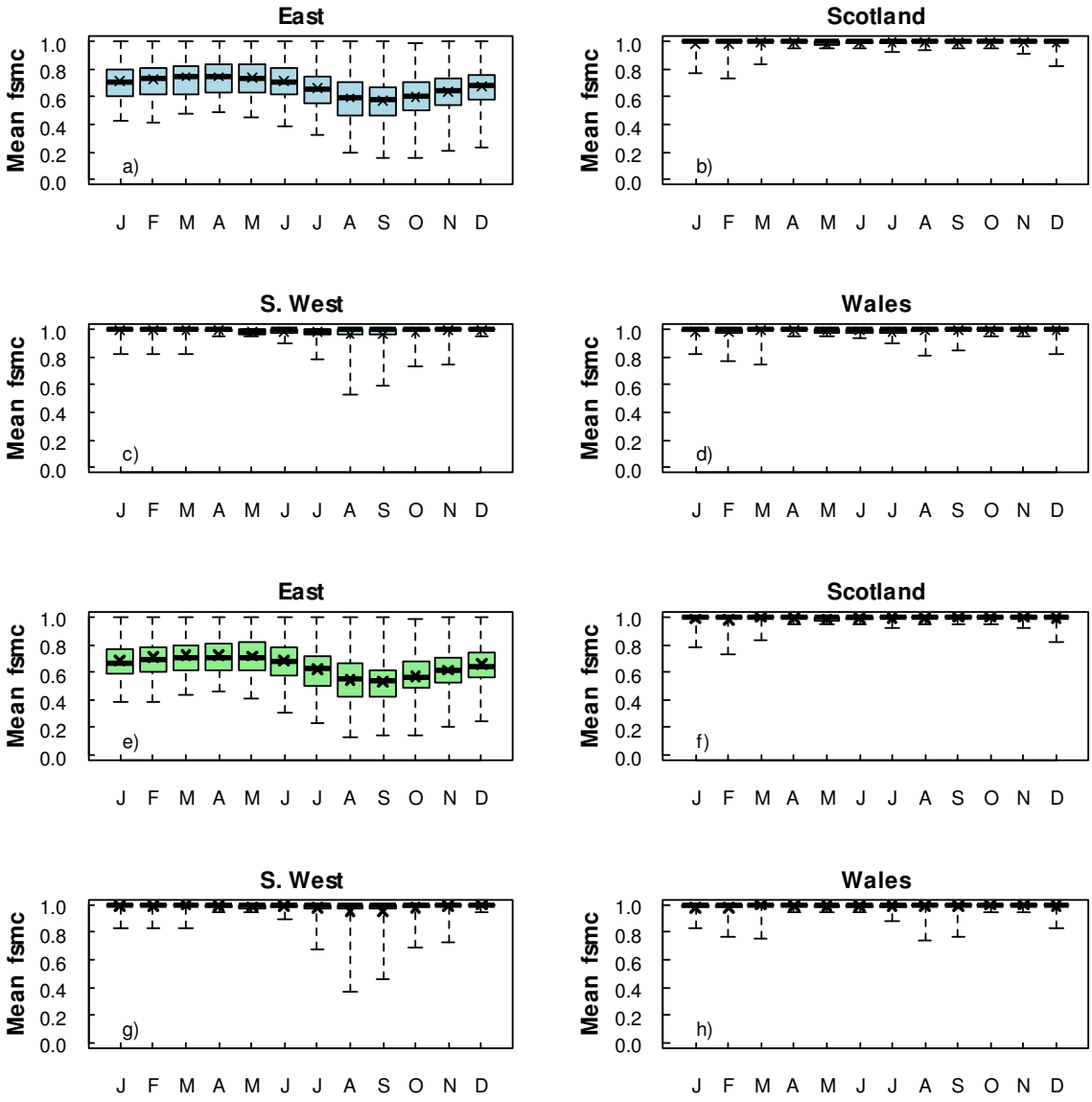

Fig. 10. Monthly mean β factor (*fsmc*) over the thirty year period of baseline climate data and with elevated atmospheric CO_2. The mean includes all three soil types; panels a - d: *P. x euramericana*, panels e - h: *P. nigra*.

6.3.3 Experiment 3: Changed climate

6.3.3 .1 Yield

The response of mean predicted yield to a changed climate alone was variable depending on site ($x^2 = 87.46, p < 0.001, n = 2640$; Fig. 11), and the magnitude of the difference compared to the baseline climate varied between genotypes. In response to a changed climate, mean predicted yield in the East and South West of England decreased compared to predicted yields under the baseline climate (Fig. 11; Table 7). The effect was greatest in the East of England, and for these two sites the magnitude of the difference was greatest in *P. nigra*. The relative difference in yield compared to the baseline climate was -59.5 % and -61.6 % for *P. x euramericana* and *P. nigra* respectively in the East, and -15.1 % and -21.0 % for *P. x euramericana* and *P. nigra* respectively in the South West (Table 7). This resulted in the East and South West becoming the lowest yielding sites, however mean predicted yields in the East were lower than in the South West (*P. x euramericana*: $x^2 = 202.07, p < 0.001, n = 1200$; *P. nigra*: $x^2 = 206.11, p < 0.001, n = 1200$). Compared to the baseline climate, mean predicted yield in Scotland and Wales increased with a changed climate. The greatest increase was seen in Scotland, with mean percentage increases of +55.0 % and +33.9 % seen in *P. x euramericana* and *P. nigra* respectively (Table 7), but the variation in predicted yield was also greatest at this site (Fig. 11). In Wales, mean percentage increases in yield of +38.2 % and +19.4 % were seen in *P. x euramericana* and *P. nigra* respectively (Table 7). In both genotypes, predicted mean yields were not different in Scotland and Wales, but mean predicted yield was detectably lower in the South West than in both Scotland and Wales (*P. x euramericana*: $x^2 = 4.05, p < 0.01, n = 1200$; *P. nigra*: $x^2 = 10.54, p < 0.001, n = 1200$; Fig. 11).

Mean predicted yield was higher in *P. nigra* at all sites except in the East ($x^2 = 35.93, p < 0.001, n = 2640$). Figs. 12 & 13 show the predictions of mean yield by the anomalies from each GCM and the large variation between these. The variation between predictions is larger for some sites (e.g. the South West) than others (e.g. Wales). There is notable variation between the GCMs, but within each prediction there is also a large amount of variation. In all cases there is a large range for the maximum and minimum predicted values, and there is a relatively large distribution of the middle 50% of the data, this is

especially noticeable in the East. These means include all soil types as soil type was only found to have a marginal impact on yield ($x^2 = 26.89$, $p < 0.05$, $n = 2640$). Sandy soils were found to have lower yields compared to both clay and silt soils in both genotypes, however this effect was minimal compared to the variation in yield explained by site.

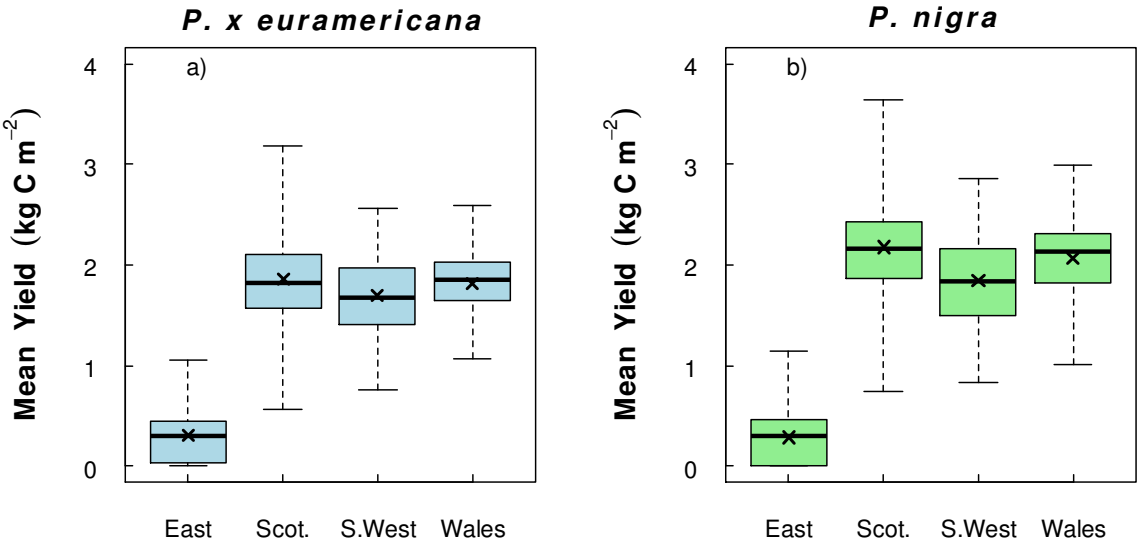

Fig. 11. Mean maximum yield (kg C m^{-2}) predicted at each site in the final year of each three year rotation over the thirty year period of driving data under a changed climate and ambient atmospheric CO_2. The mean is calculated including all three soil types.

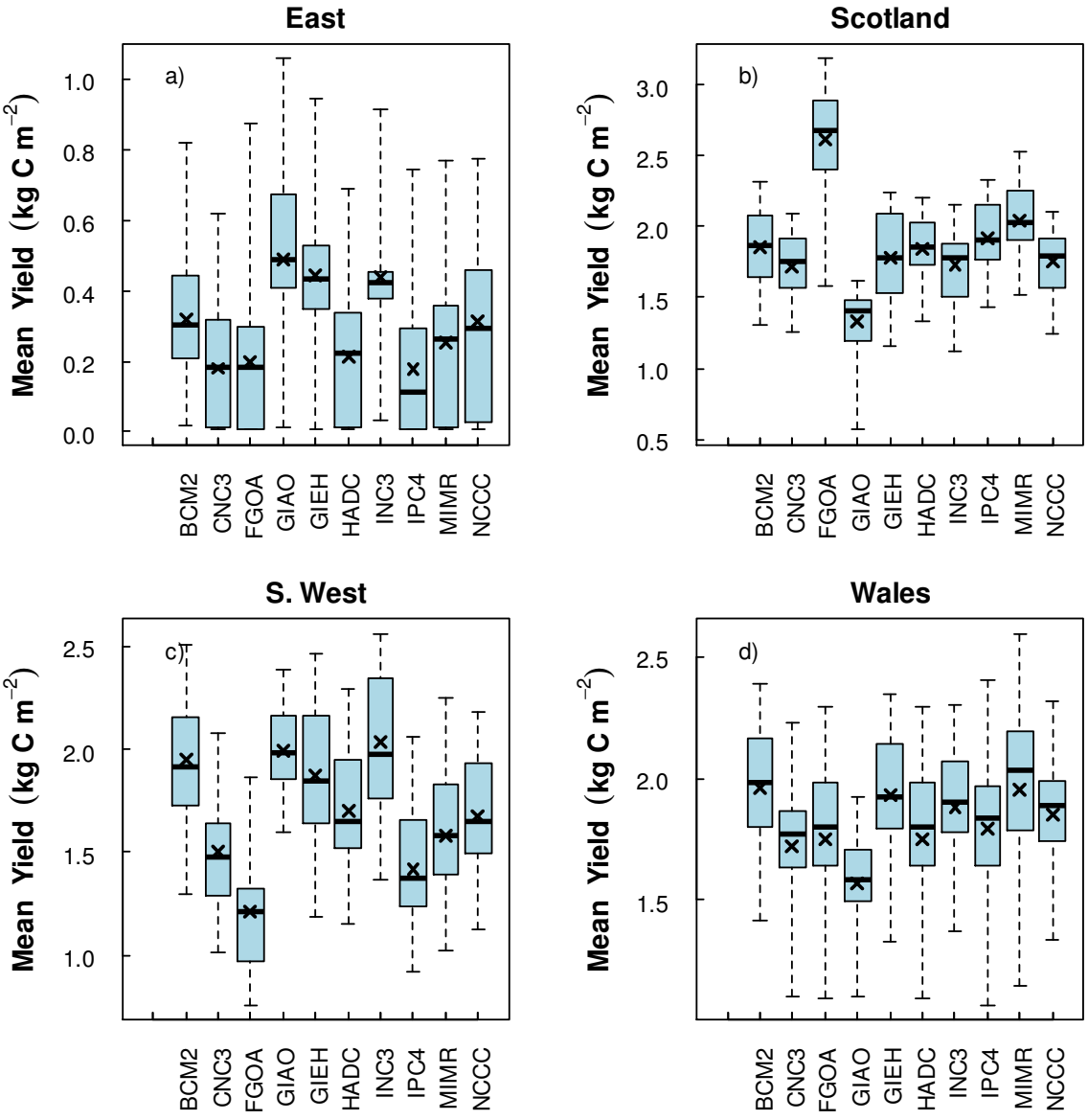

Fig. 12. The predicted yield of *P. x euramericana* at each site resulting from forcing by each of the ten GCMs (for GCM abbreviations, see Table 2). The mean is calculated as the yield at the end of each three year rotation over the thirty year period of driving data and includes all three soil types. This shows the uncertainty arising from the different GCMs.

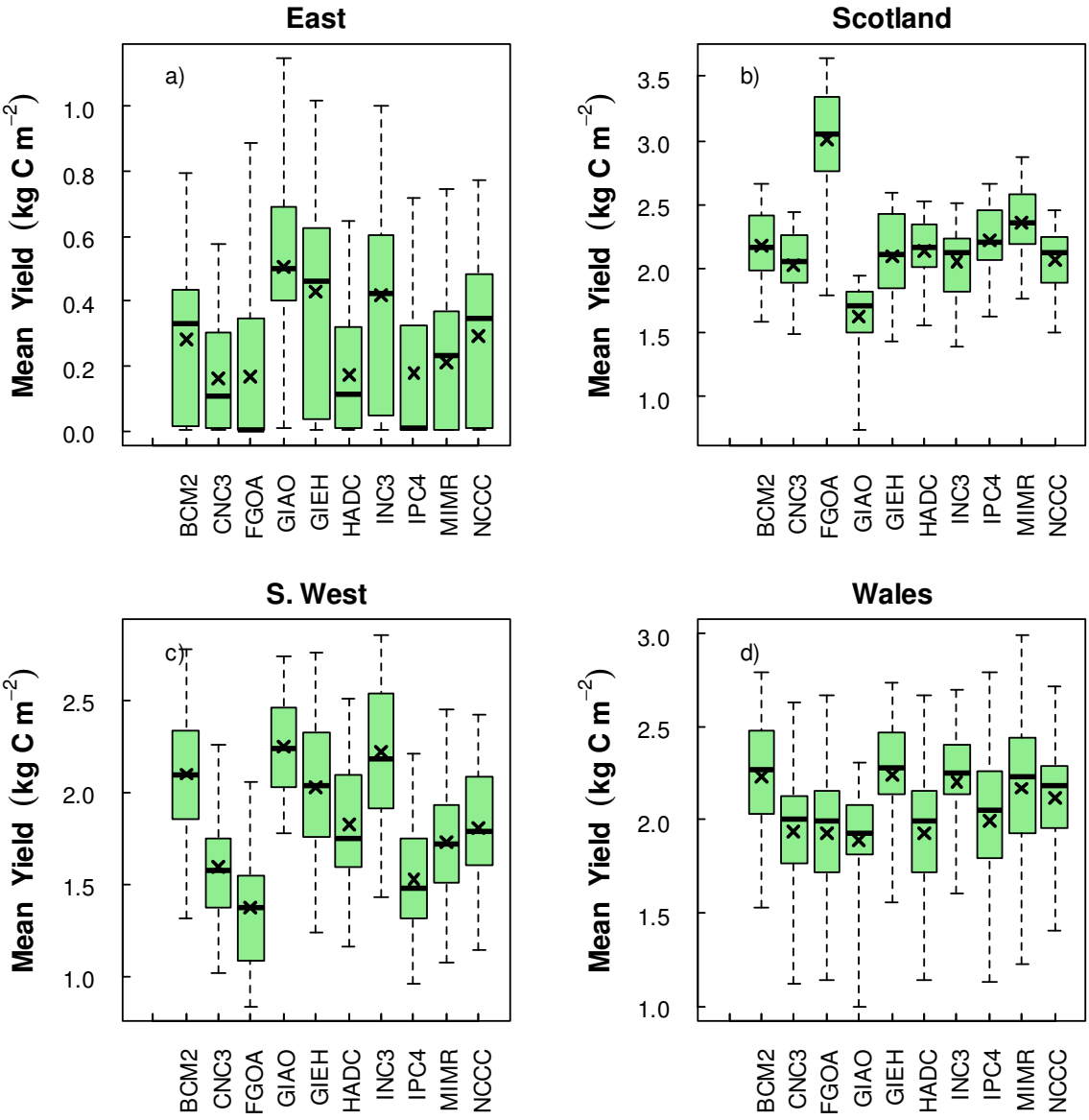

Fig. 13. The predicted yield for *P. nigra* at each site resulting from forcing by each of the ten GCMs (for GCM abbreviations, see Table 2). The mean is calculated as the yield at the end of each three year rotation over the thirty year period of driving data and includes all three soil types. This shows the uncertainty arising from the different GCMs.

6.3.3 .2 Transpiration

The response of mean predicted transpiration to a changed climate alone was variable depending on site ($x^2 = 30.23, p < 0.001, n = 7920$; Fig. 14). In the East of England, mean predicted transpiration was substantially reduced with the change in climate. At this site, the relative difference between the changed climate and baseline climate was -33.3 % for *P. x euramericana* and -34.2 % for *P. nigra* (Table 8). As a result, mean predicted transpiration in the East was lower than at all other sites (*P. x euramericana*: $x^2 = 150.86, p < 0.001, n = 3600$; *P. nigra*: $x^2 = 169.62, p < 0.001, n = 3600$; Fig. 14, Table 8). At the other sites, mean predicted transpiration increased in response to a changed climate. Considerable increases in mean predicted rates of transpiration were seen in Scotland and Wales, and transpiration was not found to be different between these two sites in either genotype (Fig. 14). The changed climate had the greatest impact on rates of transpiration at these two site, percentage increases of +113.9 % and +97.9 % were seen in Scotland for *P. x euramericana* and *P. nigra* respectively, and +102.6 % and +80.4 % in Wales for *P. x euramericana* and *P. nigra* respectively (Table 8). Despite decreased mean yield observed in the South West under a changed climate, rates of mean predicted transpiration increased so that mean transpiration remained highest at this site, and was higher than in either Scotland or Wales (*P. x euramericana*: $x^2 = 10.74, p < 0.001, n = 3600$; *P. nigra*: $x^2 = 8.87, p < 0.01, n = 3600$). The magnitude of the increase in mean predicted transpiration was much smaller in the South West, with an increase of +23.6 % for *P. x euramericana* and +18.2 % *P. nigra* (Table 8).

Rates of mean predicted transpiration were higher in *P. nigra* at all sites ($x^2 = 49.28, p < 0.001, n = 7920$). Soil type had a marginal impact on simulated tree transpiration ($x^2 = 6.67, p < 0.05, n = 7920$). Predicted rates of transpiration were found to be lower on sandy soils compared to either clay or silt soils. Mean transpiration varied between GCMs, figures 15 and 16 show the predicted mean transpiration rate by anomalies from each GCM and the variation between these. Compared to the predicted yield, there is less variation between the predicted mean transpiration rates at each site by each set of GCM anomalies.

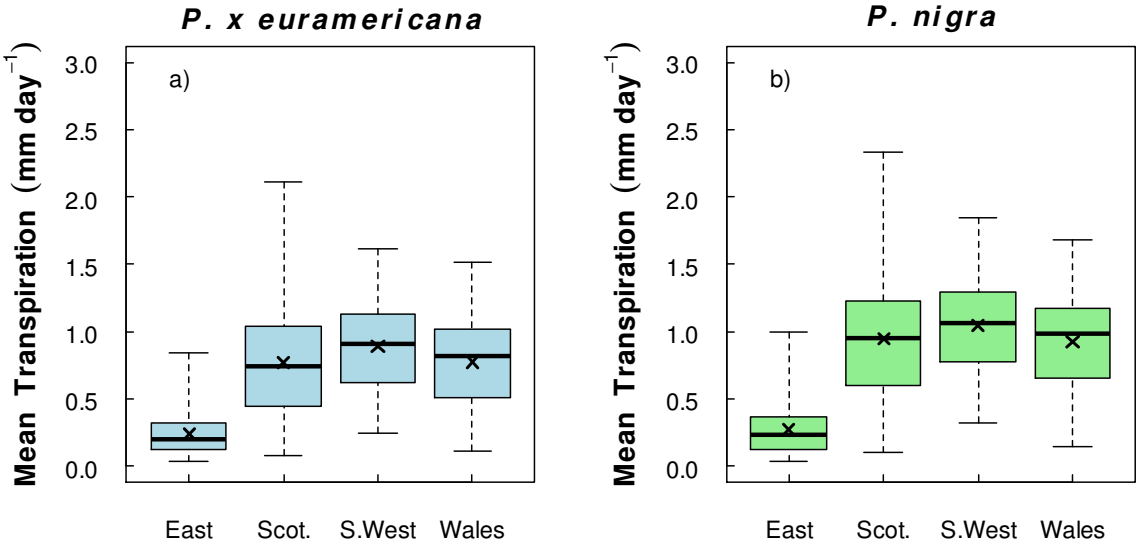

Fig. 14. Mean predicted transpiration (mm day^{-1}) at each site under a changed climate and ambient atmospheric CO_2 concentration. The mean is calculated over the thirty year period of baseline climate data, and all three soil types.

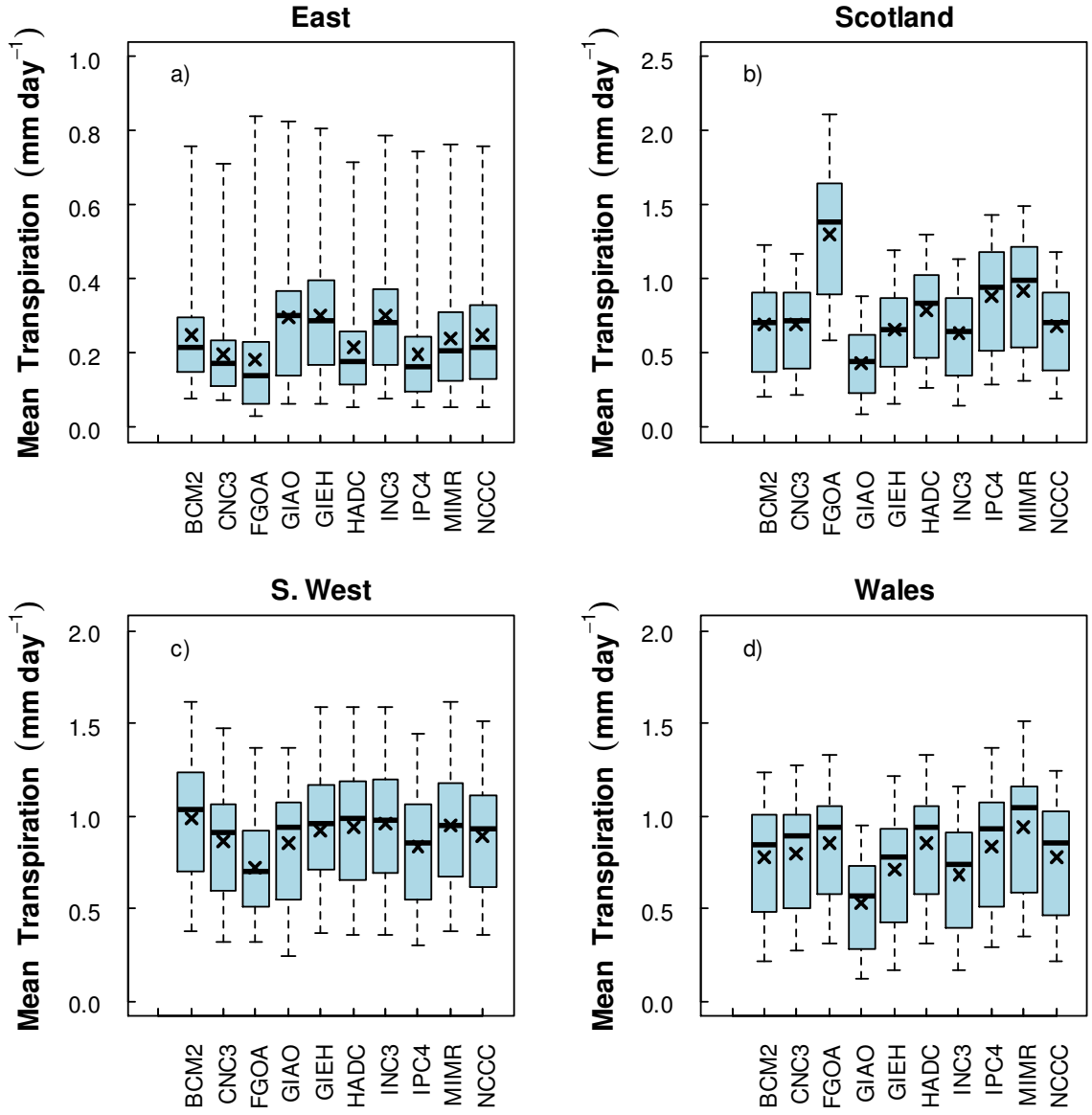

Fig. 15. The predicted transpiration for *P. x euramericana* at each site resulting from forcing by each of the ten GCMs (for GCM abbreviations, see Table 2). The mean is calculated as the mean annual transpiration over the thirty year period of driving data and includes all three soil types. This shows the uncertainty arising from the different GCMs.

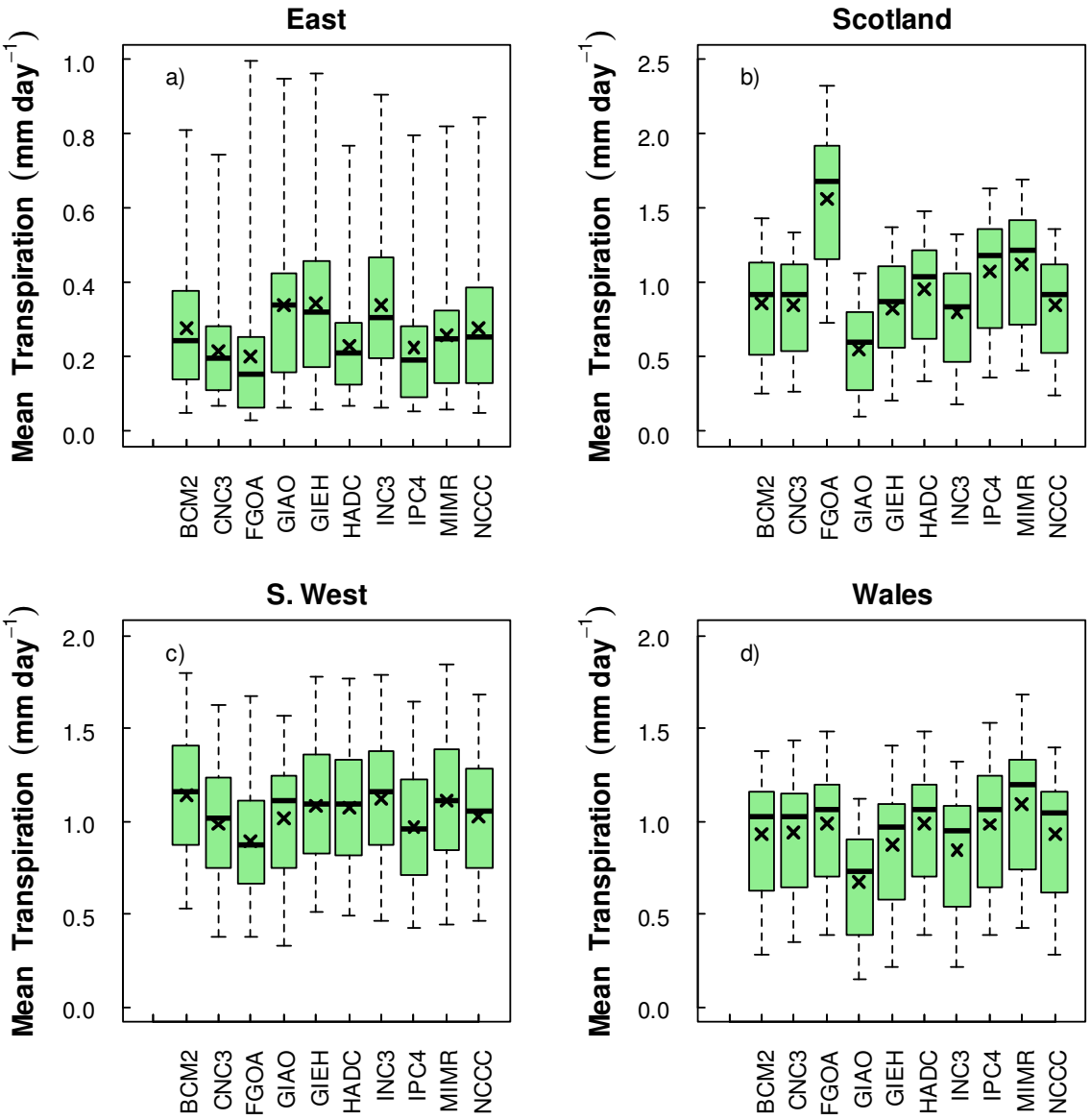

Fig. 16. The predicted transpiration for *P. nigra* at each site resulting from forcing by each of the ten GCMs (for GCM abbreviations, see Table 2). The mean is calculated as the mean annual transpiration over the thirty year period of driving data and includes all three soil types. This shows the uncertainty arising from the different GCMs.

6.3.3 .3 Soil moisture and water stress

Predicted monthly soil moisture content decreased at all sites under a changed climate compared to the baseline climate (Appendix 6B Fig. 6B-2). In the East of England, with a changed climate, the mean monthly soil moisture content was lower in all months in both genotypes compared to the baseline climate (Appendix 6B Fig. 6B-2). The mean percentage decrease in available soil moisture ranged between -17.22 % to -19.92 % for *P. x euramericana* and -16.33 % to -19.40 % in *P. nigra*. The monthly maximum and minimum soil moisture contents were also lower in a changed climate compared to the baseline climate. This decrease in available soil moisture content resulted in large decreases in the mean monthly simulated β factor in every month (more stressed). Percentage decreases in the β factor ranged between -31.87 % to -38.27 % for *P. x euramericana* and -31.12 % to -38.06 % for *P. nigra* (Fig. 17). With a change in climate the monthly minimum value of the β factor was also largely reduced. For example, in *P. x euramericana* SRC, in August the minimum value of β was at its lowest at 0.11 under the baseline climate, under a changed climate this value was reduced by a factor of ten to 0.011 (Fig. 17).

In Scotland, the mean monthly predicted soil moisture content decreased throughout the year in both genotypes with a changed climate compared to the baseline climate (Appendix 6B Fig. 6B-2). Mean percentage decreases ranged from -2.60 % to -16.67 % for *P. x euramericana* and from -2.05 % to -17.42 % for *P. nigra*. At this site, as in the South West and Wales, there was a clear trend in the annual soil moisture content. For example, the soil moisture deficit was seen to steadily increase and peak towards the end of the growing season (Sept/Oct), then decline during the autumn and winter. Changes in the β factor as a result of changes in the available soil moisture content were minimal at this site (Fig. 17). Percentage changes in the mean monthly simulated β factor as a result of the changed climate, relative to the baseline climate ranged between -7.72 % to +0.97 % and -9.39 % to +1.04 % for *P. x euramericana* and *P. nigra* respectively.

With a changed climate, the mean monthly predicted soil moisture content in the South West was lower in all months relative to the baseline climate (Appendix 6B Fig. 6B-2). Mean monthly percentage decreases were relatively large across the year in both genotypes and ranged from -19.39 % to -31.56 % in *P. x euramericana* and -19.31 % to -31.84 % in

P. nigra. The relative difference in soil moisture content was largest at this site. Large decreases in the β factor were evident as a result of the reduced mean soil moisture content in a changed climate, with decreases most pronounced during the growing season (Fig. 17). The mean and median of the predicted β factor declined as low as 0.5 under the changed climate, this is compared to roughly 0.9 under the baseline climate. Percentage decreases, relative to the baseline climate, ranged from -9.05 % to -43.31 % in *P. x euramericana* and from -9.18 % to -47.30 % in *P. nigra*.

At the Welsh site, mean monthly predicted soil moisture content decreased throughout the year in both genotypes with a changed climate, the decline in soil moisture content was most pronounced during the growing season (Appendix 6B Fig. 6B-2). Percentage decreases ranged between -7.37 % to -25.56 % for *P. x euramericana* and between -8.35 % to -27.23 % for *P. nigra*. Decreased available soil moisture content with a changed climate translated into increased soil moisture stress for both genotypes (Fig. 17). The mean monthly predicted β factor was decreased each month, with percentage decreases ranging between -0.26 % to -21.39 % in *P. x euramericana*, and between -1.02 % to -26.53 % in *P. nigra*. The biggest change in the β factor occurred in the summer months, minimum predicted values declined as low as 0.1; however, the mean and median β factor remained close to 0.8, suggesting in the majority of years the soil moisture stress imposed on the trees was not too severe.

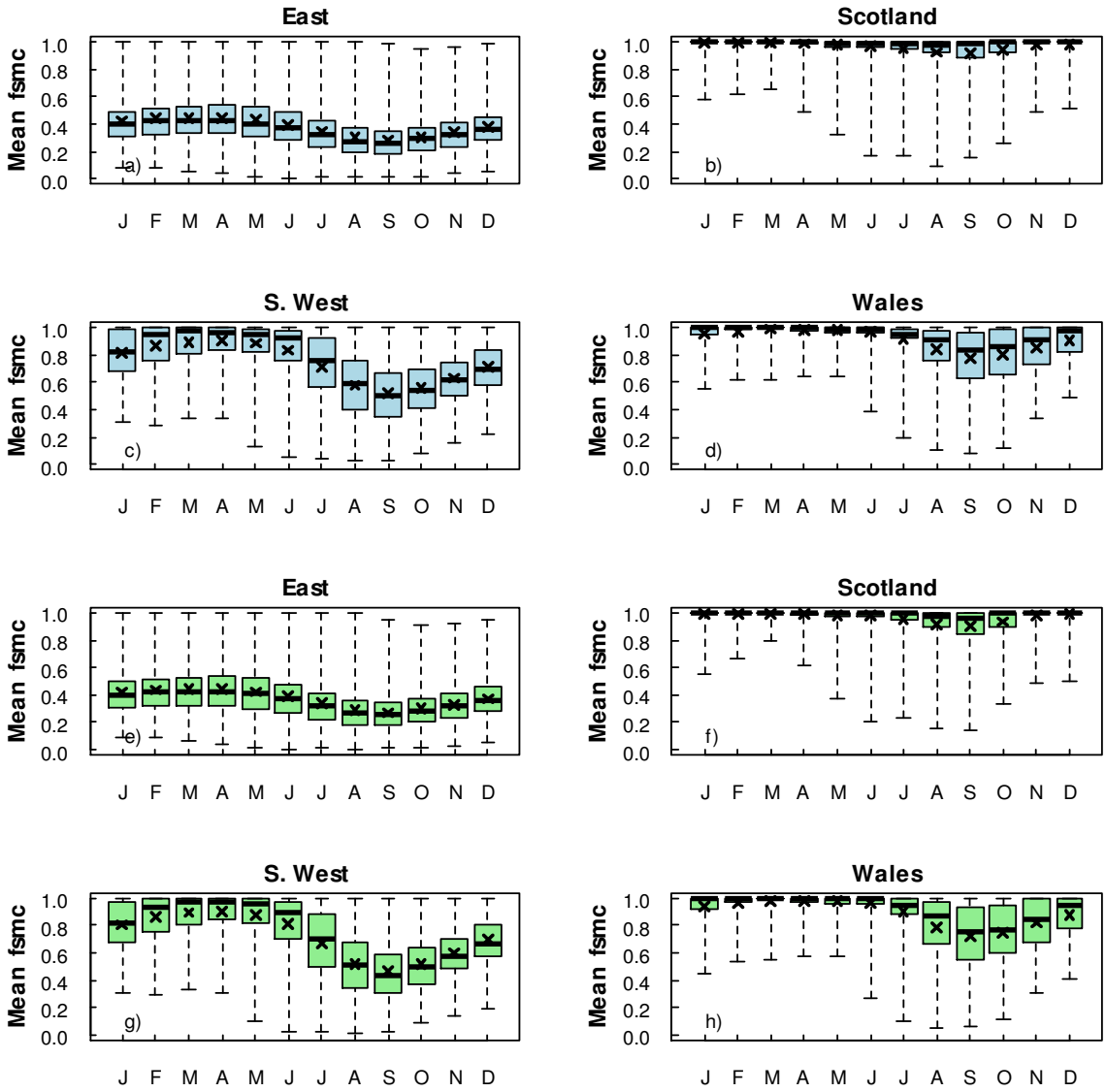

Fig. 17 Monthly mean β factor (*fsmc*) for a thirty year period with a changed climate and ambient atmospheric CO_2; panels a - d: *P. x euramericana*, panels e - h: *P. nigra*.

6.3.4 Experiment 4: Future climate

6.3.4.1 Yield

Under a future climate scenario, mean predicted yield of poplar SRC was increased at the majority of sites relative to the baseline climate, however this response was variable between sites ($x^2 = 105.4, p < 0.001, n = 5280$; Fig. 18). Additionally, the magnitude of the yield response was higher in *P. x euramericana* at the majority of sites. The exception was the East of England that saw a decline in mean predicted yield (-5.4%) in *P. x euramericana* trees relative to the baseline climate, but a marginal increase in yield in *P. nigra* (+1.4%) trees (Table 7). Thus, there was not much change in mean predicted yield under a future climate scenario, and predicted yield at this site remained the lowest. It was lower than the mean yield achieved in both Scotland and Wales (*P. x euramericana*: $x^2 = 209.61, p < 0.001, n = 1200$; *P. nigra*: $x^2 = 241.40, p < 0.001, n = 1200$; Fig. 18, Table 7). Scotland and Wales saw the greatest increase in mean predicted yield under a future climate scenario relative to the baseline climate. Mean percentage increases of +113.3 % and +107.6 % were achieved in *P. x euramericana* in Scotland and Wales respectively, and +72.8 % and +66.4 % in *P. nigra* in Scotland and Wales respectively (Table 7). In both genotypes, mean predicted yield was not detectably different between either the Welsh or Scottish sites (Fig. 18). The percentage increase in yield relative to the baseline climate was lower in the South West of England. Mean percentage increases of +54.3 % and +47.2 % were seen for *P. x euramericana* and *P. nigra* respectively (Table 7). Nevertheless, this remained the highest yielding site (*P. x euramericana*: $x^2 = 13.99, p < 0.001, n = 1200$; *P. nigra*: $x^2 = 13.39, p < 0.001, n = 1200$; Fig. 18).

Mean predicted yields were higher in *P. nigra* compared to *P. x euramericana* ($x^2 = 62.10, p < 0.01, n = 5280$; Fig. 18, Table 7). There was large variation surrounding predicted mean yield at all sites (Fig. 18). Compared to the predictions under the baseline climate, the range of predicted values was larger under the future climate, and was greatest at the Scottish site. Additionally there was more spread in the distribution of the middle 50% of the data, this was largely to do with variation between predictions resulting from the different GCM anomalies. Soil type however was not found to have any detectable impact on the mean predicted yield. Therefore, in addition to natural climate variability from year

to year, variability from the different GCM runs and also contributed to the uncertainty in the output.

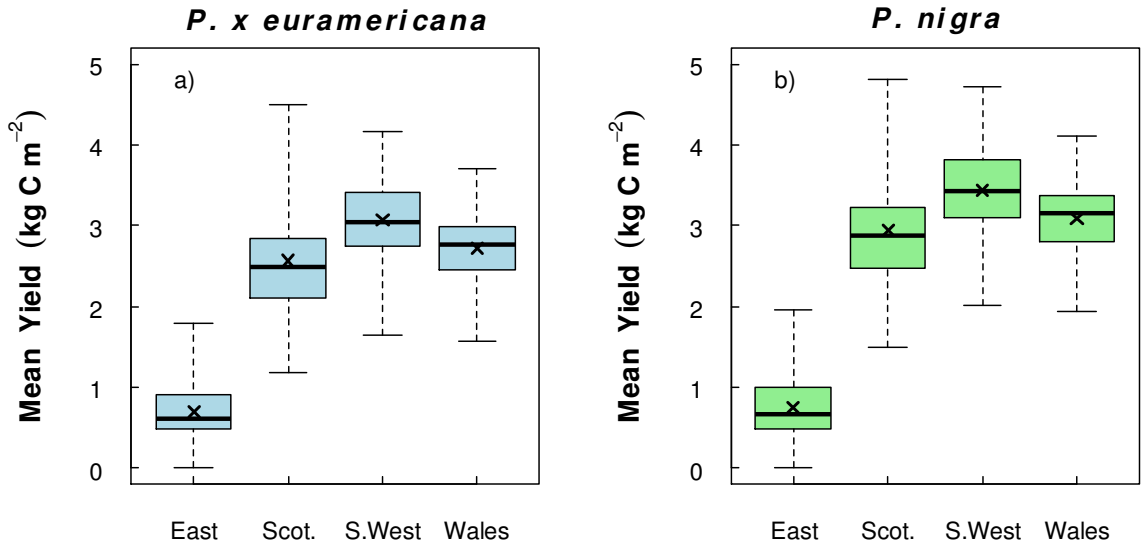

Fig. 18. Mean maximum yield (kg C m^{-2}) predicted at each site in the final year of each three year rotation over the thirty year period of driving data under a changed climate and elevated atmospheric CO_2. The mean is calculated including all three soil types.

6.3.4.2 Transpiration

Under a future climate scenario, mean predicted transpiration was increased relative to the baseline climate at all sites except in the East ($x^2 = 38.86$, $p < 0.001$, $n = 15840$; Fig. 19). The increase in transpiration relative to the baseline climate was largest in Scotland and Wales. Mean percentage increases of +61.1 % and +65.8 % were seen in Scotland and Wales respectively for *P. x euramericana*, and +47.9 % and +49.0 % in Scotland and Wales respectively for *P. nigra* (Table 8). For both genotypes, mean predicted transpiration rates were not found to be different between these two sites. Transpiration remained highest in the South West, but the percentage change under a future climate scenario was more conservative at this site (+16.7 % *P. x euramericana* and +13.6 % *P. nigra*; Table 8). Predicted mean transpiration at this site was higher than in both Scotland and Wales (*P. x euramericana*: $x^2 = 38.86$, $p < 0.001$, $n = 3600$; *P. nigra*: $x^2 = 42.42$, $p < 0.001$, $n = 3600$; Fig. 19). Predicted mean transpiration rates remained lowest in the East (*P. x euramericana*: $x^2 = 106.52$, $p < 0.001$, $n = 3600$; *P. nigra*: $x^2 = 123.17$, $p < 0.001$, $n = 3600$; Fig. 19). This site saw a decline in mean transpiration under a future climate

scenario relative to the baseline climate. A mean percentage decrease of -30.6 % and -29.3 % was seen for *P. x euramericana* and *P. nigra* respectively (Table 8).

Mean predicted transpiration saw the greatest magnitude of change from mean rates predicted under the baseline climate in *P. x euramericana* SRC, however, mean rates of transpiration were higher in *P. nigra* ($x^2 = 88.21$, $p < 0.01$, $n = 15840$; Fig. 19), except in the East where there were no detectable differences. Mean rates of transpiration as predicted by the anomalies from the different GCMs were seen to vary, however, soil type had no detectable impact on the mean transpiration. This likely contributed to the variation surrounding the mean predicted transpiration rates and the large range in the model results.

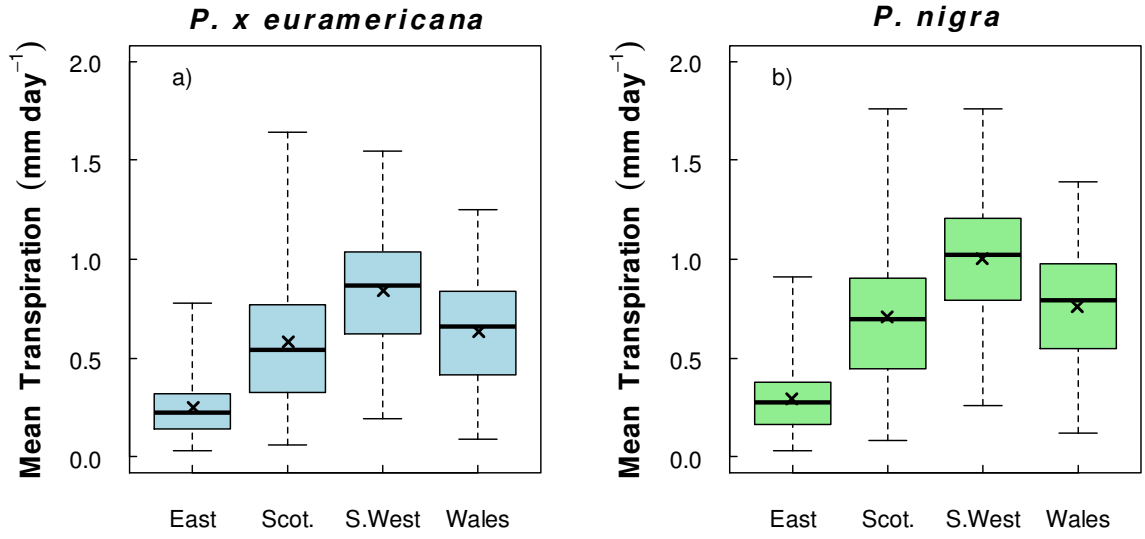

Fig. 19. Mean predicted transpiration (mm day^{-1}) at each site under a changed climate and elevated atmospheric CO_2 (future climate scenario). The mean is calculated over the thirty year period of baseline climate data, and all three soil types.

6.3.4.3 Soil moisture and water stress

Predicted monthly soil moisture content decreased at all sites under a future climate scenario relative to the baseline climate, but this response was variable depending on site (Appendix 6B Fig. 6B-3). The decline in mean monthly predicted soil moisture was greatest in the East, and the soil moisture deficit was large throughout the year ranging between -15.6 % to -18.6 % for *P. x euramericana* and -15.3 % to -18.3 % for *P. nigra*. The β factor was also substantially decreased (more stress) throughout the year (Fig. 20).

Mean percentage decreases relative to the baseline climate ranged between -29.0 % to -35.2 % for *P. x euramericana* and -28.3 % to -36.5 % for *P. nigra*.

In Scotland, the mean monthly predicted soil moisture showed a slight decline under a future climate scenario relative to the historic climate (Appendix 6B Fig. 6B-3). The mean percentage decrease ranged from -1.5 % to -9.8 % for *P. x euramericana* and from -1.0 % to -8.6 % for *P. nigra*. Minimal changes in the β factor were seen (Fig. 20).

In the South West, mean monthly predicted soil moisture content was reduced throughout the year relative to the historic climate (see Appendix 6B Fig. 6B-3). Percentage decreases ranged between -12.2 % to -20.3 % for *P. x euramericana* and -10.2 % to -17.4 % for *P. nigra*. This translated into decreases in the mean monthly predicted β factor that were most pronounced during the summer months, ranging between -4.1 % to -24.8 % for *P. x euramericana* and -3.2 % to -23.2 % for *P. nigra* (Fig. 20).

In Wales, under a future climate scenario, mean monthly predicted soil moisture decreased relative to the baseline climate. Mean monthly percentage decreases in soil moisture content gradually increased throughout the year and peaked towards the end of the growing season (Appendix 6B Fig. 6B-3). They ranged between -4.9 % to -17.4 % in *P. x euramericana* and -4.9 % to -16.9 % in *P. nigra*. Changes in the mean monthly predicted β factor also occurred, but these were minimal and ranged from -10.6 % to +1.3 % in *P. x euramericana* and from -11.9 % to +1.1 % in *P. nigra* (Fig. 20).

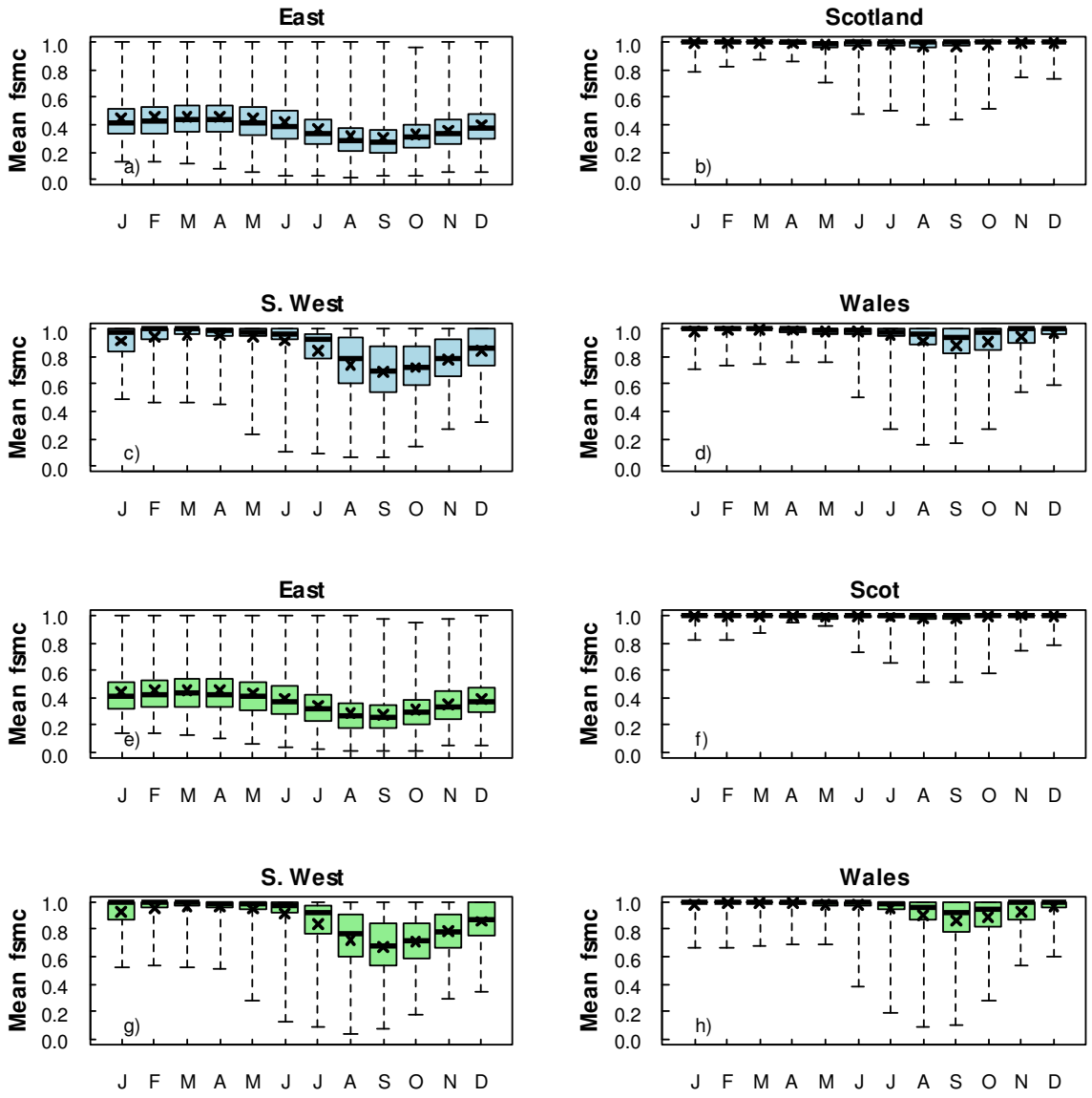

Fig. 20. Monthly mean β factor (*fsmc*) for a thirty year period with a changed climate and elevated atmospheric CO_2; panels a - d: *P. x euramericana*, panels e - h: *P. nigra*.

6.3.4.4 The interaction between CO_2 concentration and climate

These series of experiments clearly highlight the influence of climate on modifying the response of yield to elevated concentrations of atmospheric CO_2. Consequently, generalisations about the response of poplar SRC yield to future climate scenarios are difficult to make given this complex interaction between climate change and CO_2 concentration. In analysis, modification of the yield response to elevated atmospheric CO_2 as a result of climate was found for all sites ($x^2 = 8.31$, $p < 0.01$, $n = 5280$) except Scotland. At this site the response of yield to elevated atmospheric CO_2 concentration and climate was additive. To highlight this interaction, Figure 21 shows the mean predicted

yield for each site and climate scenario. Genotype and soil were pooled together as effects of site and climate on yield were similar between genotypes and soils.

In the East, for example, the response of predicted yield clearly shows the strong interaction between climate and CO_2 concentration. The large enhancement of yield as a result of the CO_2 fertilisation effect (i.e. experiment two) is clearly seen. The dramatic depression of yield as a result of drier conditions under the changed climate is evident in experiment three. The interaction between these two facets of climate change is clearly seen in experiment 4, with the evident trade off between the opposing effects of drought and elevated atmospheric CO_2 (Table 7; Fig. 21), such that there is little change in the yield under a future climate scenario relative to the baseline climate. This site is just one example however, and Fig. 21 and Table 7 show that in each experiment the mean predicted yield at each site responds differently, both in direction and magnitude of change.

At most sites, irrespective of climate, the mean predicted transpiration rate always declined in response to elevated concentrations of atmospheric CO_2, although the magnitude of the response was variable. This was with the exception of the East of England where transpiration was seen to marginally increase in response to elevated atmospheric CO_2. Therefore, an interaction between climate and CO_2 was only evident in the East for transpiration, and not apparent for the other sites. For clarity, Figure 22 shows the mean transpiration rate for each site and experiment, with genotype and soil pooled together.

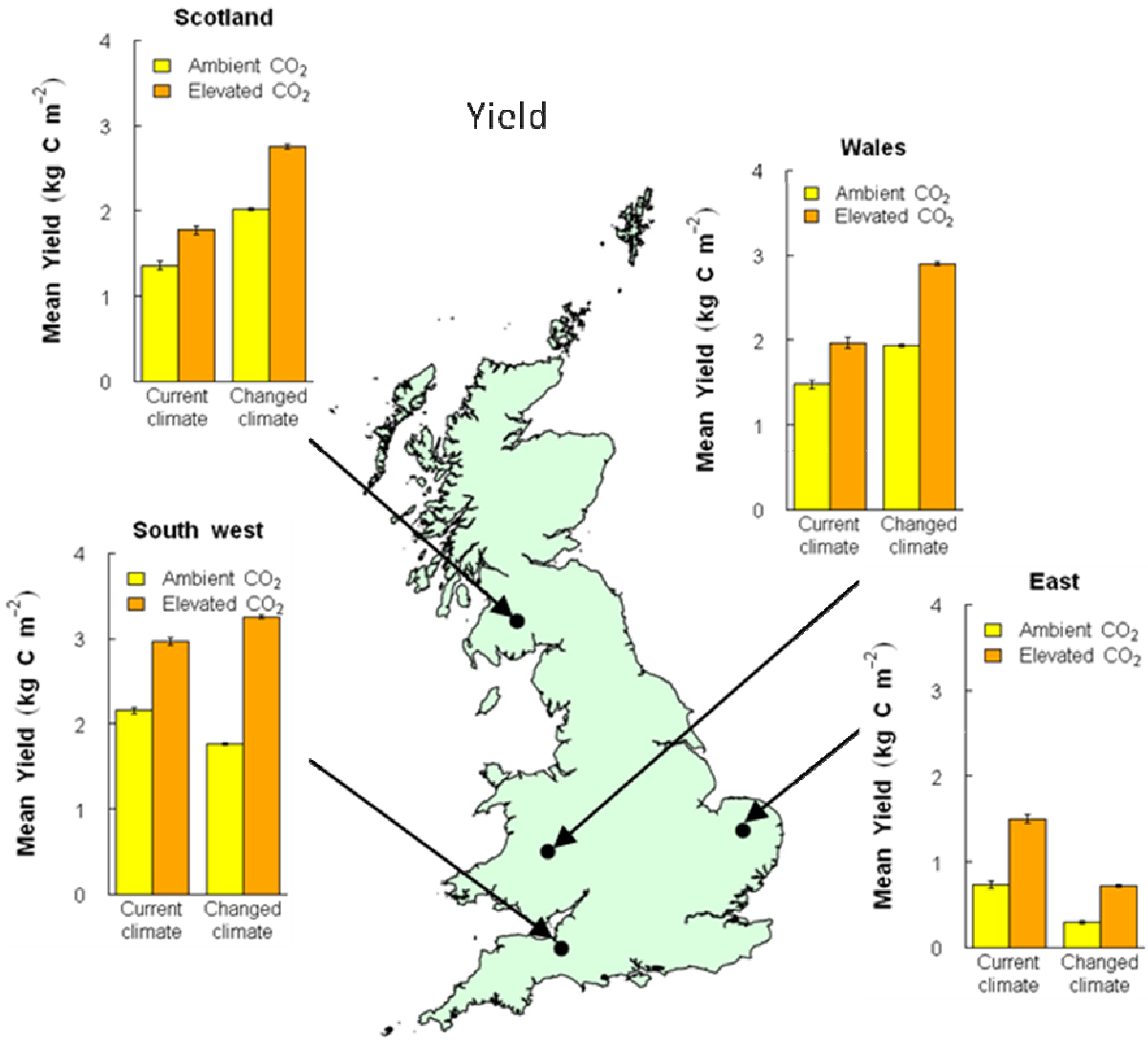

Fig. 21. Mean predicted yield in year three of the rotation at each site. Means ± s.e bars are shown for each combination of climate scenario (current or changed) and CO_2 concentration (ambient or elevated). The changed climate and elevated CO_2 represents a realistic future climate scenario for the UK predicted using a medium emissions scenario. Results for genotype and soil are pooled together.

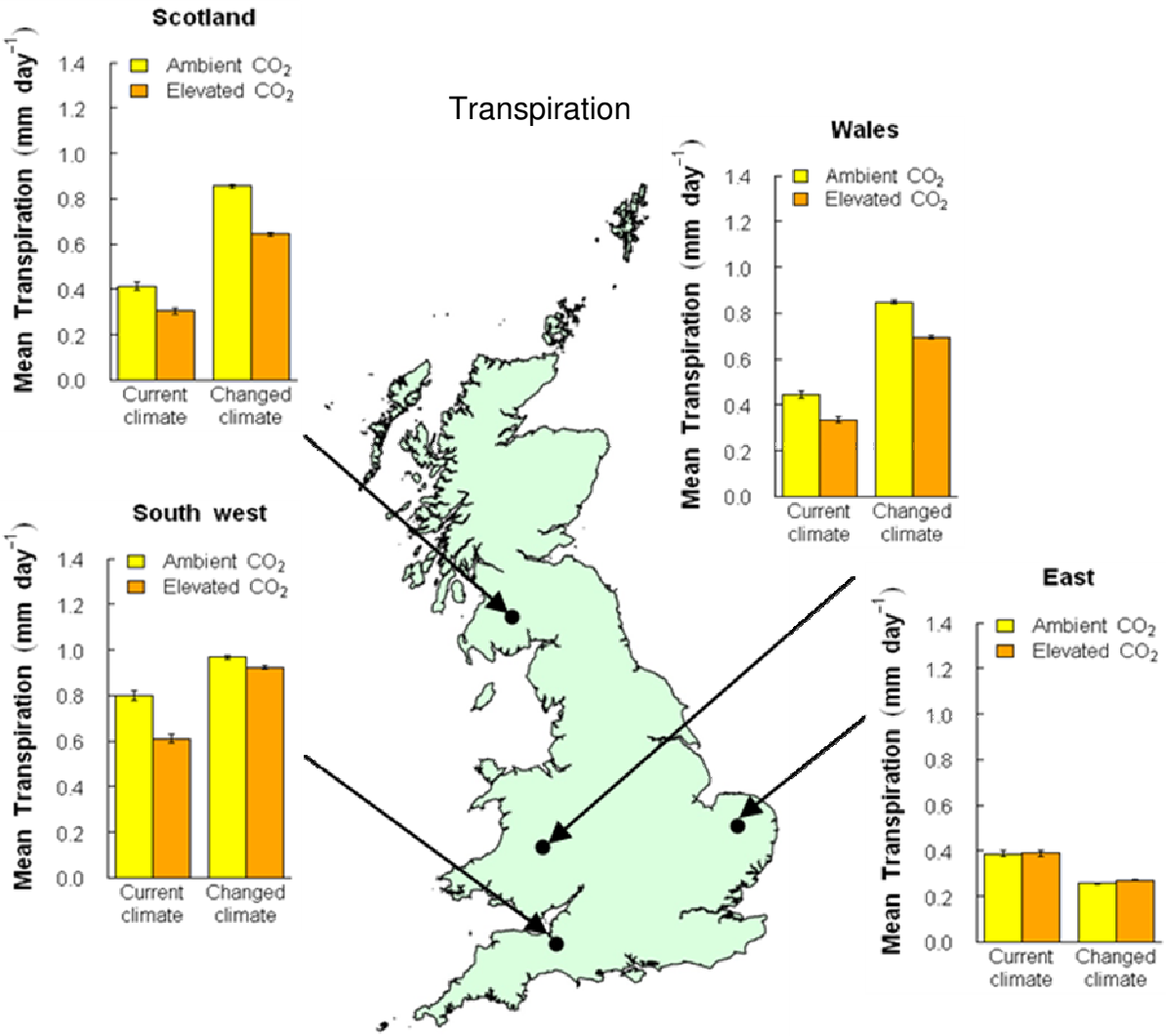

Fig. 22. Mean predicted annual transpiration at each site. Means ± s.e bars are shown for each combination of climate scenario (current or changed) and CO_2 concentration (ambient or elevated). The changed climate and elevated CO_2 represents a realistic future climate scenario for the UK predicted using a medium emissions scenario. Results for genotype and soil are pooled together.

6.4 Discussion

6.4.1 Are the responses of yield and transpiration to atmospheric CO_2 significantly modified by the interaction with climate?

These series of experiments clearly highlighted the influence of climate in modifying the yield, and to a lesser extent transpiration, responses to elevated concentrations of atmospheric CO_2. Therefore, this interaction between CO_2 and climate is important, and its impact on plant growth is not addressed by the majority of field FACE studies that manipulate concentrations of atmospheric CO_2 alone. Indeed, this study suggests that generalisations about the response of poplar SRC yield and transpiration to future climate scenarios are difficult to make given the complex, spatially dependent, interactions between climate change and CO_2 concentration.

6.4.1.1 Yield

In this study, the interaction with climate significantly modified the response of yield to elevated atmospheric CO_2 at all sites, with the exception of Scotland. The positive CO_2 fertilisation effect on yield was clearly demonstrated by the model under both climate scenarios (baseline and changed). This CO_2 fertilisation effect is a commonly documented response of plant biomass to increased concentrations of atmospheric CO_2 in C_3 plants and trees in the field (Ainsworth & Long, 2005; Calfapietra *et al.*, 2001; Ceulemans & Mousseau, 1994; Gielen & Ceulemans, 2001; Liberloo *et al.*, 2006; Lukac *et al.*, 2003; Norby *et al.*, 1995; Stulen & den Hertog, 1993). In the current experiments, substantial increases in yield were simulated at all sites, however in the East, South West and Wales, the magnitude of the yield increase was significantly larger under the changed climate scenario than under the baseline climate. This occurred despite significant decreases in yield in the East and South West of England with a change in climate alone. Therefore, at these sites, the interaction with changing climatic drivers, such as rainfall, PAR, temperature and humidity, was seen to significantly modify the yield response to rising concentrations of atmospheric CO_2. At the Scottish site, the magnitude of the change in yield response to elevated atmospheric CO_2 was similar under both climate scenarios. Therefore, at this site there was no significant interaction between climate and CO_2, the yield response to both these environmental drivers was additive.

Under the baseline climate, with an increase of atmospheric CO_2 alone, simulated increases in mean yield in the South West, Wales and Scotland ranged between +22 % to +39 % depending on genotype. The percentage stimulation of above ground biomass due to elevated atmospheric CO_2 observed in *P. x euramericana* and *P. nigra* grown in the field at a FACE experiment in Italy was between +15 % to +27 % (Calfapietra *et al.*, 2003b). These results therefore give reassurance that the magnitude of the CO_2 fertilisation effect simulated by the model was within a reasonable range of the magnitude of the CO_2 fertilisation effect observed in the field in these two genotypes of poplar SRC. The results of this study, however, indicate that with the interacting effects of climate, responses of yield to elevated atmospheric CO_2 are significantly larger than those observed in studies that manipulate concentrations of atmospheric CO_2 alone. Under the changed climate, the magnitude of the simulated yield response to elevated atmospheric CO_2 ranged between +37 % to +86 % in the South West, Scotland and Wales, depending on site and genotype. In the East of England, however, under both climate scenarios, substantial increases in yield were simulated of between +100 % to +164 %.

As a result of the interaction between climate and CO_2 concentration at the majority of sites, mean predicted yield increased at all sites relative to the simulated yield under the baseline climate, with the exception of the East of England. In the South West, Scotland and Wales, predicted mean yield increased under the future climate scenario relative to the baseline climate, but the magnitude of these increases were markedly different between sites. Whilst substantial in Wales and Scotland, in excess of +100 % in *P. x euramericana* SRC for example, in the South West these increases were large, but more conservative, in the range of +50 %. Nevertheless, the net impact was an increase in yield at these sites relative to the simulated yield under the baseline climate. In the East, however, although a positive CO_2 fertilisation effect on yield was evident under both climate scenarios, the interaction with the changed climate was such that the positive CO_2 fertilisation effect was essentially masked when compared to the predicted yield under the baseline climate. At this site there was a clear trade off between the opposing effects of increased drought and elevated atmospheric CO_2 such that, relative to the baseline climate, mean predicted yield barely increased in *P. nigra* and actually decreased in *P. x euramericana* under the future climate scenario.

Each experiment in this work clearly showed variation between sites in mean predicted yield, both in direction and magnitude of change. Therefore, a key finding of this work is that results from a single site cannot be broadly extrapolated as the multiple, simultaneous and spatially variable changes in climate make it difficult to predict how the climate will interact with elevated atmospheric CO_2 to impact on yield.

6.4.1.2 Transpiration

The predicted transpiration response of poplar SRC to elevated atmospheric CO_2 was also shown to be significantly modified by the climate, and this was spatially variable. With the exception of the East of England, simulated transpiration decreased in response to elevated atmospheric CO_2 under both climate scenarios. In response to elevated atmospheric CO_2 in the field, plant transpiration is commonly observed to decrease (Ainsworth & Long, 2005; Ainsworth *et al.*, 2003; Ainsworth & Rogers, 2007; Drake *et al.*, 1997; Gunderson *et al.*, 2002; Lee *et al.*, 2001; Medlyn *et al.*, 2001; Wand *et al.*, 1999). The modelled transpiration of poplar SRC trees in response to elevated atmospheric CO_2 alone decreased in Scotland, Wales and the South West relative to the transpiration under the baseline climate by -23 % to -32 %. This is marginally higher, but still within range of percentage decreases in transpiration observed in response to elevated atmospheric CO_2 in the field in different species of FACE-grown broadleaf tree (-13 % to -25 %) (Cech *et al.*, 2003; Leuzinger & Körner, 2007; Schäfer *et al.*, 2002; Wullschleger & Norby, 2001). Although a decrease in plant transpiration in response to elevated atmospheric CO_2 has been observed in many studies, recent studies have also observed no change, or increases in transpiration as a result of elevated atmospheric CO_2 (+12 % to +23 %) (Cech *et al.*, 2003; Ellsworth, 1999; Schäfer *et al.*, 2002; Tricker *et al.*, 2009; Uddling *et al.*, 2008). Indeed, in this study, the mean transpiration simulated in the East of England was seen to marginally increase in *P. nigra* SRC and no change in transpiration was seen in *P. x euramericana* SRC in response to elevated atmospheric CO_2.

In Scotland and Wales the reduced transpiration of the SRC trees in response to elevated atmospheric CO_2 was of a similar magnitude under both climate scenarios (baseline and changed). In the South West, the magnitude of the decrease of poplar SRC transpiration was much smaller under the changed climate than the baseline climate, but this modifying effect of climate on the CO_2 response was not statistically significant. In the East of

England, however, predicted poplar SRC transpiration increased in response to elevated atmospheric CO_2 under both climate scenarios. This increase ranged between +4 % to +7 % depending on genotype, although no change was observed in *P. x euramericana* under the baseline climate. The magnitude of the increase in predicted SRC transpiration with elevated atmospheric CO_2 was larger under the changed climate and this was statistically significant. Therefore, in the East of England and the South West, evidently interaction with other climate drivers in addition to atmospheric CO_2 modified the response to atmospheric CO_2 alone. Also, the substantially larger increases in yield at these two sites in response to CO_2 under the changed climate would have generated significant increases in the transpiring leaf area. It is possible these increases in *LAI* were of such a magnitude as to mask, or significantly reduce, the CO_2 anti-transpiration response.

Nevertheless, despite the CO_2 anti-transpiration response simulated in Scotland, Wales and the South West, relative to the baseline climate, transpiration under the future climate scenario was increased by +13 % to +66 % depending on site and genotype. This was because the increase in transpiration with a change in climate alone was substantial at these sites. In the East, however, transpiration of poplar SRC trees was on average -30% lower under the future climate scenario compared to the baseline climate.

The predicted increase in poplar SRC transpiration in response to elevated atmospheric CO_2 found in the East, and the net increase in poplar SRC transpiration relative to the baseline climate simulated in the South West, Wales and Scotland, supports more recent studies that suggest plant transpiration will increase in response elevated atmospheric CO_2 and under future climate scenarios (Tricker *et al*., 2009; Uddling *et al*., 2008). Again, this draws attention to the complex interplay between the climate and atmospheric CO_2 when determining plant responses to their environment. Potential errors that could arise from predicting plant responses to climate change from a) manipulating concentrations of CO_2 alone, and/or b) extrapolating results from a single site, are highlighted by this work.

6.4.2 Explaining the spatial variability: the model

The yield and transpiration of poplar SRC simulated by the model in this study is that resulting from the calibration of key model parameters performed in earlier chapters. These parameters were essentially responsible for getting the right balance between carbon- and

water-use by the poplars. Given the available data, this was done to the best of our ability, and results from this, and the previous chapters, suggest the current model formulation correctly represents the balance between carbon-use and water-use. Therefore, this study is an exploration of how the current model configuration for poplar SRC responds to likely future changes in climate in the UK, given the current parameterisation and representation of processes in the model. In this section, the response of the model parameterisations to the external drivers of climate and atmospheric CO_2 concentration are investigated, to determine why there was significant variation between the yield and transpiration responses of poplar SRC at the four sites under the different climate scenarios.

The model is parameterised with environmental dependencies on net photosynthesis (A_{net}) and stomatal conductance (g_s), i.e. air temperature, photosynthetically active radiation (PAR), soil moisture content, specific humidity deficit and CO_2 concentration. The responses of both A_{net} and g_s to these environmental drivers are shown in Cox *et al.*, (1998). Predicted A_{net} and g_s will therefore respond to the climate at each site through these parameterisations, which are then scaled-up to predict whole-plant productivity and water-use. In the model, both A_{net} and g_s are parameterised to increase with increasing temperature, up to a maximum, after which temperature becomes limiting to A_{net} and g_s (Cox *et al.*, 1998). C_3 photosynthesis is commonly reported to have an optimum temperature range of between 20 to 30 ^oC, beyond which temperature becomes limiting (Lambers *et al.*, 2008). The response to temperature in the model follows a bell-shaped curve, and is constrained such that A_{net} and g_s are zero below 0 ^oC and above 36 ^oC. Under the baseline climate, the South West was the warmest site during the winter and mean temperatures fell just behind those of the hottest site, the East, in the remaining months. Scotland and Wales were the coolest sites, often with no significant difference between the two. At all sites maximum monthly temperatures never exceeded 36 ^oC, the point where both A_{net} and g_s would be inhibited in the model due to high temperature, but were close in the East during the peak summer months. Nevertheless, this suggests that under the current climate, at many of the sites A_{net} and g_s would have been limited by low temperature, even if this was only marginal in some years. As the climate changed, mean seasonal temperature increased at all sites. Therefore, limitations imposed on carbon assimilation by low temperature would be relieved, likely translating into enhanced growth if other environmental factors were not limiting. Additionally, g_s would be increased as a result of higher temperatures, likely resulting in higher tree transpiration.

Cox *et al*., (1998) show both A_{net} and g_s respond to photosynthetically active radiation (PAR). Low PAR is limiting to A_{net} and g_s, both strongly increase as PAR increases, producing the typical A_{net} - P_{PFD} response curves that can easily be measured in the field. In Cox *et al*., (1998) both A_{net} and g_s follow a positive exponential curve that saturates as incident solar radiation approaches values of about 400 W m^{-2}. Although not shown, plotting leaf-level g_s against downward shortwave radiation at each site showed that g_s followed the shape of curve described in Cox *et al*., (1998) and started to saturate at similar values of incident solar radiation. Under the current climate, the maximum mean monthly values of downward shortwave radiation rarely exceeded 400 W m^{-2}. During the peak of the growing season (JJA), the mean shortwave radiation was around 200 W m^{-2} at all sites. Under the baseline climate, downward shortwave radiation was significantly higher in the South West throughout the year compared to all the other sites, and was lowest in Scotland. With climate change, the mean seasonal shortwave radiation marginally decreased during the winter, but substantial increases were seen during the rest of the year at all sites. This would therefore promote higher rates of A_{net} and g_s at each site if all other environmental conditions were favourable.

In the model, the degree of soil moisture stress experienced by the poplar SRC is calculated as the soil moisture stress factor, also called the β factor. Calculation of the β factor uses the mean volumetric soil moisture content and is shown in chapter 4, equation 5. The calculated β factor modifies the rates of A_{net} and g_s. Consequently high rates of precipitation maintain a high soil moisture content and reduce the occurrence of soil moisture stress. Under the baseline climate, rates of mean precipitation were significantly higher throughout the year at the Scottish site, followed by Wales and the South West that were not significantly different. Plots of the monthly soil moisture content predicted at all three sites showed a gradual decline throughout the growing season as soil moisture was depleted. This decline peaked around August/September and was followed by a gradual increase in mean soil moisture content as stores were re-charged. Both the Scottish and Welsh sites showed little evidence of soil moisture stress at any point in the year. Throughout the year, the mean and median of the calculated β factor did not drop below one (no stress). Despite the significantly higher transpiration of SRC poplar in the South West, little soil moisture stress occurred at this site because of the high precipitation input. Similar to the other two sites, the mean monthly β factor deviated little from one (no stress), even during the peak of the growing season. There was a degree of variation

around this, and in the summer months minimum mean values of the β factor dropped below 0.2 in *P. nigra*, for example. However, it was likely that these were due to the occurrence of a few extreme years, as both the mean and median were close to one. Mean monthly precipitation was lowest in the East, and this was significant throughout the year. Soil moisture content at this site was substantially lower and remained so. As a result, this site was significantly soil moisture stressed throughout the year. In the peak of the growing season, the mean and median of the monthly β factor was close to 0.5, even in winter months the calculated β factor was around 0.6. These results indicate that water availability was not significantly limiting to growth or transpiration in Scotland or Wales. In the South West, soil moisture became increasingly limiting as the growing season progressed, but significant stress that would seriously compromise growth only occurred in some years. At these three sites, autumn and winter precipitation was sufficient to fully re-charge stores of soil moisture. This was not the case in the East, however, and significant soil moisture stress persisted throughout the year such as to significantly impede growth. Under the changed climate, the Scottish site became wetter throughout the year, except in the summer. In Wales, mean precipitation was reduced in summer and autumn, but increased in the winter and spring. These sites were not previously water stressed, and with a change in climate the occurrence of soil moisture stress remained insignificant. Declines in soil moisture content under a changed climate relative to the ambient climate were seen. These ranged between -2 to -27 % depending on site and genotype. The soil moisture deficit was minimal in the winter, and increased as the growing season progressed, suggesting the increased deficit was due to increased extraction of water by bigger SRC trees, as opposed to a significant year-round reduction in water availability. These translated into minimal changes in the soil moisture stress seen by the SRC in Scotland. In Wales, changes in the β factor were larger, but evidently not sufficient to impact on growth or transpiration. The East was significantly water-stressed under the ambient climate. With a change in climate, precipitation increased in the winter and spring, but decreased in the summer and autumn. Declines in soil moisture content relative to the ambient climate were seen at this site, ranging between -16 % to -20 %, and these relatively large deficits were present throughout the year. The mean monthly β factor was significantly reduced at this site, with minimum predicted values dropping as low as 0.01. It is likely that this limited water availability was largely responsible for the significantly reduced yield and transpiration predicted with a changed climate. In the South West, yield declined and transpiration increased in a changed climate relative to the ambient climate. The changes predicted were

much more conservative, however, and suggested that increased soil moisture stress during the growing season as a result of the reduced summer and autumn precipitation were substantial enough to marginally impact on yield in some years, but changes in the other climate variables, such as temperature and PAR, drove increases in the transpiration.

In C_3 photosynthesis, rates of A_{net} are enhanced by increasing concentrations of atmospheric CO_2 because Rubisco, the enzyme catalysing the carboxylation reaction, is not CO_2 saturated under current ambient CO_2 concentrations, and CO_2 inhibits the competing oxygenation reaction leading to photorespiration (Rogers & Humphries, 2000). Therefore, at low atmospheric CO_2 concentrations, CO_2 is limiting to photosynthetic carbon gain. As CO_2 concentration increases, photosynthesis is increasingly limited by light availability which limits the regeneration of RuBP, the primary substrate for atmospheric CO_2 in the carboxylation reaction. At high irradiance and high CO_2 concentration, the rate of photosynthesis can be limited by the rate of export and utilisation of triose-phosphate, one of the primary photosynthate products, from the leaf. The response of A_{net} to increasing concentrations of atmospheric CO_2 can be measured in the field, and typically follows the shape of a positive exponential curve. Current ambient concentrations of atmospheric CO_2 are limiting to photosynthesis in C_3 plants (Long *et al*., 2004; Nowak *et al*., 2004), therefore, as concentrations of atmospheric CO_2 rise this limitation is reduced resulting in higher rates of carbon assimilation, which commonly translates into higher biomass accumulation. This response of A_{net} to CO_2 concentration is parameterised in the model (Cox *et al.*, 1998), and is consequently responsible for the increased yield predicted at all sites under both climate scenarios (baseline and changed) with an increase in atmospheric CO_2 alone.

In plants, water-loss is regulated by stomata on the leaf surface. Among other environmental variables, stomata are sensitive to the intercellular CO_2 concentration, which is a key variable sensed by guard cells and used to co-ordinate stomatal opening (Tricker *et al.*, 2005). In response to increased concentrations of atmospheric CO_2, g_s measured in the field is observed to decrease (Ainsworth & Long, 2005; Ainsworth & Rogers, 2007) as a result of reduced stomatal opening rather than reduced stomatal density (Radoglou and Jarvis,1990b; Tricker *et al.* 2005). This response of g_s to elevated concentrations of atmospheric CO_2 is represented in the model (Cox *et al.*, 1998) and translates into reduced poplar SRC transpiration with elevated atmospheric CO_2 at the

majority of sites, although this response is not universal. For example, in the East of England, the enhanced yield with elevated atmospheric CO_2 is of such magnitude that transpiration at the canopy-level increased in response to elevated CO_2, masking the CO_2 anti-transpiration response.

6.4.3 Does elevated atmospheric CO_2 offset the negative impact of drought on yield?

The results of these modelling experiments suggest that growth in an enriched CO_2 environment can offset the negative impacts of drought on yield by increasing soil moisture content, and thereby decreasing the soil moisture stress experienced by the poplar trees. Under the baseline climate, the East was significantly soil moisture stressed throughout the year, and the South West experienced more soil moisture stress during the growing season than either Scotland or Wales. At both sites this drought effect was exacerbated by the change in climate that reduced summer and autumn precipitation and increased temperatures and PAR. Consequently, at these two sites, yield was significantly reduced with a change in climate alone. Under both climate scenarios (baseline or changed), however, the impact of CO_2 on the enhancement of yield was always greatest in the East and South West. The CO_2 fertilisation effect on yield ranged between +100 % to +165 % depending on genotype and climate scenario in the East. In the South West this range was +36 % to +87 %. This is compared to high, but more conservative increases at the less drought prone sites, Scotland and Wales. Under the baseline climate, increases in mean monthly predicted soil moisture content with elevated atmospheric CO_2 were evident at all sites, generating increases in the mean monthly predicted β factor (less stress). The magnitude of these increases were greatest in the East and South West, sites that received the least rainfall and experienced more soil moisture stress. Together, this suggests that the CO_2 fertilisation effect on yield was greatest in drought prone areas, and that elevated atmospheric CO_2 can offset the negative impact of drought on yield.

Nevertheless, the interaction with climate determined whether any significant benefit of the CO_2 fertilisation effect was seen relative to the baseline climate. For example, in the East, because of the substantial decline in yield with a changed climate, mean predicted yield under a future climate scenario was still lower in *P. x euramericana* (-6 %) and only marginally increased in *P. nigra* (+2 %) relative to the baseline climate, despite the positive CO_2 fertilisation effect on yield. Therefore, although yield losses due to drought

were largely offset under both climate scenarios, there was no significant gain in yield under the future climate scenario relative to the baseline climate. The South West was not as dry as the East, consequently, despite significant yield losses under a changed climate, mean predicted yield under a future climate scenario was enhanced by the CO_2 fertilisation effect, such that yield was roughly 50 % higher in both genotypes relative to simulated yield under the baseline climate.

6.4.4 Does soil type significantly impact on yield and transpiration and their response to changes in climate and atmospheric CO_2?

Soil type had a minimal impact on the predicted yield and transpiration. Soil type only made a significant difference to predicted yield and transpiration under the changed climate scenario. These differences were found to be marginal, however, and were only significant for simulations with a sandy soil where the mean yield and transpiration were lower than that predicted for both the clay and silt soil types. These results are unsurprising, given that sandy soils are characteristically more free draining than either a clay or silt soil. Reduced precipitation during the growing season at the majority of sites under the changed climate generated increases in the soil moisture stress, which was exacerbated in the sandy soil given its free draining nature. Therefore predicted transpiration and yield were reduced more on the sandy soil than either the clay or silt soil. These results are supported by the literature that suggests available soil water does not impact on transpiration until a low threshold, and that differences in this response between soil textures are only apparent in sandy soils because of their free draining nature (Sinclair, 2005; Sinclair *et al.*, 1998). Although the differences between soil type were not significant under any of the other climate scenarios, these results suggest that sandy soils are least viable for poplar SRC planting, and may be best avoided in future plantings. It is noted, however, that these experiments investigated just three 'typical' soil textures and used their associated physical and thermal properties in simulations. Whilst this provides a means of investigating the impact of soil texture in this modelling experiment, in the real-world, soil textural classes and their associated properties are extremely varied, even within the same textural class. This inherent variation means that the properties of any two soils are unlikely to be similar, therefore not all sandy soils may be unsuitable for poplar SRC planting. More detailed investigation of different soil properties would be necessary.

6.4.5 How does poplar SRC yield and transpiration differ at four locations in the UK under current climatic conditions, and how does this change under a future climate scenario?

Under the current climate and ambient atmospheric CO_2 concentration, the variability of predicted yield and transpiration between locations was similar, and both genotypes followed a similar trend with yields significantly higher in *P. nigra*. The mean predicted harvestable yield in both *Populus x euramericana* and *P. nigra* was highest in the South West of England. Final harvestable yields predicted in Scotland and Wales were similar, but the mean yields at these sites were roughly -30 % to -40 % lower than the mean harvestable yield in the South West. Yield was lowest in the East of England. Mean predicted yields at this site showed a large -60 % to -70 % decline from the mean yield predicted in the South West, the most productive site. For easier comparison with the literature results were converted into units of tonnes ha^{-1} yr^{-1}. The modelled yield ranged between 5.14 to 15.82 t ha^{-1} yr^{-1} for *P. x euramerincana* and 5.07 to 16.18 t ha^{-1} yr^{-1} for *P. nigra*, depending on site. These ranges are in keeping with field studies of poplar SRC in the UK that have reported yields between 2.94 to 24.0 t ha^{-1} yr^{-1} (Andersen *et al.*, 2005; Aylott *et al.*, 2008; Bunn *et al.*, 2004; Rae *et al.*, 2004; Tubby & Armstrong, 2002), and with a further study that modelled poplar and willow SRC yields in the UK of between 1.97 to 13.34 t ha^{-1} yr^{-1} (Aylott *et al.*, 2008).

Mean predicted transpiration followed a similar pattern. In both genotypes, rates of transpiration were highest in the South West, ranging from 0.72 mm day^{-1} to 0.88 mm day^{-1} for *P. x euramericana* and *P. nigra* respectively. For *P. x euramericana* SRC, predicted mean transpiration was not significantly different between Scotland, Wales or the East of England. Plant transpiration at these sites was roughly half that of *P. x euramericana* SRC in the South West. For *P. nigra* SRC, transpiration was significantly lower in the East than in either Scotland or Wales. At all these sites, mean plant transpiration was roughly -40 % to -50 % lower than transpiration of *P. nigra* SRC in the South West. These means represent the yearly mean transpiration over the thirty year period of driving data, which includes all stages of growth in the coppice rotation from planting through to full canopy closure. Maximum rates of transpiration predicted were therefore much higher, and in the South West were in excess of 6 mm day^{-1} for *P. x euramericana* and 7 mm day^{-1} for *P.*

nigra during the peak of the growing season. These high rates of predicted transpiration were comparable to rates observed in poplar SRC (*P. trichocarpa x. deltoides*) in the South West of England, where maximum rates of 10.7 mm day^{-1} were recorded (Hall *et al.*, 1998). Another study recorded transpiration rates of up to 9 mm day^{-1} at a different site in southern England (Hall & Allen, 1997). Although these studies were on different genotypes of poplar, it gives reassurance that the model can simulate rates of transpiration for poplar SRC within a range that is not uncommon in the South of England.

Mean predicted yield simulated for a future climate scenario (i.e. changed climate and elevated atmospheric CO_2 concentration) increased at all sites relative to the yield simulated under the baseline climate, with the exception of the East of England. The magnitude of yield increase varied between sites and was greatest in Scotland for both genotypes. Nevertheless, despite the more conservative increase in yield relative to the baseline climate, the South West of England remained the highest yielding site under the future climate scenario, with predicted mean yields of 21.32 t ha^{-1} yr^{-1} for *P. x euramericana* and 23.82 t ha^{-1} yr^{-1} for *P. nigra*. Under the future climate scenario however, the difference between mean predicted yields in Scotland, Wales and the South West was reduced. Yield remained the lowest in the East. Under a future climate scenario, simulated mean yield decreased in *P. x euramericana* and only marginally increased in *P. nigra* relative to the baseline climate.

Under the future climate scenario, mean predicted transpiration was higher in the South West, Scotland and Wales relative to the baseline climate. Despite the CO_2 anti-transpiration effect in response to elevated atmospheric CO_2 under the changed climate scenario, simulated transpiration under the changed climate alone was stimulated to such an extent at these sites, a net increase in poplar SRC transpiration under the future climate scenario resulted. Mean predicted transpiration under a future climate scenario remained highest in the South West, but the relative increase from transpiration under the baseline climate was small (+17 % *P. x euramericana*, +14 % *P. nigra*). In contrast, in Scotland and Wales, mean predicted transpiration was marginally lower than in the South West, but the relative increase from the baseline climate was large. Percentage increases in mean predicted transpiration ranged between +48 % to +66 % depending on site and genotype. Transpiration remained lowest in the East of England, relative to the baseline climate, transpiration decreased on average by -30 % under the future climate.

These results suggest that the East of England is not viable for growing poplar SRC under a future climate scenario. Even under the baseline climate, the extent of soil moisture stress simulated year to year by the model was so severe that in the real-world there would be no growth. Under the future climate scenario, the soil moisture stress was increased and the yield depressed further. Therefore, the results of this modelling experiment suggest these high water using varieties of poplar SRC would not be sustainable in low rainfall area of the UK, such as the South East of England, if they were only rain-fed. Consequently, these results indicate that under both the current climate and future climate scenarios, the South West of England is most suited to poplar SRC growth, being the most productive site under both climate scenarios. However, this site also has the highest transpiration under both climate scenarios. Nevertheless, for roughly a 50 % increase in predicted yield at this site with climate change, the magnitude of the increase in transpiration was the lowest here. This suggests that environmental impacts of poplar SRC growth on water resources as a result of climate change would be smaller here compared to the other sites. The magnitude of the enhancement of yield resulting from climate change was considerably larger at the Scottish and Welsh sites than in the South West; however, this was accompanied by a significantly larger increase in transpiration. Therefore, in Scotland and Wales, whilst substantial economic benefit may be gained under a future climate scenario as a result of enhanced poplar SRC yields, this is likely to be at a greater environmental cost. Additionally, under a future climate scenario, the range of both predicted mean yield and transpiration was noticeably larger at the Scottish site, suggesting there was more variability in the year-to-year simulated yields and transpiration rates. Certainly, for economic sustainability, variability in the year-to-year supply of biomass is not desirable. This work shows that for impact assessments of the effects of climate change on bioenergy crop production, information about both the transpiration and yield is important, as there is an evident trade-off between the change in economic gain and sustainability of supply with the potential environmental impact on water resources.

The variability surrounding the prediction of mean yield and transpiration was increased under the future climate scenario relative to the baseline climate. This greater variability arose from use of the ensemble mean yield and transpiration predicted by the different sets of GCM anomalies, and the difference between the soil types, although this was seen to be marginal. There was significant variation in predicted mean yield and transpiration as simulated by the different GCM anomalies at each site. The variation associated with the

predicted yield appeared greater than the variation surrounding the predictions of mean transpiration, but both were significant. The variation was significant at all sites, but was probably largest in the South West for mean predicted yield. Plotted as the ensemble mean, however, the variation was largest at the Scottish site, largely due to two large outliers (anomalies from FGOA and GIAO) that predicted opposite and extreme ranges. This highlights the importance of this ensemble approach in impact studies. Relying on just one GCM could produce very different predicted responses to changes in climate. Using an ensemble of model predictions accounts for a wider range of possible responses to future climate change, providing a better estimate of the mean response. Nevertheless, despite the given variation, the distribution of the middle 50 % of the data around the mean and median was relatively small at each site, therefore discernable differences between sites and genotypes were evident. It is concluded that despite the spread in the data, this modelling approach, using an ensemble of predicted future changes in climate, provides useful information about the transpiration and yield of poplar SRC in the future.

6.4.6 Limitations

Limitations were identified in this study. The climate anomalies used as atmospheric forcing to simulate a changed climate were derived from GCM output. GCMs, however, tend to have a coarse horizontal resolution. GCMs have topographically smooth landscapes, with each grid cell representing average land surface properties and climate over hundreds of kilometres. RCMs (regional climate models), however, have a much higher spatial resolution. Changes in topography and vegetation distribution affect the climate, and RCMs can represent the effects of these on the weather much better than GCMs. It is well understood, for example, that the intensity, frequency and distribution of extreme precipitation events is simulated less well in GCMs (IPCC, 2007). In the UK, for example, simulation of observed winter precipitation was more accurate using RCMs as opposed to GCMs (Murphy *et al.*, 2009). From the conception of this study, output produced by the UK Climate Impacts Programme (UKCIP) 2009 was going to be used to simulate climate change. As part of their output, the UKCIP ran an eleven-member variant of the Met Office Regional Climate Model (HadRM3) at a 25 km resolution (Murphy *et al.*, 2009). This would have provided the best data available for predicted climate change in the UK at a regional scale. Unfortunately, however, although they were due out in 2008, the UKCIP outputs were delayed until July 2009. They were not available on a compatible

timescale for use in this work. Therefore, an alternative method was sought, and the GCM anomalies used provided a good alternative. Although there were known limitations, such as those described above, they gave a good indication of the spatially dependent direction and magnitude of climate change in the UK. Additionally, the GCM anomalies allowed an ensemble approach to account for uncertainty in predicted responses to future climate change resulting from variability of projected climate change by different models.

Additional uncertainties exist in the predictions of yield and transpiration responses of poplar SRC under a future climate in this study. For example, the baseline climate data are daily observations that have been disaggregated to hourly data. This may introduce errors, specifically regarding the timing, intensity and duration of rainfall. This study does not account for scenario uncertainty as only one emissions scenario was used. However, this work was primarily concerned with disaggregating and quantifying the interaction between atmospheric CO_2 and climate; consequently, it was considered adequate to use a single 'medium' emissions scenario. Nevertheless, whilst quantifying uncertainty in the baseline data is more difficult to do, a priority for future work would run simulations with additional emissions scenarios for comparison.

The results from these modelling experiments are determined by the parameterisation and representation of processes in the model. There are, however, assumptions in the model, or imperfect representation of processes in the model that may lead to erroneous responses of yield and transpiration to climate change. For example, in the model there is a fixed temperature response for photosynthesis. This follows a bell-shaped curve with an optimum temperature, below which photosynthetic rate declines, as described in section 6.4.1.3. There is evidence to suggest that photosynthetic rate will acclimate to higher growth temperatures (Hikosaka *et al.*, 2006). Consequently, this optimum temperature prescribed in the model is artificial and may not correctly describe the response of photosynthesis to temperature, which will become more important in areas where future climate change predicts an increase in growth temperature.

6.5 Conclusions

The responses of both yield and transpiration to elevated concentrations of atmospheric CO_2 were significantly affected by climate. This interaction is key and refines many of the

generalised hypotheses about plant responses to climate change. Experimental studies reported in the literature often manipulate concentrations of atmospheric CO_2 alone. These studies generally suggest that in a future high CO_2 world plant biomass will increase and transpiration decrease. This work demonstrated that the CO_2 effect was significantly modified by interactions between climatic variables in a manner that is not easily predictable. In Scotland, Wales and the South West of England, yield was significantly increased in a future climate compared to the baseline climate, although this increase was far more conservative in the South West. Under a future climate scenario however, transpiration at these three sites also increased relative to the baseline climate. Despite the CO_2 anti-transpiration effect, the increased transpiration as a result of the changed climate was such that transpiration remained higher under the future climate scenario than under the baseline climate. In the East, however, the change in yield under a future climate was marginal, even decreasing, because of the interaction with severe drought. Transpiration at this site marginally decreased under a future climate scenario relative to the baseline climate.

Therefore, at the majority of sites, the interaction of CO_2 with climate resulted in significant gains in biomass that were of much greater magnitude than gains suggested by results from studies that have manipulated concentrations of CO_2 alone (FACE). In addition, despite the CO_2 anti-transpiration effect, transpiration was significantly higher under the future climate scenario compared to the current climate, which contradicts the findings of many FACE studies. There was considerable variation between the locations however. In the East, the yield change with a future climate scenario was minimal, and transpiration marginally decreased, depending on genotype. Most notably, it was observed that the CO_2 fertilisation effect on yield was greatest at this site, along with the South West site. These two sites are the most drought prone areas, suggesting that elevated atmospheric CO_2 can offset the negative impacts of drought on yield.

This study demonstrates the importance of using ensembles of future climate projections for climate change impact studies. Large variations in simulated mean yield and transpiration were evident between the different sets of climate anomalies used. Consequently, this ensemble approach provides the best estimate of the mean response.

The results of this modelling experiment suggest that such high water-using varieties of poplar SRC would not be sustainable in low rainfall area of the UK such as the South East of England, if they were only rain-fed. The limitation of water availability significantly impeded the growth of these bioenergy crops, such that final yields were too low to be economically viable. Under both climate scenarios, the South West was the most productive site for poplar SRC growth. The Scottish and Welsh sites were also viable for poplar SRC production under both the baseline and future climate scenarios. The magnitude of the yield increase under a future climate scenario was greatest in both Scotland and Wales, however this was accompanied by substantial increases in transpiration relative to the baseline climate, suggesting the trade-off between economic gain and environmental impact on water resources may be less favourable at these sites.

Chapter 7

Conclusions

7.1 Summary

In the UK alone, significant increases are predicted for the amount of land used to grow dedicated perennial bioenergy crops such as poplar SRC (DEFRA, 2007; Haughton *et al.*, 2009). Given their favourable energy ratios and reduced emissions of greenhouse gases compared to conventional fossil fuels, the Department of Energy and Climate Change has proposed a significant contribution of bioenergy from biomass to a low carbon energy mix for the UK (DECC, 2009a). Substantial increases in the contribution of bioenergy from biomass are forecast globally (Berndes *et al.*, 2003; Sims, 2007). Many poplar varieties suitable for bioenergy have been shown to be high yielding, however this is also generally associated with high rates of water-use in addition to notorious susceptibility to drought. Therefore, a fundamental problem with poplar SRC is maintaining consistently high yields that are commercially viable in large-scale planting, across a wide variety of climatic and site conditions; without significantly compromising water resources. Future climate change scenarios for the UK in general predict warmer, wetter winters and hotter, drier summers, although this is variable depending on region (Murphy *et al.*, 2009), in addition to elevated concentrations of atmospheric CO_2. Climate change is therefore likely to significantly impact on the yield and water-use of poplar SRC and its spatial variability. How poplar SRC will respond to future climate change is currently unknown and therefore represents a significant knowledge gap in the path to a sustainable future. Given the economic and environmental importance of dedicated perennial bioenergy crops, bridging this gap is essential.

Therefore, this thesis has used the land-surface scheme JULES to predict the yield and transpiration of poplar SRC under the current climate and with future climate change in the UK. Initially, in chapter 3, fieldwork was carried out to determine the physiological responses of two genotypes of poplar SRC to drought, *Populus x euramericana* and *P.*

nigra. Biochemical photosynthetic parameters (V_{max}, J_{max}, α and g_i) were also determined for these two genotypes. This work then assessed impact of water-stress and internal CO_2 conductance on parameter estimation. In chapter 4 these data were used to calibrate and validate the leaf-level A_{net} - g_s model used in JULES. It was also investigated whether including the transfer of CO_2 from c_i to c_c would improve the accuracy of simulated A_{net} and g_s in the leaf-level model. Following calibration and validation of the leaf-level model, the JULES model was modified and parameterised in chapter 5 to simulate the growth and water-use of the two genotypes of poplar SRC. Harvesting was introduced to the model to simulate the management of poplar SRC. Changes were made to the allocation of carbon between the different plant stores in the model, and suitable plant-specific parameters were found using a Monte-Carlo sensitivity experiment. Performance of JULES was assessed against observations of canopy height, *LAI*, transpiration and carbon content of the vegetation measured from *P. x euramericana* and *P. nigra* under ambient and elevated atmospheric CO_2 at a FACE experiment in Italy. This parameterised version of JULES was used in chapter 6 to simulate the transpiration and yield of *P. x euramericana* and *P. nigra* SRC in the UK under the current climate and with climate change. The yield and transpiration responses of poplar SRC were assessed at four climatologically different regions of the UK, and for three different soil types. To simulate a changed climate an ensemble approach used atmospheric forcing from ten different GCMs. This was to account for GCM uncertainty and capture the full range of possible impacts of climate change on poplar yield and transpiration. This thesis addressed the following questions:

1. What are the genotype-dependent differences between the two varieties of poplar SRC in terms of photosynthetic parameters, stomatal conductance and carbon allocation strategies, and how do these change with water stress?

In terms of A_{net} and g_s, minimal differences were observed between *P. x euramericana* and *P. nigra* as measured across the course of the growing season. A_{net} and g_s in both genotypes of poplar declined in response to increasing soil moisture stress and atmospheric evaporative demand. Both genotypes displayed limited sensitivity to soil moisture stress, the response followed a threshold response that was best described by a sigmoid curve. Soil moisture content declined to a critical threshold of between 11-18 % vol. before the poplars responded by closing stomata which inhibited photosynthesis. This is possibly

indicative of the inherent growth strategy of poplars in the natural environment as pioneer species.

The key photosynthetic parameters (V_{max}, J_{max}, g_i and α) were only significantly different between the two genotypes at certain times during the growing season. Both V_{max} and J_{max} were significantly lower in *P. nigra* at the very start of the growing season, thereafter they were comparable between genotypes in well watered trees. Although internal conductance to CO_2 has been found to vary greatly among and within species (Ethier & Livingston, 2004; Flexas *et al.*, 2008; Niinemets *et al.*, 2009; Warren, 2008), in this study, g_i was only marginally significantly different between the genotypes and this was only at certain points in the growing season. Besides this, g_i remained fairly constant throughout the growing season in control trees, ranging between 0.83 - 2.55 µmol m^{-2} s^{-1} Pa^{-1}. These estimates of g_i fall well within reported values for g_i in *Populus spp.* in the literature, 0.4 to 5.0 µmol m^{-2} s^{-1} Pa^{-1} (Flexas *et al*., 2008). α was comparable between genotypes across the growing season. Drought-induced declines of V_{max}, J_{max} and g_i were significant and substantial. α declined with drought during the first drought period only, which occurred in concert with higher temperatures and light availability. Photosynthetic capacity was fully restored upon re-watering following drought. In fact V_{max}, J_{max} and g_i were initially 'up-regulated' to values much higher than those measured in control trees. This highlighted the 'plasticity' of these photosynthetic kinetic parameters which can be modified by the plant to adapt to changing environmental conditions. Evidently α is an inherent property of the leaf that is fairly well conserved unless exposed to extreme environmental conditions.

As a result of both diffusive and metabolic limitations to photosynthetic carbon gain, water stress was shown to significantly impede the growth of *P. x euramericana* and *P. nigra*. Stem height, diameter and total leaf area were reduced under drought, and were not significantly different between the two genotypes. In contrast, well watered *P. nigra* trees achieved a higher harvestable biomass at the end of the growing season (+ 31.6 %) compared to *P. x euramericana*, despite the latter having a greater total leaf area. In contrast, *P. nigra* trees were found to have significantly thicker stems. These results suggest genotype dependent differences in patterns of carbon partitioning in the two hybrid poplars; *P. nigra* allocates assimilated carbon primarily to structural, woody biomass, whereas *P. x euramericana* allocates carbon dominantly to leaves.

2. What is the impact of internal conductance to CO_2 on the key photosynthetic kinetic parameters used in the physiologically-based photosynthesis - stomatal conductance model in the land-surface scheme JULES?

Estimates of V_{max} made under the assumption of infinite g_i were detectably lower in well-watered and drought treated trees of both genotypes. It was shown that in these fast growing poplar genotypes, the assumption that internal CO_2 transfer is infinitely large as to have a negligible impact on the drawdown of CO_2 from c_i to c_c is invalid. Under well-watered conditions, values of V_{max} calculated from A_{net} - c_c curves were, on average, 64 % and 52 % higher than values calculated from A_{net} - c_i curves in *P. x euramericana* and *P. nigra* SRC trees respectively. Therefore, this work highlights the impact g_i has on estimates of this important photosynthetic parameter, V_{max}.

3. Using calibrated parameter values, is the accuracy of simulated leaf-level photosynthesis and stomatal conductance improved by including internal CO_2 conductance in the physiologically-based photosynthesis - stomatal conductance model used in JULES?

Different model configurations were tested to determine whether including g_i improved the accuracy of simulated leaf-level A_{net} in the JULES A_{net} -g_s model. Parameterisation and validation of model configurations assessed the ability of the models to simulate observed rates of A_{net} and g_s for the most productive, (top of canopy), leaves of *Populus x euramericana* and *P. nigra*. Results showed that including g_i in the $A_{net} - g_s$ model did not significantly improve predicted A_{net}. Model validation of the parameterised $A_{net} - g_s$ model revealed that including g_i actually marginally reduced the accuracy of simulated A_{net}. Simulated g_s was marginally improved when g_i was accounted for. However, both g_s and A_{net} were simulated to a high level of accuracy in both model configurations. Consequently, no justification was found for adding complexity to the existing $A_{net} - g_s$ model.

Validation of the calibrated parameter sets used in the leaf-level model showed that using the JULES $A_{net} - g_s$ model in its original configuration simulated leaf-level A_{net} and g_s with an acceptable level of accuracy under well-watered conditions and with increasing water stress. Comparison of the use of calibrated parameter values to default parameter values highlighted the sensitivity of predicted A_{net} to these values, especially V_{max}. Therefore, it

was concluded that given the high sensitivity of the model to V_{max}, it is important to calibrate this parameter with an appropriate value of V_{max}, i.e. based on either c_i or c_c depending on the model configuration. Because of the impact of g_i on estimates of V_{max}, it is no longer the purely biochemical parameter on which photosynthesis models, such as the Farquhar *et al*., (1980) model, are founded since estimates based on c_i contain information pertaining to g_i. V_{max} is generally considered a directly transferable parameter that can be taken from measurements and used to calibrate models of ecosystem carbon exchange, however this work suggests it is more complex and V_{max} should be used with care, especially when used for model calibration.

4. Scaling up from the leaf-level to the canopy-level, can JULES accurately simulate the managed growth cycle, productivity and water-use of poplar SRC?

The modified and parameterised JULES model simulated the growth and water-use of both genotypes of poplar SRC in ambient and elevated atmospheric CO_2 well when validated against observations from the poplar FACE experiment. In addition, the behaviour of the model captured differences in growth between genotypes and CO_2 concentrations. Replication of the managed SRC cycle was achieved by introducing a harvesting routine which provided an adequate simulation of the rotation management system. Inconsistencies between modelled output and observations were apparent and were attributed to: i) limitations in the measurements, and/or ii) constraints in the model. Key limitations in the measurements included limited replication at the plot and site scale, partial dependency of the data set used for validation, and possible erroneous inferences used to extrapolate the data set. Key constraints in the model were identified as the lack of a separate above- and below-ground 'carbon store', and required further improvements to the allocation of carbon between the different plant stores.

5. How do changes in climate and atmospheric CO_2 concentration interact to impact on yield and transpiration of poplar SRC in the UK?

In both genotypes of poplar, the response of yield and transpiration to elevated atmospheric CO_2 was modified by the interaction with climate. This interaction is key and refines many of the generalised hypotheses about plant responses to climate change. Experimental studies reported in the literature commonly manipulate concentrations of atmospheric CO_2

alone. These generally suggest that in a future high CO_2 world plant biomass will increase and transpiration decrease. This work demonstrated that the CO_2 effect was significantly modified by interaction with other climate drivers in a manner that is not easily predictable. At all sites, a large increase in yield was simulated with elevated atmospheric CO_2 under both climate scenarios. Under the changed climate, the magnitude of this yield increase was significantly larger than that predicted by FACE studies alone. In both the South West, Wales and East of England, the magnitude of the yield increase with elevated atmospheric CO_2 was significantly larger under a changed climate than under the baseline climate. In Scotland this was simply additive. The CO_2 fertilisation effect on yield was always greatest in the East and South West, which were more drought prone sites, suggesting that elevated atmospheric CO_2 can offset the negative impact of drought on yield. Nevertheless, relative to the baseline climate, the impact of a future climate scenario on yield in both genotypes of poplar SRC was a net increase in yield in the South West, Scotland and Wales, and a decrease in the East of England.

The interaction between CO_2 and climate was not significant for transpiration, except in the East. Here, transpiration marginally increased, depending on genotype, with elevated atmospheric CO_2 under the current climate, but decreased under a changed climate and elevated CO_2. In Scotland, Wales and the South West, transpiration was seen to decrease in response to elevated atmospheric CO_2 under both climate scenarios (current and changed). Nevertheless, relative to the transpiration of poplar SRC predicted under the basline climate, simulated transpiration was significantly higher under the future climate scenario, despite the CO_2 anti-transpiration effect. Therefore, relative to the baseline climate, the impact of a future climate scenario on transpiration in both genotypes of poplar SRC was a net increase in transpiration in the South West, Scotland and Wales, and a decrease in the East of England.

Taken together, these results suggest that the growth of dedicated poplar SRC in the UK under a future climate scenario will not resolve the conflict between maximising yield and minimising transpiration. On an area basis, at the majority of sites yield was increased with a concurrent increase in transpiration. Nevertheless, it may be that because of the significant and substantial enhancement of yield under a future climate scenario, the area of land required for dedicated bioenergy crops may be reduced, thereby reducing the water-use.

6. How does poplar SRC yield and transpiration vary within the UK under current climatic conditions, and how does this change under a future climate scenario?

Under the current climate, the yield of both genotypes of poplar was highest in the South West and lowest in the East. Yields in Scotland and Wales were similar. Depending on site yield ranged between 5.14 to 13.82 dry t ha^{-1} yr^{-1} for *P. x euramericana*, and 5.07 to 16.16 dry t ha^{-1} yr^{-1} for the more productive *P. nigra*. These ranges are in keeping with field and modelling studies of poplar SRC in the UK that have reported yields between 1.97 to 24.0 dry t ha^{-1} yr^{-1} (Andersen *et al.*, 2005; Aylott *et al.*, 2008; Bunn *et al.*, 2004; Rae *et al.*, 2004). Under a changed climate percentage changes in yield within the range of -5.41 to +113.33 % led to yield ranges of between 4.86 to 21.32 dry t ha^{-1} yr^{-1} for *P. x euramericana* and 5.14 to 23.82 dry t ha^{-1} yr^{-1} for *P. nigra*, depending on site. The change in yield in the East was marginal and decreased in *P. x euramericana*, consequently this remained the lowest yielding site. The percentage increase in yield was more conservative in the South West than either Scotland or Wales, nevertheless this remained the highest yielding site. Although yields in Scotland and Wales were not far behind. Soil type only had a significant impact on yield under the future climate scenario, although this was minimal and only marginally significant.

Transpiration followed a similar trend. Under the current climate, transpiration of poplar SRC was highest in the South West in both genotypes (0.72 to 0.88 mm day^{-1}). In *P. x euramericana*, transpiration was not significantly different between Scotland, Wales or the East of England and ranged between 0.36 to 0.38 mm day^{-1}. In *P. nigra*, transpiration was lowest in the East (0.41 mm day^{-1}), and was similar between Scotland and Wales (0.48 to 0.51 mm day^{-1}). Under the future climate scenario transpiration decreased in the East, consequently transpiration was lowest here (0.25 to 0.29 mm day^{-1}). Water use remained highest in the South West (0.84 to 1.00 mm day^{-1}), increasing under a future climate scenario by between 13.6 to 16.7 %. For both genotypes, transpiration in Scotland and Wales was similar (0.58 to 0.76 mm day^{-1}), however the increase in transpiration from the current climate was large at these sites ranging between +47.9 to +65.8 %.

The results of this modelling experiment suggest that such high water-using varieties of poplar SRC would not be sustainable in low rainfall area of the UK such as the South East of England, if they were only rain-fed. The limitation of water availability significantly

impeded the growth of these bioenergy crops, such that final yields were too low to be economically viable. Under both climate scenarios, the South West was the most productive site for poplar SRC growth. The Scottish and Welsh sites were also viable for poplar SRC production under both the baseline and future climate scenarios. The magnitude of the yield increase under a future climate scenario was greatest in both Scotland and Wales, however this was accompanied by substantial increases in transpiration relative to the baseline climate, suggesting the trade-off between economic gain and environmental impact on water resources may be less favourable at these sites. Additionally, under a future climate scenario, the range of both predicted mean yield and transpiration was noticeably larger at the Scottish site, suggesting there was more variability in the year-to-year simulated yields and transpiration rates. Certainly, for economic sustainability, variability in the year-to-year supply of biomass is not desirable.

7.2 Concluding remarks

The results of this work are a step to bridging the knowledge gap between current and future sustainability of bioenergy crops with respect to climate change impacts. Having successfully modified and parameterised JULES to explicitly represent poplar SRC as a new land-surface cover, this work provides a tool to assess climate impacts on this economically and environmentally important crop. This work concentrated on the UK, however JULES can be run globally. It will contribute to the modelling community by providing a means to simulate this unique vegetation type that is globally important. The initial results from this work will benefit the wider research community by providing a previously missing link in the chain to a sustainable future, and a tool to further investigate future climate impacts on poplar SRC.

7.3 Recommendations for future work

7.3.1 Further modifications to the model

Modifying the model to include a separate above- and below-ground carbon store was identified as a priority for future work. It is hoped this would improve the simulation of the coppicing and re-growth, allowing the below-ground biomass to remain in the ground when the above-ground biomass is removed.

7.3.2 Yield and water-use maps for the UK

This study assessed the variability of poplar SRC yield and transpiration in the UK by simulating the yield and transpiration at four locations within the UK. This gave good insight into the variation of poplar yield and transpiration in climatolgically different regions of the UK, and enhanced understanding of the response of poplar SRC to climate change and CO_2 concentration. However, as a tool to inform on the potential for bioenergy in the UK, future work would run JULES in a distributed mode to produce maps of yield and water-use. A land-mask could be used to exclude areas unsuitable for poplar SRC growth. The model can ultimately be run on a global scale; therefore this approach could ultimately assess the global potential for bioenergy.

7.3.3 Sampling emissions scenario uncertainty

Predictions of climate change are based on trajectories of future greenhouse gas emissions and their resultant influence on the climate. Uncertainty about future emissions arise because it is not possible to know with certainty how populations, economies, energy technologies and other social factors that influence greenhouse gas emissions will change in the future (Murphy *et al.*, 2009). The IPCC SRES emissions scenarios were developed for use in the IPCC Third- and Fourth-Assessment reports (Nakicenovic & Swart, 2000). These emissions scenarios were developed to explore future changes in the global environment with special reference to the production of greenhouse gases and aerosol precursor emissions, depending on different interactions between energy, economy, demography and land-use change (IPCC-DDC, 2009a). Consequently roughly 40 different emissions scenarios were developed within four different scenario families (Nakicenovic & Swart, 2000). This large number of scenarios covers a range of plausible ways in which the world may develop resulting in very different levels of greenhouse gases, however SRES make clear that it is not possible to put relative likelihoods on any of their emissions scenarios (Nakicenovic & Swart, 2000). This study used one ‘medium’ emissions scenario (A1B). Future work would use multiple scenarios to further quantify climate impacts on poplar SRC yield and transpiration and the associated uncertainty

Chapter 8

Appendices

8.0 Appendix 6 – Statistical analysis: output tables

Photosynthetic Parameters			
V_{max}~per+gen+treat+gi+gi:treat+gen:gi+gen:treat+per:gen+(1|treat/block)+(1|DOY)			
V_{max}	x^2	p	n
per:gen	19.64	<0.05	120
gen:treat	0.36	0.55	120
gen:gi	4.79	0.09	120
gi:treat	0.87	0.35	120
gi	40.05	<0.05	120
treat	11.78	<0.05	120
gen	*		
per	*		
J_{max}~per+gen+treat+gi+gi:treat+gen:gi+gen:treat+per:gen+(1|treat/block)+(1|DOY)			
J_{max}	x^2	p	n
per:gen	23.33	<0.05	120
gen:treat	0.35	0.56	120
gen:gi	4.07	0.13	120
gi:treat	0.39	0.53	120
gi	5.01	0.09	120
treat	14.15	<0.05	120
gen	*		
per	*		
g_i~per+gen+treat+gen:treat+per:gen+(1|treat/block)+(1|DOY)			
g_i	x^2	p	n
per:gen	12.95	<0.05	60
gen:treat	5.19	0.061	60
treat	18.43	<0.05	60
gen	*		
per	*		
a_{qe}~per+gen+treat+gen:treat+per:gen+(1|treat/block)+(1|DOY)			
a_{qe}	x^2	p	n
per:gen	4.32	0.072	60
gen:treat	2.43	0.12	60

treat	10.1	<0.05	60
gen	0.87	0.52	60
per	8.23	<0.05	60

Table 6-1. Output table of the mixed-effects models used to analyse the response of the photosynthetic parameters in Chapter 3. * Indicates that a value is not reported because it is involved in a significant interaction. Please see the main text for an explanation of the statistical method and the notation used in the statistical models. per = experimental period, gen = genotype, treat = treatment, gi = internal CO_2 transfer (g_i), block = experimental block, DOY = day of year.

Growth			
stem_biomass~treat+gen+gen:treat+(1|treat/block)			
	x^2	*p*	*n*
gen:treat	5.08	<0.05	58
gen	*		58
treat	*		58
leaf_area~treat+gen+gen:treat+(1|treat/block)			
	x^2	*p*	*n*
gen:treat	12.43	<0.05	31
gen	*		31
treat	*		31
stem_height~treat+gen+gen:treat+(1|treat/block)			
	x^2	*p*	*n*
gen:treat	1.09	0.28	58
gen	5.01	<0.05	58
treat	9.47	<0.05	58
stem_diameter~treat+gen+gen:treat+(1|treat/block)			
	x^2	*p*	*n*
gen:treat	4.72	<0.05	58
gen	*		58
treat	*		58

Table 6-2. Output table of the mixed-effects models used to analyse the growth responses of poplar SRC in Chapter 3. * Indicates that a value is not reported because it is involved in a significant interaction. Please see the main text for an explanation of the statistical method and the notation used in the statistical models. gen = genotype, treat = treatment, block = experimental block. DOY is not included as a random effect as the growth measurements were recorded on the same day at the end of the experiment.

8.1 Appendix 6A – Climate variables

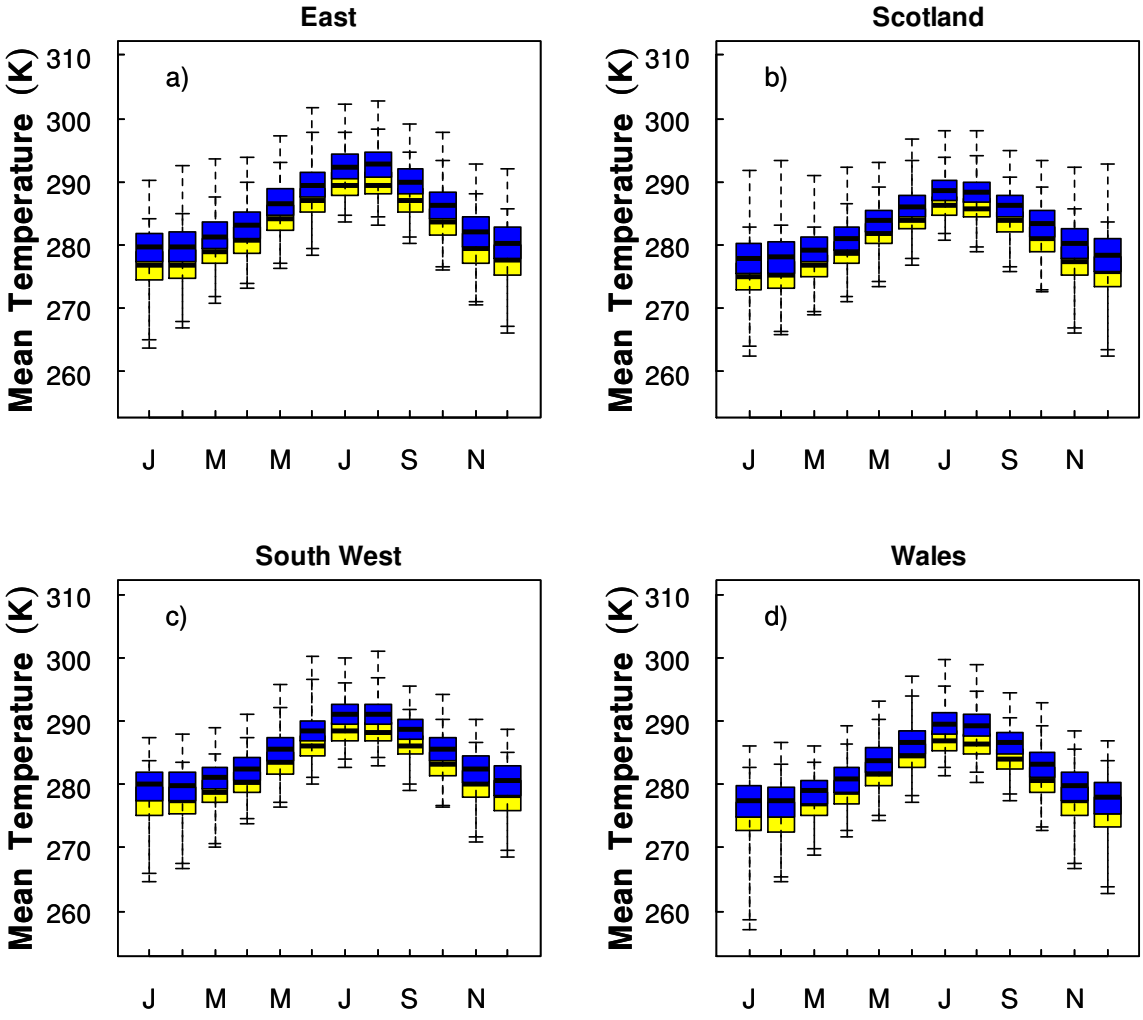

Fig. 6A-1. Temperature. The thick horizontal line represents the median, the coloured box represents the middle 50% of the data, and the vertical bars represent the minimum and maximum value. Yellow = current climate, blue = changed climate.

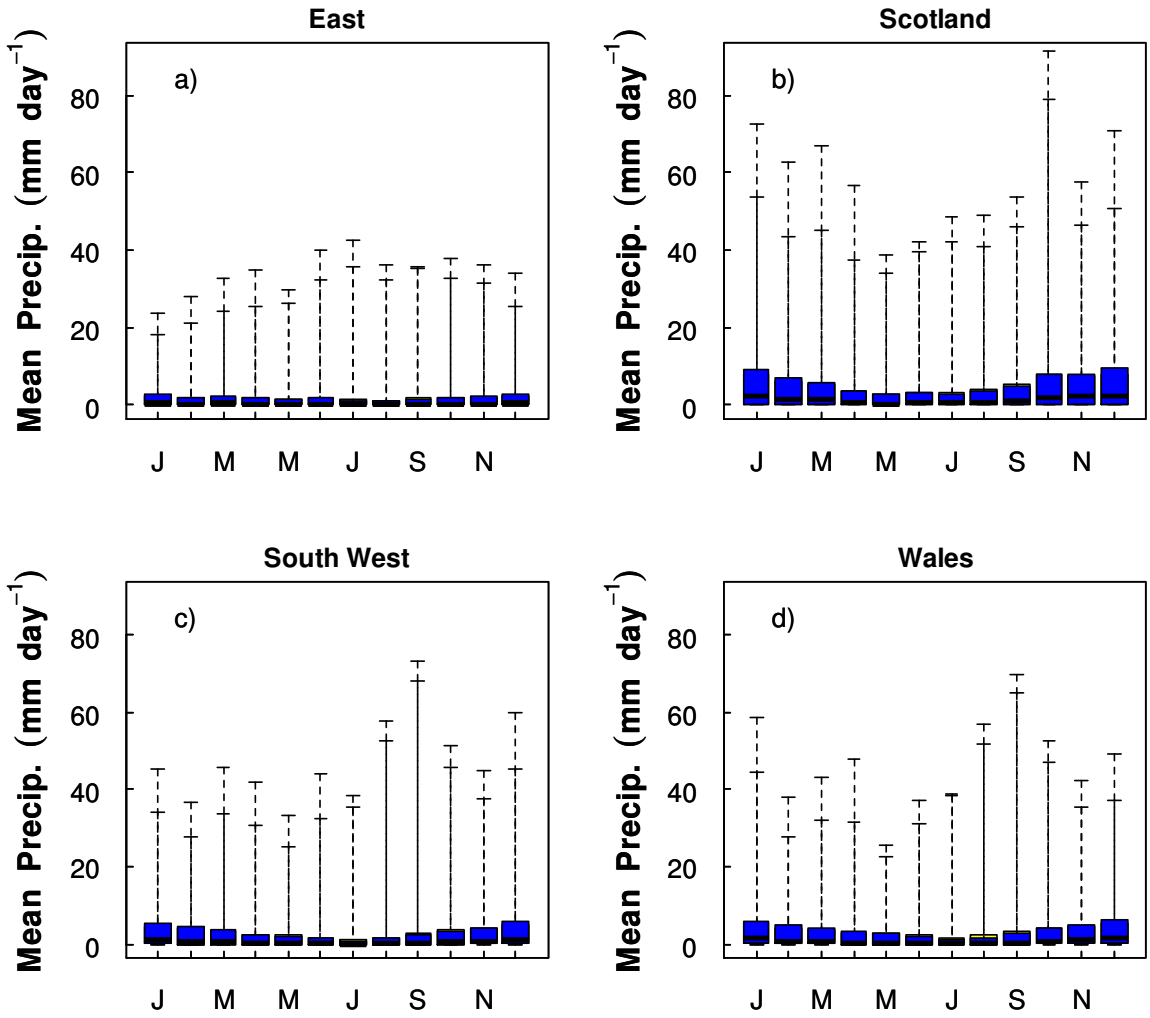

Fig. 6A-2. Precipitation. The thick horizontal line represents the median, the coloured box represents the middle 50% of the data, and the vertical bars represent the minimum and maximum value. Yellow = current climate, blue = changed climate.

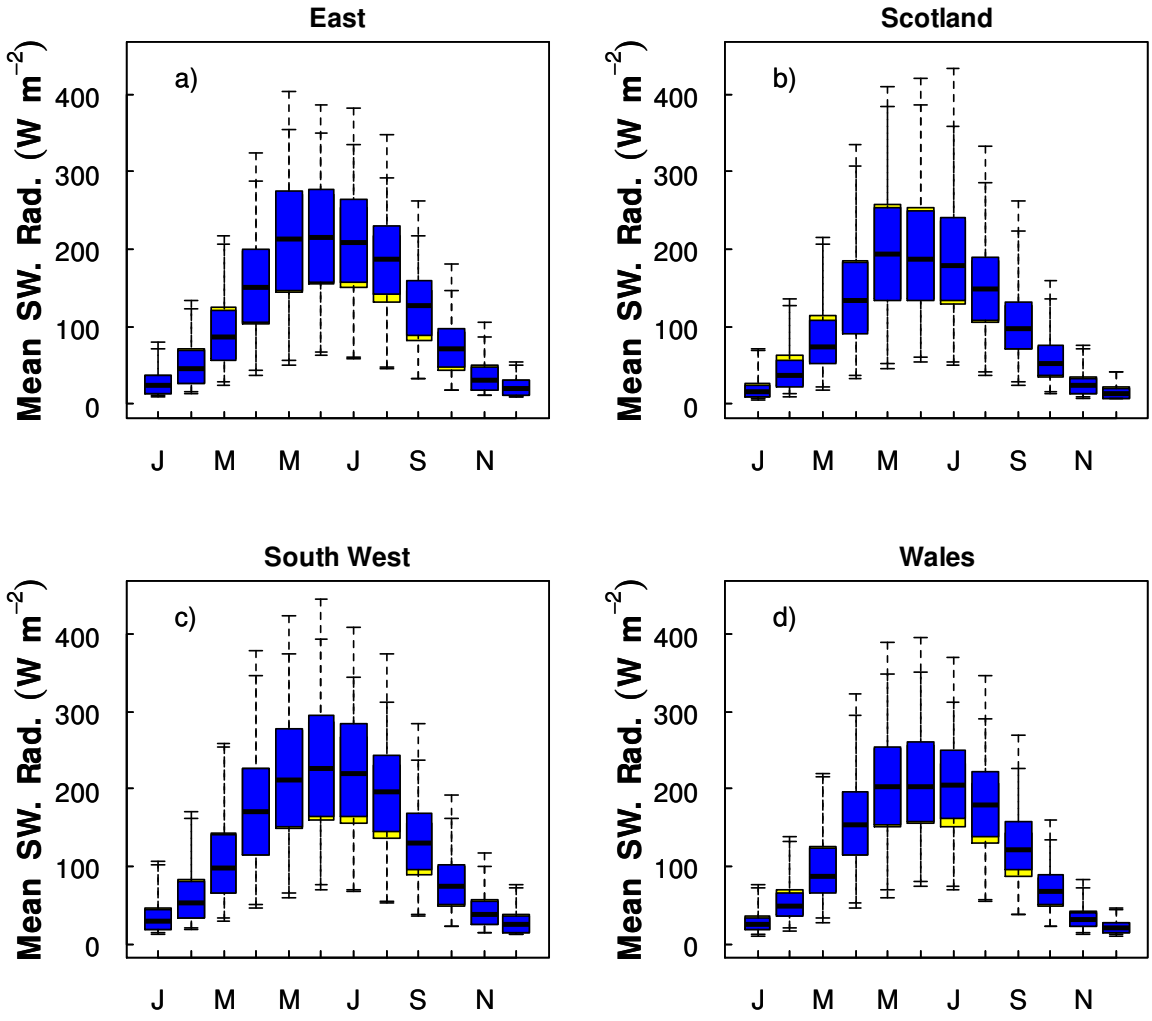

Fig. 6A-3. Downward shortwave radiation. The thick horizontal line represents the median, the coloured box represents the middle 50% of the data, and the vertical bars represent the minimum and maximum value. Yellow = current climate, blue = changed climate.

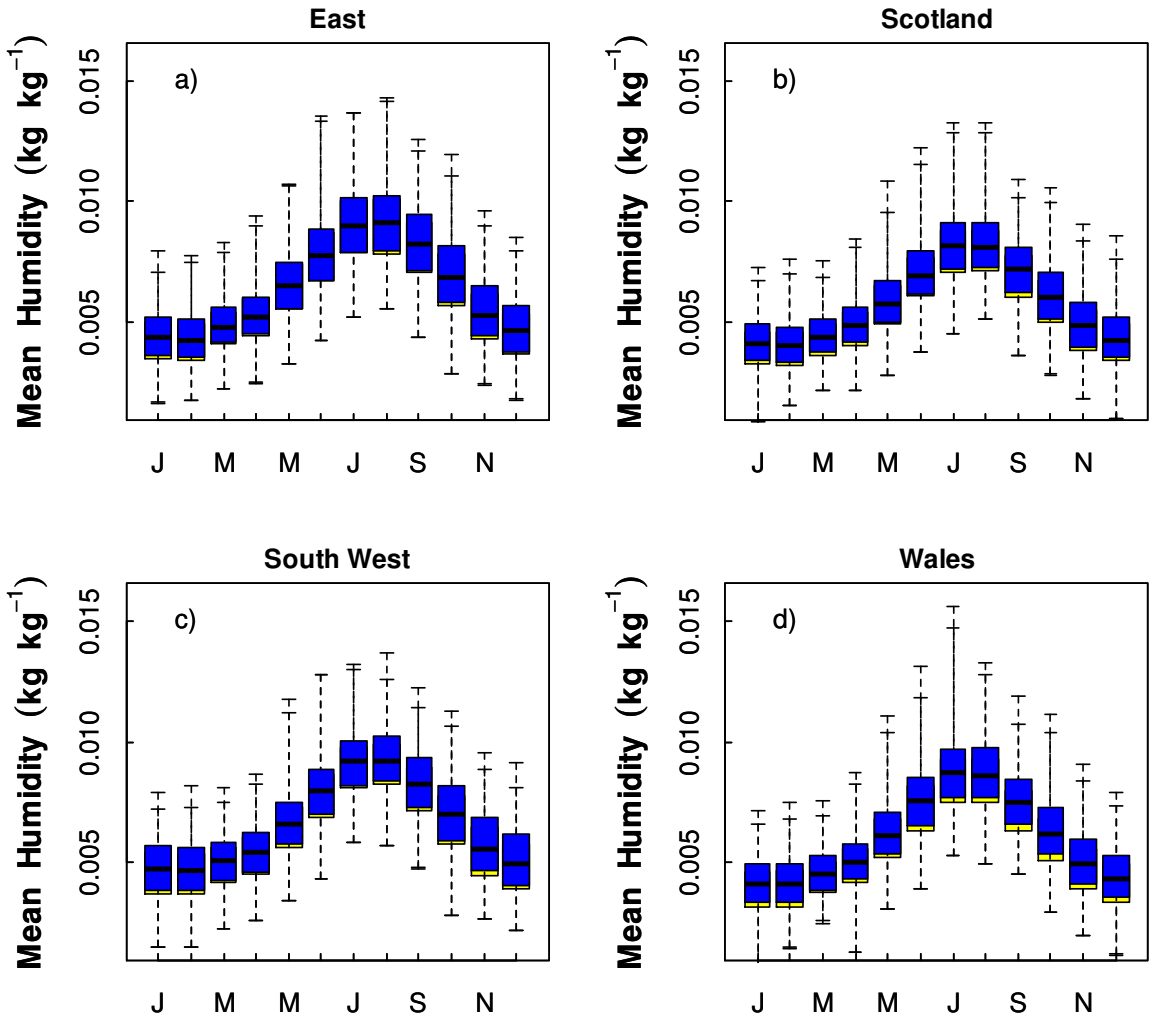

Fig. 6A-4. Specific humidity. The thick horizontal line represents the median, the coloured box represents the middle 50% of the data, and the vertical bars represent the minimum and maximum value. Yellow = current climate, blue = changed climate.

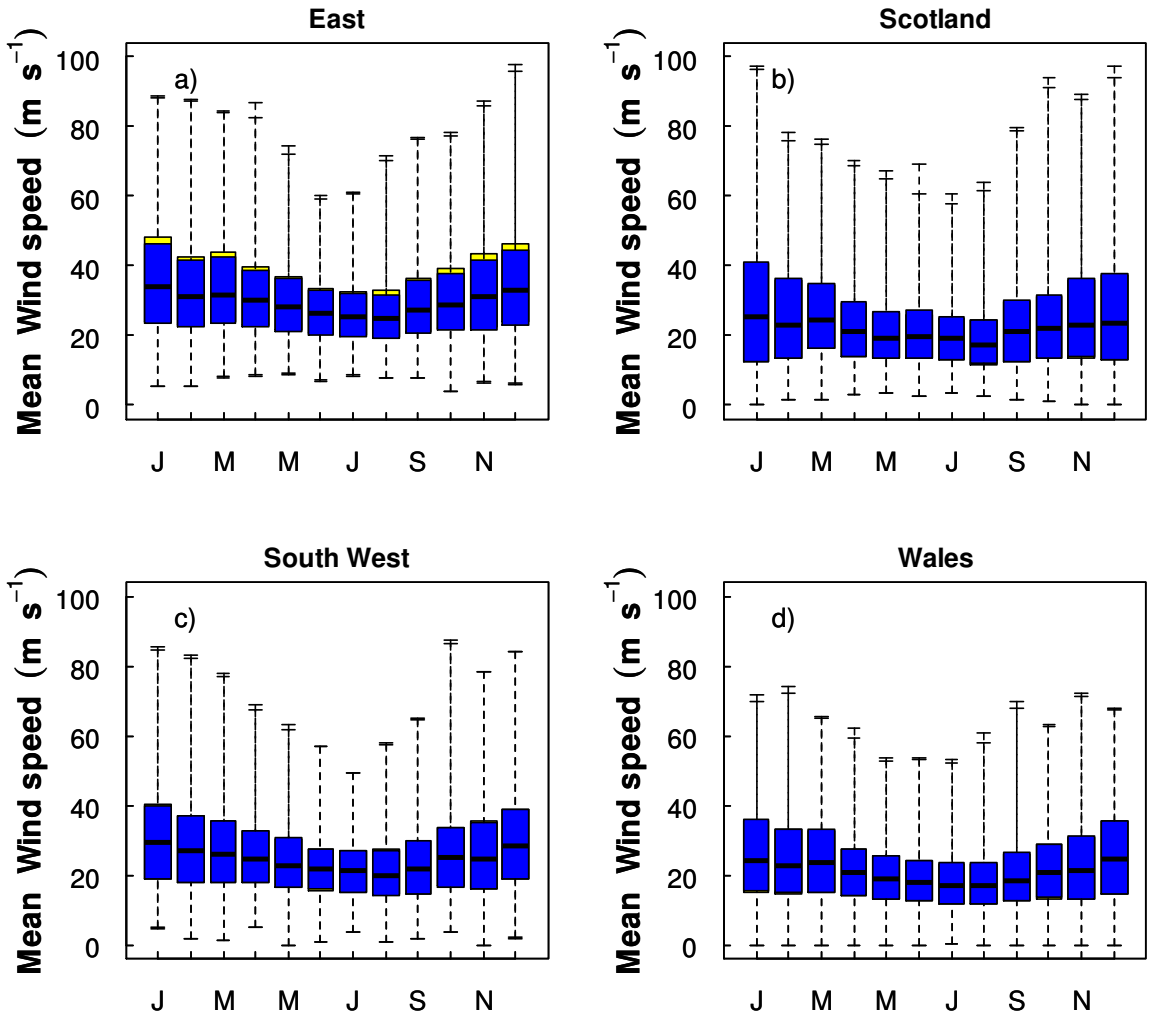

Fig. 6A-5. Wind speed. The thick horizontal line represents the median, the coloured box represents the middle 50% of the data, and the vertical bars represent the minimum and maximum value. Yellow = current climate, blue = changed climate.

8.2 Appendix 6B – Soil moisture content

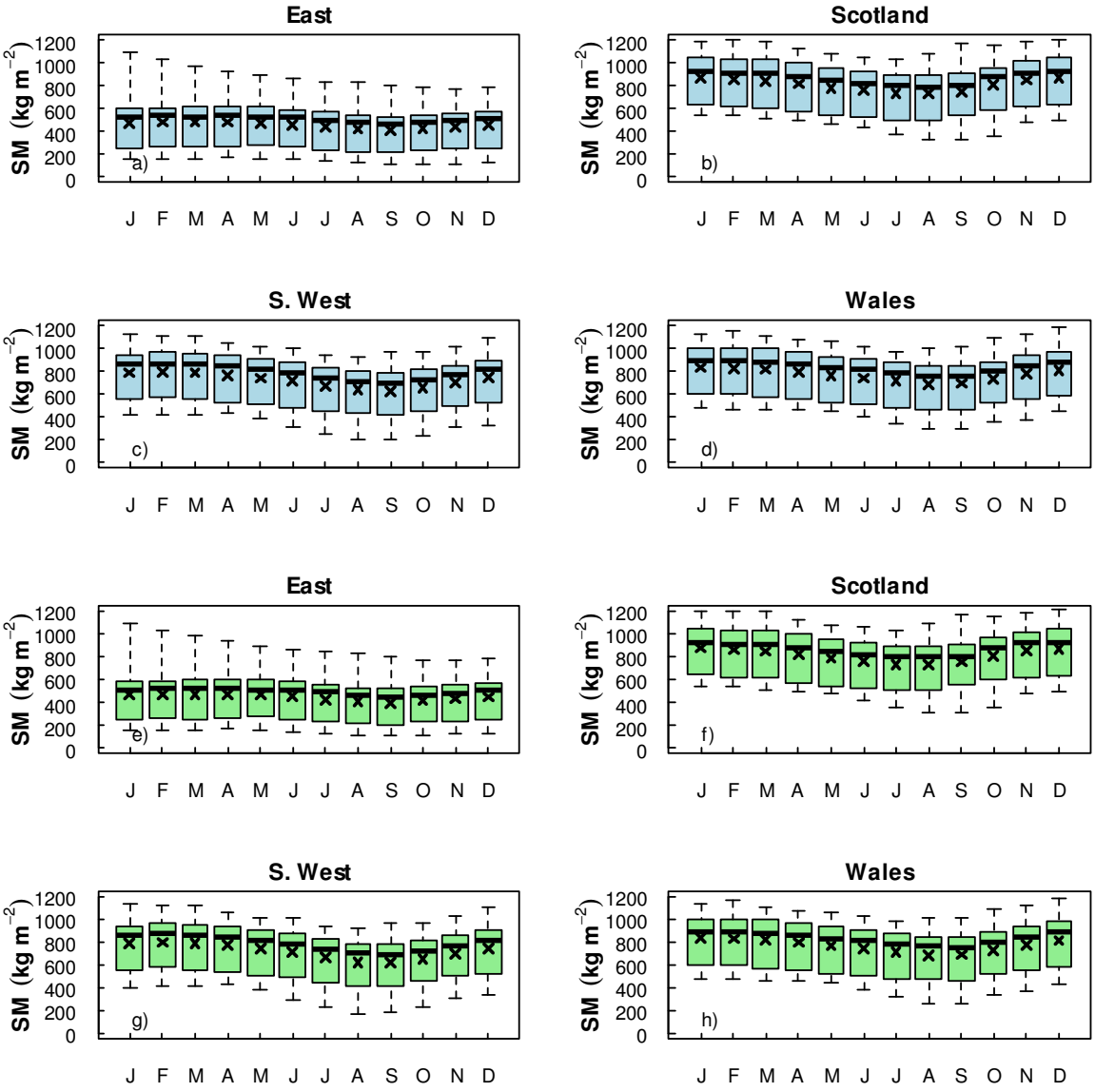

Fig. 6B-1 Mean monthly soil moisture content under elevated atmospheric CO_2. The thick horizontal line represents the median, the 'x' represents the mean, the coloured box represents the middle 50% of the data, and the vertical bars represent the minimum and maximum value. Panels a-d: *P. x euramericana* (lightblue), Panels e-h: *P. nigra* (green).

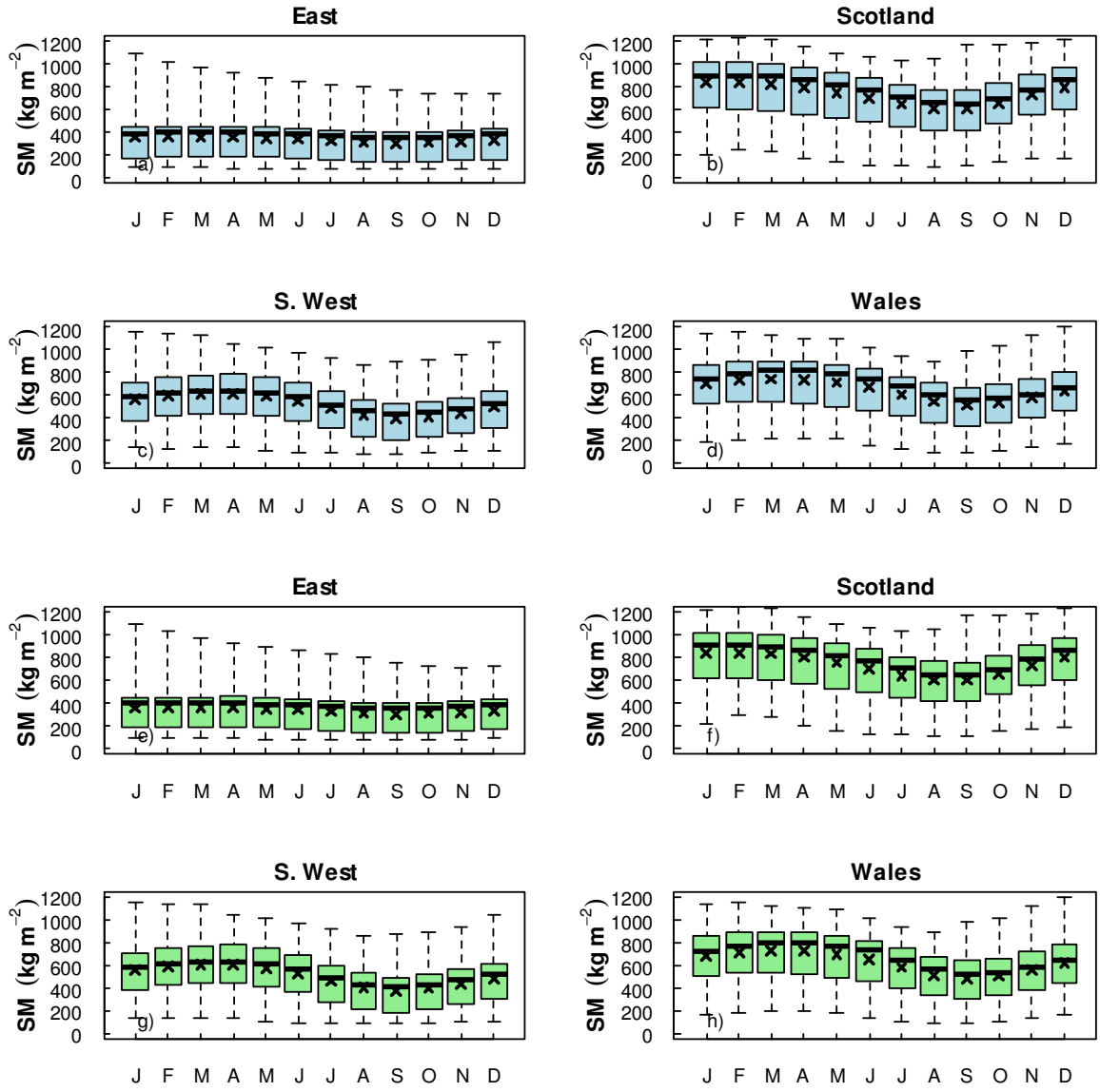

Fig. 6B-2. Mean monthly soil moisture content under a changed climate and ambient atmospheric CO_2. The thick horizontal line represents the median, the 'x' represents the mean, the coloured box represents the middle 50% of the data, and the vertical bars represent the minimum and maximum value. Panels a-d: *P. x euramericana* (lightblue), Panels e-h: *P. nigra* (green).

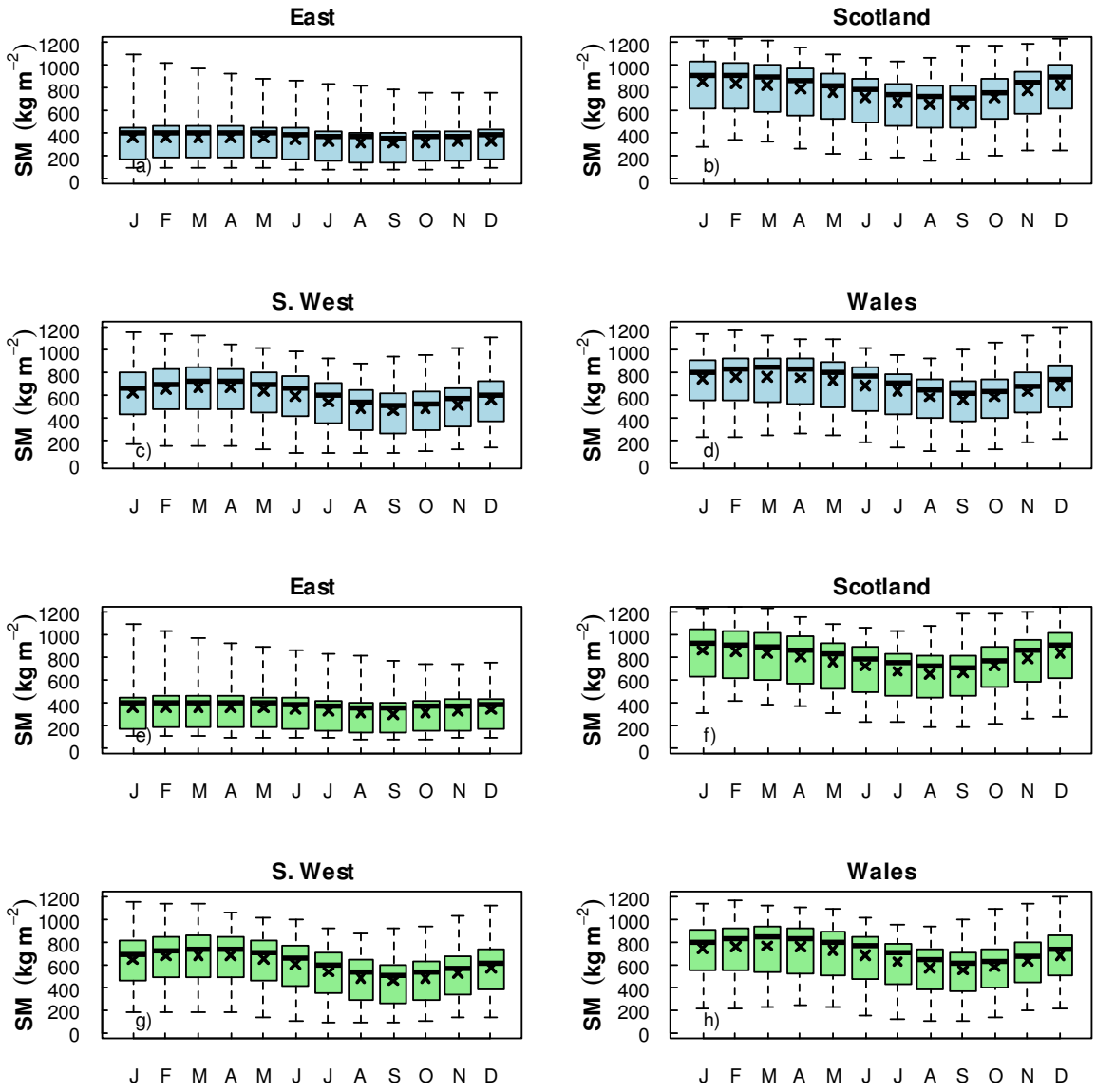

Fig. 6B-3. Mean monthly soil moisture content under a changed climate and elevated atmospheric CO_2 (future climate scenario). The thick horizontal line represents the median, the 'x' represents the mean, the coloured box represents the middle 50% of the data, and the vertical bars represent the minimum and maximum value. Panels a-d: *P. x euramericana* (lightblue), Panels e-h: *P. nigra* (green).

8.3 Appendix 6C – Statistical analysis: output tables

YIELD

Experiment 1: Current climate

yield~site+soil+genotype+site:soil+(1|block)+(1|year)

	x^2	*p*	*n*
site:soil	0.77	0.99	240
genotype	32.46	<0.05	240
soil	4.36	0.11	240
site	86.56	<0.05	240

Difference between sites

	P. x. euramericana			*P. nigra*		
	x^2	*p*	*n*	x^2	*p*	*n*
SWST 'v' WALE	42.85	<0.05	120	36.49	<0.05	120
WALE 'v' SCOT	3.2	0.07	120	2.49	0.11	120
SCOT 'v' EAST	30.16	<0.05	120	34.7	<0.05	120

Experiment 2: Elevated CO_2

yield~site+soil+genotype+co_2+co_2:site+co_2:genotype+site:soil+co_2:soil+(1|block)+(1|year)

	x^2	*p*	*n*
site:soil	0.97	0.99	480
co_2:genotype	3.27	0.07	480
co_2:site	48.3	<0.05	480
co_2:soil	0.53	0.77	480
co_2	*		480
genotype	89.7	<0.05	480
soil	0.95	0.08	480
site	*		

Difference between sites

	P. x. euramericana			*P. nigra*		
	x^2	*p*	*n*	x^2	*p*	*n*
SWST 'v' WALE	38.9	<0.05	120	36.1	<0.05	120
WALE 'v' SCOT	17.5	<0.05	120	7.8	<0.05	120
SCOT 'v' EAST	7.6	<0.05	120	15.5	<0.05	120

Experiment 3: Changed climate

yield~site+soil+genotype+climate+climate:site+climate:genotpye+site:soil+climate:soil+(1|block)+(1|year)

	x^2	*p*	*n*
site:soil	8.91	0.18	2640
climate:genotype	0.53	0.46	2640
climate:site	87.46	<0.05	2640

climate:soil	26.89	<0.05	2640
climate	*		
genotype	35.93	<0.05	2640
soil	*		
site	*		

Difference between sites

	P. x. euramericana			*P. nigra*		
	x^2	*p*	*n*	x^2	*p*	*n*
SWST 'v' WALE	4.05	<0.05	1200	10.54	<0.05	1200
WALE 'v' SCOT	0.49	0.48	1200	2.78	0.1	1200
SWST 'v' EAST	202.07	<0.05	1200	206.1	<0.05	1200

Experiment 4: Future climate

yield~site+soil+genotype+climate+co_2+site:soil+climate:site+climate:genotype+climate:soil+climate:co_2+(1|block)+(1|year)

	x^2	*p*	*n*
climate:co_2	8.31	<0.05	5280
site:soil	6.95	0.22	5280
climate:genotype	0.36	0.55	5280
climate:site	105.4	<0.05	5280
climate:soil	0.42	0.81	5280
climate	*		
genotype	62.1	<0.05	5280
soil	5.13	0.31	5280
site	*		
co_2	*		

Difference between sites

	P. x. euramericana			*P. nigra*		
	x^2	*p*	*n*	x^2	*p*	*n*
SWST 'v' WALE	13.99	<0.05	1200	13.39	<0.05	1200
WALE 'v' SCOT	2.68	0.1	1200	2.58	0.11	1200
SCOT/WALE 'v' EAST	209.61	<0.05	1200	241.4	<0.05	1200

Table 6C-1. Output table of the mixed-effects models used to analyse the response of yield in each modelling experiment in Chapter 6. * Indicates that a value is not reported because it is involved in a significant interaction. Please see the main text for an explanation of the statistical method and the notation used in the statistical models.

TRANSPIRATION

Experiment 1: Current climate

transpiration~site+soil+genotype+site:soil+(1|block)+(1|year)

	x^2	*p*	*n*
site:soil	0.58	1.01	720
genotype	53.17	<0.05	720
soil	5.26	0.08	720
site	100.27	<0.05	720

Difference between sites

	P. x. euramericana			*P. nigra*		
	x^2	*p*	*n*	x^2	*p*	*n*
SWST 'v' WALE	53.54	<0.05	360	49.21	<0.05	360
WALE 'v' SCOT	3.63	0.06	360	2.25	0.08	360
WALE/SCOT 'v' EAST	0.16	0.69	360	15.74	<0.05	360

Experiment 2: Elevated CO_2

transpiration~site+soil+genotype+co_2+co_2:site+co_2:genotype+site:soil+co_2:soil +(1|block)+(1|year)

	x^2	*p*	*n*
site:soil	1.17	0.98	1440
co_2:genotype	2.4	0.86	1440
co_2:site	65.21	<0.05	1440
co_2:soil	0.83	0.66	1440
co_2	*		
genotype	116.28	<0.05	1440
soil	1.72	0.96	1440
site	*		

Difference between sites

	P. x. euramericana			*P. nigra*		
	x^2	*p*	*n*	x^2	*p*	*n*
SWST 'v' EAST	37.33	<0.05	360	37.03	<0.05	360
EAST 'v' WALE	15.54	<0.05	360	7.11	<0.05	360
SCOT 'v' WALE	4.47	<0.05	360	4.08	<0.05	360

Experiment 3: Changed climate

transpiration~site+soil+genotype+climate+climate:site+climate:genotype+site: soil+climate:soil+(1|block)+(1|year)

	x^2	*p*	*n*
site:soil	2.24	0.9	7920
climate:genotype	0.09	0.77	7920
climate:site	30.23	<0.05	7920
climate:soil	0.18	0.92	7920
climate	*		

genotype	49.28	<0.05	7920
soil	6.67	<0.05	7920
site	*		

Difference between sites

	P. x. euramericana			*P. nigra*		
	x^2	*p*	*n*	x^2	*p*	*n*
SWST 'v' WALE	10.74	<0.05	3600	8.87	<0.05	3600
WALE 'v' SCOT	0.07	<0.05	3600	0.34	0.56	3600
SCOT/WALE 'v' EAST	150.86	<0.05	3600	169.6	<0.05	3600

Experiment 4: Future climate

transpiration~site+soil+genotype+climate+co_2+site:soil+climate:site+climate:genotype+climate:soil+climate:co_2+(1|block)+(1|year)

	x^2	*p*	*n*
climate:co_2	0.18	0.67	15840
site:soil	2.37	0.88	15840
climate:genotype	0.21	0.65	15840
climate:site	38.86	<0.05	15840
climate:soil	0.17	0.92	15840
climate	*		15840
genotype	88.21	<0.05	15840
soil	5.52	0.065	15840
site	*		15840
co_2	107.88	<0.05	15840

Difference between sites

	P. x. euramericana			*P. nigra*		
	x^2	*p*	*n*	x^2	*p*	*n*
SWST 'v' WALE	38.86	<0.05	3600	42.42	<0.05	3600
WALE 'v' SCOT	2.83	0.09	3600	2.2	0.14	3600
SCOT/WALE 'v' EAST	106.52	<0.05	3600	123.2	<0.05	3600

Table 6C-2. Output table of the mixed-effects models used to analyse the response of transpiration in each modelling experiment. * Indicates that a value is not reported because it is involved in a significant interaction. Please see the main text for an explanation of the statistical method and the notation used in the statistical models.

Glossary

a_{wl}	Allometric coefficient relating the target woody biomass to the *LAI*	(kg C m^{-2})
a_{ws}	Relates the woody biomass to the live stem biomass	
A_{max}	Maximum photosynthetic rate	(µmol CO_2 m^{-2} s^{-1})
A_{net}	Net photosynthesis	(µmol CO_2 m^{-2} s^{-1})
A_{sat}	Light-saturated photosynthesis	(µmol CO_2 m^{-2} s^{-1})
b_{wl}	Allometric exponent relating the target woody biomass to the *LAI*	
C_{dry}	Dry soil heat capacity	(J m^{-3} K^{-1})
C_v	Total carbon content of the vegetation	(kg C m^{-2})
c_a	Atmospheric CO_2 concentration	(Pa)
c_c	Chloroplastic CO_2 concentration	(Pa)
c_i	Intercellular CO_2 concentration	(Pa)
c_p	Specific heat capacity of air	(J kg^{-1} K^{-1})
D_c	The critical humidity deficit	(kg kg^{-1})
D_Q	The humidity deficit at the leaf surface	(kg kg^{-1})
E	Total evaporation	(kg m^{-2} s^{-1})
F_0	The c_i/c_a for specific humidity deficit in canopy	
F_v/F_m	The maximum potential quantum efficiency of PSII	
G	Ground heat flux	(W m^{-2})
GPP	Gross primary productivity	(kg C m^{-2} s^{-1})
g_c	Canopy conductance	(m s^{-1})
g_i	Internal CO_2 conductance	(µmol CO_2 m^{-2} s^{-1} Pa^{-1})
g_s	Stomatal conductance	(m s^{-1}; mmol m^{-2} s^{-1})
H	Sensible heat flux	(W m^{-2})
h	Canopy height	(m)
ha	Hectares	
I_{par}	Incident photosynthetically active radiation	(µmol m^{-2} s^{-1})
J	The rate of electron transport dependent on irradiance	(µmol e^- m^{-2} s^{-1})
J_{max}	The maximum rate of electron transport	(µmol e^- m^{-2} s^{-1})
k	PAR extinction coefficient	
K_c	Michaelis-Menton constants for CO_2	(Pa)
K_o	Michaelis-Menton constants for O_2	(kPa)
k_s	Hydraulic conductivity at saturation	(kg m^{-2} s^{-1})
L	Carbon content of leaves	(kg C m^{-2})
LAI	Leaf area index	(m^2 m^{-2})
L_b	Balanced *LAI*	(m^2 m^{-2})
L_w	Downward long-wave radiation	(W m^{-2})
N_r	Nitrogen content of the roots	(kg N kg C^{-1})
N_s	Nitrogen content of the stem	(kg N kg C^{-1})
N_l	Nitrogen content of the leaves	(kg N kg C^{-1})
NPP	Net primary productivity	(kg C m^{-2} s^{-1})
O_2	Oxygen	
O_a	Partial pressure of atmospheric oxygen	(kPa)
P_{PFD}	Photosynthetic photon flux density	(µmol m^{-2} s^{-1})
q_*^s	Saturated specific humidity at the surface	(kg kg^{-1})
q_1	Unsaturated specific humidity at the reference level	(kg kg^{-1})
R	Carbon content of roots	(kg C m^{-2})

R_d	Dark respiration	(μmol CO_2 m^{-2} s^{-1})
R_{dc}	Canopy dark respiration	(μmol CO_2 m^{-2} s^{-1})
R_n	Net radiation	(W m^{-2})
R_p	Total autotrophic (plant) respiration	(kg C m^{-2} s^{-1})
r_a	Aerodynamic resistance	(m s^{-1})
r_g	Growth respiration factor	
r_s	Stomatal resistance	(m s^{-1})
S	Respiring stem carbon	
S_w	Insolation (direct and diffuse)	(W m^{-2})
T_*	Land surface temperature	(K)
T_l	Leaf surface temperature	(K)
T_1	Reference level temperature	(K)
T_{s1}	Top soil layer temperature	(K)
TPU	Triose-phosphate use limitation	(μmol CO_2 m^{-2} s^{-1})
V_{max}	The maximum rate of carboxylation of Rubisco	(μmol CO_2 m^{-2} s^{-1})
VPD	Vapour pressure deficit	(kPa)
W	Carbon content of stem	(kg C m^{-2})
W_c	Canopy photosynthesis	(μmol CO_2 m^{-2} s^{-1})
W_{carb}	The rate of CO_2 is limited gross photosynthesis	(μmol CO_2 m^{-2} s^{-1})
W_{carbc}	The rate of CO_2 is limited gross photosynthesis determined at c_c	(μmol CO_2 m^{-2} s^{-1})
$W_{\exp}$	The rate of photosynthesis limitation associated with transport of the photosynthetic products	(μmol CO_2 m^{-2} s^{-1})
W_{lite}	The rate of light-limited gross photosynthesis	(μmol CO_2 m^{-2} s^{-1})
W_{litec}	The rate of light-limited gross photosynthesis determined at c_c	(μmol CO_2 m^{-2} s^{-1})
z_{om}	Roughness length for momentum	
α_{app}	The apparent quantum efficiency	(mol e^- mol^{-1} quanta)
α_{int}	The intrinsic quantum efficiency	(mol CO_2 mol^{-1} quanta)
Θ	Curvature factor	
λE	Latent heat flux	(W m^{-2})
α	Surface albedo	
ε	Emissivity of the surface	
σ	The Stefan-Boltzmann constant	
ρ	Air density	(kg m^{-3})
Δz	Thickness of the top soil layer	
σ_l	Specific density of leaf carbon	(kg C m^{-2} $LA\Gamma^{1}$)
η_{sl}	Live stemwood coefficient	(kg C m^{-2})
$1/(n\text{-}1)$	Exponent used in the van Genuchten model	
$1/\alpha$	A parameter of the van Genuchten model	
θ_{sat}	Volumetric soil moisture content at saturation	(m^3 m^{-3})
θ_{crit}	Volumetric soil moisture concentration at the critical point	(m^3 m^{-3})
θ_{wilt}	Volumetric soil moisture concentration at the wilting point	(m^3 m^{-3})
λ_{dry}	Dry soil thermal conductivity	(W m^{-1} K^{-1})
β	Soil moisture stress factor	
Γ	CO_2 photorespiration compensation point	(Pa)
Γ^*	Chloroplastic CO_2 photorespiration compensation point	(Pa)
ω	Leaf scattering coefficient for I_{PAR}	
τ	The Rubisco specificity factor for CO_2 relative to O_2	
ΔH_a	Enthalpy of activation	

ΔH_d	Enthalpy of deactivation
ΔS	Entropy

References

Ainsworth E. & Long S. (2005) What have we learned from 15 years of free-air CO_2 enrichment (FACE)? A mete-analytic review of the responses of photosynthesis, canopy properties and plant production to rising CO2. *New Phytologist*, **165**, 351-372.

Ainsworth E.A., Davey P.A., Hymus G.J., Osborne C.P., Rogers A., Blum H., Nosberger J. & Long S.P. (2003) Is stimulation of leaf photosynthesis by elevated carbon dioxide concentration maintained in the long term? A test with *Lolium perenne* grown for 10 years at two nitrogen fertilization levels under Free Air CO_2 Enrichment (FACE). *Plant, Cell and Environment*, **26**, 705-714.

Ainsworth E.A. & Rogers A. (2007) The response of photosynthesis and stomatal conductance to rising [CO_2]: mechanisms and environmental interactions. *Plant Cell and Environment*, **30**, 258-270.

Andersen R.S., Towers W. & Smith P. (2005) Assessing the potential for biomass energy to contribute to Scotland's renewable energy needs. *Biomass and Bioenergy*, **29**, 73-82.

Anderson R.S., Towers W. & Smith P. (2005) Assessing the potential for biomass energy to contribute to Scotland's renewable energy needs. *Biomass and Bioenergy*, **29**, 73-82.

Ångström A. (1918) A study of the radiation of the atmosphere. *Smithsonian Institute miscellaneous collection.*, **65**, 159-161.

Arp W.J. (1991) Effects of source-sink relations on photosynthetic acclimation to elevated CO_2. *Plant, Cell & Environment*, **14**, 869-875.

Aylott M.J., Casella E., Tubby I., Street N.R., Smith P. & Taylor G. (2008) Yield and spatial supply of bioenergy poplar and willow short-rotation coppice in the UK. *New Phytologist*, **178**, 358-370.

Baker J.T., Allen L.H.J., Boote K.J. & Pickering N.B. (1997) Rice responses to drought under carbon dioxide enrichment. 1. Growth and yield. *Global Change Biology*, **3**, 119-128.

Bates D. & Maechler M. (2009) *lme4*: Linear mixed-effects models using S4 classes. R package version 0.999375-32. (ed http://CRAN.R-project.org/package=lme4).

Bates J., Edberg O. & Nuttall C. (2009) Minimising greenhouse gas emissions from biomass energy generation. *Environment Agency*.

Beerling D.J., Heath J., Woodward F.I. & Mansfield T.A. (1996) Drought and CO_2 interactions in trees observations and mechanisms. *New Phytologist*, **134**, 235-242.

Bernacchi C., Portis A.R., Nakano H., von Caemmerer S. & Long S.P. (2002) Temperature response of mesophyll conductance. Implications for the determination of Rubisco enzyme kinetics and for limitations to photosynthesis *in vivo*. *Plant Physiology*, **130**, 1992-1998.

Bernacchi C.J., Calfapietra C., Davey P.A., Wittig V.E., Scarascia-Mugnozza G.E., Raines C.A. & Long S.P. (2003) Photosynthesis and stomatal conductance responses of poplars to free-air CO_2 enrichment (PopFACE) during the first growth cycle and immediately following coppice. *New Phytologist*, **159**, 609-621.

Bernacchi C.J., Singsaas E.L., Pimentel C., A. R. Portis J. & Long S.P. (2001) Improved temperature response functions for models of Rubisco-limited photosynthesis. *Plant, Cell & Environment*, **24**, 253-259.

Berndes G., Hoogwijk M. & Broek R. (2003) The contribution of biomass in the future global energy supply: a review of 17 studies. *Biomass and Bioenergy*, **25**, 1-28.

Bown H.E., Watt M.S., Mason E.G., Clinton P.W. & Whitehead D. (2009) The influence of nitrogen and phosphorus supply and genotype on mesophyll conductance limitations to photosynthesis in *Pinus radiata*. *Tree Physiology*.

Boyer J.S., Wong S.C. & Farquhar G.D. (1997) CO_2 and water vapour exchange across leaf cuticle (epidermis) at various water potentials. *Plant Physiology*, **114**, 185-191.

Buckley T.N., Farquhar G.D. & Mott K.A. (1997) Qualitative effects of patchy stomatal conductance distribution features on gas-exchange calculations. *Plant , Cell and Environment*, **20**, 867-880.

Bunn S.M., Rae A.M., Herberst C.S. & Taylor G. (2004) Leaf-level productivity traits in *Populus* grown in short rotation copice for biomass energy. *Forestry*, **77**, 307-323.

Calfapietra C., Gielen B., Galema A.N.J., Lukac M., De Angelis P., Moscatelli M.C., Ceulemans R. & Scarascia-Mugnozza G. (2003b) Free-air CO_2 enrichment (FACE) enhances biomass production in a short-rotation poplar plantation. *Tree Physiology*, **23**, 805-814.

Calfapietra C., Gielen B., Sabatti M., De Angelis P., Miglietta F., Scarascia-Mugnozza G. & Ceulemans R. (2003a) Do above-ground growth dynamics of poplar change with time under CO_2 enrichment? *New Phytologist*, **160**, 305-318.

Calfapietra C., Gielen B., Sabatti M., De Angelis P., Scarascia-Mugnozza G. & Ceulemans R. (2001) Growth performance of populus exposed to "Free Air Carbon dioxide Enrichment" during the first growing season in the POPFACE experiment. *Annals of Forest Science*, **58**, 819-828.

Calvet J.C., Noilhan J., Roujean J.L., Bessemoulin P., Cabelguenne M., Olioso A. & Wigneron J.P. (1998) An interactive vegetation SVAT model tested against data from six contrasting sites. *Agricultural and forest meteorology*, **92**, 73-95.

Cannell M.G.R. (2003) Carbon sequestration and biomass energy offset: theoretical, potential and achievable capacities globally, in Europe and the UK. *Biomass and Bioenergy*, **24**, 97-116.

Cech P.G., Pepin S. & Korner C. (2003) Elevated CO_2 reduces sap flux in mature deciduous forest trees. *Oecologia*, **137**, 258-268.

Centritto M., Lee H.S.J. & Jarvis P.G. (1999a) Interactive effects of elevated [CO_2] and drought on cherry (*Prunus avium*) seedlings I. Growth, whole-plant water use efficiency and water loss. *New Phytologist*, **141**, 129-140.

Centritto M., Loreto F. & Chartzoulakis K. (2003) The use of low CO_2 to estimate diffusional and non-diffusional limitations of photosynthetic capacity of salt-stressed olive saplings. *Plant, Cell & Environment*, **26**, 585-594.

Centritto M., Magnani F., Lee H.S.J. & Jarvis P.G. (1999b) Interactive effects of elevated [CO_2] and drought on cherry (*Prunus avium*) seedlings II. Photosynthetic capacity and water relations. *New Phytologist*, **141**, 141-153.

Ceulemans R. & Mousseau M. (1994) Effects of elevated atmospheric CO_2 on woody plants. *New Phytologist*, **127**.

Challinor A.J., Ewert F., Arnold S., Simelton E. & Fraser E. (2009) Crops and climate change: progress, trends, and challenges in simulating impacts and informing adaptation. *Journal of Experimental Botany*, **60**, 2775-2789.

Chaves M., M. (1991) Effects of water deficits on carbon assimilation. *Journal of Experimental Botany*, **42**, 1-16.

Chaves M.M., Maroco J.P. & Pereira J.S. (2003) Understanding plant responses to drought - from gene to whole plant. *Functional Plant Biology*, **30**, 239-264.

Chaves M.M., Pereira J.S., Maroco J., Rodrigues M.L., Ricardo C.P.P., Osorio M.L., Carvalho I., Faria T. & Pinheiro C. (2002) How plants cope with water stress in the field? Photosynthesis and growth. *Annals Botany*, **89**, 907-916.

Clifton-Brown J.C. & Lewandowski I. (2000) Water use efficiency and biomass partitioning of three different *Miscanthus* genotypes with limited and unlimited water supply. *Annals Botany*, **86**, 191-200.

Clifton-Brown J.C., Lewandowski I. & Jones M.B. (2002) Comparative responses to water stress in stay-green, rapid- and slow senescing genotypes of the biomass crop, *Miscanthus*. *New Phytologist*, **154**, 335-345.

Collatz G.J., Ball J.T., Grivet C. & Berry J.A. (1991) Physiological and environmental regulation of stomatal conductance, photosynthesis and transpiration: A model that includes a laminar boundary layer. *Agricultural and Forest Meteorology*, **54**, 107-136.

Collatz G.J., Ribas-Carbo M. & Berry J.A. (1992) A coupleed photosynthesis-stomatal conductance model for leaves of C_4 plants. *Australian Journal of Plant Physiology*, **19**, 519-538.

Conley M.M., Kimball B.A., Brooks T.J., Pinter P.J., Hunsaker D.J., Wall G.W., Adam N.R., LaMorte R.L., Matthias A.D., Thompson T.L., Leavitt S.W., Ottman M.J., Cousins A.B. & Triggs J.M. (2001) CO_2 enrichment increases water-use efficiency in sorghum. *New Phytologist*, **151**, 407-412.

Cousins A.B., Adam N.R., Wall G.W., Kimball B.A., Pinter P.J., Leavitt S.W., LaMorte R.L., Matthias A.D., Ottman M.J., Thompson T.L. & Webber A.N. (2001) Reduced photorespiration and increased energy-use efficiency in young CO2-enriched sorghum leaves. *New Phytologist*, **150**, 275-284.

Cowley J.P. (1978) The distribution over Great Britain of global solar radiation on a horizontal surface. *Meteorological Magazine.*, **107**, 357-372.

Cox P.M. (2001) Description of the TRIFFID dynamic global vegetation model. *Hadley Centre technical note 24*.

Cox P.M., Huntingford C. & Harding R.J. (1998) A canopy conductance and phtosynthesis model for use in a GCM land surface scheme. *Journal of Hydrology*, **212-213**, 79-94.

Crookshanks M., Taylor G. & Broadmeadow M. (1998) Elevated CO_2 and tree growth: contrasting responses in *Fraxinus excelsior*, *Quercus petraea* and *Pinus sylvestris*. *New Phytologist*, **138**, 241-250.

Curtis P.S. & Wang X. (1998) A meta-analysis of elevated CO_2 effects on woody plant mass, form, and physiology. *Oecologia*, **113**, 299-313.

Dai Z.Y., Ku M.S.B. & Edwards G.E. (1995) C4 photosynthesis. The effects of leaf development on the CO2-concentrating mechanism and photorespiration in maize. *Plant Physiology*, **107**, 815-825.

Davey P.A., Olcer H., Zakhleniuk O., Bernacchi C.J., Calfapietra C., Long S.P. & Raines C.A. (2006) Can fast-growing plantation trees escape biochemical down-regulation of photosynthesis when grown throughout their complete production cycle in the open air under elevated carbon dioxide? *Plant , Cell and Environment*, **29**, 1235-1244.

DECC (2009a) The UK Low Carbon Transition Plan: National strategy for climate and energy *HM Government*.

DECC (2009b) The UK Renewable Energy Strategy. *HM Government*.

DEFRA (2001a) Planting and growing miscanthus: Best practice guidelines: For applicants to DEFRA's Energy Crops Scheme. (ed DEFRA). Department for Environment Food and Rural Affairs, London.

DEFRA (2001b) Growing short rotation coppice: Best practice guidelines: For applicants to DEFRA's Energy Crops Scheme (ed DEFRA). Department for Environment Food and Rural Affairs, London.

DEFRA (2007) UK Biomass Strategy (ed F.a.R.A. Department for Environment), London.

Dharssi I. (2010) New high resolution soil ancillaries for the Unified Model. *In preparation*.

Dilley A.C. & O'Brien D.M. (1998) Estimating downward clear sky long-wave irradiance at the surface from screen temperature and precipitable water. *Quarterly Journal of the Royal Meteorological Society.*, **124**, 1391-1401.

Drake B.G., Gonzalez-Meler M.A. & Long S.P. (1997) More efficient plants: A consequence of rising atmospheric CO_2? *Annual Review of Plant Physiology and Plant Molecular Biology*, **48**, 609-639.

DTI (2006) The government's response to the biomass task force report (eds DTI & DEFRA), London.

During H. (2003) Stomatal and mesophyll conductances control CO_2 transfer to chloroplasts in leaves of grapevine (*Vitis vinifera L.*). *Vitis*, **42**, 65-68.

Ellsworth D.S. (1999) CO_2 enrichment in a maturing pine forest: are CO_2 exchange and water status in the canopy affected? *Plant, Cell and Environment*, **22**, 461-472.

Enquist B.J., Brown J.H. & West G.B. (1998) Allometric scaling of plant energetics and population density. *Nature*, **395**, 163-165.

Essery R.L.H., Best M.J. & Cox P.M. (2001) MOSES 2.2 technical documentation. In: *Hadley Centre technical note 30*.

Ethier G.J. & Livingston N.J. (2004) On the need to incorporate sensitivity to CO_2 transfer conductance into the Farquhar-von Caemmerer-Berry leaf photosynthesis model. *Plant, Cell & Environment*, **27**, 137-153.

FAO/IIASA/ISRIC/ISS-CAS/JRC (2008) *Harmonised world soil database (version 1.0).* FAO

IIASA.

Faraway J., J. (2006) *Extending the linear model with R: generalized linear, mixed effects and nonparametric regression models*. Chapman & Hall.

Farquhar G.D., Von Caemmerer S. & Berry J.A. (1980) A biochemical model of photosynthetic CO_2 assimilation in leaves of C_3 species. *Planta*, **149**, 78-90.

Ferris R., Sabatti M., Miglietta F., Mills R.F. & Taylor G. (2001) Leaf area is stimulated in *Populus* by free air CO_2 enrichment (POPFACE), through increased cell expansion and production. *Plant, Cell and Environment*, **24**, 305-315.

Finch J.W., Hall R.L., Rosier P.T.W., Clark D.B., Stratford C., Davies H.N., Marsh T.J., Roberts J.M., Riche A. & Christian D. (2004) *The Hydrological Impacts of Energy Crop Production in the UK: Final report*. The Centre for Ecology and Hydrology for the Department of Trade and Industry.

Flexas J., Bota J., Cifre J., Escalona J.M., GalmeS J., GulÍas J., Lefi E.K., MartÍnez-Canellas S.F., Moreno M.T., Ribas-Carbo M., Riera D., Sampol B. & Medrano H. (2004b) Understanding down-regulation of photosynthesis under water stress: future prospects and searching for physiological tools for irrigation management. *Annals of Applied Biology*, **144**, 273-283.

Flexas J., Bota J., Galmes J., Medrano H. & Ribas-Carbo M. (2006) Keeping a positive carbon balance under adverse conditions: responses of photosynthesis and respiration to water stress. *Physiologia Plantarum*, **127**, 343-352.

Flexas J., Bota J., Loreto F., Cornic G. & Sharkey T.D. (2004a) Diffusive and metabolic limitations to photosynthesis under drought and salinity in C_3 plants. *Plant Biology*, **6**, 269-279.

Flexas J., Diaz-Espejo A., Galmes J., Kaldenhoff R., Medrano H. & Ribas-Carbo M. (2007) Rapid variations of mesophyll conductance in response to changes in CO_2 concentration around leaves. *Plant, Cell & Environment*, **30**, 1284-1298.

Flexas J., Escalona J.M., Sampol B. & Medrano H. (2002) Effects of drought on phtosynthesis in grapevines under field conditions: an evaluation of stomatal and mesophyll limitations. *Functional Plant Biology*, **29**, 461-471.

Flexas J., Ribas-Carbo M., Diaz-Espejo A., Galmes J. & Medrano H. (2008) Mesophyll conductance to CO_2: current knowledge and future prospects. *Plant, Cell & Environment*, **31**, 602-621.

Gallé A. & Feller U. (2007) Changes of photosynthetic traits in beech saplings (Fagus sylvatica) under severe drought stress and during recovery. *Physiologia Plantarum*, **131**, 412-421.

Gallé A., Haldimann P. & Feller U. (2007) Photosynthetic performance and water relations in young pubescent oak (*Quercus pubescens*) trees during drought stress and recovery. *New Phytologist*, **174**, 799-810.

Gedney N., Cox P.M., Bett R.A., Boucher O., Huntingford C. & Stott P.A. (2006) Detection of a direct carbon dioxide effect in continental river runoff records. *Nature*, **439**, 835-838.

Ghannoum O., Caemmerer S.V., Ziska L.H. & Conroy J.P. (2000) The growth response of C_4 plants to rising atmospheric CO_2 partial pressure: a reassessment. *Plant, Cell & Environment*, **23**, 931-942.

Ghannoum O., Siebke K., von Caemmerer S. & Conroy J.P. (1998) The photosynthesis of young *Panicum* C_4 leaves is not C_3-like. *Plant, Cell and Environment*, **21**, 1123-1131.

Gielen B., Calfapietra C., Lukac M., Wittig V.E., De Angelis P., Janssens I.A., Moscatelli M.C., Grego S., Cotrufo M.F., Godbold D.L., Hoosbeek M.R., Long S.P., Miglietta F., Polle A., Bernacchi C.J., Davey P.A., Ceulemans R. & Scarascia-Mugnozza G.E. (2005) Net carbon storage in a poplar plantation (POPFACE) after three years of free-air CO_2 enrichment. *Tree Physiology*, **25**, 1399-1408.

Gielen B., Calfapietra C., Sabatti M. & Ceulemans R. (2001) Leaf area dynamics in a closed poplar plantation under free-air carbon dioxide enrichment. *Tree Physiology*, **21**, 1245-1255.

Gielen B. & Ceulemans R. (2001) The likely impact of rising atmospheric CO_2 on natural and managed *Populus*: a literature review. *Environmental Pollution*, **115**, 335-358.

Gielen B., Liberloo M., Bogaert J., Calfapietra C., De Angelis P., Miglietta F., Scarascia-Mugnozza G. & Ceulemans R. (2003) Three years of free-air CO_2 enrichment (POPFACE) only slightly affect profiles of light and leaf characteristics in closed canopies of *Populus*. *Global Change Biology* **9**, 1022-1037.

Grassi G. & Magnani F. (2005) Stomatal, mesophyll conductance and biochemical limitations to photosynthesis as affected by drought and leaf ontogeny in ash and oak trees. *Plant, Cell & Environment*, **28**, 834-849.

Gregory S. (1976) *Regional climates*. Longman Group Ltd, New York.

Guan B.T. (2000) Effects of correlation among parameters on prediction quality of a process-based forest growth model. *Forest Science*, **46**, 269-276.

Gunderson C.A., Sholtis J.D., Wullschleger S.D., Tissue D.T., Hanson P.J. & Norby R.J. (2002) Environmental and stomatal control of photosynthetic enhancement in the canopy of a sweetgum (*Liquidambar styraciflua L.*) plantation during 3 years of CO_2 enrichment. *Plant, Cell and Environment*, **25**, 379-393.

Gunderson C.A. & Wullschleger S.D. (1994) Photosynthetic acclimation in trees to rising atmospheric CO_2: A broader perspective. *Photosynthesis Research*, **39**, 369-388.

Hall R.L. (2002) Aerodynamic resistance of coppiced poplar. *Agricultural and forest meteorology*, **114**, 83-102.

Hall R.L. & Allen S.J. (1997) Water use of poplar clones grown as short-rotation coppice at two sites in the United Kingdom. *Aspects of Applied Biology*, **49**, 163-171.

Hall R.L., Allen S.J., Rosier P.T., Smith D.M., Hodnett M.G., Roberts J.M., Hopkins R., Davies H.N., Kinniburgh D.G. & Gooddy D.C. (1996) *Hydrological Effects of Short Rotation Energy Coppice: Final Report to ETSU*. NERC / Institute of Hydrology.

Hall R.L., Allen S.J., Rosier P.T.W. & Hopkins R. (1998) Transpiration from coppiced poplar and willow measured using sap-flow methods. *Agricultural and Forest Meteorology*, **90**, 275-290.

Hansen E.A. (1988) Irrigating short rotation intensive culture hybrid poplars. *Biomass*, **16**, 237-250.

Harley P.C. & Sharkey T.D. (1991) An improved model of C_3 photosynthesis at high CO_2: reversed O_2 sensitivity explained by lack of glycerate reentry into the chloroplast. *Photosynthesis Research*, **27**, 169-178.

Harley P.C., Thomas R.B., Reynolds J.F. & Strain B.R. (1992) Modelling photosynthesis of cotton grown in elevated CO_2. *Plant , Cell and Environment*, **15**, 271-282.

Haughton A.J., Bond A.J., Lovett A.A., Dockerty T., Sunnenberg G., Clark S.J., Bohan D.A., Sage R.B., Mallott M.D., Mallott V.E., Cunningham M.D., Riche A.B., Shield I.F., Finch J.W., Turner M.M. & Karp A. (2009) A novel, integrated approach to assessing social, economic and environmental implications of chnaging rural land-use: a case study of perennial biomass crops. *Journal of Applied Ecology* **46**, 315-322.

Herrick J.D., Maherali H. & Thomas R.B. (2004) Reduced stomatal conductance in sweetgum (*Liquidambar styraciflua*) sustained over long-term CO_2 enrichment. *New Phytologist*, **162**, 387-396.

Herrick J.D. & Thomas R.B. (2001) No photosynthetic down-regulation in sweetgum trees (*Liquidambar styraciflua* L.) after three years of CO_2 enrichment at the Duke Forest FACE experiment. *Plant, Cell & Environment*, **24**, 53-64.

Hibbs D.E., Chan S.S., Castellano M. & Niu C.-H. (1995) Response of red alder seedlings to CO_2 enrichment and water stress. *New Phytologist*, **129**, 569-577.

Hikosaka K., Ishikawa K., Borjigidai A., Muller O. & Onoda Y. (2006) Temperature acclimation of photosynthesis: mechanisms involved in the changes in temperature dependence of photosynthetic rate. *Journal of Experimental Botany*, **57**, 291-302.

Hinckley T.M., Brooks J.R., Cermak J., Ceulemans R., Kucera J., Meinzer F.C. & Roberts D.A. (1994) Water flux in a hybrid poplar stand. *Tree Physiology*, **14**, 1005-1018.

Hough M.N. & Jones R.J.A. (1997) The United Kingdom Meteorological Office Rainfall and Evaporation Calculation System: MORECS version 2.0 - an overview. *Hydrology and Earth System Sciences*, **1**, 227-239.

Hovenden M.J. (2003) Photosynthesis of coppicing poplar clones in a free-air CO_2 enrichment (FACE) experiment in a short-rotation forest. *Functional Plant Biology*, **30**, 391-400.

Hughes J.K., Lloyd A.J., Huntingford C., Finch J.W. & Harding R.J. (2010) The impact of extensive planting of *Miscanthus* as an energy crop on future CO_2 atmospheric concentrations. *Global Change Biology Bioenergy*, **2**, 79-88.

Huxman T.E., Hamerlynck E.P., Moore B.D., Smith S.D., Jordan D.N., Zitzer S.F., Nowak R.S., Coleman J.S. & Seemann J.R. (1998) Photosynthetic down-regulation in Larrea tridentata exposed to elevated atmospheric CO_2: interaction with drought

under glasshouse and field (FACE) exposure. *Plant, Cell & Environment*, **21**, 1153-1161.

Ibrahim L., Proe M.F. & Cameron A.D. (1997) Main effects of nitrogen supply and drought stress upon whole-plant carbon allocation in poplar. *Canadian Journal of Forest Research*, **27**, 1413-1419.

IEA (2010) Sustainable production of second-generation biofuels: Potential and perspectives in major economies and developing countries. *International Energy Agency*.

IPCC-DDC (2009a) The SRES emissions scenarios. In: *Intergovernmental Panel on Climate Change Data Distribution Centre* (ed http://sedac.ciesin.columbia.edu/ddc/sres/).

IPCC-DDC (2009b) Carbon Dioxide: Projected emissions and concentrations (ed http://www.ipcc-data.org/ddc_co2.html).

IPCC-TGICA (2007) *General Guidelines on the Use of Scenario Data for Climate Impact and Adaptation Assessment. Version 2.*

IPCC (2007) *Climate change 2007 - The physical science basis. Contribution of working group I to the fourth assessment report of the Intergovernmental Panel on Climate Change (IPCC)*. Cambridge University Press, Cambridge, United Kingdom and New York, NY, USA.

Iqbal M. (1983) *An introduction to solar radiation.*

Jacobs C. (1994) *Direct impact of atmospheric CO_2 enrichment on regional transpiration*, Wageningen Agricultural University.

Jenkins G.J., Murphy J.M., Sexton D.M.H., Lowe J.A., Jones P. & Kilsby C.G. (2009) UK Climate Projections: Briefing report. *Met Office Hadley Centre, Exeter, UK.*

Johnson J.D., Tognetti R. & Paris P. (2002) Water relations and gas exchange in poplar and willow under water stress and elevated atmospheric CO_2. *Physiologia Plantarum*, **115**, 93-100.

Jones H.G. (1992) *Plants and Microclimate: A quantitative approach to environmental plant physiology*. (2nd ed.). Cambridge University Press.

Kao W.Y. & Forseth I.N. (1992) Diurnal leaf movement, chlorophyll fluorescence and carbon assimilation in soy-bean grown under different nitrogen and water availabilities. *Plant , Cell and Environment*, **15**, 703-710.

Karnosky D.F., Zak D.R., Pregitzer K.S., Awmack C.S., Bockheim J.G., Dickson R.E., Hendrey G.R., Host G.E., King J.S., Kopper B.J., Kruger E.L., Kubiske M.E., Lindroth R.L., Mattson W.J., McDonald E.P., Noormets A., Oksanen E., Parsons W.F.J., Percy K.E., Podila G.K., Riemenschneider D.E., Sharma P., Thakur R., Sober A., Sober J., Jones W.S., Anttonen S., Vapaavuori E., Mankovska B., Heilman W. & Isebrands J.G. (2003) Tropospheric O_3 moderates responses of temperate hardwood forests to elevated CO_2: a synthesis of molecular to ecosystem results from the Aspen FACE project. *Functional Ecology*, **17**, 289-304.

Karp A. & Shield I. (2008) Bioenergy from plants and the sustainable yield challenge. *New Phytologist*, **179**, 1-18.

Keller V., Young A.R., Morris D.G. & Davies H. (2006) *Task 1.1: Estimation of precipitation inputs.* Centre for Ecology and Hydrology.

Kimball B.A., Idso S.B. & Aase J.K. (1982) A model of thermal radiation from partly cloudy and overcast skies. *Water Resources Research.*, **18**, 931-936.

Knutti R. (2008) Should we believe model predictions of future climate change? *Philosophical Transactions of the Royal Society A*, **366**, 4647-4664.

Körner C. (2006) Plant CO_2 responses: an issue of definition, time and resource supply. *New Phytologist*, **172**, 393-411.

Körner C., Asshoff R., Bignucolo O., Hattenschwiler S., Keel S.G., Pelaez-Riedl S., Pepin S., Siegwolf R.T.W. & Zotz G. (2005) Carbon Flux and Growth in Mature Deciduous Forest Trees Exposed to Elevated CO_2. *Science*, **309**, 1360-1362.

Körner C., Morgan J.A. & Norby R.J. (2007) CO_2 fertilization: when, where, how much? In: *Terrestrial ecosystems in a changing world* (eds J.G. Canadell, D.E. Pataki, & L.F. Pitelka), pp. 9-22. Springer, Berlin.

Laisk A., Oja V., Rasulov B., Ramma H., Eichelmann H., Kasparova I., Pettai H., Padu E. & Vapaavuori E. (2002) A computer-operated routine of gas exchange and optical measurements to diagnose photosynthetic apparatus in leaves. *Plant , Cell and Environment*, **25**, 923-943.

Lambers H., Chapin III F.S. & Pons T.L. (2008) *Plant Physiological Ecology*. (Second ed.). Springer, New York.

Lange O.L. (1971) Responses of stomata to changes in humidity. *Planta*, **100**, 76-86.

Lawlor D.W. (2002) Limitation to photosynthesis in water-stressed leaves: stomata vs. metabolism and the role of ATP. *Ann Bot*, **89**, 871-885.

Lawlor D.W. & Cornic G. (2002) Photosynthetic carbon assimilation and associated metabolism in relation to water deficits in higher plants. *Plant , Cell and Environment*, **25**, 275-294.

Leakey A.D.B., Bernacchi C.J., Dohleman F.G., Ort D.R. & Long S.P. (2004) Will photosynthesis of maize (*Zea mays*) in the US Corn Belt increase in future [CO_2] rich atmospheres? An analysis of diurnal courses of CO_2 uptake under free-air concentration enrichment (FACE). *Global Change Biology*, **10**, 951-962.

Leakey A.D.B., Uribelarrea M., Ainsworth E.A., Naidu S.L., Rogers A., Ort D.R. & Long S.P. (2006) Photosynthesis, Productivity, and Yield of Maize Are Not Affected by Open-Air Elevation of CO_2 Concentration in the Absence of Drought. *Plant Physiol.*, **140**, 779-790.

Lee T.D., Tjoelker M.G., Ellsworth D.S. & Reich P.B. (2001) Leaf gas exchange responses of 13 prairie grassland species to elevated CO_2 and increased nitrogen supply. *New Phytologist*, **150**, 405-418.

Leuzinger S. & Körner C. (2007) Water savings in mature deciduous forest trees under elevated CO_2. *Global Change Biology*, **13**, 2498-2508.

Leuzinger S., Zotz G., Asshoff R. & Körner C. (2005) Responses of deciduous forest trees to severe drought in Central Europe. *Tree Physiology*, **25**, 641-650.

Liberloo M., Calfapietra C., Lukac M., Godbold D., Luos Z., Polles A., Hoosbeek M.R., Kull O., Marek M., Raines C., Rubino M., Taylor G., Scarascia-Mugnozza G. & Ceulemans R. (2006) Woody biomass production during the second rotation of a bio-energy *Populus* plantation increases in a future high CO_2 world. *Global Change Biology*, **12**, 1094-1106.

Liberloo M., Dillen S.Y., Calfapietra C., Marinari S., Luo Z.B., De Angelis P. & Ceulemans R. (2005) Elevated CO_2 concentration, fertilization and their interaction: growth stimulation in a short-rotation poplar coppice (EUROFACE). *Tree Physiology*, **25**, 179-189.

Liberloo M., Gielen B., Calfapietra C., Veys C., Pigliacelli R., Scarascia-Mugnozza G. & Ceulemans R. (2004) Growth of a poplar short rotation coppice under elevated atmoshperic CO_2 concentrations (EUROFACE) depends on fertilization and species. *Annals of Forest Science*, **61**, 299-307.

Liberloo M., Tulva I., Raim O., Kull O. & Ceulemans R. (2006a) Photosynthetic stimulation under long-term CO_2 enrichment and fertilization is sustained across a closed *Populus* canopy profile (EUROFACE). *New Phytologist*, **173**, 537-549.

Linderson M., Iritz Z. & Lindroth A. (2007) The effect of water availability on stand-level productivity, transpiration, water use efficicency and radiation use efficiency of field-grown willow clones. *Biomass and Bioenergy*, **31**, 460-468.

Lindroth A. & Cienciala E. (1996) Water-use efficiency of short rotation Salix viminalis at leaf, tree and stand scales. *Tree Physiology*, **16**, 257-262.

Lindroth A., Verwijst T. & Halldin S. (1994) Water-use efficiency of willow: variation with season, humidity and biomass allocation. *Journal of Hydrology*, **156**, 1-19.

Long S.P., Ainsworth E.A., Leakey A.D.B., Nosberger J. & Ort D.R. (2006) Food for Thought: Lower-Than-Expected Crop Yield Stimulation with Rising CO_2 Concentrations. *Science*, **312**, 1918-1921.

Long S.P., Ainsworth E.A., Rogers A. & Ort D., R. (2004) Rising atmospheric carbon dioxide: plants FACE the future. *Annual reveiw of plant biology*, **55**, 591-628.

Long S.P. & Bernacchi C.J. (2003) Gas exchange measurements, what can they tell us about the underlying limitations to photosynthesis? Procedures and sources of error. *J. Exp. Bot.*, **54**, 2393-2401.

Long S.P., Postl W.F. & Bolhar-Noedenkampf H.R. (1993) Quantum yields for uptake of carbon dioxide in C_3 vascular plants of contrasting habitats and taxonomic groupings. *Planta*, **189**, 226-234.

Lukac M., Calfapietra C. & Godbold D.L. (2003) Production, turnover and mycorrhizal colonization of root systems of three *Populus* species grown under elevated CO_2 (POPFACE). *Global Change Biology*, **9**, 838-848.

Luo Z.-B., Calfapietra C., Liberloo M., Scarascia-Mugnozza G. & Polle A. (2006) Carbon partitioning to mobile and structural fractions in poplar wood under elevated CO_2 (EUROFACE) and N fertilization. *Global Change Biology*, **12**, 272-283.

Manter D.K. & Kerrigan J. (2004) A/C_i curve analysis across a range of woody plant species: influence of regression analysis parameters and mesophyll conductance. *J. Exp. Bot.*, **55**, 2581-2588.

Maxwell K. & Johnson G.N. (2000) Chlorophyll fluorescence--a practical guide. *J. Exp. Bot.*, **51**, 659-668.

Medlyn B.E., Badeck F.W., De Pury D.G.G., Barton C.V.M., Broadmeadow M., Ceulemans R., De Angelis P., Forstreuter M., Jach M.E., Kellomaki S., Laitat E., Marek M., Philippot S., Rey A., Strassemeyer J., Laitinen K., Liozon R., Portier B., Roberntz P., Wang K. & Jstbid P.G. (1999) Effects of elevated [CO_2] on photosynthesis in European forest species: a meta-analysis of model parameters. *Plant, Cell & Environment*, **22**, 1475-1495.

Medlyn B.E., Barton C.V.M., Broadmeadow M.S.J., Ceulemans R., De Angelis P., Forstreuter M., Freeman M., Jackson S.B., Kellomaki S., Laitat E., Rey A., Roberntz P., Sigurdsson B.D., Strassemeyer J., Wang K., Curtis P.S. & Jarvis P.G. (2001) Stomatal conductance of forest species after long-term exposure to elevated CO_2 concentration: a synthesis. *New Phytologist*, **149**, 247-264.

Miglietta F., Peressotti A., Vaccari F.P., Zaldei A., De Angelis P. & Scarascia-Mugnozza G. (2001) Free-air CO_2 enrichment (FACE) of a poplar plantation: the POPFACE fumigation system. *New Phytologist*, **150**, 465-476.

Miller D.A. & White R.A. (1998) A conterminous United States multilayer soil characteristics dataset for regional climat and hydrology modelling. *Earth Interactions 2*, **paper no. 2**, 1-26.

Monclus R., Dreyer E., Villar M., Delmotte F.M., Delay D., Petit J., Barbaroux C., Le Thiec D., Bréchet C. & Brignolas F. (2006) Impact of drought on productivity and water use efficiency in 29 genotypes of *Populus deltoides* x *Populus nigra*. *New Phytologist*, **169**, 765-777.

Moore B.D., Cheng S.H., Rice J. & Seeman J.R. (1998) Sucrose cycling, Rubisco expression, and prediction of photosynthetic acclimation to elevated atmospheric CO_2. *Plant, Cell and Environment* **21**, 905-915.

Moore B.D., Cheng S.H., Sims D. & Seeman J.R. (1999) The biochemical and molecular basis for photosynthetic acclimation to elevated CO2. *Plant, Cell and Environment* **22**, 567-582.

Morison J.I.L. & Lawlor D.W. (1999) Interactions between increasing CO_2 concentration and temperature on plant growth. *Plant, Cell and Environment*, **22**, 659-682.

Morison L.J.I. & Gifford R.M. (1983) Stomatal sensitivity to carbon dioxide and humidity: a comparison of two C_3 and two C_4 grass species. *Plant Physiology*, **71**, 789-796.

Morse S.R., Wayne P., Miao S.L. & Bazzaz F.A. (1993) Elevated CO_2 and drought alter tissue water relations of birch (*Betula populifolia* Marsh.) seedlings. *Oecologia*, **95**, 599-602.

Murphy J.M., Sexton D., Barnett D.N., Jones G.S., Webb M.J., Collins M. & Stainforth D.A. (2004) Quantification of modelling uncertainties in a large ensemble of climate change simulations. *Nature*, **430**, 768-772.

Murphy J.M., Sexton D.M.H., Jenkins G.J., Boorman P.M., Booth B.B.B., Brown C.C., Clark R.T., Collins M., Harris G.R., Kendon E.J., Betts R.A., Brown S.J., Howard T.P., Humphrey K.A., McCarthy M.P., McDonald R.E., Stephens A., Wallace C., Warren R., Wilby R. & Wood R.A. (2009) UK Climate Projections Science Report: Climate change projections. *Met Office Hadley Centre, Exeter, UK*.

Nakicenovic N. & Swart R. (2000) Special report on emissions scenarios. *Cambridge, UK: Cambridge University Press.*

Nie D., He H., Kirkham M.B. & Kanemasu E.T. (1992) Photosynthesis of a C_3 and a C_4 grass under elevated CO_2. *Photosynthetica*, **26**, 189-198.

Niinemets Ü., Cescatti A., Rodeghiero M. & Tosens T. (2006) Complex adjustments of photosynthetic potentials and internal diffusion conductance to current and previous light availabilities and leaf age in Mediterranean evergreen species *Quercus ilex*. *Plant, Cell and Environment*, **29**, 1159-1178.

Niinemets Ü., Diaz-Espejo A., Flexas J., Galmes J. & Warren C.R. (2009) Importance of mesophyll diffusion conductance in estimation of plant photosynthesis in the field. *Journal of Experimental Botany*, **60**, 2271-2282.

Nonhebel S. (2002) Energy yields in intensive and extensive biomass production systems. *Biomass and Bioenergy*, **22**.

Norby R.J., DeLucia E.H., Gielen B., Calfapietra C., Giardina C.P., King J.S., Ledford J., McCarthy H.R., Moore D.J.P., Ceulemans R., De Angelis P., Finzi A.C., Karnosky D.F., Kubiske M.E., Lukac M., Pregitzer K.S., Scarascia-Mugnozza G.E., Schlesinger W.H. & Oren R. (2005) Forest response to elevated CO2 is conserved across a broad range of productivity. *Proceedings of the National Academy of Sciences of the United States of America*, **102**, 18052-18056.

Norby R.J., Ledford J., Reilly C.D., Miller N.E. & O'Neill E.G. (2004) Fine-root production dominates responses of a deciduous forest to atmospheric CO_2 enrichment. *PNAS*, **101**, 9689-9693.

Norby R.J., Wullschleger S.D., Gunderson C.A., Johnson D.W. & Ceulemans R. (1999) Tree responses to rising CO_2 in field experiments: implications for the future forest. *Plant, Cell and Environment*, **22**, 683-714.

Norby R.J., Wullschleger S.D., Gunderson C.A. & Nietch C.T. (1995) Increased growth efficiency of *Quercus alba* trees in a CO_2 enriched atmosphere. *New Phytologist*, **131**, 91-97.

Nowak R.S., Ellsworth D.S. & Smith S.D. (2004) Functional responses of plants to elevated atmospheric CO_2- do photosynthetic and productivity data from FACE experiments support early predictions? *New Phytologist*, **162**, 253-280.

Openshaw K. (2000) A review of Jatropha curcas: an oil plant of unfulfilled promise. *Biomass and Bioenergy*, **19**, 1-15.

Oren R., Ellsworth D.S., Johnsen K.H., Phillips N., Ewers B.E., Maier C., Schäfer K.V.R., McCarthy H., Hendrey G., McNulty S.G. & Katul G.G. (2001) Soil fertility limits carbon sequestration by forest ecosystems in a CO_2-enriched atmosphere. *Nature*, **411**, 469-472.

Oren R., Sperry J.S., Katul G.G., Pataki D.E., Ewers B.E., Phillips N. & Schafer K.V.R. (1999) Survey and synthesis of intra- and interspecific variation in stomatal sensitivity to vapour pressure deficit. *Plant , Cell and Environment*, **22**, 1515-1526.

Ottman M.J., Kimball B.A., Pinter P.J., Wall G.W., Vanderlip R.L., Leavitt S.W., LaMorte R.L., Matthias A.D. & Brooks T.J. (2001) Elevated CO_2 increases sorghum biomass under drought conditions. *New Phytologist*, **150**, 261-273.

Owensby C., Ham J., Knapp A., Bremer D. & Auen L. (1997) Water vapour fluxes and their impact under elevated CO_2 in a C_4-tallgrass prairie. *Global Change Biology*, **3**, 189-195.

Parsons R. & Ogston S.A. (1998) Photosynthesis Assistant - Windows software for analysis of photosynthesis. Dundee Scientific, Dundee, Scotland.

Piñeiro G., Perelman S., Guerschman J.P. & Paruelo J.M. (2008) How to evaluate models: Observed vs. predicted or predicted vs. observed? *Ecologicla Modelling*, **216**, 316-322.

Pons T.L., Flexas J., von Caemmerer S., Evans J.R., Genty B., Carbo-Ribas M. & Brugnoli E. (2009) Estimating mesophyll conductance to CO_2: methodology, potential errors, and recommendations. *Journal of Experimental Botany*, **60**, 2217-2234.

Poole I., Weyers J.D.B., Lawson T. & Raven J.A. (1996) Variations in stomatal density and index: implications for paleoclimatic reconstructions. *Plant , Cell and Environment*, **19**, 705-712.

Poorter H. & Navas M. (2003) Plant growth and competition at elevated CO_2: on winners, losers and functional groups. *New Phytologist*, **157**, 175-198.

Pregitzer K.S., Dickmann D.I., R. H. & Nguyen P.V. (1990) Whole-tree carbon and nitrogen partitioning in young hybrid poplars. *Tree Physiology*, **7**, 79-93.

Prescott J.A. (1940) Evaporation from a water surface in relation to solar radiation. *Transaction of the Royal Society of South Australia*, **64**, 114-125.

Prioul J.L. & Chartier P. (1977) Partitioning of transfer and carboxylation components of intracellula resistance to photosynthetic CO_2 fixation: A critical analysis of the methods used. *Annals of Botany*, **41**, 789-800.

Prudhomme C. & Lafon T. (2008) Climate Change Data Portal. In: *SuCCInCT: Scenarios for uncertainty in climate change impact*. Centre for Ecology and Hydrology, Wallingford.

R2.10.1 (2009) R Core Development Team: A language and environment for statistical computing. In: *ISBN 3-900051-07-0, URL http://www.R-project.org*. (ed V. R Foundation for Statistical Computing, Austria.).

Radoglou K.M. & Jarvis P.G. (1990b) Effects of CO_2 enrichment on four poplar clones. II. Leaf surface properties. *Annals of Botany*, **65**, 627-632.

Rae A.M., Robinson K.M., Street N.R. & Taylor G. (2004) Morphological and physiological traits influencing biomass productivity in short-rotation coppice poplar. *Canadian Journal of Forest Research*, **34**, 1488-1498.

RCEP (2004) *Biomass as a renewable energy source*. Royal Commission on Environmental Pollution.

Reich P.B., Tilman D., Craine J., Ellsworth D., Tjoelker M.G., Knops J., Wedin D., Naeem S., Bahauddin D., Goth J., Bengtson W. & Lee T.D. (2001) Do species and functional groups differ in acquisition and use of C, N and water under varying atmospheric CO_2 and N availability regimes? A field test with 16 grassland sprecies. *New Phytologist*, **150**, 435-448.

Ripley B.S., Gilbert M.E., Ibrahim D.G. & Osborne C.P. (2007) Drought constraints on C_4 photosynthesis: stomatal and metabolic limitations in C_3 and C_4 subspecies of Alloteropsis semialata. *Jouranl of Experimental Botany*, **58**, 1351-1363.

Rogers A. & Ellsworth D.S. (2002) Photosynthetic acclimation of Pinus taeda (loblolly pine) to long-term growth in elevated pCO_2 (FACE). *Plant, Cell & Environment*, **25**, 851-858.

Rogers A. & Humphries S.W. (2000) A mechanistic evaluation of photosynthetic acclimation at elevated CO_2. *Global Change Biology*, **6**, 1005-1011.

Saliendra N.Z., Sperry J.S. & Comstock J.P. (1995) Influence of leaf water status on stomatal responses to humidity, hydraulic conductance, and soil drought in *Betula occidentalis*. *Planta*, **196**, 357-366.

Sanchez-Rodriguez J., Perez P. & MartInez-Carrasco R. (1999) Photosynthesis, carbohydrate levels and chlorophyll fluorescence-estimated intercellular CO2 in water-stressed Casuarina equisetifolia Forst. & Forst. *Plant, Cell & Environment*, **22**, 867-873.

Saxe H., Ellsworth D.S. & Heath J. (1998) Tree and forest functioning in an enriched CO_2 atmosphere. *New Phytologist*, **139**, 395-436.

Scarascia-Mugnozza G.E., Ceulemans R., Heilman P.E., Isebrands J.G., Stettler R.F. & Hinckley T.M. (1997) Production physiology and morphology of Populus and their hybrids grown under short rotation. II. Biomass components and harvest index of hybrid and parental species clones. *Canadian Journal of Forest Research* **27**, 285-294.

Schäfer K.V.R., Oren R., Lai C. & Katul G.G. (2002) Hydrologic balance in an intact temperate forest ecosystem under ambient and elevated atmospheric CO_2 concentration. *Global Change Biology*, **8**, 895-911.

Sellers P., Berry J.A., Collatz G.J., Field C. & Hall F. (1992) Canopy reflectance, photosynthesis and transpiration, III. a reanalysis using enzyme kinetics - electron transport models of leaf physiology. *Remote Sensing of Environment*, **42**, 187-216.

Sharkey T.D., Bernacchi C.J., Farquhar G.D. & Singsaas E.L. (2007) Fitting photosynthetic carbon dioxide response curves for C_3 leaves. *Plant , Cell and Environment*, **30**, 1035-1040.

Sims R.H. (2007) *Good practice guidelines: bioenergy project development and biomass supply*.

Sinclair T.R. (2005) Theoretical analysis of soil and plant traits influencing daily plant water flux on drying soils. *Agronomy Journal*, **97**, 1148-1152.

Sinclair T.R., Hammond L.C. & Harrison J. (1998) Extractable soil water and transpiration rate of soybean on sandy soils. *Agronomy Journal*, **90**, 363-368.

Stainforth D.A., Aina T., Christensen C., Collins M., Faull N., Frame D.J., Kettleborough J.A., Knight S., Martin A., Murphy J.M., Piani C., Sexton D., Smith L.A., Spicer R.A., Thorpe A.J. & Allen M.R. (2005) Uncertainty in predictions of the climate response to rising levels of greenhouse gases. *Nature*, **433**, 403-406.

Stitt A. & Krapp M. (1999) The interaction between elevated carbon dioxide and nitrogen nutrition: the physiological and molecular background. *Plant, Cell and Environment*, **22**, 583-628.

Stocker R., Leadley P.W. & KÖrner C.H. (1997) Carbon and water fluxes in a calcareous grassland under elevated CO_2. *Functional Ecology*, **11**, 222-230.

Stott P.A. & Kettleborough J.A. (2002) Origins and estimates of uncertainty in predictions of twenty-first century temperature rise. *Nature*, **416**, 723-726.

Street N.R., Skogstrom O., Sjodin A., Tucker J., Rodriguez-Acosta M., Nilsson P., Jansson S. & Taylor G. (2006) The genetics and genomics of the drought response in *Populus*. *Plant Journal*, **48**, 321-341.

Stulen I. & den Hertog J. (1993) Root growth and functioning under atmospheric CO_2 enrichment. *Vegetatio*, 99-115.

Taylor G. (2002) *Populus Arabidopsis* for forestry: Do we need a model tree? *Annals of Botany*, **90**, 681-689.

Taylor G., Ceulemans R., Ferris T., Gardner S.D.L. & Shao B.Y. (2001a) Increased leaf area expansion of hybrid poplar in elevated CO_2. From controlled environments to open-top chambers and to FACE. *Environmental Pollution*, **115**, 463-472.

Taylor G., Tricker P.J., Zhang F.Z., Alston V.J., Miglietta F. & Kuzminsky E. (2003) Spatial and temporal effects of free-air CO_2 enrichment (POPFACE) on leaf growth, cell expansion, and cell production in a closed canopy of poplar. *Plant Physiol.*, **131**, 177-185.

Tezara W., Mitchell V.J., Driscoll S.D. & Lawlor D.W. (1999) Water stress inhibits plant photosynthesis by decreasing coupling factor and ATP. *Nature*, **401**, 914-917.

Thompson N., Barrie I.A. & Ayles M. (1981) *The Meteorological Office rainfalll and evaporation calculation system: MORECS.*

Tissue D.T., Thomas R.B. & Strain B.R. (1997) Atmospheric CO_2 enrichment increases growth and photosynthesis in Pinus taeda: a 4-year experiment in the field. *Plant, Cell and Environment*, **20**, 1123-1134.

Tognetti R., Longobucco A., Raschi A., Miglietta F. & Fumagalli I. (1999) Responses of two Populus clones to elevated atmospheric CO_2 concentration if the field. *Annals of Forest Science* **56**, 493-500.

Tognetti R., Minnocco A., Penuelas J., Raschi A. & Jones M.B. (2000) Comparative field water relations of three Mediterranean shrub species co-occurring at a natural CO_2 vent. *Journal of Experimental Botany*, **51**, 1135-1146.

Tricker P.J., Pecchiari M., Bunn S.M., Vaccari F.P., Peressotti A., Miglietta F. & Taylor G. (2009) Water use of a bioenergy plantation increases in a future high CO_2 world. *Biomass and Bioenergy*, **33**, 200-208.

Tricker P.J., Trewin H., Kull O., Clarkson G.J.J., Eensalu E., Tallis M.J., Colella A., Doncaster C.P., Sabatti M. & Taylor G. (2005) Stomatal conductance and not stomatal density determines the long-term reduction in leaf transpiration of poplar in elevated CO_2. *Oecologia*, **143**, 652-660.

Triggs J.M., Kimball B.A., Pinter P.J., Wall G.W., Conley M.M., Brooks T.J., LaMorte R.L., Adam N.R., Ottman M.J., Matthias A.D., Leavitt S.W. & Cerveny R.S. (2004) Free-air CO_2 enrichment effects on the energy balance and evapotranspiration of sorghum. *Agricultural and Forest Meteorology*, **124**, 63-79.

Tubby I. & Armstrong A. (2002) Establishment and management of short rotation coppice. A practice note (ed B.F. Commission).

Tuskan G.A., DiFazio S., Jansson S., Bohlmann J., Grigoriev I., Hellsten U., Putnam N., Ralph S., Rombauts S., Salamov A. & *al. e.* (2006) The genome of black cottonwood, *Populus trichocarpa* (Torr. & Gray). *Science*, **313**, 1596-1604.

Uddling J., Teclaw R.M., Kubiske M.E., Pregitzer K.S. & Ellsworth D.S. (2008) Sap flux in pure aspen and mixed aspen-birch forests exposed to elevated concentrations of carbon dioxide and ozone. *Tree Physiology*, **28**, 1231-1243.

Van der Burgh J., Visscher H., Dilcher D.L. & Kurschner W.M. (1993) Paleoatmospheric signatures in neogene fossil leaves. *Science*, **260**, 1788-1790.

Vanloocke A., Bernacchi C.J. & Twines T.E. (2010) The impacts of *Miscanthus* x *giganteus* production on the Midwest US hydrologic cycle. *Global Change Biology Bioenergy*, **2**, 180-191.

Vavasseur A. & Raghavendra A. (2005) Guard cell metabolism and CO_2 sensing. *New Phytologist*, **165**, 665-682.

Von Caemmerer S. (2000) *Biochemical models of leaf photosynthesis.* CSIRO Publishing, Canberra, Australia.

von Caemmerer S. & Furbank R.T. (2003) The C_4 pathway: an efficient CO_2 pump. *Photosynthesis Research*, **77**, 191-207.

Voogt M.H., Van den Hurk B.J.J.M. & Jacobs C.M.J. (2005) The ECMWF land surface scheme extended with a photosynthesis and LAI module tested for a coniferous forest site.

Vu J.C.V. & Allen Jr L.H. (2009) Growth at elevated CO2 delays the adverse effects of drought stress on leaf photosynthesis of the C4 sugarcane. *Journal of Plant Physiology*, **166**, 107-116.

Wall G.W., Brooks T.J., Adam N.R., Cousins A.B., Kimball B.A., Pinter P.J., LaMorte R.L., Triggs J., Ottman M.J., Leavitt S.W., Matthias A.D., Williams D.G. & Webber A.N. (2001) Elevated atmospheric CO_2 improved Sorghum plant water status by ameliorating the adverse effects of drought. *New Phytologist*, **152**, 231-248.

Wall G.W., Garcia R.L., Kimball B.A., Hunsaker D.J., Pinter P.J., Long S.P., Osborne C.P., Hendrix D.L., Wechsung F., Wechsung G., Leavitt S.W., LaMorte R.L. & Isdo S.B. (2006) Interactive effects of elevated carbon dioxide and drought on wheat. *Journal of Agronomy*, **98**, 354-381.

Wand S.J.E., Midgley G.F., Jones M.H. & Curtis P.S. (1999) Responses of wild C_4 and C_3 grass (*Poaceae*) species to elevated atmospheric CO_2 concentration: a meta-analytic test of current theories and perceptions. *Global Change Biology*, **5**, 723-741.

Ward J.K., Tissue D.T., Thomas R.B. & Strain B.R. (1999) Comparative responses of model C_3 and C_4 plants to drought in low and elevated CO_2 *Global Change Biology*, **5**, 857-867.

Warren C.R. (2008) Stand aside stomata, another actor deserves centre stage: the forgotten role of the internal conductance to CO_2 transfer. *Journal of Experimental Botany*, **59**, 1475-1487.

Warren C.R. & Adams M.A. (2006) Internal conductance does not scale with photosynthetic capacity: implications for carbon isotope discrimination and the economics of water and N use in photosynthesis. *Plant, Cell & Environment*, **29**, 192-201.

Warren C.R. & Dreyer E. (2006) Temperature response of photosynthesis and internal conductance to CO_2: results from two independent approaches. *Journal of Experimental Botany*, **57**, 3057-3067.

Warren C.R., Livingston N.J. & Turpin D.H. (2004) Water stress decreases the transfer conductance of Douglas-fir (*Pseudotsuga menziesii*) seedlings. *Tree Physiology*, **24**, 971-979.

Watling J.R. & Press M.C. (1997) How is the relationship between the C_4 cereal *Sorghum bicolor* and the C_3 root hemi-parasite *Striga hermonthica* and *Striga asiatica* affected by elevated CO_2? *Plant, Cell and Environment*, **20**, 1292-1300.

Wheeler T.R., Batts G.R., Ellis R.H., Hadley P. & Morison J.I.L. (1996) Growth and yield on winter wheat (*Triticum aestivum*) crops in response to CO_2 and temperature. *The Journal of Agricultural Science*, **127**, 37-48.

Wheeler T.R., Morison J.I.L., Ellis R.H. & Hadley P. (1994) The effects of CO_2, temperature and their interaction on the growth and yield of carrot (*Daucus carota L.*). *Plant, Cell and Environment*, **17**, 1275-1284.

Wilkinson S. & Davies W.J. (2002) ABA-based chemical signalling: the co-ordination of responses to stress in plants. *Plant, Cell and Environment*, **25**, 195-210.

Williams M., Rastetter E.B., Fernandes D.N., Goulden M.L., Wofsy S.C., Shaver G.R., Melillo J.M., Munger J.W., Fan S.M. & Nadelhoffer K.J. (1996) Modelling the soil-plant-atmosphere continuum in a *Quercus-Acer* stand at Harvard Forest: the regulation of stomatal conductance by light, nitrogen and soil/plant hydraulic properties. *Plant, Cell & Environment*, **19**, 911-927.

Woodward F.I. (1987) Stomatal numbers are sensitive to increases in CO_2 from pre-industrial levels. *Nature*, **327**, 617-618.

Wosten J.H., Lilly A., Nemes A. & Le Bas C. (1999) Development and use of a database of hydraulic properties of European soils. *Geoderma*, **90**, 169-185.

Wullschleger S.D., Gunderson C.A., Hanson P.J., Wilson K.B. & Norby R.J. (2002b) Sensitivity of stomatal and canopy conductance to elevated CO_2 concentration; interacting variables and perspectives of scale. *New Phytologist*, **153**, 485-496.

Wullschleger S.D. & Norby R.J. (2001) Sap velocity and canopy transpiration in a sweetgum stand exposed to free-air CO_2 enrichment (FACE). *New Phytologist*, **150**, 489-498.

Wullschleger S.D., Tschaplinski T.J. & Norby R.J. (2002a) Plant water relations at elevated CO_2 - implications for water-limited environments. *Plant, Cell and Environment*, **25**, 319-331.

www.co2now.org (last accessed 01.05.10).

Yin C., Wang X., Duan B., Luo J. & Li C. (2005) Early growth, dry matter allocation and water use efficiency of two sympatric Populus species as affected by water stress. *Environmental and Experimental Botany*, **53**, 315-322.

Yin C.Y., Berninger F. & Li C.Y. (2006) Photosynthetic responses of *Populus przewalski* subjected to drought stress. *Photosynthetica*, **44**, 62-68.

Zhang X., Zang R. & Li C. (2004) Population differences in physiological and morphological adaptations of Populus davidiana seedlings in response to progressive drought stress. *Plant Science*, **166**, 791-797.

Ziska L.H. & Bunce J.A. (1997) Influence of increasing carbon dioxide concentration on the photosynthetic and growth stimulation of selected C_4 crops and weeds. *Photosynthesis Research*, **54**, 199-208.

Ziska L.H., Sicher R.C. & Bunce J.A. (1999) The impact of elevated carbon dioxide on growth and gas exchange of three C_4 species differing in CO_2 leak rates. *Physiol Plant* **105**, 74-80.